Pingju Li

An Experimental Investigation of Velocity Distribution and Head Loss of Oscillatory Flow in a Rectangular Duct with Sand Roughness

PhD-thesis 2004:04

Faculty of Engineering Science and Technology
Department of Energy and Process Engineering

◉ NTNU

An Experimental Investigation of Velocity Distribution and Head Loss of Oscillatory Flow in a Rectangular Duct with Sand Roughness

Pingju Li

Department of Energy and Process Engineering
Faculty of Engineering Science and Technology
Norwegian University of Science and Technology
Trondheim, Norway

This thesis is submitted to
the Norwegian University of Science and Technology
in partial fulfillment of the Ph.D. degree

January 2004

Abstract

Frequency and amplitude dependency of velocity distribution and head loss of oscillatory flow in a rectangular duct have been studied experimentally with a model tunnel system.

Tests were carried out with the duct of both smooth and rough walls. The smooth wall was made of Plexiglas. Sand roughness was used for the rough wall. Velocity, pressure and differential pressure of stationary flow, pure oscillatory flow and combined oscillatory flow were measured. The combined oscillatory flow was classified as oscillation dominant flow, stationary dominant flow, and oscillation-and-stationary balanced flow. Various oscillating frequencies, amplitudes and steady flow percentages were tested for oscillatory flows. The oscillating frequencies tested were varied from 0.01 Hz to 1.00 Hz. Oscillatory amplitude and stationary part were varied from 10 to 100%. Velocity of the flow was measured with a 2D PIV (Particle Image Velocimetry) and a 2D LDV (Laser Doppler Velocimetry) respectively at different test stages. The maximum mainstream velocity was ranged from 0.05 m/s to 1.1 m/s. Data of pressure variations along the tunnel were collected with differential pressure sensors. Flow rate and instant wall pressures at multiple points along the test tunnel were measured simultaneously. The static pressure in the test tunnel was about 1.0 mWC. The differential pressure along the tunnel was less than 20 mmWC per meter.

Examples of velocity distribution in the test rig from LDV measurement are presented, for both stationary flow and oscillatory flow. The dimensionless velocity distributions of stationary flow are in good agreement with the universal velocity distribution law. Deviations are obvious between the velocity distributions of oscillatory flow and the universal velocity distribution law, when the measured velocity is scaled to dimensionless by friction velocity from Clauser chart.

Examples of PIV velocities of different flow regimes are presented in the forms of velocity profile and velocity waveform. Generally, the velocity distributions are in good agreement with the results from LDV, in agreement with the normal turbulent velocity distribution in a duct, if the velocity magnitude is not too small. Dimensionless velocity profiles at various phase angles of the same oscillatory flow regime have quite consistent distribution. The annular effect is observed in some cases. Its occurrence depends on the complex actions of oscillating frequency, amplitude and stationary flow percentage. The velocity waveform confirms the characteristics of mass oscillation of the flow. No significant phase shift is displayed between the velocity waveform of the boundary and centreline in most cases tested. The vertical velocity, which is normal to the mainstream, is quite small and has similar features to the mainstream velocity.

The velocity profiles got from both LDV and PIV show that the flows in the test tunnel were typical turbulence, with typical velocity distribution of turbulence. No transition between laminar and turbulence is observed even at the turning point of oscillation.

Pressure variations measured along the tunnel of different flow regimes are presented. The accelerative heads of oscillatory flow are calculated. The friction head losses along the tunnel are evaluated. The dependencies of pressure variation and friction head loss on oscillatory frequency and amplitude are investigated for both pure oscillatory flow and combined oscillatory flow. It is proven that the friction head loss of oscillatory flow increases along with the increase of frequency if the mean flow rate is kept constant. The peak friction head loss increases along with the increase of oscillatory amplitude. Comparison of pressure variation and friction head loss between stationary flow and oscillatory flow shows that the friction head loss of unsteady flow is much bigger than that of steady flow. This is in good agreement with the expectancy based on the experimental results of laminar flow. The head loss of pure oscillatory flow was greater than that of the stationary flow for dozens or more times for various flow regimes running at equivalent flow rate. The ratio of head loss of combined oscillatory flow to stationary flow running at equivalent flow rate is smaller than that of pure oscillatory flow to stationary flow, several times to dozen times. In general, the frequency dependency of head loss on oscillatory frequency and amplitude is clear, though the measuring length is only 9 metres and the absolute magnitude of pressure variation is less than 0.20 mWC.

i

ii

Acknowledgements

This work has been performed at the Hydropower Laboratory, Faculty of Engineering Science and Technology, Norwegian University of Science and Technology (NTNU). The measurement was carried out at the Norwegian Hydraulic Laboratory (NHL).

iv

Contents

Nomenclature

u^*	friction velocity	[m/s]	Ch. 4
V	Velocity in general sense for theoretical development	[m/s]	
V	Mean velocity in *y* direction	[m/s]	
v	Velocity component in *y* direction	[m/s]	
v^+	Dimensionless velocity component in *y* direction	[-]	
$v^{'}$	Fluctuation of the velocity in *y* direction	[m/s]	
W	Mean velocity in *z* direction	[m/s]	
w	Velocity component in *z* direction	[m/s]	
w	Deflection of a plate	[m]	Only in Ch. A.3
w^+	Dimensionless velocity component in *z* direction	[-]	
$w^{'}$	Fluctuation of the velocity in *z* direction	[m/s]	
x	Streamwise coordinate	[m]	
y	Distance from side wall of the duct	[m]	
y^+	Dimensionless distance from side wall of the duct	[-]	
z	Distance from the test duct bottom	[m]	
z^+	Dimensionless distance from the test duct bottom	[-]	

Greek letters

Δ	Total boundary layer thickness	[m]	
δ	Boundary layer displacement thickness	[m]	
ε	Height of surface roughness	[m]	
$ε^+$	Dimensionless roughness	[-]	
μ	Dynamic viscosity	[kg/m-s]	$1.005 \cdot 10^{-3}$
ν	Kinematic viscosity	[m^2/s]	$= μ / ρ$
π	Constant	[-]	
ρ	Density	[kg/m^3]	Water: 998.20
τ	Shear stress	[N/m^2]	
φ	Phase angle	[rad]	
Θ	Boundary layer momentum thickness	[m]	
θ	Angle	°	
Ω	Number of periods	[-]	
ω	Angular velocity / frequency	[rad/s]	
ψ	Phase angle	[rad]	

Subscript

0	Time mean value
amp	Amplitude
e	Free stream
w	Wall
-	(Over score) averaged value
Φ	Phase averaged value
'	(Prime) Velocity fluctuation value

Chapter 1

Introduction

Main topics of this chapter

- General Definitions
- Scope of the work
- Review of previous work

1.1 General Definitions

1.1.1 Unsteady turbulent flow

In a numerical analysis, the turbulence is generally decomposed into the time averaged part, and the fluctuating part. The velocity component of turbulent flow in x direction can be written as

$$(1.1) \qquad \vec{u}(x,t) = \bar{u}(\vec{x}) + u'(\vec{x},t)$$

where

- $\bar{u}(\vec{x})$: time averaged part (*mean* part)

- $u'(\vec{x},t)$: fluctuation (*disordered* part)

For unsteady turbulent flow, the "*mean*" motion is also time dependent. It is generally made up of a time independent part and a time dependent part. The velocity component of unsteady turbulent flow in x direction can be written as

$$(1.2) \qquad \vec{u}(x,t) = \bar{u}(\vec{x}) + \tilde{u}(\vec{x},t) + u'(\vec{x},t)$$

where $\tilde{u}(\vec{x},t)$ is the time dependent *ordered* part. $\tilde{u}(\vec{x},t)$ and $\bar{u}(\vec{x})$ represent the "*mean*" motion. For the oscillatory flow discussed in this thesis, $\tilde{u}(\vec{x},t)$ is the oscillatory part and $\bar{u}(\vec{x})$ is the base flow. The *phase average* of the velocity is obtained by measuring the unsteady turbulent velocity at the same phase angle of multiple periods and then average, as shown in Equation (1.3)

$$(1.3) \qquad \left\langle \vec{u}(x,t) \right\rangle = \frac{1}{\Omega} \sum_{i=0}^{\Omega-1} \vec{u}(x,t+i\cdot T)$$

where T is the period of unsteady turbulent flow and W is the number of periods measured.

1

In this thesis, Equation (1.3) is applied not only to the analysis of the velocity but also to the analysis of other flow characteristics discussed, i.e., Equation (1.3) is valid for velocity, pressure, and flow rate if u in the equation is substituted by a specific symbol of the variable. The fluctuation, $u'(\vec{x},t)$ in Equation (1.2), is not the main topic of this thesis.

1.1.2 Flow regime definitions

1.   Stationary Flow

   Stationary Flow (SF) is a flow regime the characteristics of which keep constant in both time and space, or typically, $Q(t) = Q_0 = Constant$.

2.   Oscillatory Flow

   Oscillatory Flow (OF) is a periodical flow that can be expressed as $Q(t)=Q_0 + q\,sin(\omega t)$, resulting in a water head of flow as $H(t)=H_0 + h\,cos(\omega t)$. Theoretically, the flow can be separated into two parts: steady part (bulk flow) Q_0 and oscillatory part $q sin(\textbf{\textit{w}}t)$. A typical oscillatory flow is shown in Figure 1-1. The characteristic parameters of an oscillatory flow include:

   − Q_0: base flow (steady part)
   − q: oscillatory amplitude
   − $\textbf{\textit{w}}$: oscillatory angular frequency, $\textbf{\textit{w}} = 2\pi f_r$, f_r is the oscillatory frequency.

3.   Pure Oscillatory Flow

   An oscillatory flow is defined as *Pure Oscillatory Flow* (POF) when $Q_0 = 0$.
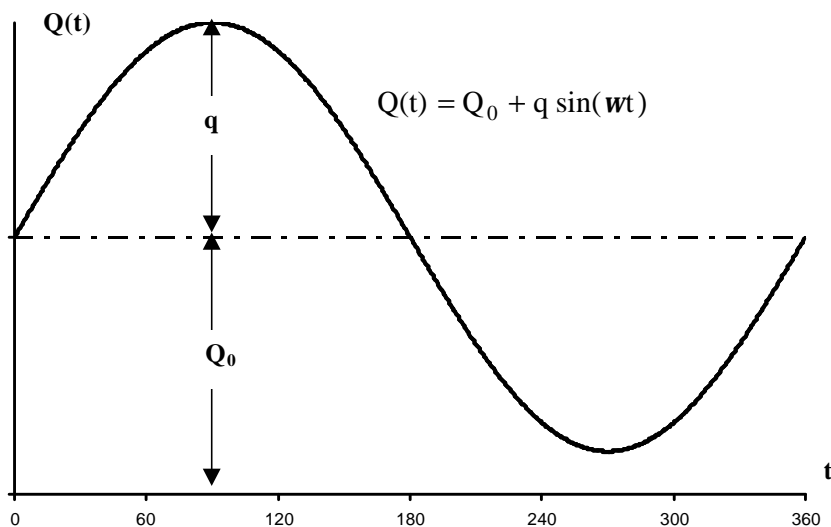
Figure 1-1 Oscillatory flow regime

4.   Combined Oscillatory Flow

   An oscillatory flow is defined as *Combined (Superimposed) Oscillatory Flow* (COF) if all of Q_0, q and $\textbf{\textit{w}}$ are nonzero.

5. Stationary Dominant Flow

    If $Q_0 >> q$ in the case of combined oscillatory flow, the flow is classified as *Stationary Dominant Flow* (SDF).

6. Balanced Flow.

    If $Q_0 = q$ or the difference between Q_0 and q is quite small in the case of combined oscillatory flow, the flow is classified as *Balanced Flow* (BF).

7. Oscillatory Dominant Flow

    If $Q_0 << q$ in the case of combined oscillatory flow, the flow is classified as *Oscillatory Dominant Flow* (ODF).

1.1.3 Pressure related definitions

1. Friction Loss

    Friction Loss is found by the difference in pressure between two points along the conduit. It is a result of the wall friction to the flow.

2. Dynamic Pressure Oscillations

    Dynamic Pressure Oscillations is found by the difference in pressure between two points along the conduit, which is caused by acceleration or deceleration of the flow. It is also called accelerative head in related literatures.

3. Differential Pressure

    Differential Pressure is the difference of wall pressure between two points along the mainstream. For stationary flow it is the friction loss caused by wall friction. For non-stationary flow it is the sum of friction loss and the dynamic wall pressure variation. In the measurement the wall pressure differences are found by means of readings of the differential pressure sensors located along the model tunnel.

    Figure 1-2 illustrates the definitions of water pressure for oscillatory flow.
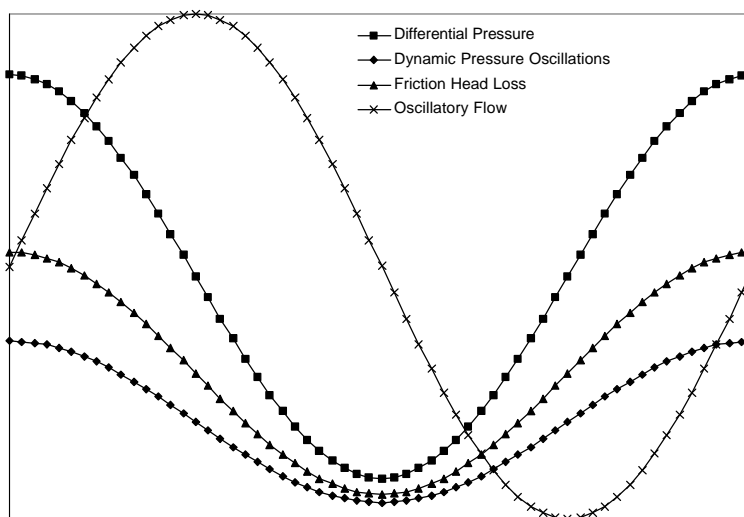
Figure 1-2 Different heads in the flow

4. Wall Pressure

    Wall Pressure is the reading of a pressure sensor attached to a single point of the tunnel wall. As shown in Figure 1-3, pressure sensor *P* gets the wall pressure of the flow passing by point *A*.

5. Cross Sectional Averaged Pressure

    Cross Sectional Averaged Pressure is the mean pressure in the whole cross section of the tunnel, as shown in Figure 1-4, pressure sensor *P* gets the averaged pressure of points *A* through *D*. Points *A* to *D* were connected by flexible tubes, which are shown in dash lines in Figure 1-4.
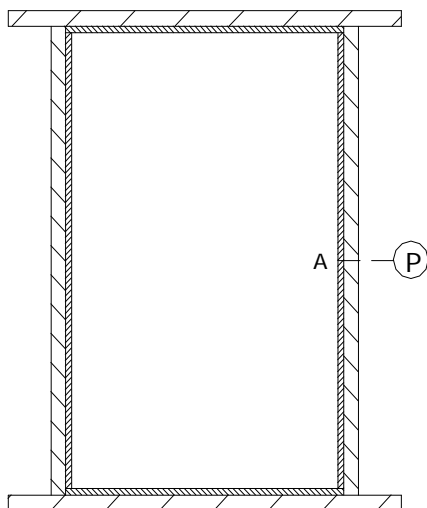
Figure 1-3 Wall pressure sensor
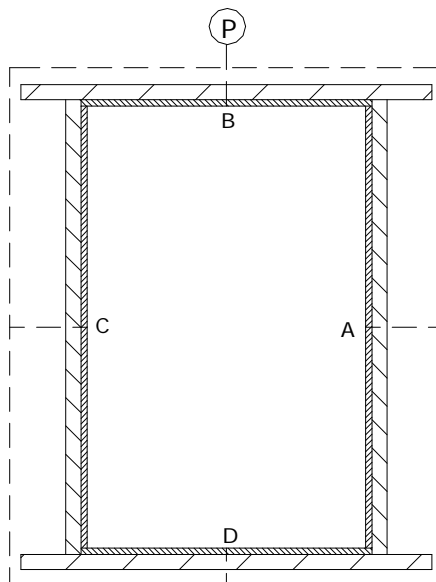
Figure 1-4 Cross section averaged pressure sensor

1.2 Scope of the Work

The aim of this work was to investigate the dependency of friction loss on the amplitudes and frequencies of oscillatory flow in a non-circular conduit, with and without sand roughness. The goal was to get a better understanding of the friction loss increment from the steady flow to the oscillatory flow. This work was mainly carried out by experiment, i.e., measuring the velocity, pressure, and differential pressure along the streamline.

The flow conduit had a rectangular cross section, which was simulated to a non-circular (e.g. horse-shoes shape) tunnel of a hydropower plant.

Measurements were carried out as followings:

− stationary flow: mean velocity ranged from 0.10 m/s – 0.81 m/s.
− pure oscillatory flow: peak velocity ranged from 0.07 m/s to 1.03 m/s; frequency from 0.01 Hz to 1.00 Hz.
− superimposed oscillatory flow: peak velocity ranged from 0.1 m/s to 0.99 m/s; frequency from 0.01 Hz to 1.00 Hz.

Measurements were carried out on both smooth conduit and conduit with sand roughness deployed on its four inner sidewalls.

1.3 Previous Work

Many measurements have been carried out on unsteady flows for boundary layer study, for fully developed pipe flow investigation, for turbulence model evaluation, for comparison with stationary flow, etc. Both flow without pressure gradient and flow with adverse pressure gradient have been measured. Some tests are carried out in channels; others are carried out in circular pipes, which are dominant in all cases. The oscillation is produced either by moving the flow or by moving the boundary.

The recent measurement by Vennatrø (2000) is carried out with a rigid circular smooth pipe in diameter of 100 mm. The velocity profiles in oscillatory flow are measured with LDA (Laser Doppler Anemometry) and compared with steady-state measurement. The oscillating frequency varies in the range of 2.7 to 73.9 Hz. The amplitude of the oscillation is about 20% of the averaged bulk flow; the time mean Reynolds number is of the magnitude of $Re \sim 1 \cdot 10^4$. The results show that when a phase dependent friction velocity $u^*(\boldsymbol{j})$ is used to normalize the oscillatory velocity profile, the time mean and phase dependent velocity profiles follow the universal logarithmic law. The flows measured behave as quasi-steady at all frequencies tested. The results show further that in smooth pipes the head loss is independent of the frequency when the amplitude of oscillation is less than 20% of the time mean bulk velocity.

Brekke (1984) measures the full size rough tunnel systems in multiple hydropower plants, in which the roughness is 0.05m to 0.45 m. The flow in this case cannot be regarded as a turbulent boundary layer problem with a laminar sub layer for the large eddies formed in the flow by waviness of the wall. The cross sectional area of tunnels measured ranges from 3 to 50 m^2 and the frequency ranges from 0.006 to 8 rad/s (approximately 0.001 – 1.27 Hz). It is concluded from the measurement that the head loss in the tunnel with oscillatory flow is frequency dependent. Friction factor of rough tunnel is expressed as:

$$(1.4) \qquad K_r = \frac{Q_0 |\hat{q}|}{\boldsymbol{v}} \cdot \frac{1}{A} \cdot \left(\frac{\ln f + 5.973}{5.213} \right)^{5.155}$$

The relation between K_r and Nikuradse's sand roughness K_s is proposed by Brekke (1984) as:

$$(1.5) \qquad K_r = \frac{K_s}{R_h^2}$$

The general empirical formula for K_r which is suitable for tunnels tested and other tunnels, is developed by setting $Q_0 |\hat{q}| = 1.0$ and $\boldsymbol{w} = 0.0025$:

$$(1.6) \qquad K_r = \frac{400}{A} \cdot \left(\frac{\ln f + 5.977}{5.213} \right)^{5.155}$$

There is a phase shift of $\boldsymbol{p}/4$ between the flow oscillation and the shear force at the wall according to Brekke (1984).

Jonsson L. (1991) measures the rapid decelerating flows, velocity profiles of which are obtained by using of a laser velocity meter. Two different cases are reported: flow changes due to pump trip only and flow changes due to rapid valve closure. Jonsson L. (1991) classifies the flow by means of the factor

$$(1.7) \qquad k = \sqrt{\frac{\boldsymbol{w}}{\boldsymbol{n}}} R$$

where w is the angular frequency of oscillation, R is the pipe radius and n is the kinematic viscosity. The flow was classified as quasi-steady when $k < 1$.

In the first case, the velocity is diminished from 2.6 m/s to 1.0 m/s in approximately 10 seconds. The test results show that the velocity profile keeps the original shape during the deceleration.

In the other case, the bulk flow is shut off in about 1 second, the bulk velocity was 0.312 m/s and the wave travelling time $2L/a = 0.2$ s. The measurement shows that the velocity profiles in the core and at the wall have opposite directions for a period.

One of the odd observations in the measurement is that the velocity near to the wall is reversed all the time whereas the velocity in the core changes direction according to the pressure oscillation.

Jonsson I. G. (1980) also carries out measurements on a rough seabed with oscillatory flow. The roughness is in 2D regular waviness. Constant phase lead (relative to the free stream) of velocity (relative to the wall) is confirmed. A relation between friction factor and the boundary layer thickness to roughness ratio is presented as

$$(1.8) \qquad f_w = \frac{0.0605}{\log^2 \frac{27\delta}{\kappa}}$$

or in terms of the ratio between amplitude and boundary thickness:

$$(1.9) \qquad f_w \approx \frac{0.0605}{\log^2 \frac{27a_{1m}}{11d}}$$

The annular effect is confirmed in velocity profile presented by the experiments of Jonsson (1980). The annular effect is called characteristic overshooting in his publications.

Tu and Ramaprian (1983) measure the velocity profile of oscillatory pipe flow at two different frequencies, 0.5 Hz and 3.6 Hz. The amplitude of oscillation is 65% of the mean bulk flow at 0.5 Hz and 15% of the mean bulk flow at 3.6 Hz. They compare the oscillatory properties with the properties found in steady state or quasi-steady state flows. They find that the time mean profile is affected by the imposed oscillation when the oscillation frequency approaches the characteristic frequency of turbulence, and neither the time mean nor the ensemble averaged velocity profile follows the universal logarithmic law.

Binder and Kueny (1981) measure velocity profiles of turbulent channel flow with small periodic velocity oscillation, the time mean $Re_h = 8.8 \cdot 10^3$. They find that the mean flow and the mean turbulent intensity are not affected by the forced oscillation. The oscillating frequency tested ranges from 0.07 to 1.4 Hz with amplitude of 2.5% of the bulk flow. The amplitude near to the wall is closely following the laminar Stokes flow for both frequencies as far as $y^+ \cong 12$. The phase of the velocity oscillation at the highest frequency tested is almost exactly the same as predicted by the Stokes solution, and at the lower frequency the phase is completely different from the Stokes solution. Phase shift of $p/4$ is shown.

Fully developed pipe flow of pulsating turbulence in a water tunnel is measured by Lu et al. (1973). Time averaged longitudinal velocity at the edge of boundary layer U_0 is in the range of 0.0 to 0.7 cm/s with Reynolds number as 16 000 to 81 600. The oscillation amplitude at the edge of boundary layer is 0.0 to 25% of U_0, wRe^2/n is from 0 to 3 130. It is shown that the long-time average velocity distributions are coincident with steady flow. However, the distribution of the measured pulsating velocity component depends on the dimensionless frequency parameter. At low values of wRe^2/n, the unsteady component of velocity shows turbulent-flow-type profiles, while at higher values, the maximum velocity point moves from the centreline towards the wall, and a constant-speed region exists over the central portion of the tube.

Fully developed pipe flow of pulsating turbulence in a circular tube is also measured by Mizushina et al. (1973). Time averaged longitude velocity at the edge of boundary layer U_0 is 100 cm/s with Reynolds number as 10^4. The oscillation amplitude at the edge of boundary layer is 32% to 43% of U_0, oscillatory frequency is 0.12 to 1.3 Hz. It is found that the flow behaviour depends on whether the driving frequency is above or below a critical value associated with the bursting frequency of a steady turbulent boundary layer. For low frequency oscillation, the velocity profiles vary through the cycle and are similar to steady state profiles. The turbulence intensity does not vary through the cycle; the flow is not in full equilibrium. For high frequency, all the measured parameters ($u,\ u^c,\ t,\ -\overline{u'v'}$) are significantly different from that of steady flow.

Lodahl et al. (1998) study the combined oscillatory flow and current in a circular, smooth pipe with LDA. They find that a turbulent current can be laminarized by superimposing an oscillatory flow. The overall average value of the wall shear stress (the mean wall shear stress) may retain its steady-current value, it may decrease, or it may increase, depending on the flow style.

Borghei (1982) investigates the oscillatory flow under gravity waves above smooth, two-dimensional and three-dimensional rough beds. For the smooth bed case, it was found that the velocity profile throughout the depth is well presented by the Stokes second order shear wave equation. A linear relationship is obtained for the velocity coefficients between the two sets of values. As for mean velocity, the profile is in close agreement with the Longuet-Higgins conduction solution, and it is found to have a negative value (in opposite direction to wave progression) in the bulk of fluid and always-positive values within the boundary layer. The rough beds make little change to the flow in the bulk of fluid. As for inside the boundary layer, the laminar boundary layer is eliminated due to the large size of the rough bed. For a small size rough bed, the flow becomes laminar at the edge of the boundary layer, and a perturbed laminar boundary layer velocity profile is traceable. However, the two rough beds have similar influences on the flow except for the roughness size and Reynolds number values. Inside the roughness elements of the rough beds, vortex formation is clearly observed.

The experimental study of Kongeter (1980) on oscillatory flow is based on a 300 mm diameter oscillating Plexiglas pipe with the water inside locked in between two pistons. The friction factor K increases linearly along with the frequency in the whole frequency range investigated (from 0 to bigger than 1.5Hz) according to Kongeter (1980)

1.4 Concluding Remarks

Due to the complexity of unsteady flow, the results from the previous work are far from sufficient for practical application. The available results are very limited. Some results are not completely consistent with each other.

Based on the earlier work, the dimension and roughness was determined for a closed test loop in the laboratory as described in next chapter. It was decided to measure the velocity profiles with laser Doppler equipment, to collect the water head variation along the test loop with pressure / differential pressure sensors, and test with various of frequency and amplitude of oscillatory flow.

It was also decided to put the main effort into the experiment part since more documentation of oscillatory flow on rough wall was needed.

7

Chapter 2

Experimental Setup

Main topics of this chapter:

- Rig configuration
- Introduction to velocimetry (anemometry) systems
- Description of other sensors used
- Data acquisition system
- Flow regime build up and control

2.1 The Rig

Three different rig arrangements were tested in different stages of the measurement. They were:
- smooth tunnel with water supply of constant head.
- smooth tunnel with circulating water supply from pumps.
- rough tunnel with circulating water supply from pumps.

Most of the measurements presented in this thesis were carried out mainly on the last rig arrangement as shown in Figure 2-1 and Figure 2-2. Some measurements conducted on the second rig arrangement will be presented in the Appendix B "Other Measurements".

2.1.1 Layout of the rig

An overview photo of the test rig, the third rig arrangement, is shown in Figure 2-1. A detail sketch of the test rig with a list of parts is shown in Figure 2-2. The whole system was composed of:
- Model tunnel with oscillatory pumping system
  A model tunnel was constructed for the work described in the thesis. It included six rectangular sections (items 9 - 14 in Figure 2-2) as the flow-developing channel and sampling control volume. The cross section of the rectangular sections was 230×360 mm^2 without inner rough layer and 220×350 mm^2 with inner rough layer. The length of each section was 3 meters. The total length of the test section in rectangular was 18 meters. There were inlet expanding and outlet contracting sections (items 8 and 15 in Figure 2-2), which were in the shape of cone and connected to the ends of the rectangular parts to smooth the flow developing process.
  The oscillatory pumping system is described in detail in 2.5.1.
- Wall roughness
  Similar to the model build by Nikuradse (1933), sand roughness was build on all four sidewalls of the rectangular model tunnel: small sand particles were glued to Plexiglas

plate. It was taken as inner rough layer, which was inserted into the model tunnel and fixed to the tunnel wall tightly. This roughness was classified as small-scale roughness. The thickness of the sand layer was about 0.4—0.5 mm. (*Refer to section 2.1.2 for more details*).

−   Water flow circulation system

A water tank (item 1 in Figure 2-2) and connecting pipes in circular (items 5 - 7 and 16 - 18 in Figure 2-2) built up a closed circuit with the model tunnel in rectangular. Pumps (items 2 and 3 in Figure 2-2) were installed in the tank to produce different flow regimes in the model tunnel, such as pure oscillatory flow, stationary flow, combined oscillatory flow, etc.

−   Velocimeter (anemometry) systems

In the test, three velocimeter systems have been used in different stages of the measurement to get the velocity of the flow. They were: the Acoustic Doppler Velocimeter (ADV, item 31 in Figure 2-2), the Laser Doppler Anemometry (LDA, item 34 in Figure 2-2) and the Particle Image Velocimeter (PIV, items 32 and 33 in Figure 2-2). The results from PIV are presented mainly in this thesis. The velocity from ADV and LDV are presented briefly in the Appendix B "Other Measurements". (*Refer to sections 2.2 and 2.3 for more details about LDV and PIV instrument.*)

−   Flow regime control system

The frequency and amplitude of oscillatory flow, the magnitude of the base stationary flow could be set over a wide range to produce flows with various characteristic parameters. These parameters were controlled from a PC by mean of a LabView VI (Virtual Instrument) named PumpControl and frequency motor controllers (item 4 in Figure 2-2). The controller operated the pumps following the signal from PumpControl VI. (*Refer to section 2.5.1 for more details on PumpControl).*

−   Data acquisition system

The data acquisition system (DAQ) consisted of sensors, data acquisition unit, control PC, and DAQ software.

The sensors used included 4 differential pressure sensors (items 26 - 29 in Figure 2-2), the velocimeter systems (ADV, LDA, PIV), 6 pressure cells (items 19 - 24 in Figure 2-2), and a flow rate meter (item 25 in Figure 2-2).

The data acquisition unit consisted of a HP Data Acquisition / Switch Unit from the Hewlett-Packard Company (HP), a Data Acquisition Board from the National Instruments Corporation (NI), and a connecting board from the Flow Design Bureau (FDB).

The control PCs included the PC for velocimeter sub-systems, and the PC for other data collection and flow regime control.

The DAQ software included the velocimetry analysis software Insight for PIV from the TSI Incorporated (TSI), BSA Flow Software from the Dantec Dynamics A/S (DanTec), ExploreV from the Nortek AS, a flow regime control LabView VI, a HP BenchLink Data Logger, and TecPlot 7.5 from the Amtec Engineering, Inc. (*Refer to section 2.4 and 2.5 for more details of DAQ*).

PIV Sampling
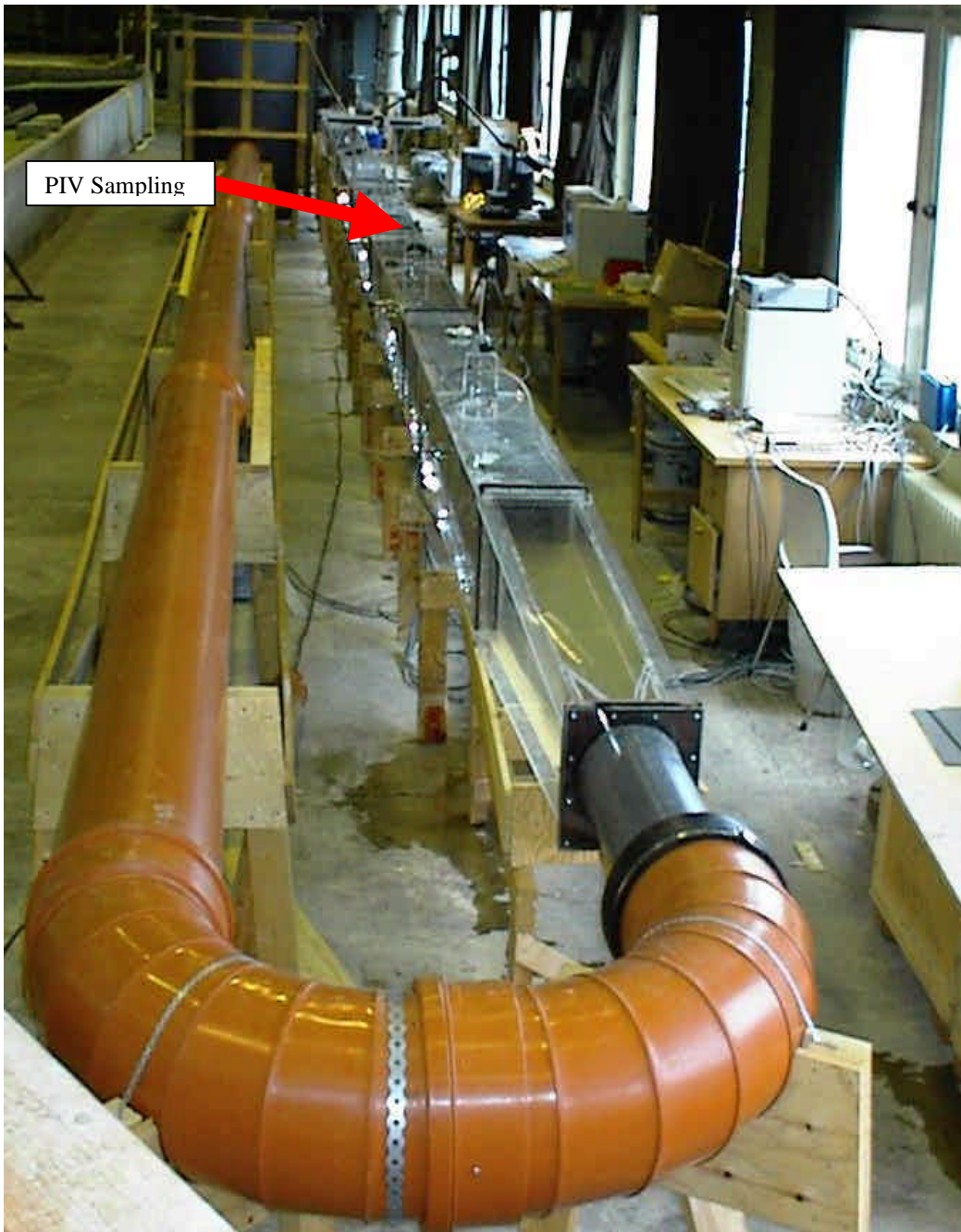
Figure 2-1 Overview of the test rig
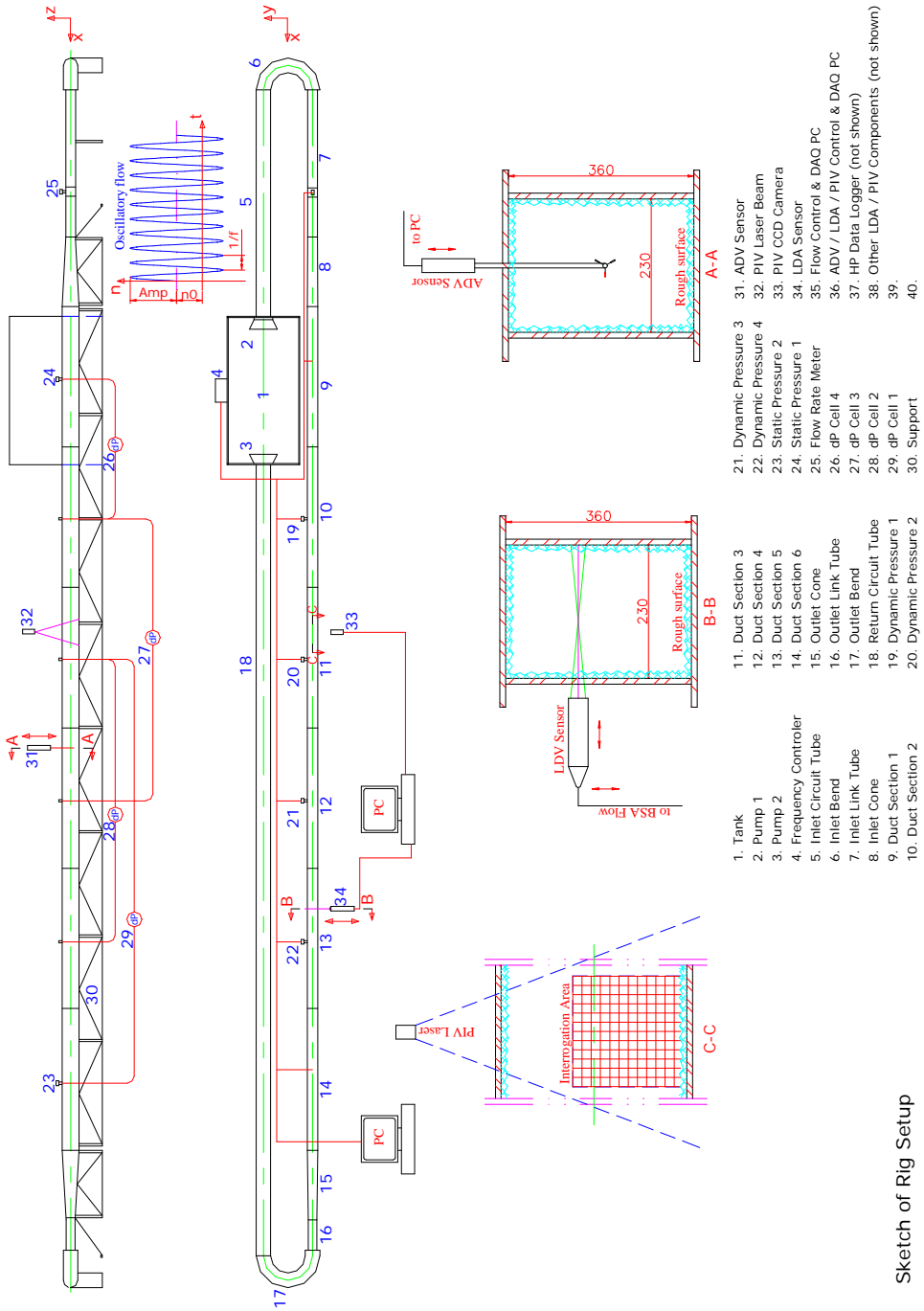
Figure 2-2 Test rig layout

2.1.2 Wall roughness

The roughness used in the model was very similar to the sand roughness built by Nikuradse (1933) in a circular pipe. Figure 2-3 is a picture of the sand roughness.

Figure 2-3 Picture of the sand roughness (the dark dots were water drops)

− The roughness was made by gluing sand particles to a plate of Plexiglas with grey paint. The original thickness of the plate was 5 mm. The plate was taken as an inner layer to the model tunnel.
− The inner layer was inserted into the model tunnel and fixed tightly on the wall of the model tunnel with screws.
− The inner layer was deployed on all four sidewalls of the rectangular model tunnel (Figure 2-4).
− The average height of the sand roughness was about 0.4--0.5 mm.
− No sand was glued to the small part of the sampling windows of PIV camera, entrance of PIV laser sheet and LDV laser beams.

A cross section of the tunnel with the rough inner layer inserted is shown in Figure 2-4 schematically. The cross sectional area of the duct was about 220×350 mm^2 after the inner rough layer was inserted into the model tunnel. The hydraulic diameter D_h of the test duct is:

$$(2.1) \qquad D_h = \frac{4 \cdot A}{P} = \frac{4 \cdot a \cdot b}{2(a+b)} = 0.2702(m)$$

where A is the cross sectional area, P is the wet perimeter, a and b are the side length of the rectangular duct.

The relative roughness is:

$$(2.2) \qquad \frac{\varepsilon}{D_h} = 1.8505 \cdot 10^{-3}$$
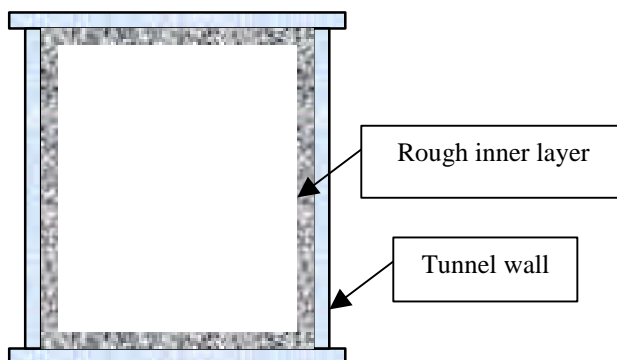
Figure 2-4 Rough inner layer in the tunnel

The hydraulic diameter D_h of the test duct without inner rough layer (smooth tunnel) is:

(2.3) $$D_h = 0.2807(m)$$

2.2 The PIV System

The Particle Image Velocimetry (PIV) system was used to measure the velocity of flow in the final stage of the measurement. Most of the velocity data presented in this thesis was obtained from the PIV system.

2.2.1 Introduction of PIV

The Particle Image Velocimetry system measures velocity by determining particle displacement over time using a double-pulsed laser technique. A laser light sheet illuminates a plane in the seeded flow, and the positions of particles (seeds) in that plane are recorded using a CCD camera. A fraction of a second (*dT*) later, another laser pulse illuminates the same plane, creating a second particle image (Figure 2-5). From these two particle images (or frames, Figure 2-6), unique PIV analysis algorithms obtain the particle displacements for the entire flow region imaged, and give out velocity information at hundreds or thousands of locations. Flow properties such as vorticity and strain rates are obtained for the entire region. Other properties, such as mean, turbulence and other higher order flow statistics can also be obtained.
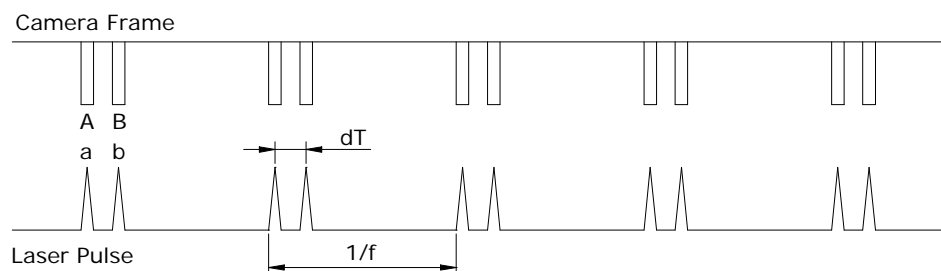
Figure 2-5 Laser pulse and camera frame taken

In Figure 2-5: *dT* is the time interval between two consecutive pulses in micro seconds. *f* is the sampling frequency of PIV, with a maximum value of 15Hz for the PIV system used in the measurement. *1/f* is the time interval between two pairs of picture.

14
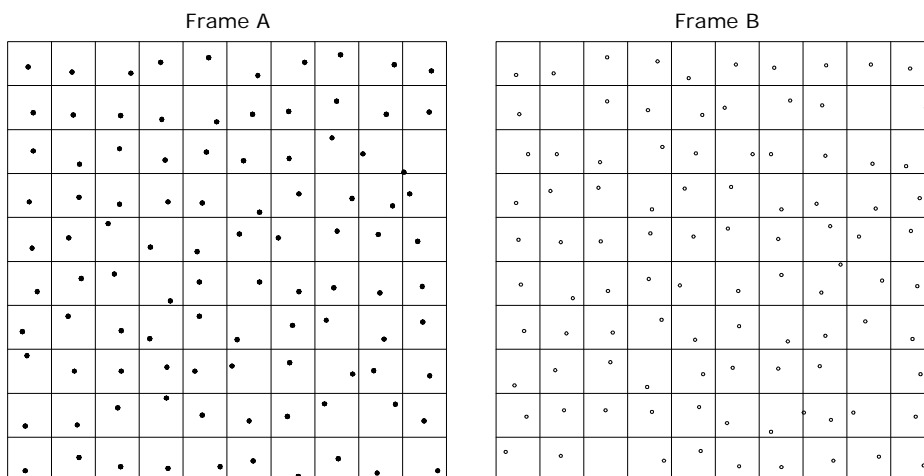
Figure 2-6 A pair of frame from PIV

Frame A and Frame B shown in Figure 2-6 are pictures of particles in flow at moment *t* and *t* + *dT*.

2.2.2 PIV system used in the measurement

The PIV system used in the measurement for velocity data acquisition is a 2D global velocimeter from the TSI Incorporated, which is called POWERVIEW™ 2-D PIV Systems. It includes:

 – LASERPULSE™ integrated dual Nd:YAG laser system. It produces laser pulse with a wavelength of 532nm. Laser energy is up to 120mJ per pulse. The maximum pulse frequency is 15Hz. Two units included in the system to produce the double pulses in very short time interval and keep the laser energy constant at a specific level. This allows PIV camera to capture image pairs continuously at a rate of 15 Hz while the camera operates at 30 frames per second.

 – LASERPULSE™ Synchronizer, which is controlled by computer to synchronize the operation of laser system and camera to capture appropriate images in correct time interval and sequence set in the PIV software Insight™ or triggered by external signal.

 – Beam Delivery and Light Sheet Systems delivers laser pulse from laser producers to sampling control volume and converts the laser beam to a flat and diverging light sheet. It consists of LASERPULSE™ Light Arm and Light Sheet Optics. Light sheet optics consists of a cylindrical lens and a spherical lens. The cylindrical lens diverges the incident laser beam in one direction, creating a flat sheet of light. The spherical lens controls the thickness of the sheet by focussing it in the direction normal to the sheet. The narrowest region, or "waist region", of the light sheet is typically centred on the control volume of the flow. The nominal thickness of the light sheet is normally less than 1 mm.

 – PIVCAM 10-30 Cross/Autocorrelation CCD Camera (1024 x 1024 pixels resolution and a frame rate of 30 frames/sec), using a "frame straddling" technique, captures two laser pulses on consecutive video frames. Image on the two frames are transferred to the host computer of PIV system at the full camera frame rate that is only limited by the physical memory of the computer. Images pairs are then analysed using cross correlation to compute a two-dimensional flow field. The correlation technique enables

vector field computation without directional ambiguity; no external image shifting hardware is needed. Image pairs can also be captured directly to the computer disk drive.

−   High-speed CCD camera interface, is used to transfer the images from the CCD camera to the computer. It is a high-speed digital frame, which offers 8-bit resolution, giving 256 grey scales to represent the captured image. It couples with the CCD camera and Synchronizer to transfer images to the host computer RAM at the full camera frame rate (i.e. 30 Mbytes/sec). It has a maximum data transfer rate of 90 Mbytes/sec, which ensures that no successive images are lost during data acquisition.

−   INSIGHT-NT, image capturing and analysing software of PIV system from TSI, controls the entire PIV system, from set-up, optimisation, and image acquisition to processing and presentation of the data. It controls the setup and operation of the Synchronizer during the measurement, to further control the laser system and camera. After power supply of laser is turned on, the software operates all others of the ongoing measurement.

−   The Insight comes with TecPlot from Amtec Engineering to visualize the data. Insight presents instantaneous and ensemble averaged PIV data in both 2-D and 3-D and data animation of instantaneous velocity fields. TecPlot can be used for further processing and presentation of the data.

−   Control PC runs the software Insight and operates the system.

Figure 2-7 shows the components of the PIV system.
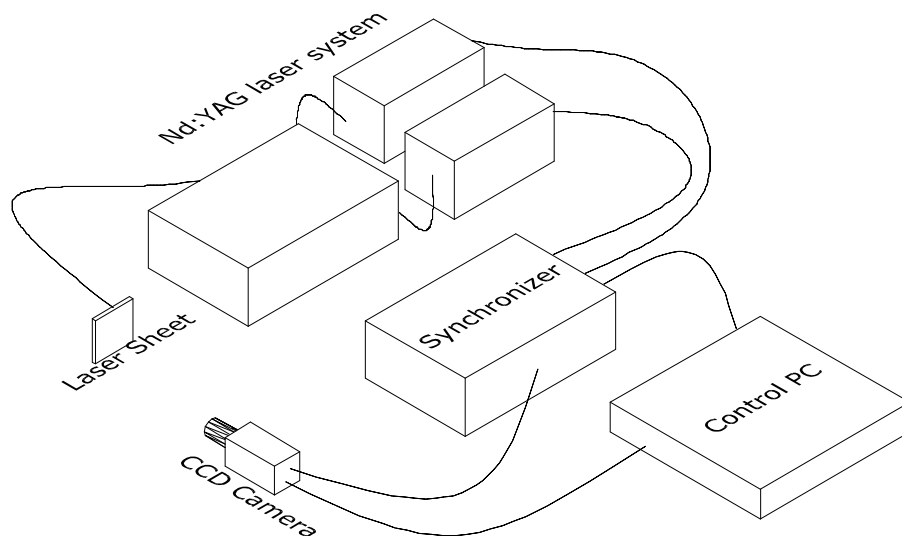
Figure 2-7 Schematic drawing of PIV system used

2.2.3 PIV measurement process

−   Seeding the flow
    When measuring with PIV, generally flow is seeded and seed particles are suspended in the fluid to trace the motion of the fluid and provide signal to the camera. The seeding used in the measurement for PIV was Metallic Coated Particles from TSI, Inc.

It was in shape of spherical, its density was 2.6 g/cm^3, its mean diameter was 12 µm, and geometric standard deviation was 1.6.

− Flow field illumination

The laser beam is produced by dual Nd:YAG laser system and transferred via Light Arm to a group of lenses, including a cylindrical lens and a spherical lens. The laser beam is reformed to a light sheet and is used to illuminate the flow.

When a thin slice of the flow field is illuminated by the light sheet, the illuminated seeding in the flow scatters the light. This is detected by the CCD camera placed at right angles to the light sheet. The light sheet is pulsed twice at a known interval in µs (*dT* in Figure 2-5). The flow is illuminated twice at the interval. Light is scattered twice by the seeding at the time interval.

− Image acquisition

The first pulse of the laser freezes an image of the initial positions of seeding particles onto the first frame of the camera (Frame A in Figure 2-6). The camera frame is advanced and the second frame of the camera is exposed to the light scattered by the particles from the second pulse of laser light (Frame B in Figure 2-6). There are thus two camera images, the first showing the initial positions of the seeding particles and the second their final positions due to the movement of the flow field in the time interval between two pulses.

− Vector processing

The two camera frames are then processed to find the velocity vector map of the flow field. This involves dividing the camera frames into small areas called interrogation regions (the grid in Figure 2-6). In each interrogation region, the displacement d_x and d_y of groups of particles between Frame A and Frame B are measured using correlation techniques (which are implemented using FFT algorithms). The 2D velocity vectors of u and w, of this area in the flow field are then calculated using the equations (2.4) and (2.5)

(2.4) $u = S \dfrac{d_x}{t}$ (main stream velocity)

(2.5) $w = S \dfrac{d_y}{t}$ (velocity normal to the main stream)

where S is the object to image scale factor between the camera's CCD chip and the measurement area. S is set in the software of PIV during the calibration by assigning the width and height of measuring area to the software. If suitable unit was used, the velocity u and w from PIV would be in the unit of *m/s*. If S were not set the PIV software, the software would give out the velocity in the unit of *pixels/s*.

The velocity vectors of all interrogation regions compose the velocity fields of the measuring area.

The vector field can be saved in a file with velocity vectors of u and w of each interrogation region and coordinates of the region. The vector fields can also be converted to a format that accessible to TecPlot for further processing and visualization.

− In the real measurement conducted, sequential vector fields were obtained for both oscillatory flow and stationary flow. The maximum number of sequence depended on the memory of the controlling PC. Normally about 200 pairs of picture could be obtained and saved in the PC RAM in one session with the PC used in the measurement, in which 512MB memory was installed.

− Phase average over periods was carried out later for oscillatory flow.

Refer to section 3.3 for the details of data processing of PIV data used in this project.

2.2.4 Results dependent factors

The PIV output was dependent on the following measuring conditions and parameters:

– Seeding quantity: enough seeding to get sufficient lights scattered and effective signals.

– The size of the control volume (in fact it was a thin slice): it was calibrated with the lens used and setting it in the software of PIV.

– The time delay between two laser pulses: this was adjusted according to the magnitude of the target velocity.

– Focus precision of the camera. A clear picture was essential to get an accurate result.

– The reflection of the laser light from the boundary wall. The amount of reflection had effects on both the measurement of boundary layer and adjacent area for reflected light could be scattered by the seeding in the flow outside of the laser sheet.

– Ambient light source besides laser beam was being as less as possible.

– The laser power level: was adjusted within the limit of the laser producer. It was not the higher the better.

– The dimension of the grid to the picture. It was adjusted from the software of PIV in data processing.

– Air bubbles in the flow had significant influence on the image captured.

– The alignment of camera and laser sheet to the target flow. The centre line of the camera must be normal to the laser sheet. The laser sheet must be parallel to the direction of the mainstream flow.

– Transparency of the flow was fatal to the measurement of PIV. The laser sheet had to go through the flow and illuminated the flow. The camera had to be able to see clearly through the flow or the scattered light from particles in the flow had to be seen clearly by the camera.

– Particles other than seeding exposed to the light sheet were captured by the camera and might produce errors in the analysis of velocity vectors.

2.3 The LDV System

Laser Doppler Velocimetry (LDV or LDA for Laser Doppler Anemometry) was used to measure the velocity at the second stage of the measurement. Due to the limitation of LDV system, it was not used in the final stage of the measurement. Part results from LDV measurement are shown in "Appendix B Other Measurements".

2.3.1 Introduction of LDV

Laser Doppler velocimetry is a technique that measures fluid velocity in high accuracy without disturbing the flow.

– Laser light illuminates the flow. Typically, the laser beam is divided into two beams and the focusing lens forces the two beams to intersect to form the measuring volume.

– Particles moving through the measuring volume scatter light of varying intensity, some of which are collected by a detector.

– The scattered light contains a Doppler shift to the source laser light, the Doppler frequency, which is proportional to the velocity component perpendicular to the bisector of the two laser beams.

- The signal conditioner and signal processing remove noise from the signal and extract the Doppler frequency and hence the velocity information.
- With a known wavelength of the laser light and a known angle between the intersecting beams, a conversion factor between the Doppler frequency and the velocity can be calculated.
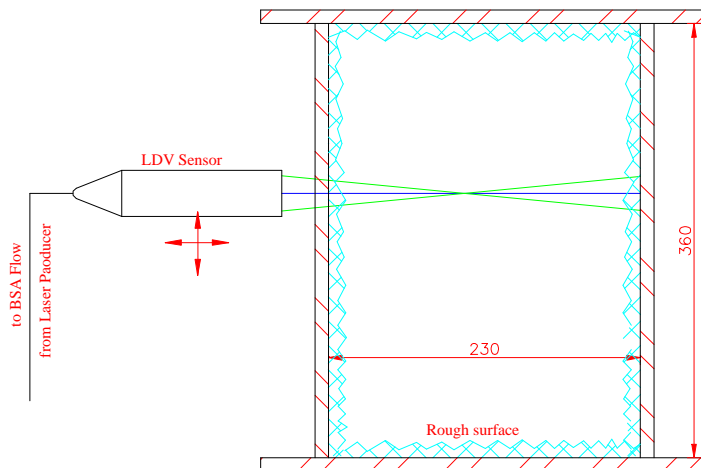
Figure 2-8 LDV measurement

- The addition of one or two more beam pairs of different wavelengths to the transmitting optics and one or two detectors and interference filters permits two or all three velocity components to be measured. A 2D LDV system was used in this measurement, as shown in Figure 2-8.
- The basic configuration gives the same output for opposite velocities of the same magnitude. In order to distinguish between positive and negative flow direction, frequency shift is employed. An acoustic-optical modulator in the transmitting optics introduces a fixed frequency difference between the two beams. The resulting output frequency is the Doppler frequency plus the frequency shift. This is important to the measurement of the oscillatory flow.
- Signal processors use correlation or FFT algorithms efficiently to determine the Doppler frequency from the noisy signals received from the detectors.
- The advantages of LDV over Particle Image Velocimetry (PIV) are the high spatial and temporal resolution.

2.3.2 LDV system used in the measurement

The LDV system used in this measurement was a one probe, 2D LDV (or LDA as it is called by the manufacture) from Dantec Dynamics A/S. The system includes:
- LDA signal processor - BSA F60
- BSA/FVA Flow Software v. 1.23.
- FiberFlow optical system.
- 3D Lightweight traverse systems
- Seeding particles for LDA

The LDV system had two laser beams in blue and green respectively. It measured two velocity components of oscillatory flow.

The traverse systems moved the probe in 3D. It was quite easy to move the probe across the tunnel flow and measured velocity profile continuously. The movement was controlled by the BSA/FVA Flow Software.

To get a relatively accurate result, big number of samples was needed for each measuring volume. This always caused problem in the application of the LDV system when trying to get the whole velocity profile across the tunnel in one continuous session. The PC crashed frequently before the end of the measurement and the measurement had to be repeated in most of the cases.

2.3.3 Results dependent parameters

Two types of parameters could have effects on the results of LDV measurement. One was the setting of the LDA system. The other was the environment condition.

1. Setting of LDA system, such as

    − Laser power level

    − Laser alignment and size of the control volume

    − Data rate and number of samples collected

    − Distance between adjacent measuring volumes. To get a good accuracy of measuring result and to cut the measuring time for each velocity profile, different steps were used in the different velocity area. In the mainstream area, bigger step was used, e.g. 5 mm. In the area near to the boundary, medium step was used, e.g. 1 mm. In the near wall boundary layer, smaller step was applied, e.g. 0. 5 mm.

    − Adjustable settings in LDA signal processor – BSA, such as values of record length, high voltage, signal gains and so on.

2. Test condition, such as

    − Seeding density, seeding type. The seeding used in the measurement was a special seeding for LDV from Dantec Dynamics A/S.

    − Refractory of different material on the laser way from probe to the measuring volume. The moving distance of Lightweight traverse systems was not equal to the displacement of the measurement volume all of the way crossing the test tunnel. Special calibration was carried out based on the effects of the refractory. Figure 2-9 shows the effects of the refractory. When the sensor moved a distance of d_1, the displacement of the control volumes was d_2. For the rig tested and the LDV system used, the ratio of d_1 and d_2 was about: $d_2/d_1 = 1.3529$.

    − Reflection from the tunnel wall, the nearer of the sampling volume to the boundary, the bigger of errors caused by the wall reflection of laser light.

    − Vibration of the tunnel wall under pressure transient, the nearer of the sampling volume to the boundary, the bigger of errors caused by the vibration of the tunnel wall.

2.3.4 Comparison of LDV and PIV measurement

According to the usage of PIV and LDV in the measurement, the author had the following notes of the difference between two velocimetry systems:

    − LDV got the 2D velocity of one point (control volume); PIV got the 2D velocity of all points in a plane.
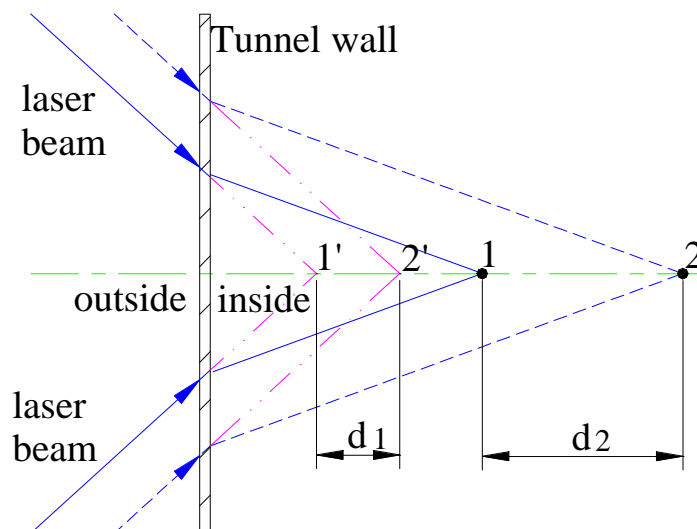
Figure 2-9 LDV Movement

- Control volume of LDV was a tiny cylinder and control volume of PIV was a thin plane.
- Accurate LDV measurement took very long time for turbulent flow. The result was a long time averaged value. PIV measurement always took quite short time to capture images. LDV measurement was not sensitive to the accidental noise (disturbance) but PIV measurement was quite sensitive to any noise.
- LDV data took reasonable disk space and physical memory of controlling PC during the measurement; PIV data needed large amount of disk space and physical memory during the measurement.
- Refractory was not a problem in PIV measurement; Refractory had to be taken into account in LDV measurement. LDV measurement was sensitive to the vibration of both the tunnel wall of the laser inlet window and the boundary wall near to the control volume in measuring of points near to the wall. PIV measurement was only sensitive to the vibration of the boundary wall near to the control volume in measuring of points near to the wall.
- LDV measurement was not so sensitive to the environmental light as the PIV measurement was.

2.4 Other Measuring Instrument

Besides the velocimetry systems used in the measurement, some other instruments were used in the measurement, to set up the data acquisition for other variables than velocity.

1. HP 34970A Data Acquisition/Switch Unit

Used to collect data from various sensors, excluding the velocity measurement. The software for communication between this unit and sensors, and for control of data acquisition was BenchLink Data Logger from HP.

HP 34970A Data Acquisition / Switch Unit setup a unique channel for each sensor input. It scanned all channels used with a constant time interval for input from the sensors. The time

series obtained from every sensor connected with HP 34970A Data Acquisition / Switch Unit was displayed on time and saved on disk by BenchLink Data Logger for later processing.

The scan rate of the unit was up to 250 channels/sec. However, it was difficult to use it at high frequency data sampling. One thing was the scan rate of the unit and the number of channels used. Another thing was the limit of the PC that ran the BenchLink Data Logger software.

```
                              ┌──────────┐
                              │   Flow   │
                              └──────────┘
        ┌────────────────────────┼────────────────────────┐
        ▼                        ▼                        ▼
 ┌──────────────┐        ┌──────────────┐        ┌──────────────────┐
 │ P Cells (6)  │        │ dP Cells (4) │        │ Flow rate meter  │
 └──────────────┘        └──────────────┘        └──────────────────┘
        └────────────────────────┼────────────────────────┘
                                 ▼
                     ┌────────────────────────┐
                     │   HP 34970A DA/SU       │
                     └────────────────────────┘
                                 ▼
                ┌───────────────────────────────────┐
                │   HP BenchLink Data Logger         │
                └───────────────────────────────────┘
        ┌───────────────┬──────────────┬───────────────┬───────────────┐
        ▼               ▼              ▼               ▼
 ┌──────────────┐ ┌──────────────┐ ┌──────────────┐ ┌────────────────────┐
 │  Waveform    │ │  Bar chart   │ │  Readings    │ │ Save data into file│
 └──────────────┘ └──────────────┘ └──────────────┘ └────────────────────┘
```
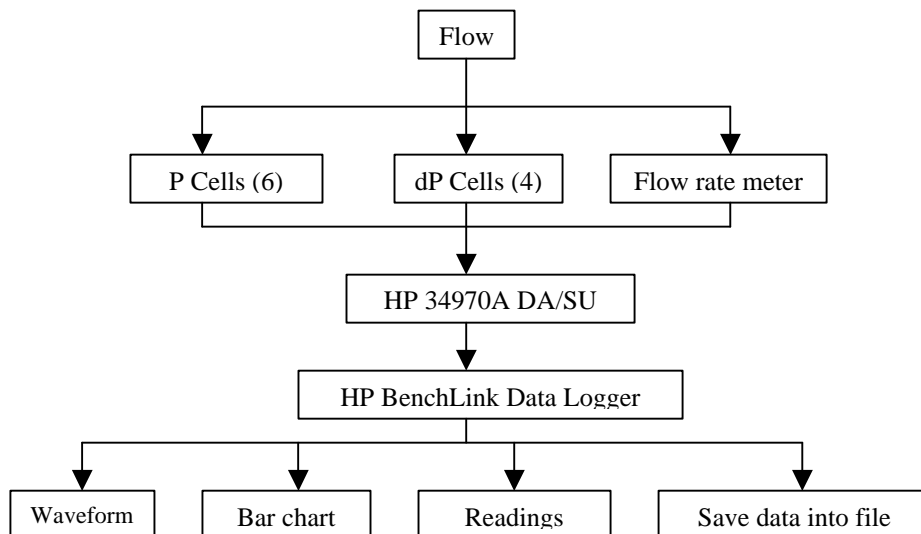
Figure 2-10 Data acquisition process of HP 34970A

The data acquisition process of HP 34970A DA/SU is shown in Figure 2-10. Settings of data acquisition with HP 34970A DA/SU included:

–   Created a setup before sampling, including set a unique channel for each sensor.
–   Calibration of each sensor, determine the gain and offset for each channel and sensor. This was only needed before the first run after the rig setup. It was not necessary to calibrate them before each measurement if there was not any significant change in the rig setup.
–   Set input signal range and conversion ratio. The signals from sensors were in the form of normalized voltage or current. They were converted into water column in meters (*mWC*) for pressure and differential pressure, and *l/s* for flow rate. Signal range and conversion ratio needed to be set before the first measurement after the rig setup. It was not necessary to set them before each measurement if there was not any significant change in the rig setup.
–   Set scan rate for each session. The value of scan rate was set according to the flow parameters, such as the frequency of oscillatory flow.
–   Set number of samples to collect in one session, or scanned continuously, or controlled the scan with time, or started and stopped scanning manually.

2.   Pressure sensors

Six pressure sensors were used in the measurement. Two of them (item 23 and 24 in Figure 2-2) were used to measure the cross sectional averaged pressure. The other four of them (item 19 to 22 in Figure 2-2) were used respectively to measure the wall point pressure along the test duct.

The detail arrangement of pressure sensors is listed in Table 2-1. The pressure sensors were installed approximately at the mid point of each test section.

Table 2-1 Pressure sensor arrangement

Tunnel Section No.	1	2	3	4	5	6
Pressure Cell	P1	dynP1	dynP2	dynP3	dynP4	P2
Type	Averaged	Wall	Wall	Wall	Wall	Averaged

The readings of all pressure sensors were scanned by HP 34970A DA/SU in a suitable sampling rate. Only readings of wall point pressure were collected by LabView virtual instrument PumpControl (discussed later).

The pressure cells were from IMT Industrie-Messtechnik GmBH with a measuring range of 0—1.6 bar. Output signal is 0 – 10V and input signal is DC 10 – 30V.

3.   Differential pressure sensors

The differential pressure sensors (dP cell) used in the measurement includes:
- The Model 3051 pressure transmitter from Fisher-Rosemount Systems (dP1 and dP2 in the measurement) with maximum water pressure as 138 bars. The output is DC 4-20mA signal with power supply of 10.5 – 55VDC. The measuring accuracy of these dP cells is 0.075%.
- Pressure transmitters FCX-AII series from Fuji Electric Instruments Co., Ltd (dP3 and dP4 in the measurement) with maximum water pressure as 32 bars. The output is DC 4-20mA signal with power supply of 28VDC.

The differential pressure sensors were deployed in the system as follows:
- dP1: from the mid point of Section 3 to the mid point of Section 6, distance in between was about: 9.14 m; (item 29 in Figure 2-2)
- dP2: from the mid point of Section 3 to the mid point of Section 5, distance in between was about: 6.09 m; (item 28 in Figure 2-2)
- dP3: from the mid point of Section 2 to the mid point of Section 4, distance in between was about: 6.08m ; (item 27 in Figure 2-2)
- dP4: from the mid point of Section 1 to the mid point of Section 2, distance in between was about: 3.01 m; (item 26 in Figure 2-2)

Only dP1 was used for all measurements. Other dP cells were only used for part of the measurements. Pressure transmitters FCX-AII could only get the differential pressure greater than zero. The negative differential pressure was treated as zero in the output of dP3 and dP4.

The readings of all dP sensors were scanned by HP 34970A DA/SU in a suitable sampling rate. Only readings of dP1 and dP2 were collected by LabView virtual instrument PumpControl (discussed later).

4.   Flow rate meter

A flow rate meter, MagMaster from ABB, was installed in the system (item 25 in Figure 2-2). It is an electromagnetic flow rate meter. It measures the mean flow rate output from the pump. It can measure flow rate from 0.236 l/s to 313.889 l/s with measuring accuracy as 0.15% and fluid pressure of 10 bars. The nominal diameter of the flow rate meter is 200 mm.

The flow rate meter used in the measurement could measure both forward and backward flow; display the flow rate in both directions, but it could only output the flow rate of forward flow to the data acquisition unit, with the existed configuration. For oscillatory flow, the output of the meter was zero when the flow was running backward (corresponding to the direction marked on the gauge).

The readings of the flow rate meter were scanned by both HP 34970A DA/SU and LabView virtual instrument PumpControl (discussed later).

5. Multifunction I/O board

PCI-6052E Multifunction I/O board from National Instrument (NI) was used for the interface between the LabView virtual instrument PumpControl (discussed later) and the hardware controlled, i.e., sensors and pumps. The board can stream to disk at rates up to 333 kS/s. The PumpControl can collect sample at quite high rate without significant losses. Two output lines of the board were used to control the two pumps and 7 input lines were used to collect data from flow rate meter, pressure sensors (4) and differential sensors (2).

6. SCB-68 quick linker

The SCB-68 from National Instrument (NI) is a shielded I/O connector block for interfacing I/O signals to plug-in DAQ devices with 68-pin connectors. It was the connector between PCI-6052E Multifunction I/O board and MICROMASTER frequency inverter in the rig setup.

7. MICROMASTER frequency inverters

Two microprocessor controlled frequency inverters MICROMASTER from SIMENS were used to control the rotation speed of the pumps, which were driven by three phases AC motors. The input of MICROMASTER came from PumpControl VI via PCI-6052E Multifunction I/O and SCB-68 quick linker. The output of MICROMASTER was send to the motor of the pump to control the rotating speed of the pumps and further the flow rate in the system.

8. Pumps

Two PP-pump 4640 from the ITT Flygt AB (item 2 and 3 in Figure 2-2) were used to build the flow finally. They were controlled by PumpControl VI via PCI-6052E Multifunction I/O, SCB-68 quick linker and MICROMASTER frequency inverter. The output of one pump could be up to 300 l/s with head of 0.3 m and about 75 l/s with head of 1.0 m. The horizontally centre line of the pump was close to the horizontally centre line of the test tunnel.

One pump was installed at each end of the water-running loop, i.e., they were installed as standing back to back. Each pump was controlled by one MICROMASTER frequency inverter. Two pumps were always running at the same speed and in the same direction so that one pumped water out of the tank and the other sucked in the same amount of water to the tank at the same time and theoretically there was not water level surging in the tank.

Refer to the Figure 3-2 for the pump locations in the water tank.

The function relation of instruments mentioned above is shown in Figure 2-11.

2.5 Oscillatory Flow Control

The flow running in the test tunnel was produced and controlled by a LabView Virtual Instrument (VI) PumpControl. The VI functioned for data acquisition at the same time.

2.5.1 Pump control virtual instrument

As described in the last section of the previous chapter, the pumps were controlled by the PumpControl VI to produce the required flow regime. The main functions of PumpControl VI were:

–   control the rotating direction and speed of the pumps to produce various flow regime
–   display the waveform of pump speed
–   send trigger signal to velocimetry system

- collect data from differential pressure sensors, pressure sensors and flow rate meter
- display the readings or waveform of the samples from the sensors mentioned above
- save the data collected into specified file.

The procedure of the pump control and DAQ is shown in Figure 2-11.

- for the meaning of Q_0, q and f_r, refer to sub-chapter 2.5.2.
- for the hardware shown in the chart, refer to sub-chapter 2.4.
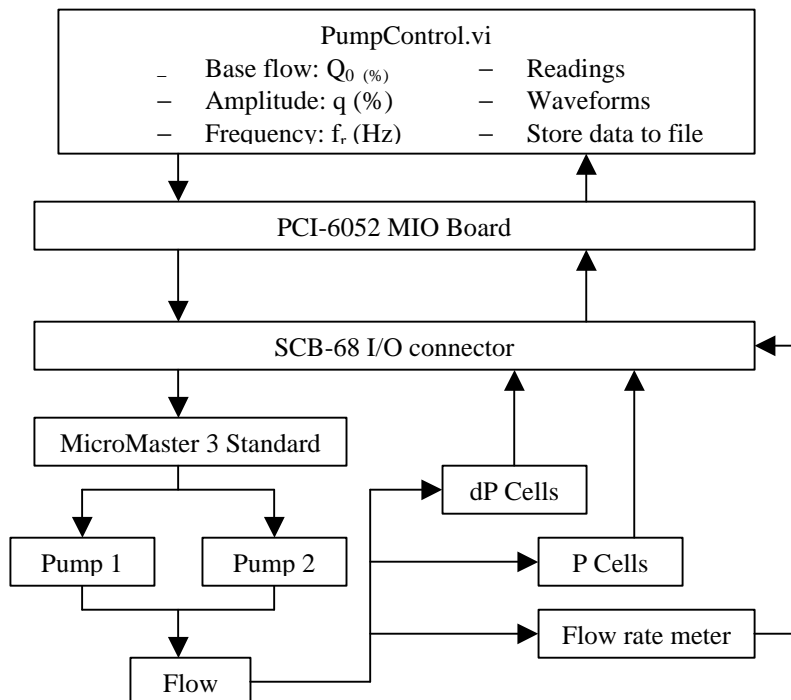
Figure 2-11 Flow control and DAQ of PumpControl

2.5.2 Flow regimes

Based on the intrinsic function of LabView, PumpControl could produce different harmonic waves, including sine, saw, square and so on. For a specific wave, there was several parameters could be controlled: the base flow (stationary part), amplitude and frequency of the oscillation. The two pumps could run synchronously in the same direction or reverse direction, with or without phase difference. Various flow regimes could be produced in the test tunnel, even the very complicate waveform, if only it could be expressed by a suitable equation. Generally the flow regime could be build up in the tunnel with the VI if the flow regime could be expressed explicitly in a form of superposition of harmonic waves.

All flow regimes tested could be treated as the superposition of a stationary part and an oscillatory part. There were three characteristic parameters to specify the flow regime:

- stationary base flow Q_0 (%), $Q_0 \geq 0$.
- oscillatory amplitude q (%) of the oscillatory part, $q \geq 0$
- oscillatory frequency f_r (Hz) of the oscillatory part, $f_r = 2p w$, w is the angular frequency of the oscillatory flow.

The parameters were controlled through the rotation speed and direction of water supply pumps. Both the stationary base flow Q_0 and oscillatory amplitude q were in percentage of the pump rotating speed at full load (Figure 2-12).

Based on the different value range of q and Q_0, the flows were classified in following ways (this is an extension and specified description of the definitions mentioned in Chapter 1):

- *Stationary flow* (SF): the amplitude of oscillatory flow $q = 0$; base flow Q_0 **¹** 0.
- *Pure Oscillatory flow* (POF): the amplitude of oscillatory flow q **¹** 0 and oscillatory frequency f_r **¹** 0; base flow $Q_0 = 0$.
- *Combined oscillatory flow* (COF): all three parameters were not equal to zero, i.e., Q_0 **¹** 0 and q **¹** 0 and f_r **¹** 0.
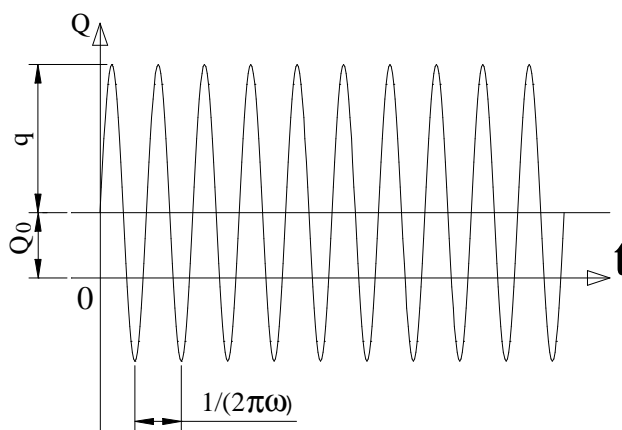
Figure 2-12 Schematic of the flow regime

The COF was further divided into sub-group:

- *Oscillatory dominant flow* (ODF): the oscillatory amplitude of flow was 20% or more higher than base flow, i.e., $q = Q_0 + 20\%$.
- *Stationary dominant flow* (SDF): the oscillatory amplitude of flow was 20% or more lower than base flow, i.e., $q = Q_0 - 20\%$.
- *Balanced flow* (BF): the amplitude of oscillating flow was equal to that of the base flow or with difference in between less than 20%, i.e., $Q_0 - 20\% < q < Q_0 + 20\%$.
- *Other oscillatory flow* (OOF): oscillatory flow not falling in any group mentioned above.

It ought to be noted that in all cases, $Q_0 + q$ **£** 100%.
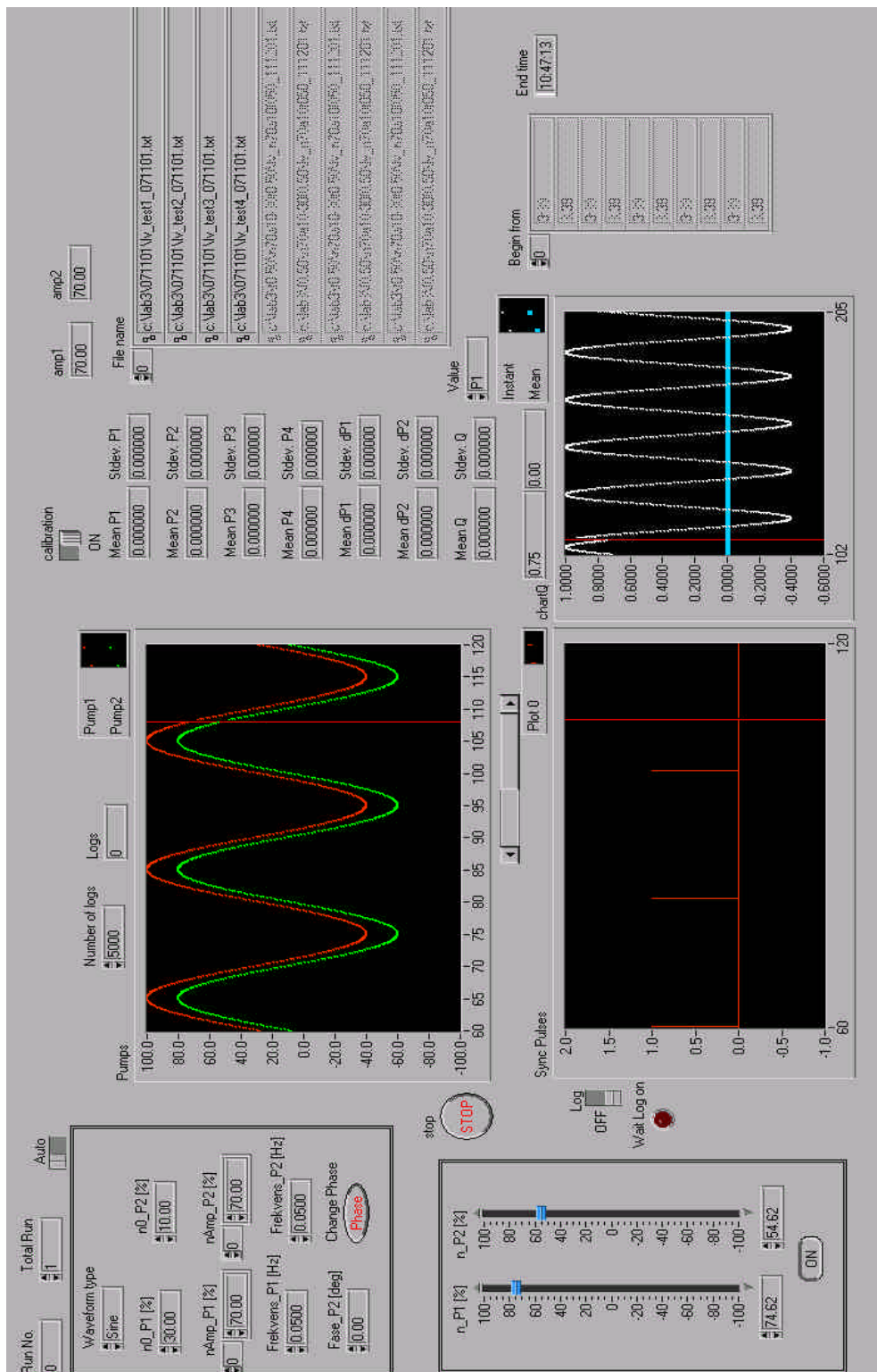
Figure 2-13 Snapshot of the front panel of PumpControl

Chapter 3

Measurement and Data Processing

Main topics of this chapter:

- Description of measurement
- Data processing
- Overview of measured flow regimes
- Examples of data collected

3.1 Measurement

3.1.1 Calibration

Calibration included *initial calibration* and *daily calibration*. The former was carried out before the first measurement after the rig setup and when there was any significant change to the setup. The latter was carried out everyday before the daily measurement.

1. Initial calibration was carried out before any practical measurement:
    - Flow rate meter calibration for the offset and gain factor;
    - Pressure sensors calibration for the offsets and gain factors;
    - Differential pressure sensors calibration for the offsets and gain factors (measuring range, unit, output and so on);
    - Velocimetry calibration, for the PIV mainly included (after the setup of the hardware including the alignment of the laser beam): image to object ratio, light power level, time interval between pulses, camera focus length, camera aperture, camera alignment to the control volume etc.

   Generally, the gain of sensors did not change significantly in the test period; the sensors were not recalibrated for gain factors and offsets after the initial calibration.

2. Daily calibration

   Daily calibration was conducted when the water was still, normally before the first start-up of the pumps.
   - Zero reset of differential sensors (zero trim)
   - Zero reset of pressure sensors
   - Zero reset of flow rate meter

   The above calibrations were carried out from both the PumpControl VI and HP BenchLink Data Logger at the same time.

Sometimes there was air encompassed and accumulated at the top of the tunnel, it was released before the daily calibration.

3.1.2 Measuring procedure

Set the PumpControl VI (refer to Chapter 2.5 for the description of this VI) to run in "manual" mode and started the pump after the daily calibration. First set the pump speed to medium level and ran the flow in steady state for some minutes so that the seeding for PIV measurement were mixed with the water sufficiently and the water temperature were distributed evenly. Then set the PumpControl VI to run in "auto" mode with suitable parameter settings to build the flow regime to measure:

- Set the number of logs (samples to collect).
- Set the sampling rate (setup it in the diagram of the PumpControl VI).
- For stationary flow measurement, set the frequency to zero, set the base flow Q_0 to a specific value, and ran.
- For oscillatory flow, set the base flow Q_0, oscillatory amplitude q, oscillatory frequency f_r, and ran.

The following measurements were carried out after flow was build:

1. Velocity measurement with PIV

    - Powered on all hardware of PIV system (Laser producer and the synchronizer were turned on respectively).
    - Started the laser beam (set it to minimum laser level and pressed the "Start" button on the control panel, set it to maximum laser level after start up)
    - Opened Insight and setup an experiment (laser power levels, velocity grid, pulses interval, capture mode, number of pictures taken in sequence and so on)
    - Taking pictures with CCD camera, controlled by Insight via synchronizer.
    - Vectoring the flow picture to produce VEC file (coulf process later by self made special code after the measurement)
    - Created TecPlot files (could be created later after the measurement)
    - Data processing (refer to section 3.3 on page 38 for more details)

2. DAQ with HP BenchLink Data Logger

    - Created setup for the measuring session
    - Setup the data acquisition related parameters (scanning rate, number of samples, number of channels to scan etc.)
    - Scanned the sensors, displayed the readings and waveform for monitoring the measurement
    - Saved and exported the data (format could be defined before save and export)

3. DAQ with LabView VI PumpControl

    - The number of logs (samples) to collect and the sampling rate were set before building the flow regime.
    - The readings and waveforms from different sensors could be viewed on time from the moment when the VI started.
    - Started to log data after all other measurement finished or controlled by time (using the computer time).
    - The VI stopped automatically after the sampling finished and data saved.

```
┌─────────────────────────────────────────────┐
│            Initial calibration               │
│     (Run once after the rig was setup)       │
└─────────────────────────────────────────────┘
                      │
                      ▼
┌─────────────────────────────────────────────┐
│             Daily calibration                │
│  (Run daily before the first start of the    │
│                 pump)                         │
└─────────────────────────────────────────────┘
                      │
                      ▼
┌─────────────────────────────────────────────┐
│  Run stationary flow in medium flow rate to  │
│                 mix flow                      │
└─────────────────────────────────────────────┘
                      │
                      ▼
        ┌───────────────────────────┐
        │    Build test flow regime  │
        └───────────────────────────┘
            │                   │
            ▼                   ▼
┌───────────────────────┐  ┌───────────────────────┐
│  Velocity measueremnt │  │   DAQ by Data Logger  │
└───────────────────────┘  └───────────────────────┘
                      │
                      ▼
        ┌───────────────────────────┐
        │     DAQ by PumpControl     │
        └───────────────────────────┘
                      │
                      ▼
        ┌───────────────────────────┐
        │      Data Processing       │
        └───────────────────────────┘
```
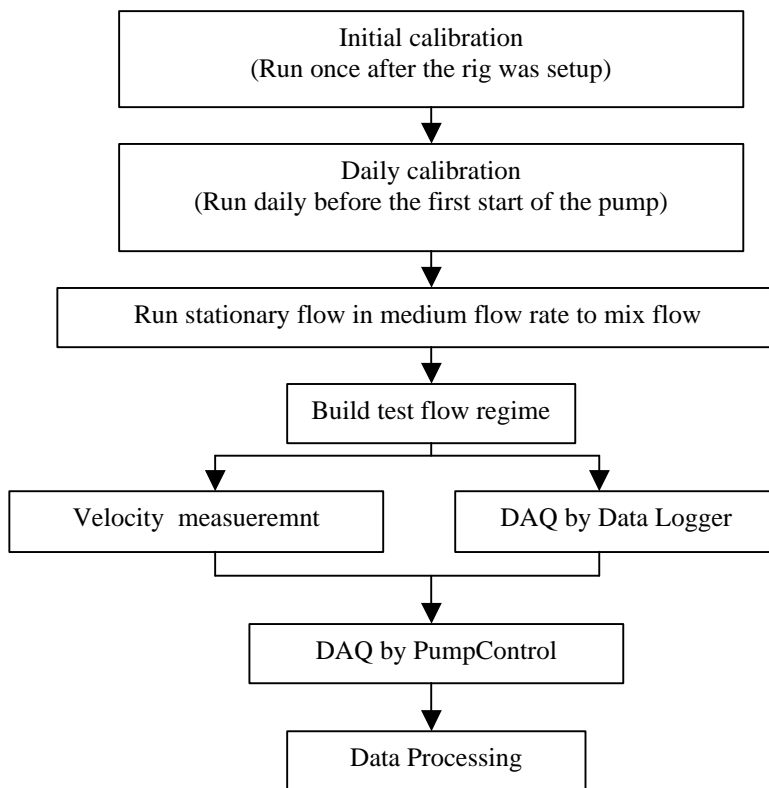
Figure 3-1 Measuring procedure

The general measuring procedure is shown in Figure 3-1.

The measurement could be carried out in the mode of measuring one flow regime in one session or measuring multiple flow regimes in one session. The parameters and data files related were updated automatically according to the configuration before the starting up of the virtual instrument if ran the experiment in the latter mode. Be sure that no air was accumulated at the top of the tunnel during the measurement if ran the test in the mode of measuring multiple flow regimes in one session.

3.1.3 Example of measurement notes

Measurement notes recorded the basic information of each measuring session, including the flow regime parameters, data acquisition settings, file names for the data collected, and special things happened during the session, if there were any. Following is an example of this.

Measurement notes of oscillatory flow with $f_r = 0.01$Hz; $n_0 = 70\%$; $amp = 10\%$ -- 30%

Timestamp: measurement carried out on 2001-12-05 11:00—11:40 AM

Table 3-1 Information of Sampling

	PIV	LV PumpControl	HP Logger	Remarks
Sampling Rate (Hz)	0.25	10	2	
Number of samples	125	5000	1000	

Table 3-2 Information of file names

Amp (%)	PIV Exp.	LV PumpControl	HP Logger Export	HP Logger Data
10	n70a10f001_a	lv_ n70a10f001_051201.txt	hp_ n70a10f001_051201.csv	Data 12/05/101 11:08:44
20	n70a20f001_a	lv_ n70a20f001_051201.txt	hp_ n70a20f001_051201.csv	Data 12/05/101 11:23:07
30	n70a30f001_a	lv_ n70a30f001_051201.txt	hp_ n70a30f001_051201.csv	Data 12/05/101 11:36:06

Table 3-3 Pressure bottom flat and flow rate top flat

Amp (%)	P1 & P6	dynP1 to dynP4	Q
10	Yes	No	No
20	Yes	Yes	Yes
30	Yes	Yes	Yes

Table 3-4 Air at the top points

Amp (%)	Points	Amount	
10	P2, P4 to P6	A little	Released before next test
20	P2, P4 to P6	"	"
30	P2, P5 to P6	A little	Released before next test

Other notes:

− The measurement was tried for the 1st time on 2001-12-04. Bottom flat in pressure curves from pressure cells was found. The reason was that the pressure at the point around maximum flow rate was lower than the atmospheric pressure, i.e. lower than "zero". Test was stopped on 2001-12-04.

− Water was added to the tank to increase the level of water, to increase the absolute head along the tunnel, in order to get rid of the bottom flat mentioned above. Actually the lowest pressure was still smaller than "zero" when amplitude was bigger, refer to the results got on 2001-12-05 when the test was carried out again.

− To solve this problem, absolute pressure sensor could be used, instead of the relative pressure sensor used in the measurement.

3.1.4 Problems and maintenance of the system

The measurement had been continued for a quite long period of time. Some problems occurred during the measurement. Most of them were related to the rig setup as described in the following pages.

1.   Looseness and disintegration of the honey comb

To even the flow at the inlet of the model tunnel, a honeycomb was build in the connection tube (Item 7 in Figure 2-2 Test rig layout) in front of the inlet of the test tunnel. The honeycomb was made by gluing several plastic tubes with smaller diameter together first. The whole honeycomb (grouped tubes) was glued to the connection tube later. First one or two small pipes loosed off the assembly after long time running of the rig with oscillatory flow, sometimes with quite high flow velocity and oscillatory frequency. Then the whole honeycomb disintegrated. The loosed pipe from the honeycomb wandered in the connection pipes for some time (could be weeks) and popped out from the gap between blades of the pump. Some of them popped out without disturbing the running pump significantly. Some of them blocked the high speed rotating blades and pump was stopped. The disintegration of the honeycomb resulted in:

- The flow was not consistent at the different stage of measurement. This was confirmed by the flow rate data. Special effort was made in the data processing to get rid of the influence.
- Stop of the pump. Measurements related had to be repeated. The bad thing was the flow regimes stopped were mainly those with strong vibration and noise, those that ran with more risk to endanger the rig, including causing heavy leakage.
- Verify measurement had to be carried out each time when there was a small pipe came out from the honeycomb, no matter the pump was stopped or not.
- Broken of the flow guiding blades at the outlet side of pump 1 (discussed more later).
- Must contribute to the translocation of one pump (discussed more later).

2. Fractured of the flow guiding blade

Between one pump and the connection pipe, guide blades were installed to improve flow condition. The guide blades were made of Plexiglas. All of the blades were broken at the second time of the loosen tubes of the honeycomb popping out from the pump. The test was run without guide blades afterwards.

The location of the guide blades was shown in Figure 3-2.

3. Translocation of one pump

The pump was aligned with the connection pipe in the same horizontal centre line. Once upon a time, one pump removed from its installed position and turned 90 degrees and faced to the sidewall of the water tank. As shown in Figure 3-2, the pump 2 was installed in the position shown in solid lines. In the accident, pump 2 turned to the position shown in dash lines.
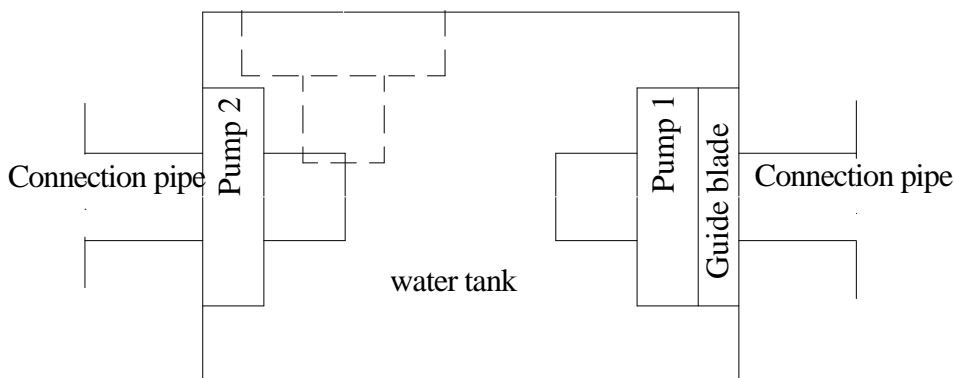

Figure 3-2 Pump position before and after translocation

4. Deformation of the inner rough layer

The inner rough layer was made by gluing sand on Plexiglas plate with a thickness of 5 mm. The Plexiglas plate would absorb 2-5% water of its volume if it stayed in the water for enough time. The water would evaporate if the plate was taken out of the water and dry up. This would cause the change of dimensions of the plate to certain extent. When the plate was inserted into the tunnel for the first time, its dimension was set to just fit to the space inside the tunnel and fixed very well to the tunnel wall. It deformed a lot after the tunnel was filled with water for some days. The inner layer was not attached very well to the tunnel wall and longitude waviness of the plate was observed, especially after the tunnel was drained off the water again. Two measures were taken to fix this:

33

- Cut the plate to a minor smaller size so that when it expended again it could fit to the space in the tunnel better, at least without visible longitude waviness.
- More fasten screws added to fix it more tightly to the tunnel wall.

Big headaches were experienced during the reinstallation of the reformed inner rough layer.

- It was very difficult to let the plate adhere to the wall sufficiently without support from the inside. Support was not easy for the great section length and small cross section of the test tunnel. Also the sand glued on the plate ought to be protected from any damages during the installation.
- The original screw hole on the inner plate did not fit well to the hole on the wall of the tunnel during reinstallation. Sometimes bigger holes were drilled on the wall to fit the hole on the inner plate. Sometimes bigger screws were used to replace the smaller one for the hole on the inner plate had to be enlarged. Sometimes new holes were added and old holes were blocked.

Only this reinstallation took 2-3 days of 2–3 technicians every time. Multiple reinstallations were conducted due to the modification of the rig or fix of the leakage.

5. Leakage

The leakage happened mainly at the screw holes for fastening of inner rough layer to the tunnel wall, though silicon was used to seal the screw holes. It was hard to fasten the screw very tight once. Most of the screws had to be tightened again after water was filled to the tunnel for sometime. The reasons were:

- The length of thread in the inner rough layer was very short, only 2-3 mm, the Plexiglas used was quite brittle and the surface was broken a little when began drilling hole on one side and when drilled through the other side.
- The screw length was limited by the thickness of the inner rough layer, the screw could not pop out of the inner layer and disturb the flow in tunnel, any minor disturb ought to be avoided.
- If too much strength were applied when fasten the screw, the thread would be destroyed or the inner rough layer would break. This happened at several points. If big leakage happened measures had to be taken to fix it.

The leakage did not happened at the connections of tunnel sections, though the connecting screws needed fastening again after water was filled and sometime later.

6. Encompassed air

Encompassed air in the flow, if existed, would cause significant errors in the result. Encompassed air was found in following cases.

- After water was filled into the tunnel, there was air accumulated at the top points of the tunnel due to temperature and pressure change of the water. It was always necessary to run the pump for 3—5 days to get rid of the air in the tunnel each time after the test tunnel was refilled with fresh water. The air could be released from the check valve next to the pressure sensor at each section of the tunnel if it was accumulated into the tubes for the pressure sensor. After most of the air was released the left air was encompassed at the top point of the tunnel where there was not any release outlet and located away from any check valve for pressure sensor. The left air could be released by running the flow in very high speed and the air will be brought to the tank and released at the open surface. However air could be sucked in from the connection point or screw hole when the flow velocity was high enough and the pressure inside the tunnel was lower than atmosphere pressure.

 − During the measurement, air could be accumulated again at the top of tunnel, especially when ran the flow at high velocity. If the pressure was too low in the tunnel, the air could be sucked into the tunnel from section connections and screw holes, especially the one with minor leakage. Water level in the tank could be increased to avoid too low pressure in the tunnel at high flow velocity if the leakage was under control.

7. Reflection of laser from the boundary

The power of laser was quite strong and the Plexiglas reflected a lot of the laser beam, no matter for LDV or for PIV, though grey paint was used to make the sand roughness darker and the inner rough layer was opaque to normal light.
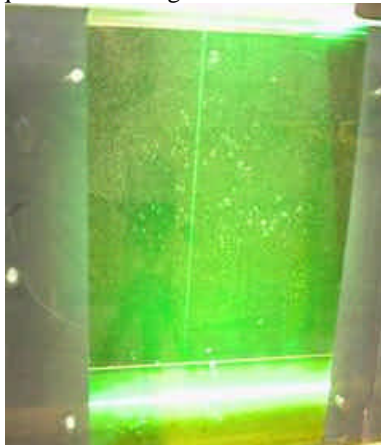
Figure 3-3 Laser sheet of PIV

Figure 3-3 shows the reflection of PIV laser sheet from the bottom of the tunnel. This reflection resulted in that it was difficult for the PIV camera to see clearly what happened in the near wall boundary layer, which was very important to the analysis of the shear stress of the flow.

In all of the results from PIV and some results from LDV, information of near wall boundary layer was not displayed.

8. Vibration of the test tunnel

When the flow was oscillating in the tunnel with high frequency, such as f_r was bigger than 0.5 Hz, or with greater amplitude, e.g., q was greater than 50%, visible vibration was observed on the tunnel wall. When the oscillatory amplitude was big enough and oscillatory frequency was low, the sidewall of tunnel bended forth and back in the same frequency as the flow inside. The length of each section of tunnel was 3 meters and there were 2 enforcement plates on the side of the wall. This limited the bend effect to some extent. But it was still visible in some cases of measurements.

3.2 Overview of Measurements

Part of the flow regimes tested is listed in Figure 3-4. The flow can be classified as two main groups: steady flow and oscillatory flow.

3.2.1 Steady flow

Steady flow was tested for the purposes of comparison and analysis. The key parameter of steady flow was the mean flow rate, which was controlled by the rotating speed of the water supplying pumps in the rig. The minimum mean flow rate tested was about 7.6 l/s, i.e., the mean velocity of mainstream was about 0.1 m/s. The maximum mean flow rate tested was about 120 l/s, i.e., the mean velocity of mainstream was about 1.6 m/s. The Reynolds numbers was ranged from 25561 to 416646 (Ref. to Appendix A.4 Reynolds number of flow tested on page 150). The flow was always turbulent flow.

For each flow rate of stationary flow, about 2000 samples were collected from each of the differential pressure sensors, pressure sensors, and flow rate meter. The sampling rate for LabView VI PumpControl was 10 Hz and for HP DAU was about 1 Hz to 2Hz.

Velocity pictures were captured with PIV system in a sampling rate of about 1 Hz. 50 pairs of picture were taken for each flow regime. The time interval between two laser pulses was 2000 µs. The area of the PIV picture was 195 mm * 193 mm.

In different stages of the measurement, steady flow measurements were conducted repeatedly to verify the status of the whole system.

3.2.2 Oscillatory flow

There were three characteristic parameters to specify the flow regime of oscillatory flow:

   − the stationary base flow Q_0 (%), or the bulk flow part.
   − the frequency f_r (Hz) of the oscillatory part
   − the oscillatory amplitude q (%) of the oscillatory part

Here both the stationary base flow Q_0 and oscillatory amplitude q were in percentage of the pump rotating speed at full load. All three parameters were controlled through a LabView VI PumpControl (refer to section 2.5 for details).

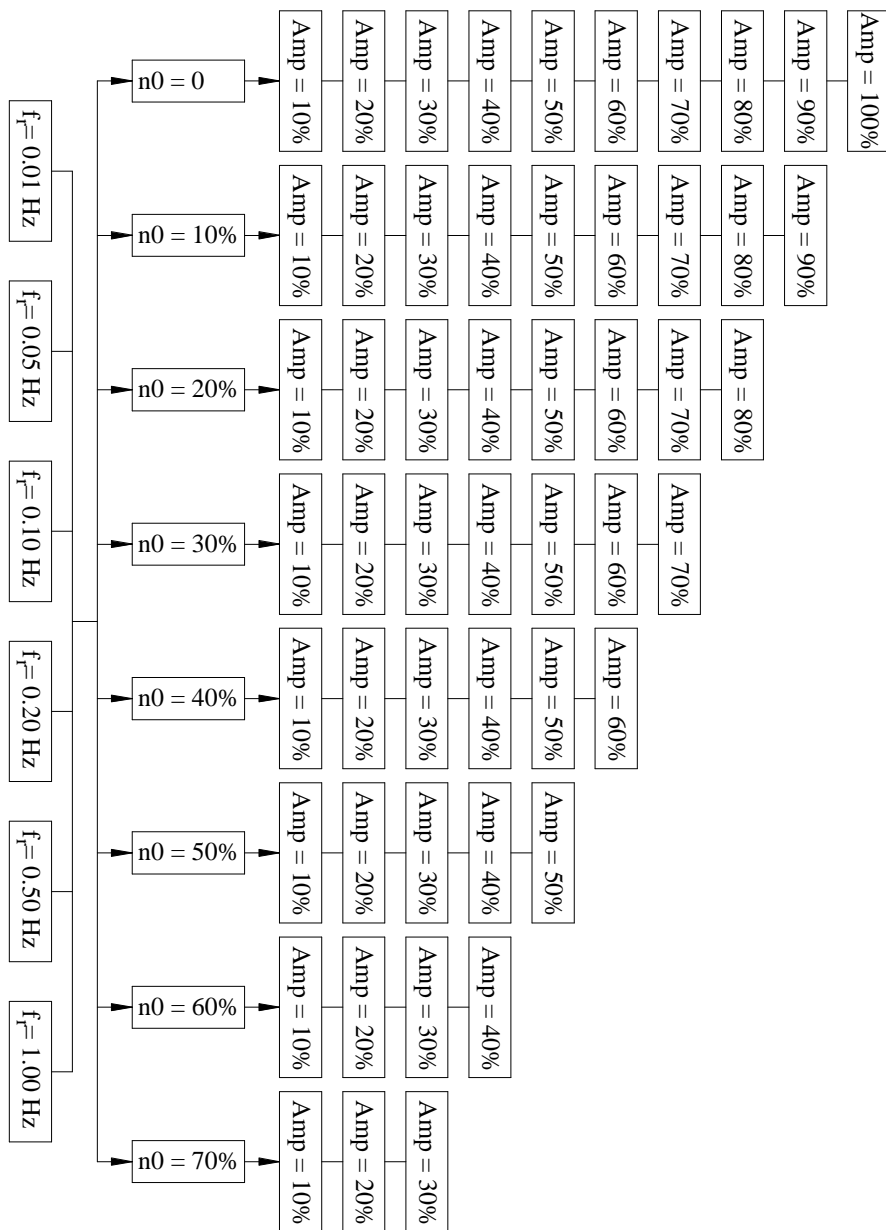In the measurement of oscillatory flow, the value ranges of the three parameters were:

   − stationary base flow Q_0 varied from 10% to 70% of full pump load
   − the frequency f_r varied from 0.01 Hz to 1.00 Hz
   − the amplitude q varied from 10% to 100% of the full pump load
   − the sum of the stationary base flow Q_0 and amplitude q was always smaller than or equal to 100%, i.e., $q + Q_0 = 100\%$

Totally there were about 260 flow regimes tested for oscillatory flow. More than 300 flow regimes were tested totally if taking into account of the stationary flow.

The detail parameters of all flow regimes tested for oscillatory flow are listed in Figure 3-4.

For each flow regime, about 5000 samples were collected from each of the differential pressure sensors, pressure sensors and flow rate meter. The sampling rates were 10 Hz (for frequency f_r from 0.01 to 0.20 Hz) and 50 Hz (for frequency f_r = 0.50Hz) for LabView PumpControl VI and 1 Hz to 10 Hz for HP DAU.

Velocity profiles of the flow were captured with PIV system in a sampling rate from 1 Hz to 15 Hz for different flows. The time interval between two laser pulses ranged from 500 µs to 3000 µs. Due to the limitation of storage capability of the PC for PIV, the number of samples varied from 100 to 150. The area of the PIV picture was 195 mm * 193 mm.

36

f_r = 0.01 Hz
f_r = 0.05 Hz
f_r = 0.10 Hz
f_r = 0.20 Hz
f_r = 0.50 Hz
f_r = 1.00 Hz

n0 = 0 → Amp = 10% | Amp = 20% | Amp = 30% | Amp = 40% | Amp = 50% | Amp = 60% | Amp = 70% | Amp = 80% | Amp = 90% | Amp = 100%

n0 = 10% → Amp = 10% | Amp = 20% | Amp = 30% | Amp = 40% | Amp = 50% | Amp = 60% | Amp = 70% | Amp = 80% | Amp = 90%

n0 = 20% → Amp = 10% | Amp = 20% | Amp = 30% | Amp = 40% | Amp = 50% | Amp = 60% | Amp = 70% | Amp = 80%

n0 = 30% → Amp = 10% | Amp = 20% | Amp = 30% | Amp = 40% | Amp = 50% | Amp = 60% | Amp = 70%

n0 = 40% → Amp = 10% | Amp = 20% | Amp = 30% | Amp = 40% | Amp = 50% | Amp = 60%

n0 = 50% → Amp = 10% | Amp = 20% | Amp = 30% | Amp = 40% | Amp = 50%

n0 = 60% → Amp = 10% | Amp = 20% | Amp = 30% | Amp = 40%

n0 = 70% → Amp = 10% | Amp = 20% | Amp = 30%

Data collected:

Velocity by velocimetry

dP1, dP2, dynP1, dynP2, dynP3, dynP4, P1, P6, Q

Figure 3-4 List of tests

3.3 Data Processing

The data processing included

- *the velocity data processing*: including PIV data processing, LDV data processing, ADV data processing. Only PIV data processing is described below.
- *the head loss data processing*: processed the data from all of the differential pressure sensors.
- *other data processing*: including processing of the data from all pressure sensors and flow rate meter.

3.3.1 Process PIV data

PIV data processing was carried out in three steps:
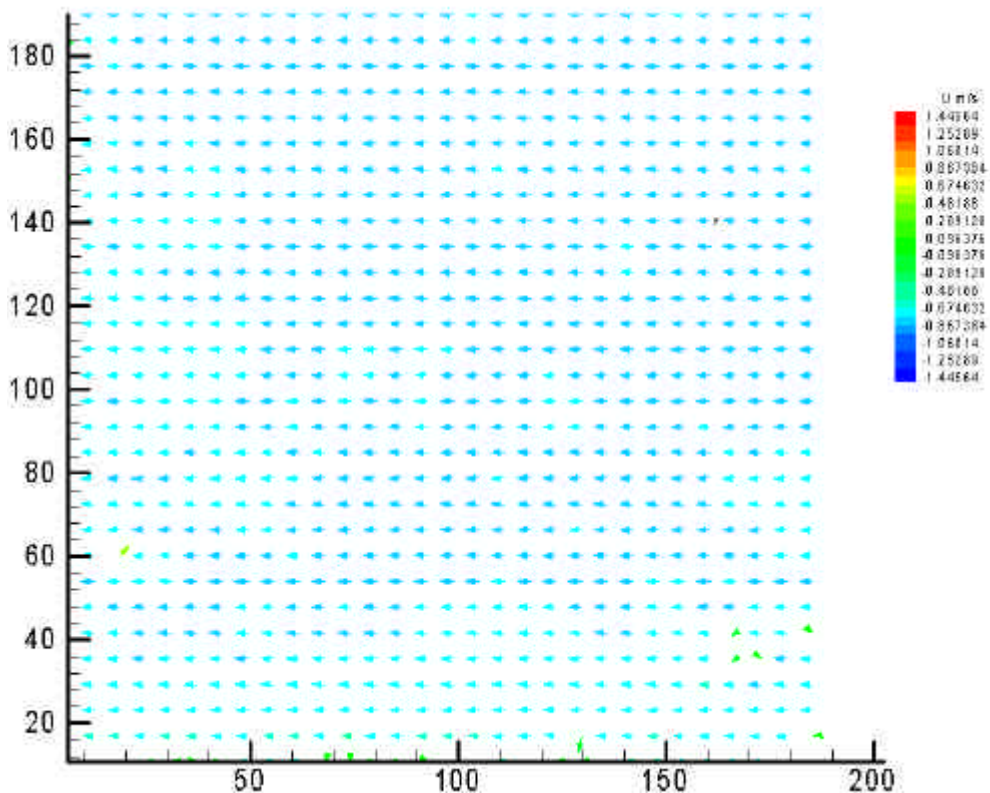
Figure 3-5 Example of vector fields from TecPlot

- *Preliminary processing*, which could only be handled by the software with PIV system, i.e., Insight from TSI in the measurement. The main purpose of this processing was to extract the velocity from the pictures taken for the flow studied, and prepare for the further processing and analysis.
- *Intermediate processing* which was implemented in commercial software TecPlot from AMTEC. Insight of PIV could export the velocity data into a format that was accessible to TecPlot. TecPlot features visualizing the velocity vector field in 2D and 3D and exporting velocity figures in various formats and data of velocity field. Figure 3-5 is an example of vector fields exported from TecPlot.

   −   *Final processing,* which was conducted with special code made only for this thesis work. It used the PIV velocity directly and built the profile of velocity and carried out other analysis needed in this thesis.

Figure 3-6 shows the processing of PIV data in flow chart.
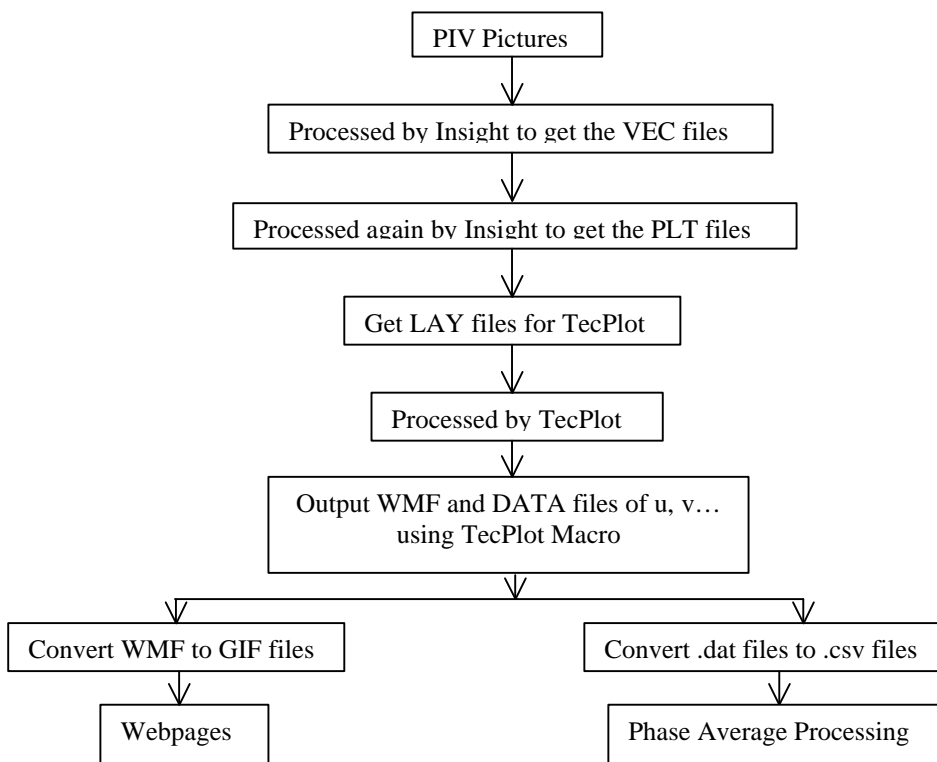
Figure 3-6 Flow chart of PIV data processing

To deal with the large amount of measured results from PIV, a TecPlot macro was made to process the PIV data in automatic batch mode. The main function of the macro was to read in PIV velocity in sequence, process each one, and export the needed figures or velocity data. The version of TecPlot used could not read multiple files at the same time if only using the "Open" file menu item. This was a big problem to process large amount of data measured from oscillatory flow. TecPlot could read series of files by a special made *Layout* file. This is limited that the path to each file had to keep unchanged. Any change to the path of data file ought to be updated in the *Layout* file before running Tecplot. This was quite inconvenience when measurement was carried out on one PC and processing of data on another PC.

Another limitation of processing PIV data with TecPlot was that it was not easy to carry out the phase average and space average of PIV velocity. To get the vector field of velocity was quite easy with acceptable accuracy. To get the velocity profile was not that simple. All of these processing was handled by the special made macro in TecPlot.

To average the PIV velocity in space and over phase for oscillatory flow, special code was made. The code read the velocity data from PIV and did the followings:

   −   Space average to get a velocity profile. Velocity field got from PIV was a 2D plane, including many velocity profiles. To get a mean profile for each PIV picture, space

average was implemented. The picture was meshed into small grids. Each cell was specified by a pair of coordinates and had a velocity. Space average was carried out based on the coordinates.

As shown in Figure 3-7, there were multiple profiles along the streamline in a PIV picture, space average was to average the profiles in different locations along the streamline.

If you define the grid index in a meshed PIV picture as i and j. i is the index along the streamline (horizontal in the measurement) and j is the index in the direction normal to the streamline (vertical in the measurement). The velocity of the cell is expressed as $u_{i,j}$, then

$$(3.1) \qquad \left. \overline{u_j} \right|_{j=1}^{M} = \frac{1}{N} \sum_{i=1}^{N} u_{i,j}$$

where N is the number of grids along the streamline. $\overline{u_j}$ is the space averaged velocity at index j. $\overline{u_j}$ (j = 1,…M, M is the number of grids in the direction normal to the streamline) constructs a profile of one PIV picture.
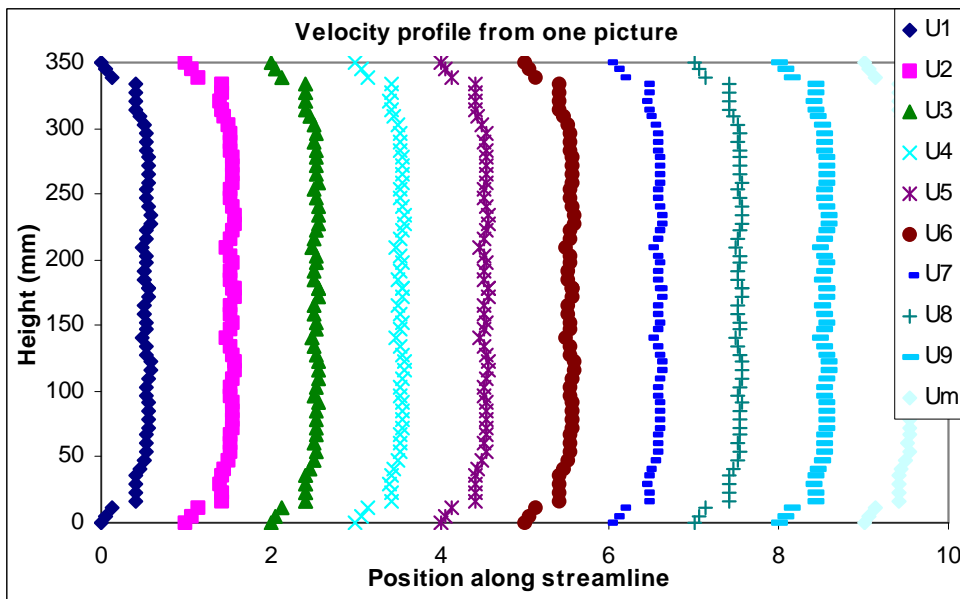
Figure 3-7 Schematic of space average

For example, a series of velocity profiles from a PIV picture is shown in Figure 3-7. There are 10 profiles showed in the figure, i.e., profile U1 to profile Um. Every profile is composed of lot of velocity points $u_{i,j}$. The space averaged velocity profile of this picture is

$$\left. \overline{u_j} \right|_{j=1}^{M} = \frac{1}{10} \sum_{i=1}^{10} u_{i,j}$$

–   Phase average to get a profile for each flow regime. Velocity of multiple periods measured for each flow regime of oscillatory flow. Average points over periods on the

basis of phase to get the phase-averaged profile. If the velocity at phase angle j is $u_{j,k}$, it is one of the $\overline{u_j}$ got from equation (3.1), then

(3.2)
$$\overline{u_\phi} = \frac{1}{\Omega} \sum_{k=1}^{\Omega} u_{\phi,k}$$

where $\overline{u_f}$ is the mean velocity at phase angle j. Ω is the period numbers measured. $\overline{u_f}$ (j = 1 ,…, S, S is the number of samples in one oscillatory period) constructs the waveform of velocity at one specific point. Figure 3-8 displays the phase average schematically.

Average Ω pictures for Ω periods
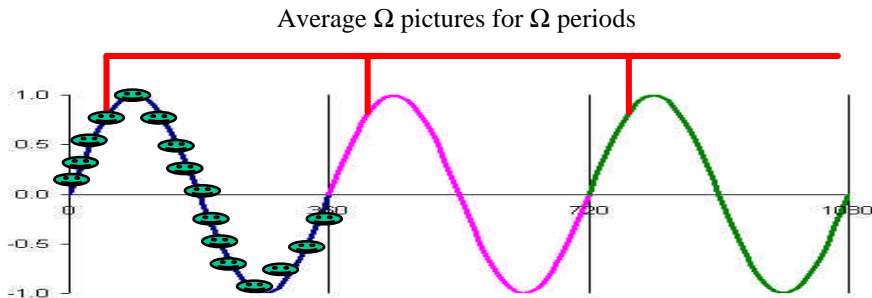
Figure 3-8 Schematic of phase average

For example, in Figure 3-8, three periods of velocity are measured. 16 pictures are taken in each period. There are 16 phase-averaged velocities which can be obtained by

$$\overline{u_f} = \frac{1}{3} \sum_{k=1}^{3} u_{f,,k}$$

After space average and phase average, multiples velocity profiles were available for each flow regime. Each velocity profile is corresponding to a phase point (angle). Velocity profile for each flow regime could be drawn in two ways:

− All profiles for different phase points was drawn in one figure based on vertical coordinates, in which the changes of velocity magnitude and profile were shown, the velocity changes along the coordinates were shown. Figure 3-9 is an example of this kind of profile. In the figure 25 profiles are shown for 25 different phase angles (P1 to P25). *X*-axis is the velocity magnitude and *Z*-axis is the location of the sampling point coordinates (height coordinate in the measurement). Each point in Figure 3-9 is corresponding to a set of $(\overline{u_j}$, $z)$ from equation (3.1). If *M = 30* and *N = 30*, and 10 periods is measured for the flow regime, each profile in Figure 3-9 is based on 9000 velocity vectors.

− Velocity is drawn in a figure based on the phase points (angles), i.e., the phase points are the *X* coordinates and velocities are the *Z* coordinates, from which the phase shift of velocity at different oscillating points could be displayed. Figure 3-10 is an example of velocity by phase points. 30 waveforms are shown in the figure, each waveform corresponding to a different height of the sampling point. For instance, waveform with legend 60 is the velocity waveform of points that are 60 mm from the bottom. Waveform with legend 177.6 corresponding to the velocity around the centre line of test duct.

41
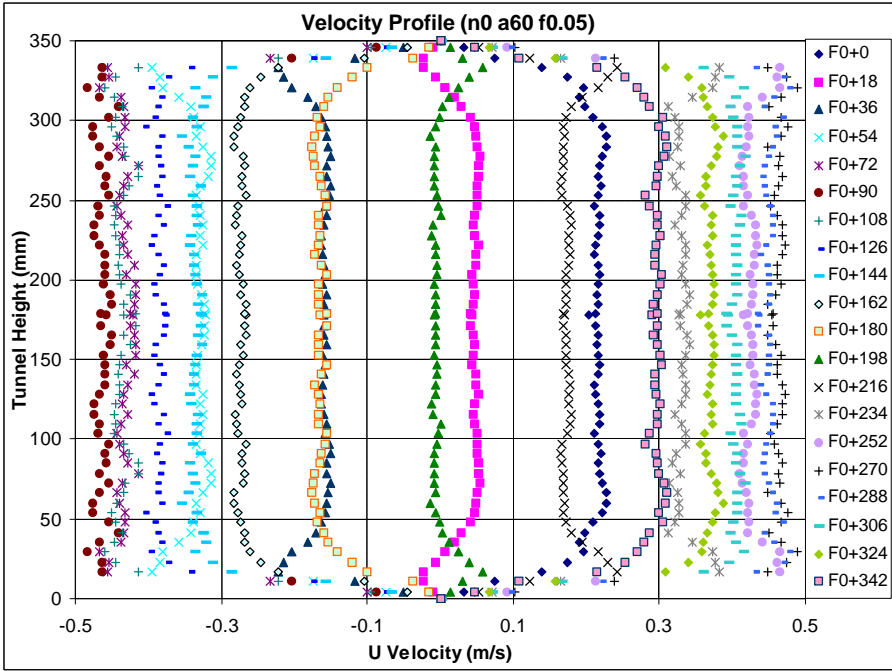
Figure 3-9 Example of velocity profile for a flow regime
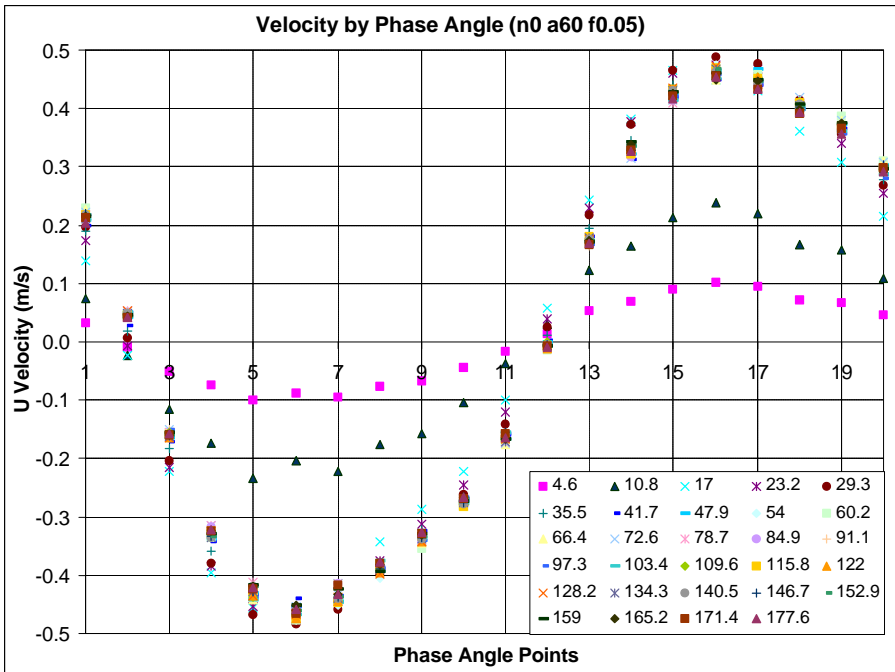
Figure 3-10 Example of velocity by phase points

Each point in Figure 3-10 is corresponding to a set of ($\overline{u_f}$, z) from equation (3.2). If 10 periods was measured for the flow regime, i.e., $W = 10$, and $M = 30$, each waveform in Figure 3-10 is based on 7500 velocity vectors.

In Figure 3-10 the phase interval between two adjacent points on one waveform is $360/26 = 14.4°$. Phase points number is used for *X-axis*, instead of the phase angle itself for the initial angle of the waveform is not specified.

3.3.2 LabView data processing

LabView VI PumpControl collected data from pressure sensors, differential pressure sensors and flow rate meter. The data collected was saved into a text file along with the flow control data (input of the MACROMASTER frequency inverter).

The data collected by PumpControl was processed in two steps:

− Rearrange data to make the first data of all data set synchronized with the same phase angle of the flow control waveform. Refer to the appendix for detail description of the rearrange of data

− Average all data over phase of oscillatory flow. This treatment is similar to that of PIV data processing mentioned in section 3.3.1.

As an example, Figure 3-11 shows one time series from readings of a differential pressure sensor in 500 seconds, 5 oscillatory periods. Totally 5000 samples are shown in the series. Figure 3-12 shows the phase-averaged data of the time series in Figure 3-11. 500 phase-averaged points are included in the figure. Figure 3-13 is the standard deviation (Stdev) of the phase-averaged value to the original time series.
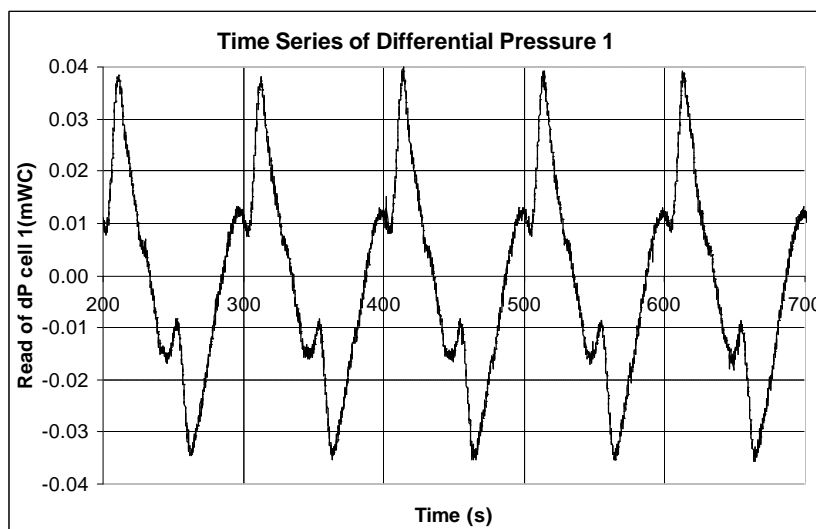
Figure 3-11 Time series of the reading from a dP cell 1

Similar processing is carried out for the readings of other differential pressure sensors, pressure sensors and flow rate meters for all flow regimes tested. Only the results from one of the differential pressure are presented in the thesis. However, examples for each sensor are shown in Figure 3-14 to Figure 3-25.
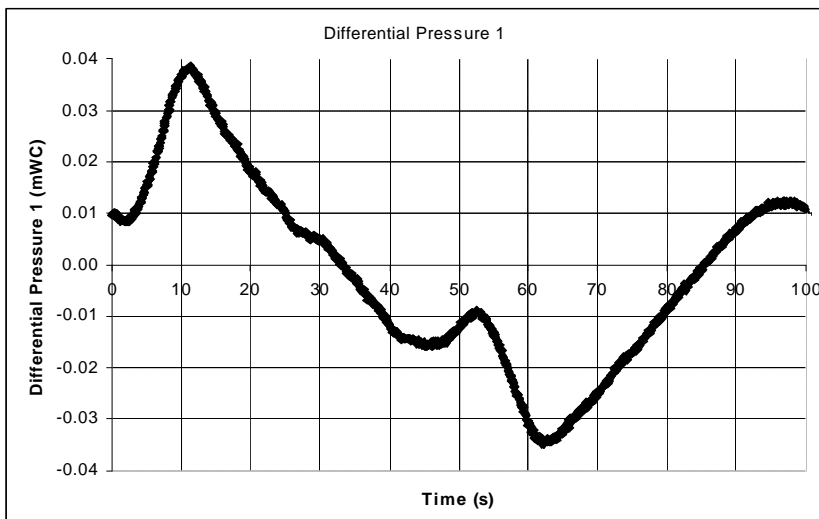
Figure 3-12 Phase average of the time series
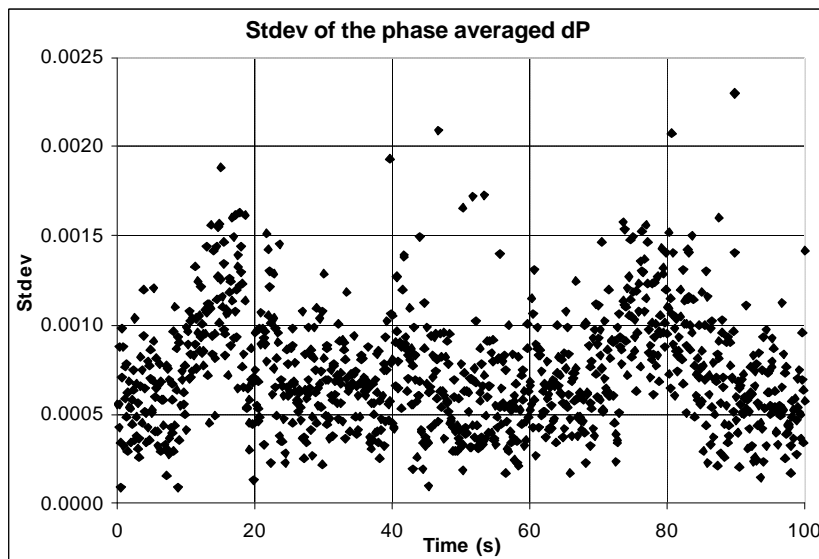
Figure 3-13 Stdev of phase averaged values

In Figure 3-14 to Figure 3-25
- *dP2*: readings of differential pressure sensor 2.
- *dynP1 – dynP4*: readings of dynamic pressure sensor 1 – 4.
- *Q*: Flow rate meter

The characteristic parameters of the flow:

- Flow type: pure oscillatory flow
- Oscillatory amplitude of flow rate: 42 l/s (-42 l/s < Q < 42 l/s).
- Oscillatory frequency: 0.01 Hz
- Sampling rate for PumpControl: 10 Hz
- Total samples from each sensor: 5000.
- Period number scanned: 5
- Scanning time: 500 s.
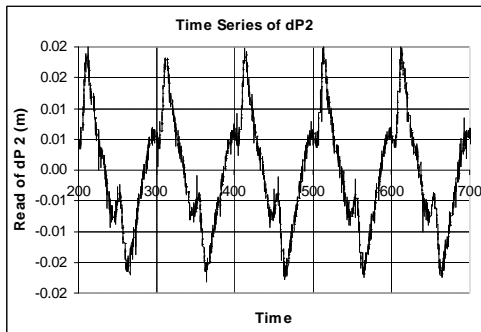
Figure 3-14 Time series of dP2
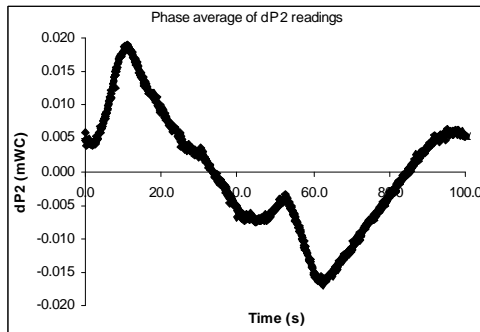
Figure 3-15 Phase average of dP2
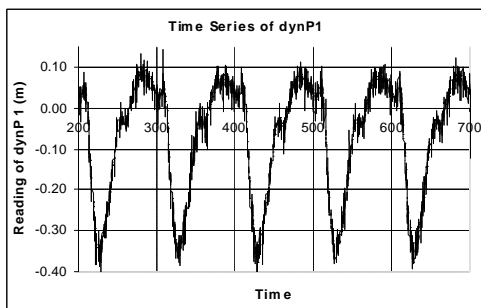
Figure 3-16 Time series of dynP1
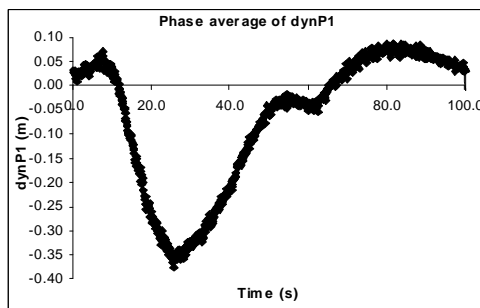
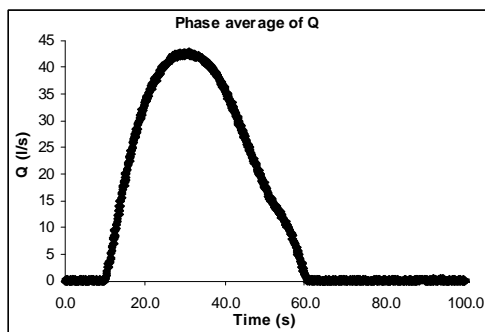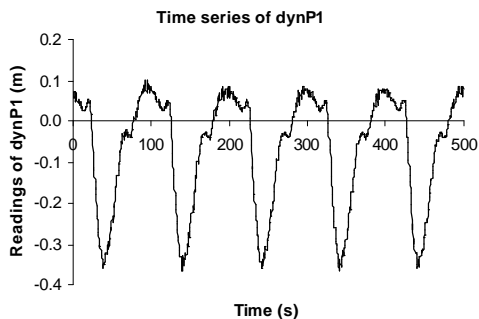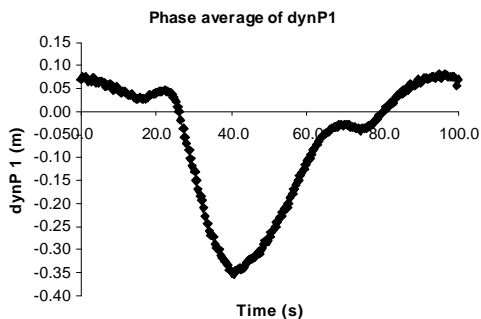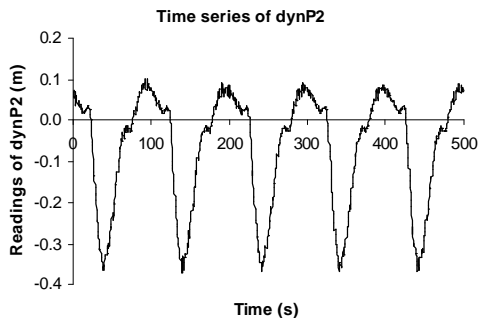Figure 3-17 Phase average of dynP1
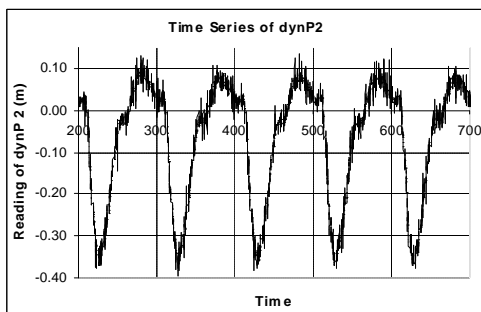
Figure 3-18 Time series of dynP2
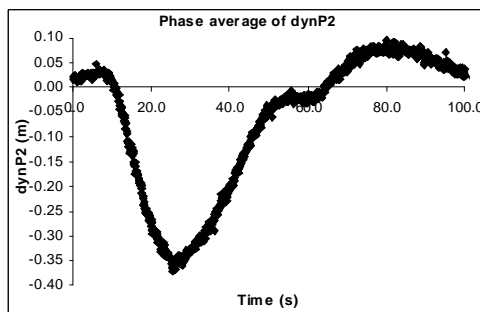
Figure 3-19 Phase average of dynP2
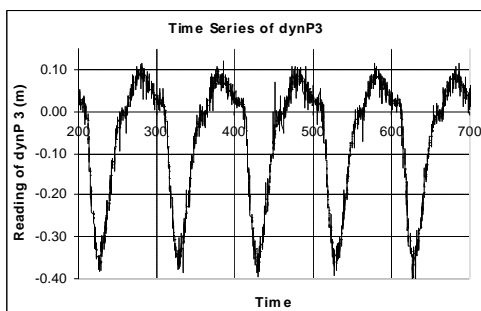
Figure 3-20 Time series of dynP3
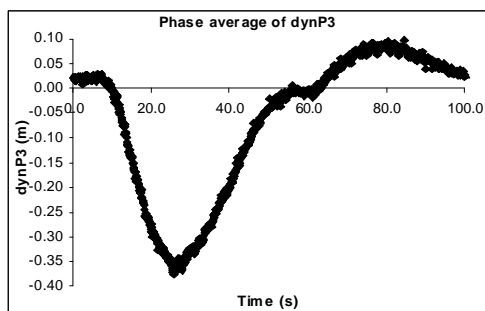
Figure 3-21 Phase average of dynP3
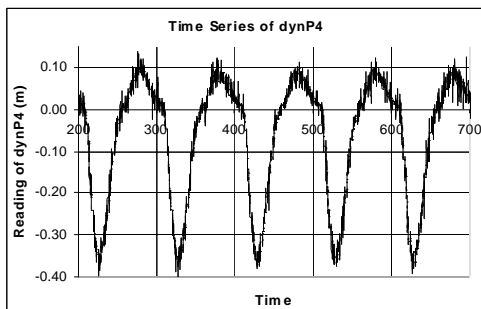
Figure 3-22 Time series of dynP4
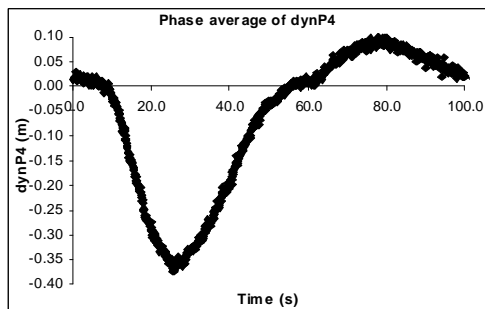
Figure 3-23 Phase average of dynP4
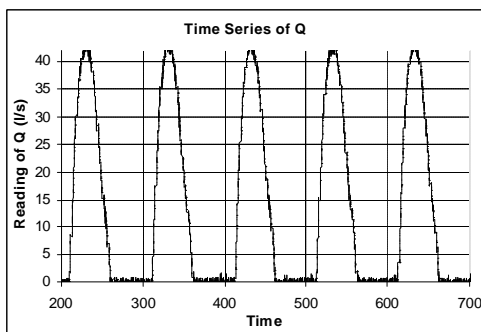
Figure 3-24 Time series of Q

Figure 3-25 Phase average of Q

The main problem for LabView data processing (variables other than velocity) is still the huge amount of data to process. A special code was made for this purpose. The code reads the data from original text file from LabView VI PumpControl, processes the data in two steps as mentioned above, draws various charts for each variable and each flow regime. The total processing time for all flow regimes tested is about 12 hours running continuously on a PC of Pentium III 677 MHz with 384MB memory.

3.3.3 HP DA/SU data processing

HP DA/SU data processing is similar to that of the LabView data processing. Only the original data formats from two DAQ means are different. Main data for different variables, such as pressure, differential pressure, flow rate, is similar. Only the auxiliary data such as time stamp

and so on is different. A code was also made for HP DA/SU data processing, which is similar to the one for LabView data processing, which was discussed in the previous section.

The result presented in this thesis is mainly based on the data collected by LabView VI PumpControl, because the sampling rate of HP DA/SU is not fast enough in some cases.

Examples of data collected by HP DA/SU for each sensor are shown in Figure 3-26 to Figure 3-45.

It is from the same flow and same sensors as shown in the previous section, and:

− Sampling rate for HP DA/SU: 2 Hz
− Total samples from each sensor: 1000.
− Period number scanned: 5
− Scanning time: 500 s

Figure 3-26 Time series of dynP1

Figure 3-27 Phase average of dynP1

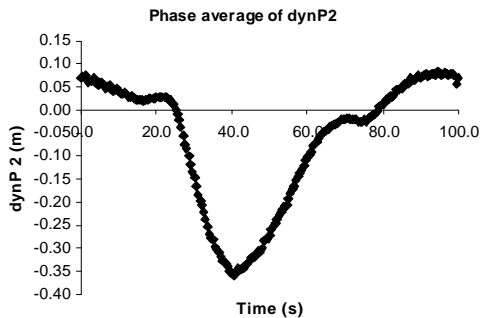Figure 3-28 Time series of dynP2

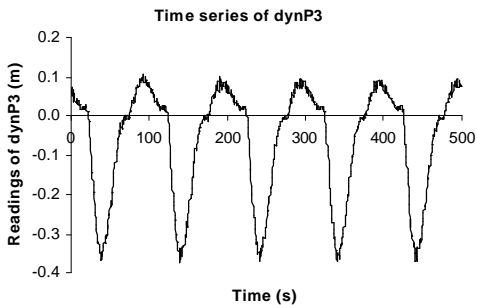Figure 3-29 Phase average of dynP2
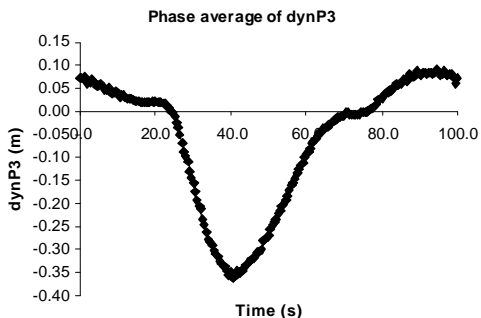
Figure 3-30 Time series of dynP3
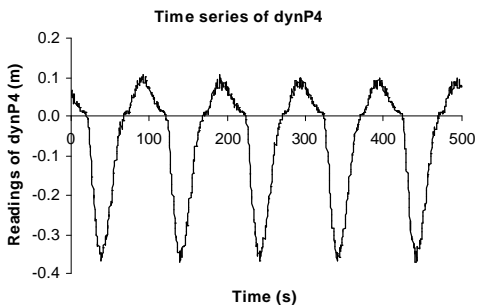

Figure 3-31 Phase average of dynP3

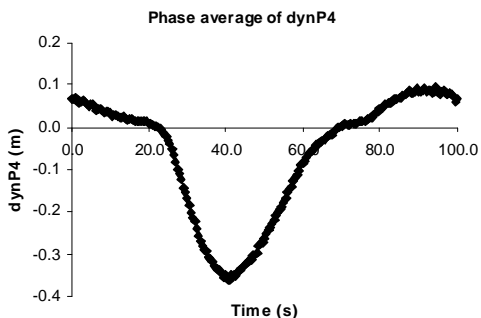Figure 3-32 Time series of dynP4

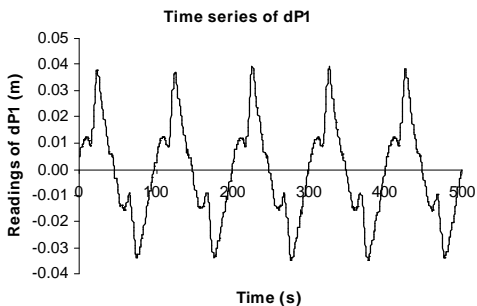Figure 3-33 Phase average of dynP4

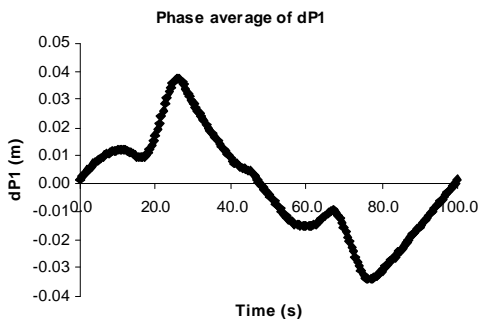Figure 3-34 Time series of dP1
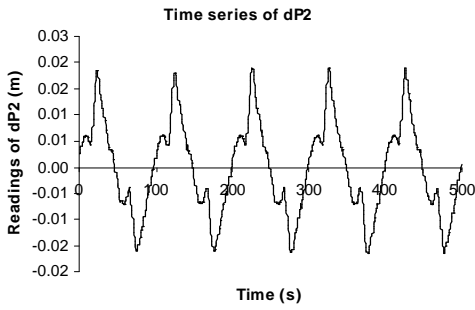

Figure 3-35 Phase average of dP1
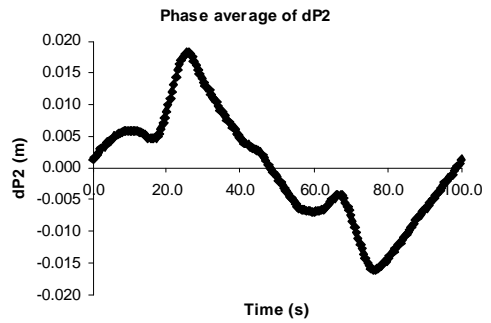
48

Figure 3-36 Time series of dP2
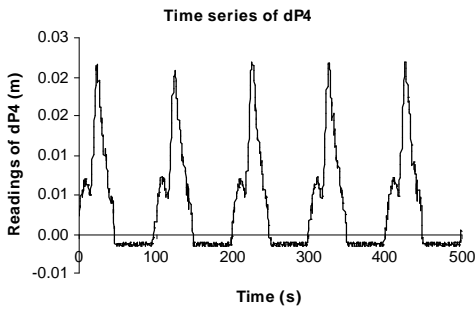

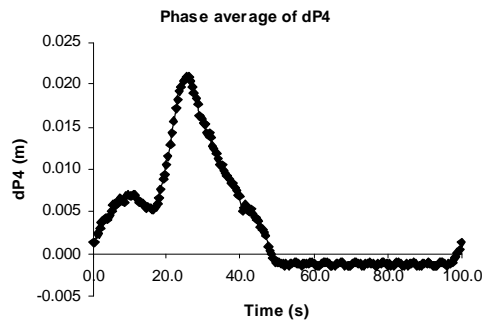Figure 3-37 Phase average of dP2

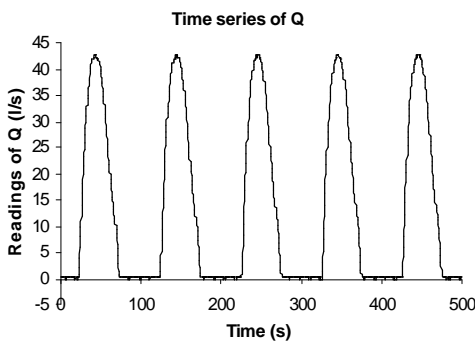Figure 3-38 Time series of dP4

Figure 3-39 Phase average of dP4

Figure 3-40 Time series of Q
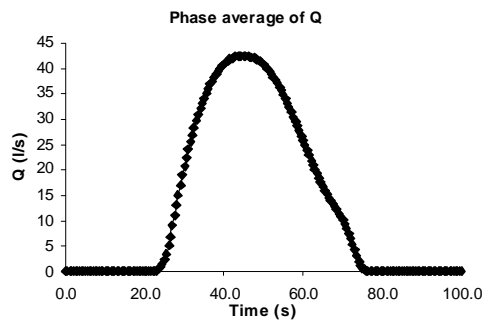
Figure 3-41 Phase average of Q

49
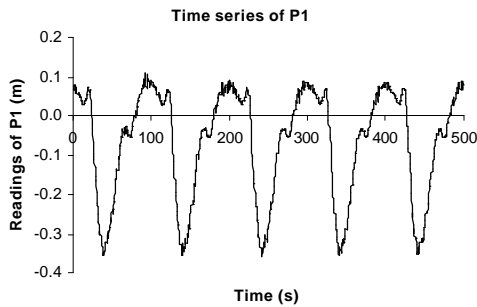
Time series of P1

Figure 3-42 Time series of P1
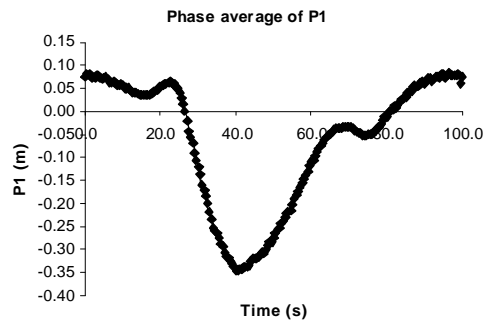
Phase average of P1

Figure 3-43 Phase average of P1
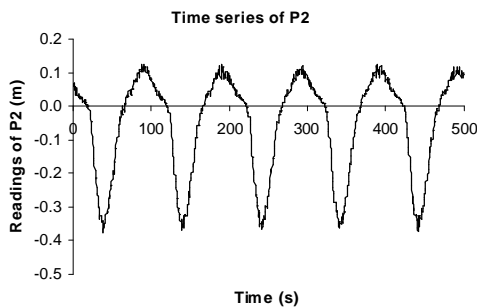
Time series of P2

Figure 3-44 Time series of P2
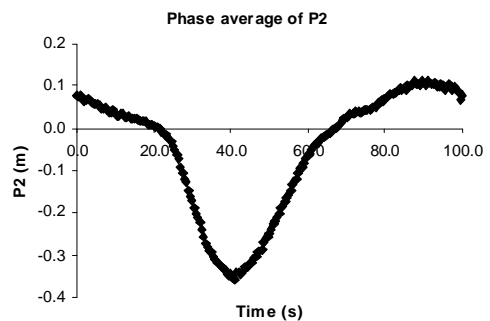
Phase average of P2

Figure 3-45 Phase average of P2

Notes on the figures shown above:

- P1 – P2 are the cross sectional averaged pressure readings. Distance between P1 and P2 is about 15 meters streamwise.
- The flow rate meter and differential pressure cell dP4 can only read out the values in one direction. Only positive readings are shown in the figure. All negative readings are treated as zero.
- The readings of all pressure sensors are the dynamic head. The static head when the water is still is set as datum.

Compare Figure 3-14 to Figure 3-25 with Figure 3-26 to Figure 3-45, we can see that within the same scanning time PumpControl collected 5 times data as HP DA/SU did. The time series from the data of PumpControl is not as smooth as the one from HP DA/SU. The phase averaged value displays similar difference.

Chapter 4

Velocity Measurements

Main topics of this chapter:

- Overview of LDV measurement
- Examples of LDV velocity
- LDV velocity and universal distribution law
- PIV velocity instructions
- PIV velocity of steady flow
- PIV velocity of pure oscillatory flow
- PIV velocity of combined oscillatory flow

4.1 Overview of LDV Measurement

Laser Doppler Velocimeter (LDV or LDA for Laser Doppler Anemometry) was used for the velocity measurements before the Particle Image Velocimeter (PIV) was available for this project.

LDV was used for both stationary flow measurement and part of the oscillatory flow measurement. It was first used for flow measurement of the smooth tunnel. And later it was also applied for flow measurement in the rough tunnel. It was also used for flow measurement when the rig was not build up as a closed loop.

Symmetry of velocity distribution across the tunnel was assumed. Only half of the cross section of flow in the tunnel was measured with LDV. The LDV sensor was installed on one side of the tunnel and movable in three dimensions by lightweight traverse system. The horizontal velocity profile normal to the mainstream flow direction was measured. The sensor only moved in horizontal direction perpendicular to the longitude axis of the test tunnel. Mostly the measurement started from the sidewall near to the LDV sensor, stepped forward to the centreline, and ended at a point where it was a little bit passed over the centreline of the cross section (Figure 2-8). Some measurements were also carried out in the inverse direction for the purpose of comparison, i.e., the measurement started from the sidewall away from the LDV sensor and moved toward to the sensor step by step. There was a window on the sidewall for the laser to pass through the sidewall and enter into the flow. The part of the sidewall, where the window was located, was smooth. Other parts of the sidewall were rough.

Parameters of part of the flow regimes measured by LDV are listed below in Table 4-1:

Table 4-1 List of tests with LDV

Test	f_r (Hz)	n0_P1 (%)	n0_P2 (%)	Amp_P1&P2 (%)	Q (l/s)
1	0.05	-3.00	0.00	40.00	0.00
2	0.05	10.00	0.00	40.00	13.00
3	0.05	20.00	0.00	40.00	23.00
4	0.05	30.00	0.00	40.00	32.00
5	0.00	10.00	9.80	0.00	13.40
6	0.00	17.00	16.75	0.00	22.90
7	0.00	23.00	22.00	0.00	31.20
8	0.10	-3.00	0.00	59.00	8.29
9	0.10	10.00	0.00	59.00	15.00
10	0.10	20.00	0.00	59.00	27.00
11	0.10	30.00	0.00	59.00	37.00
12	0.00	8.00	0.00	0.00	7.00
13	0.00	8.20	8.20	0.00	10.00
14	0.00	15.00	15.00	0.00	20.00
15	0.00	28.30	28.30	0.00	39.90
16	0.00	41.90	41.90	0.00	60.00
17	0.00	55.55	55.55	0.00	80.00
18	0.00	69.20	69.20	0.00	100.00
19	0.00	85.00	85.00	0.00	120.00
20	0.05	42.00	42.00	10.00	60.71
21	0.05	42.00	42.00	20.00	62.00
22	0.05	38.00	38.00	30.00	60.00
23	0.05	30.00	0.00	40.00	32.79
24	0.10	30.00	0.00	40.00	35.22
25	0.20	30.00	0.00	40.00	35.92
26	0.01	30.00	0.00	40.00	23.02
27	0.05	-3.00	0.00	40.00	0.20
28	0.05	10.00	0.00	40.00	13.58
29	0.05	20.00	0.00	40.00	23.49
30	0.10	-3.00	0.00	40.00	0.15
31	0.10	10.00	0.00	40.00	15.73
32	0.10	20.00	0.00	40.00	25.65
33	0.20	-3.00	0.00	40.00	-0.08
34	0.20	10.00	0.00	40.00	16.1
35	0.20	20.00	0.00	40.00	26.63
36	0.01	-3.00	0.00	40.00	2.22
37	0.01	10.00	0.00	40.00	11.17
38	0.01	20.00	0.00	40.00	17.73

Notation of column names used in the table:

− f_r: frequency of flow, Hz

− *n0_P1*: base flow input to pump I , %

− *n0_P2*: base flow input to pump II, %

- *Amp_P1 & P2*: oscillatory flow input to pump I & II, %. Generally *Amp_P1 = Amp_P2*.
- *Q*: mean flow rate, l/s

Not all tests by LDV are listed in Table 4-1. The LDV measurements that are not listed in Table 4-1 include:

- The comparing tests of different laser power levels applied, while flow parameters and other parameters of LDV system were kept constant.
- The comparing tests of measurement from different sides of the tunnel, while all flow parameters and settings of LDV system were kept constant.
- The comparing tests of different parameter settings of LDA system applied, while all flow parameters were kept constant.
- Other measurements.

The *Q* in Table 4-1 was a mean flow rate over oscillatory periods for oscillatory flow, and it was a time mean for stationary flow. It was averaged from the readings of flow rate meter. The flow rate meter used could display both positive and negative readings of flow rate, however it could not output the negative signal in voltage to the data acquisition computer with the settings used. If the reading of flow rate of oscillatory flow crossed the zero point, i.e., the minimum flow rate was negative (flow in inverse direction) and the maximum flow rate was positive, then some minimum flow rate points were recorded on site manually and averaged afterwards. For the oscillatory flow whose flow rate was always positive, the mean flow rate in Table 4-1 was obtained from the samples recorded by HP DA/SU logger or the LabView VI PumpControl.

As mentioned above, it was assumed that the flow in the rectangular duct was symmetry about the longitude centreline. To save the measuring time, only half of the cross section was measured, i.e., the half velocity profile was measured. The measured part of flow was divided into three regions and the LDV sensor was moved with different steps in different regions as shown in Table 4-2. In the boundary area, region 1 as shown Table 4-2, where flow variance was greater, more sampling volumes were measured. The moving step of the sensor in this area was 0.1 mm (reading of the lightweight traverse system). In the area away from the boundary wall, region 3 as listed in Table 4-2, where velocity profile was almost flat, and the distance between adjacent sampling volumes was bigger, 5.0 mm (reading of the lightweight traverse system). In the area in between, region 2 as shown Table 4-2, the intermediate area, where flow varied, but not so steep as in region 1, the distance between sampling points was moderate, 1.0 mm (reading of the lightweight traverse system). The total moving distance of the sensor in a single measurement was 81.4 mm (reading of the lightweight traverse system) and 39 points measured across the test tunnel.

Table 4-2 Regions and steps of LDV measurement

Region	From (x, y, z)	To (x, y, z)	Displacement (mm)	Step (mm)	Points	Note
1	(0, 0, 0)	(0, 1.4, 0)	1.4	0.1	15	Boundary area
2	(0, 2.4, 0)	(0, 11.4, 0)	10.0	1.0	10	Intermediate
3	(0, 16.4, 0)	(0, 81.4, 0)	70.0	5.0	14	Main area
Sum			81.4 mm		39	

As described in the sub-chapter 2.3.3, the displacement readings of the lightweight traverse system were the physical displacements of the sensor itself. There was a coefficient of 1.3529 between the physical displacement of the sensor and the displacement of the control volume. The steps of sampling volume in the three measuring regions were 0.13529 mm, 1.2529 mm,

and 6.7645mm respectively. The total measured length of a session was about 110 mm across the test tunnel.

4.2 Examples of LDV Velocity

LDV was used for measurement of both stationary flow and oscillatory flow. Example results of LDV measurement from both stationary flow and oscillatory flow are shown below respectively.

4.2.1 LDV velocity of steady flow

 Figure 4-1 and Figure 4-2 are the LDV measured velocity U and V of stationary flow, with flow rate changing from $Q = 30$ l/s to 87 l/s. The *RMS* of the velocities U and V by LDV is shown in Figure 4-3 and Figure 4-4.
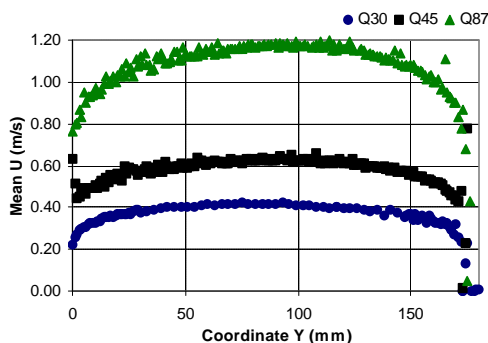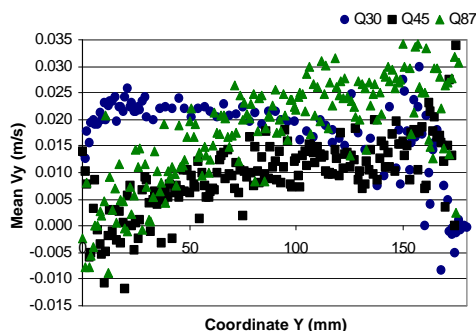
Figure 4-1 Profile of *U* by LDV
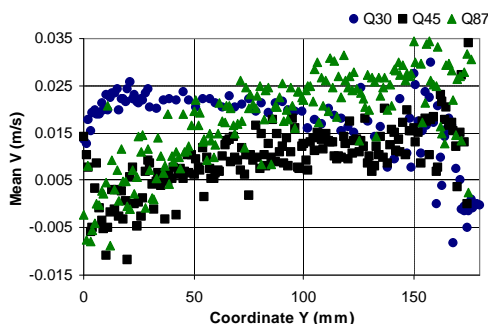
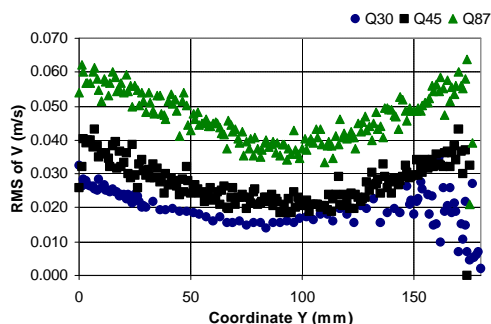Figure 4-2 Profile of *V* by LDV

Figure 4-3 *RMS* of *U* by LDV

Figure 4-4 *RMS* of *V* by LDV

It is shown that the results from LDV for stationary flow were quite good. The velocity profiles of the boundary area were quite smooth, though the vibration and reflection of tunnel wall were visible to naked eyes when the sampling volume was near to the wall during the LDV measurement.

4.2.2 LDV velocity of oscillatory flow

LDV was used to measure velocity of oscillatory flow at different frequencies and different flow rates. Examples of LDV results of flow with frequencies of 0.05 Hz and 0.10Hz, flow rates

at about 15l/s, 27l/s and 37l/s are shown from Figure 4-5 to Figure 4-16. Velocity profiles in absolute velocity values and in dimensionless velocity values are presented side by side.
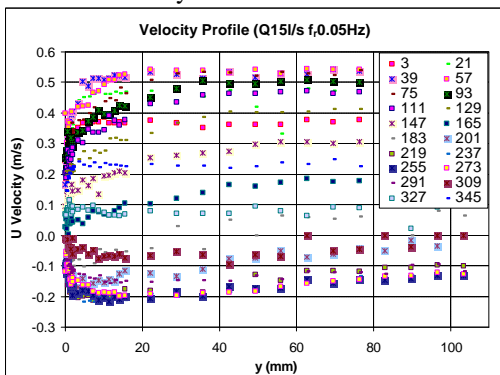

Figure 4-5 Profiles with absolute value (0.05Hz, 15l/s)
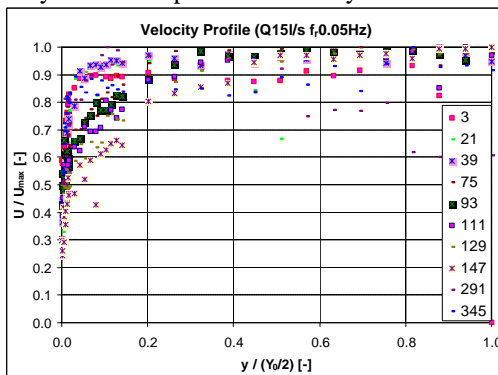

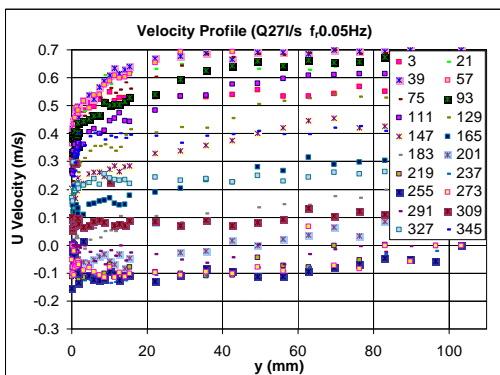Figure 4-6 Profiles with dimensionless value (0.05Hz, 15l/s)

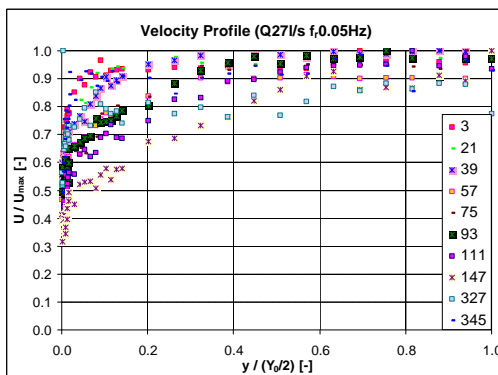Figure 4-7 Profiles with absolute value (0.05Hz, 27l/s)

Figure 4-8 Profiles with dimensionless value (0.05Hz, 27l/s)
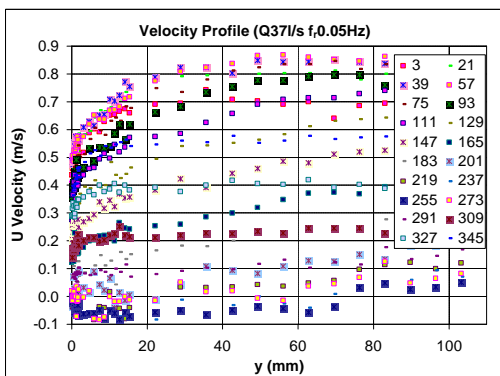
Figure 4-9 Profiles with absolute value (0.05Hz, 37l/s)
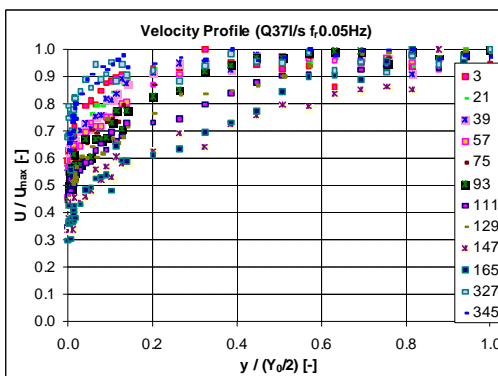
Figure 4-10 Profiles with dimensionless value (0.05Hz, 37l/s)

Figure 4-11 Profiles with absolute value
(0.10Hz, 15l/s)
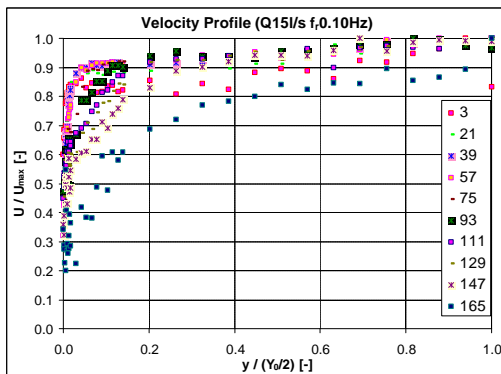
Figure 4-12 Profiles with dimensionless value
(0.10Hz, 15l/s)

Figure 4-13 Profiles with absolute value
(0.10Hz, 27l/s)
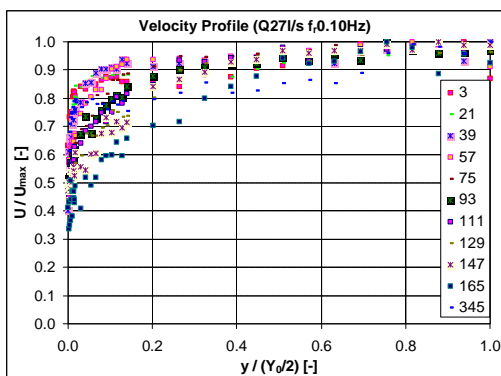
Figure 4-14 Profiles with dimensionless value
(0.10Hz, 27l/s)
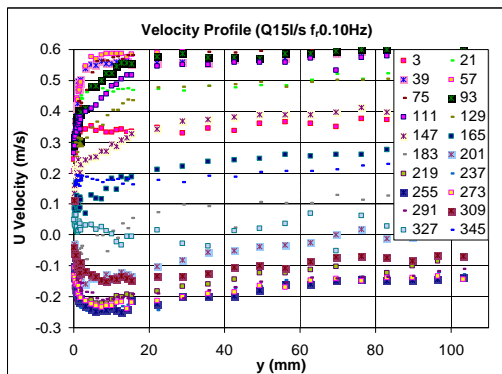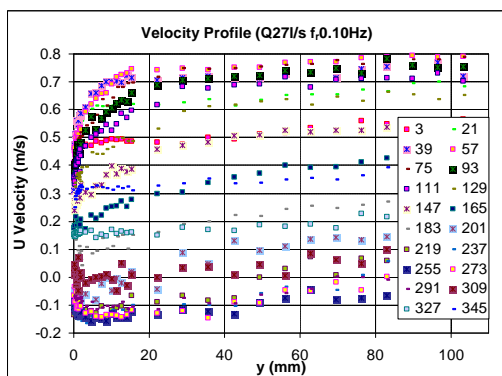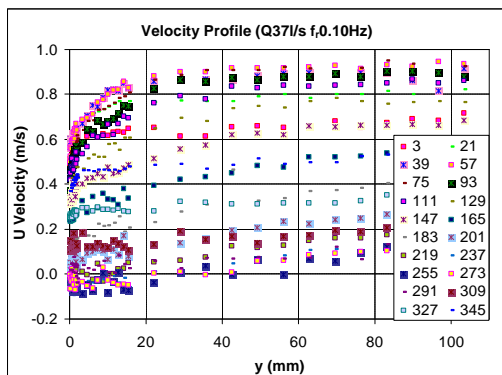

Figure 4-15 Profiles with absolute value
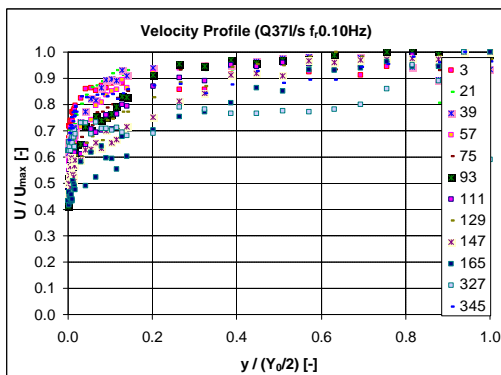(0.10Hz, 37l/s)

Figure 4-16 Profiles with dimensionless value
(0.10Hz, 37l/s)

Generally speaking, the velocity profiles of steady flow and oscillatory flow were quite similar. The profiles of oscillatory flow at near wall area were steeper than that of the stationary flow, though the mean flow rates for oscillatory flow were smaller relatively.

Basically, there was not significant difference between the velocity profiles of two oscillatory frequencies shown above.

For oscillatory flow, the advantage of velocity profile in absolute value was that the oscillation was obvious by the locations of profiles at different phase angles. This could not be shown in the dimensionless velocity profiles. However, it is shown in the dimensionless velocity profiles that the velocity profiles at different phase angles had the similar shape.

4.3 LDV Velocity and Universal Distribution Law

Universal Distribution Law is the general presentation of turbulent velocity in a pipe. In the following, some efforts are made to compare the LDV velocity measured with the universal distribution law. The starting point is to make dimensionless the measured velocity with a friction velocity.

4.3.1 Equations for Clauser chart

Wall shear stress is expressed as

(4-1)
$$\tau_w = \rho\nu\left(\frac{du}{dy}\right)_{y=0}$$

Boundary layer thickness is expressed as

(4-2)
$$\Delta = \frac{\delta}{3.3715}\sqrt{\frac{2}{C_f}}$$

Friction velocity is expressed as

(4-3)
$$u^* = \sqrt{\frac{\tau_w}{\rho}} = U_e\sqrt{\frac{C_f}{2}}$$

Then, the Law of the wall (inner law)

(4-4)
$$\frac{U}{u^*} = f\left(\frac{y \cdot u^*}{\nu}\right)$$

For outer region (Outer law, velocity-defect law);

(4-5)
$$\frac{U_e - U}{u^*} = g\left(\frac{y}{\Delta}, \xi\right), \ \xi = \frac{\Delta}{\tau_w}\frac{dp_e}{dx}$$

Overlap layer (overlap law), $u_{inner} = u_{outer}$, i.e.,

(4-6)
$$\frac{u}{u^*} = f\left(\frac{\Delta \cdot u^*}{\nu}\frac{y}{\Delta}\right) = \frac{U_e}{u^*} - g\left(\frac{y}{\Delta}\right)$$

It can be true only if both f and g are logarithmic functions. Then in the overlap layer:
For inner variables:

(4-7)
$$\frac{U}{u^*} = \frac{1}{\kappa}\ln\frac{y \cdot u^*}{\nu} + B$$

57

For outer variables:

$$(4\text{-}8) \qquad \frac{U_e - U}{u^*} = -\frac{1}{\kappa} \ln \frac{y}{\Delta} + A$$

Multiply u^*/u_e to the equation of inner variables, Clauser (1956)

$$(4\text{-}9) \qquad \frac{U}{U_e} = \frac{1}{\kappa} \sqrt{\frac{C_f}{2}} \ln\left(\frac{yU_e}{\nu}\right) + \frac{1}{\kappa} \sqrt{\frac{C_f}{2}} \ln\left(\sqrt{\frac{C_f}{2}}\right) + B\sqrt{\frac{C_f}{2}}$$

or

$$(4\text{-}10) \qquad \frac{U}{U_e} = \sqrt{\frac{C_f}{2}}\left[\frac{1}{\kappa} \ln\left(\frac{yU_e}{\nu}\right) + \frac{1}{\kappa} \ln\left(\sqrt{\frac{C_f}{2}}\right) + B\right]$$

or , Skåre (1994)

$$(4\text{-}11) \qquad \frac{U}{U_e} = \sqrt{\frac{C_f}{2}}\left[A \cdot \log_{10}\left(\frac{yU_e}{\nu}\right) + A \cdot \log_{10}\left(\sqrt{\frac{C_f}{2}}\right) + B\right]$$

4.3.2 Basic Clauser chart

In equation (4-10), Clauser (1956) chose $\kappa = 0.41$ and $B = 4.9$. Example calculations are shown below in Table 4-3 and a basic Clauser chart is shown Figure 4-17:

Table 4-3 Example calculations of Clauser chart

$\dfrac{yU_e}{\nu}$	C_f	$\dfrac{U}{U_e}$	Chart
10^2	0.0001	0.0287	
10^6		0.1875	
10^2	0.0005	0.0951	
10^6		0.4503	
10^2	0.0010	0.1535	
10^6		0.6558	
10^2	0.0015	0.2015	
10^6		0.8167	
10^2	0.0020	0.2437	
10^6		0.9541	
10^2	0.0025	0.2821	
10^6		1.0764	
10^2	0.0030	0.3177	
10^6		1.1877	
10^2	0.0035	0.3510	
10^6		1.2907	
10^2	0.0040	0.3825	

Figure 4-17 Example of Clauser chart

4.3.3 Analysis on measured velocity of steady flow

Three examples of Clauser chart are shown below with the velocity data measured by LDV. The flows are steady flow.

With each pair of y and U, a pair of $\dfrac{yU_e}{\nu}$ and $\dfrac{U}{U_e}$ was calculated, and a point was drawn in the basic Clauser chart shown in Figure 4-17. With all pairs of y and U from a flow regime, a series of points was drawn, from which the coefficient C_f was extracted. The friction velocity u^* could be calculated with equation (4-3) after C_f was available.

In all three cases shown below, as shown in Figure 4-18, Figure 4-20, and Figure 4-22, the series points of ($\dfrac{yU_e}{\nu}$, $\dfrac{U}{U_e}$) developed almost linearly along with the increase of y coordinate, i.e., the increase of value $\dfrac{yU_e}{\nu}$. All series were developed in parallel or near to parallel to the isometric lines of C_f. It was not difficult to get a suitable value of C_f for all of the three cases.

The velocity profiles from the three cases are shown in Figure 4-19, Figure 4-21, and Figure 4-23. The velocity profiles were good enough for all three cases.

1. Measured velocity of steady flow, example I

    Flow type: steady flow

    Flow parameters:
    − $\mathbf{n} = 1.007 \times 10^{-6}\,\mathrm{m^2/s}$
    − $Q = 13.41$ l/s (measured by flow rate meter, averaged value of 5000 readings)
    − $U_e = 0.1891$ m/s (from LDV velocity at $y = 110.11$ mm)

The calculation results and charts were shown below.

Figure 4-18 Clauser chart with LDV data   Figure 4-19 Velocity profile with LDV data

From the Clauser chart shown in Figure 4-18, the value of C_f for this flow regime was about 0.0043. The friction velocity u^* calculated for this flow regime from equation (4-3) was 0.008768 m/s.

2. Measured velocity of steady flow, example II

    Flow type: steady flow

    Flow parameters:
    − $\mathbf{n} = 1.007 \times 10^{-6}\,\mathrm{m^2/s}$

59

- Q = 22.88 l/s (measured by flow rate meter, averaged value of 5000 readings)
- U_e = 0.3193 m/s (from LDV data at y = 110.11 mm)

The calculation results and charts were shown below.
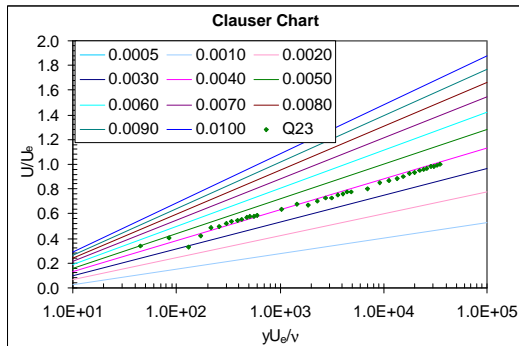
Figure 4-20 Clauser chart with LDV data   Figure 4-21 Velocity profile with LDV data
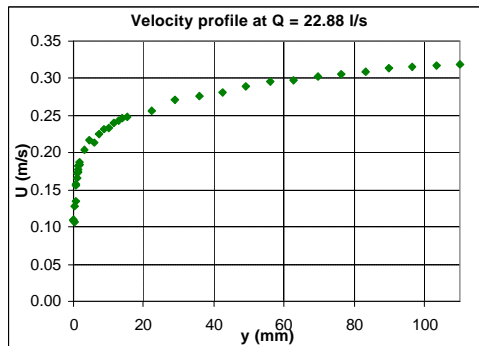
From the Clauser chart shown in Figure 4-20, the value of C_f for this flow regime was about 0.0040. The friction velocity $u*$ calculated for this flow regime from equation (4-3) was 0.001428 m/s.

3. Measured velocity of steady flow, example III

Flow type: steady flow

Flow parameters:
- $\mathbf{n} = 1.007 \times 10^{-6}\,\text{m}^2/\text{s}$
- Q = 31.24 l/s (measured by flow rate meter, averaged value of 5000 readings)
- U_e = 0.4327 m/s (from LDV data at y = 110.11 mm)

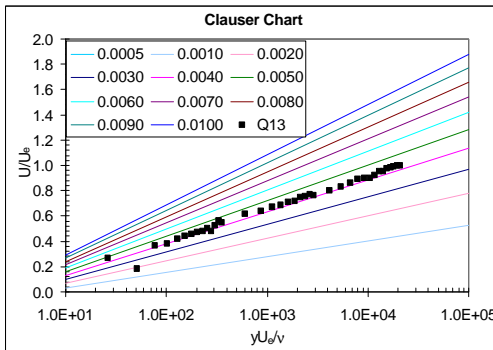The calculation results and charts were shown below.

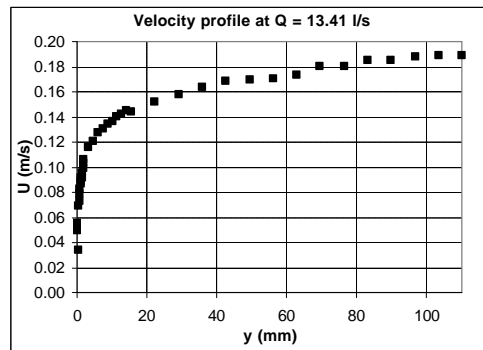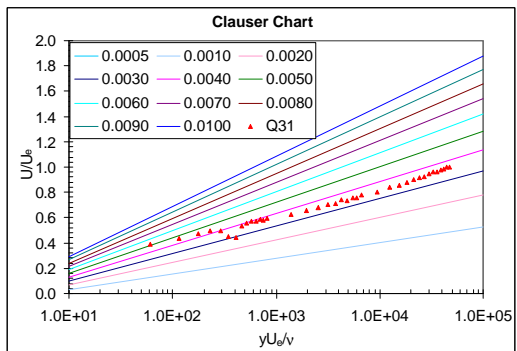
Figure 4-22 Clauser chart with LDV data   Figure 4-23 Velocity profile with LDV data
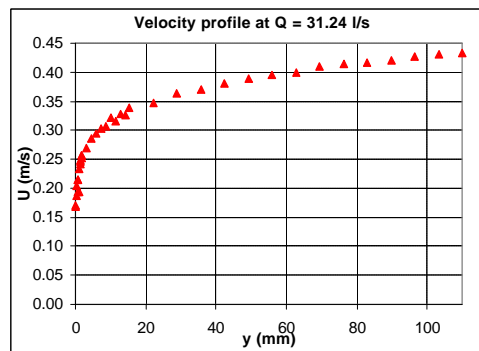
From the Clauser chart shown in Figure 4-22, the value of C_f for this flow regime was about 0.0035. The friction velocity $u*$ calculated for this flow regime from equation (4-3) was 0.01810 m/s.

With the friction velocity calculated above, the dimensionless velocity profiles for the three flow regimes shown above are drawn below in Figure 4-24 to Figure 4-27.

It is shown in Figure 4-27 that the velocity profiles shown in all three cases were coincidence well with the universal velocity distribution law shown by Schlichting (1979), e.g.

when y+ = 10, u+ is a little more than 10; when y+ = 100, u+ is around 16-17; when y+ = 1000, u+ is about 22 – 23.
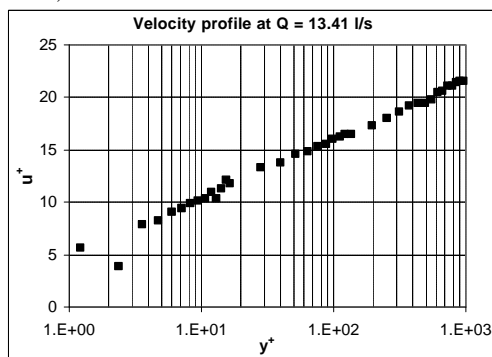
Figure 4-24 Dimensionless velocity profile
with data from LDV
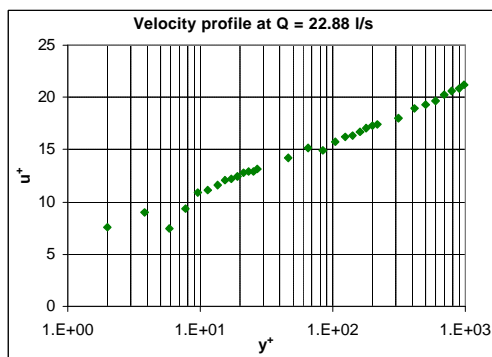
Figure 4-25 Dimensionless velocity profile
with data from LDV
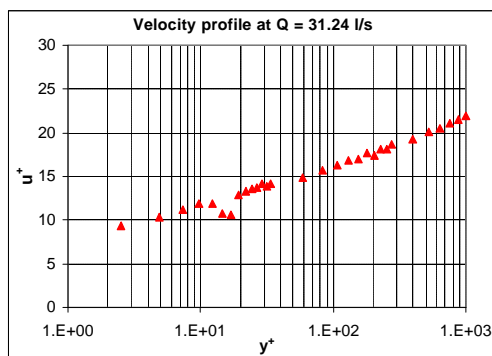
Figure 4-26 Dimensionless velocity profile
with data from LDV
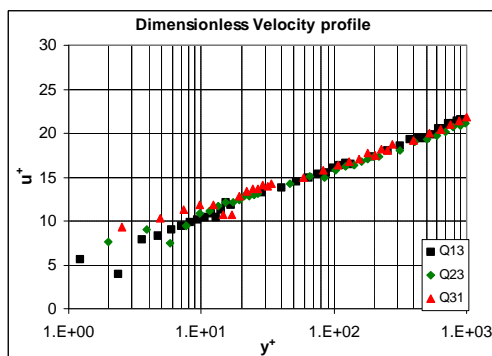
Figure 4-27 Dimensionless velocity profiles
with data from LDV (3 in one)

4.3.4 Analysis on measured velocity of oscillatory flow

The examples shown above were results from steady flows measurement. The friction velocity of oscillatory flow varies for different phase angles of the flow. There is a unique friction velocity for each phase angle of the oscillatory flow. The process to determine the friction velocity for each phase angle is similar to the process for steady flow shown above.

- Get the mean velocity U_φ of each phase angle j at each physical location y.
- If there are N points are measured across the tunnel ($N = 39$ in the previous examples), there are N U_φ for each j, i.e., there is a series of U_φ, as the U in the previous examples. There is a U_e too.
- A series of $\dfrac{yU_e}{\nu}$ and $\dfrac{U}{U_e}$ can be evaluated for each j.
- C_f can be estimated for each phase angle j with the help of Clauser chart.
- Friction velocity u^* can be calculated for each phase angle j.
- The dimensionless velocity profile can be drawn for the velocity at the phase angle.

An example analysis is shown below. The flow parameters are:

- $\boldsymbol{n} = 1.007 \times 10^{-6}\,\mathrm{m^2/s}$

  − f_r = 0.05 Hz
  − Q_0 = 31.5 l/s
  − q = 30 l/s

As examples, calculations waere carried out on several special phase angles of the flow, i.e., phase angles of 3, 30, 60, 90, 120, 150, and 180 degrees. First a series of $\dfrac{yU_e}{\nu}$ and $\dfrac{U}{U_e}$ was calculated for each phase angle. Then the series was drawn in the Clauser chart, as shown in Figure 4-28. The coefficient C_f of each phase angle was evaluated from the figure. The friction velocity u^* for each phase angle was calculated afterwards. The calculation results of C_f and u^* were listed below in Table 4-4
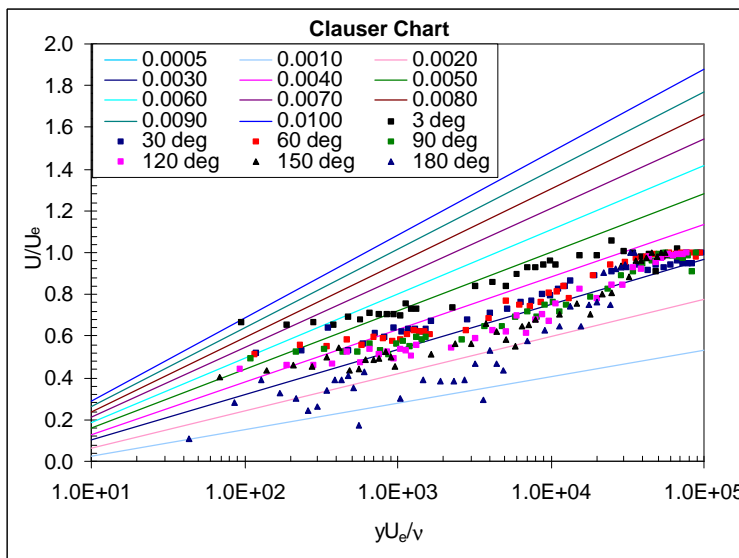
Figure 4-28 Clauser chart of the oscillatory flow at different phase angles

Table 4-4 Calculated C_f and u^* of oscillatory flow

Phase angle	3	30	60	90	120	150	180
C_f	0.0046	0.0035	0.0033	0.0030	0.0027	0.0024	0.0021
u^* (m/s)	0.03371	0.03513	0.03347	0.03155	0.02572	0.01760	0.00989

With the calculated u^* of oscillatory flow shown in Table 4-4, a series of y^+ and u^+ were calculated for each phase angle with the original velocity measured by LDV. The dimensionless velocity profiles of oscillatory flow at each phase angle were drawn then, as shown in Figure 4-29.
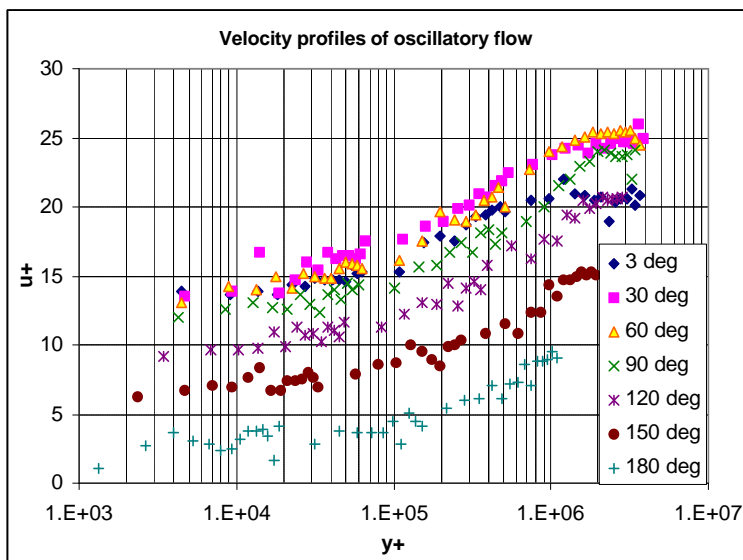
Figure 4-29 Velocity profiles of the oscillatory flow at different phase angles

It is shown in Figure 4-29 that

- The velocity profiles were better fitted with the universal velocity distribution law at phase angles of 3, 30, 60, 90, and 120 degrees. The velocity profiles were more and more away from the universal velocity distribution law from phase angle of 120 to 180 degrees. The reason could be that the flow discussed was combined oscillatory flow. At phase angles of 3, 30, 60, and 90 degrees, the absolute magnitudes of the flow were greater than that of at phase angles of 120 and 180 degrees, as shown in Figure 4-30. When the absolute velocity was smaller, the relative error could be bigger.

- Comparing with the examples of steady flow shown above, the values of y^+ were bigger for the oscillatory flow.

- The scattering of points in the Clauser chart of oscillatory flow, as shown in Figure 4-28, could contribute to the divergence of the velocity profile in Figure 4-29 .
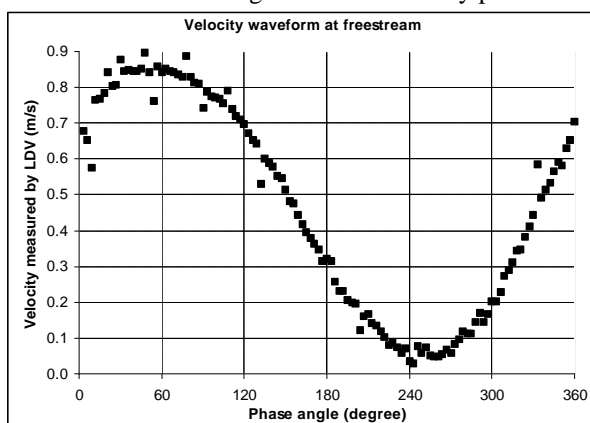
Figure 4-30 Velocity waveform of the oscillatory flow at the free stream

63

4.4   Introductions to PIV Velocity Results

Some special definitions used in this chapter and general instructions on the figures presented in this chapter are given below.

4.4.1   Definitions of PIV velocity

The Particle Image Velocimeter (PIV) system used in the measurement was a 2D Velocimeter. Two velocity components of the target flow were obtained at the same time in the measurement. One of them was named as mainstream velocity; the other was named as vertical velocity.

1.   Mainstream velocity

Mainstream velocity was the velocity component of the flow in the mainstream direction. It was horizontal and was parallel to the centreline of the test duct; it was denoted as *u*; it was the dominant velocity in all cases.

2.   Vertical velocity

Vertical velocity was the velocity component of the flow in vertical direction, and which was normal to the mainstream velocity. It was the minor velocity for the flow discussed in this thesis; it was denoted as *v*.

3.   Velocity phase shift

*Velocity phase shift* was the phase difference between the velocities at two different physical locations. The most important velocity phase shift discussed in the thesis was the phase difference between the velocity of centreline and the velocity near to the boundary wall.

4.   Instant velocity profile

Instant velocity profile was the velocity distribution of points with different heights (vertical coordinates) and the same horizontal coordinate in a PIV picture. All points in an instant velocity profile were located on the same vertical line.

5.   Space averaged velocity profile

Space averaged velocity profile was obtained by averaging all instant velocity profiles got in one PIV picture. It was taken as the velocity profile of the PIV picture (refer to Figure 3-7).

Mass oscillation was assumed for the oscillatory flow discussed in this thesis. This was the base on which space average of velocity was carried out.

6.   Phase averaged velocity profile

Phase averaged velocity profile was obtained by averaging all space averaged velocity profiles that have the same oscillatory phase angle in a series of PIV pictures taken from a oscillatory flow. It was taken as the velocity distribution of a flow regime at the phase angle (refer to Figure 3-8).

7.   Initial phase angle

Initial phase angle was the phase angle of the flow at the instant when the first pair of PIV pictures was taken. It was denoted as *F0* (as $\boldsymbol{j}_0$) in the velocity profile figures presented below.

The initial phase angle varied from flow regime to flow regime. This was due to that the PIV measurement was not triggered at the same phase angle for different oscillatory flow regimes. The flow velocity, flow-travelling time in certain distance varied from flow regime to flow regime. It was difficult to trigger the PIV measurement at exactly the same phase angle for all oscillatory flow regimes.

4.4.2 Instructions on the figures

To show the flow velocity from PIV, normally a pair of figures was presented. One was the velocity profile. The other was the velocity by phase angle, or the velocity waveform.

For each flow regime, *W* periods of oscillatory flow were measured; *K* points were captured on each period; a PIV picture was meshed into *M* cells in horizontal direction and *N* cells in vertical direction. *W* and *K* were different from flow regime to flow regime. *M* and *N* were *30* in all cases shown below.

- Total number of PIV pictures taken for a flow regime in one session was: *W* * *K* (pairs).
- Total number of cells in one PIV picture: *M* * *N*. There were *M* * *N* velocity vectors for each velocity component in a PIV picture. All velocity vectors of each velocity component in a PIV picture built up the corresponding velocity vector field.
- There were *M* instant velocity profiles in a PIV picture, *N* points on each profile.
- There were *K* phase averaged velocity profiles for a flow regime. There were *W* * *K* space averaged velocity profiles in one oscillatory period.
- The phase angle interval between two adjacent sampling points in an oscillating period was *360° / (K + 1)*.

1. Velocity profile figures

Velocity profile figure was composed of phase averaged velocity profiles in one test session. It was drawn in a 2D chart.

- The *x-axis* was the velocity magnitude in *m/s* and *z-axis* was the height of the test duct in *mm*.
- The legends of the figure were the relative phase angles of the velocity profiles shown. The phase angles of the *K* profiles in one figure changed from *F0* to *K * 360° / (K + 1) + F0*.
- *K* profiles were shown in the figure, with a phase interval of *360° / (K + 1)* in between two adjacent profiles. There were *N* points on each profile.
- It was assumed that the velocity profile of upper half of the duct was symmetry to that of the lower half, so only the velocity profile of the lower half, i.e., from the height of 0 to the height of about 178 mm, is shown.
- Each velocity profile in the figure was obtained by averaging *W* same-phase-profiles from *W* PIV pictures, and each same-phase-profile was obtained by space averaging of *M* instant profiles in one PIV picture.
- In the practical measurement carried out, the minimum value of *K* was 15, the maximum value of *K* was 30. If all the velocity profiles got for one flow regime were presented in one chart, there would be 15 – 30 velocity profiles in one chart and 30 points on each profile. It was easy to be confused with so much information in one figure. In this chapter, only a simplified version is presented and about 1/3 of velocity profiles got from PIV are shown in each figure, except the one for steady flow. A full version of the velocity profiles from PIV is presented in the Appendix D, in the same order, under the same headings as those of this chapter. A dimensionless version of the velocity profiles from PIV is presented in the Appendix E in the same order, under the same headings as those of this chapter

  Refer to Appendix D and E for details.

Example of velocity profile figure:

Simplified version: Figure 4-36 Velocity profiles at amp=10%

Corresponding full version: Figure D-1 Velocity profile with amp=10%

Corresponding dimensionless version: Figure E-1 Velocity profile with amp=10%

2. Velocity by phase angle

Velocity by phase angle was obtained by rearranging the data in velocity profile figures. It was built up by putting the velocities of the same space point at different phase angles of the oscillatory flow into a waveform. It was the result of the space average and the phase average too. It was drawn in a 2D chart.

- The *x-axis* was the sequence number of phase angle points, 1 to *K*, corresponding to the phase angle from *F0* to *K * 360° / (K + 1) + F0* as mentioned above. The *z-axis* was the velocity of the space point at the phase angle.

- The legends were the heights (vertical coordinates) of the space points in the test duct, of whose velocity waveforms were shown. The first point was the boundary wall and its velocity was set to zero always. The last point was located close to the centre of the test duct. The distance between two adjacent points was 6.2 mm.

- *N* waveforms of velocity were shown in one figure. Each waveform was corresponding to a physical point in the test duct. Each waveform was composed of *K* points.

- The starting point on each waveform had a phase angle of *F0* and the phase angle of the last point on each waveform was *K * 360° / (K + 1) + F0*.

- To keep consistent with the figure of velocity profile, the velocity waveform presented in this chapter is also a simplified version, i.e., only 1/3 of waveforms at different space points are shown in each figure of velocity by phase angle. A full version with all waveforms included from different space points (30 points) is shown in Appendix D, in the same order, under the same headings as those of this chapter.

  Refer to Appendix D for details.

Example of velocity by phase angle:

  Simplified version: Figure 4-37 Velocity waveforms at amp=10%

  Corresponding full version: Figure D-2 Velocity by phase angle (amp=10%)

3. Velocity vector field

Velocity vector field was obtained by meshing a PIV picture into small cells and presenting the velocity of each cell as a vector. This was the primitive result from the PIV picture, on which velocity profile and velocity by phase were based.

The *x-axis* of velocity vector field was the horizontal coordinate along the tunnel and *z-axis* was the height of the point in the test duct or its vertical coordinate. There were *M * N* velocity vectors in a velocity vector field. The arrow of the vector showed the direction of the velocity. Both the colour and the length of the arrow displayed the magnitude of the velocity.

Example of velocity vector field: Figure 4-31.

4.5 PIV Velocity of Steady Flow

As an example and reference for further analysis, velocity of stationary flow was measured first by PIV. During the different stages of the measurement, stationary flows were always measured as verifications to the configuration of the rig.

A series of steady flows was always measured continuously, with the pump load ranged from 10—100% of the full pump load, flow velocity ranged from 0.08 m/s to 0.8 m/s. The results from one test series are shown below.

For stationary flow measurements with PIV, *W = 50* (sample number), *K = 1*.

Figure 4-31 is an example of the vector field of the mainstream velocity from a PIV picture. It is shown in the figure that generally the amplitude of velocity increased along with the height (vertical coordinate), with random fluctuations. The velocity was not constant everywhere along a horizontal line of the vector field in some cases. Velocity fluctuates in both horizontal and vertical directions.

Figure 4-32 is an example of the vector field of the vertical velocity from the same PIV picture.

The maximum, minimum, and mean mainstream velocity by PIV and the Reynolds number of the series of steady flows are listed in Table 4-5. The Reynolds number was only based on the mainstream velocity by PIV. The relation between the mean mainstream velocity and the pump load was found to be:

(4-12) $$U = 0.0079 \cdot Amp$$

Table 4-5 Velocities of the flow

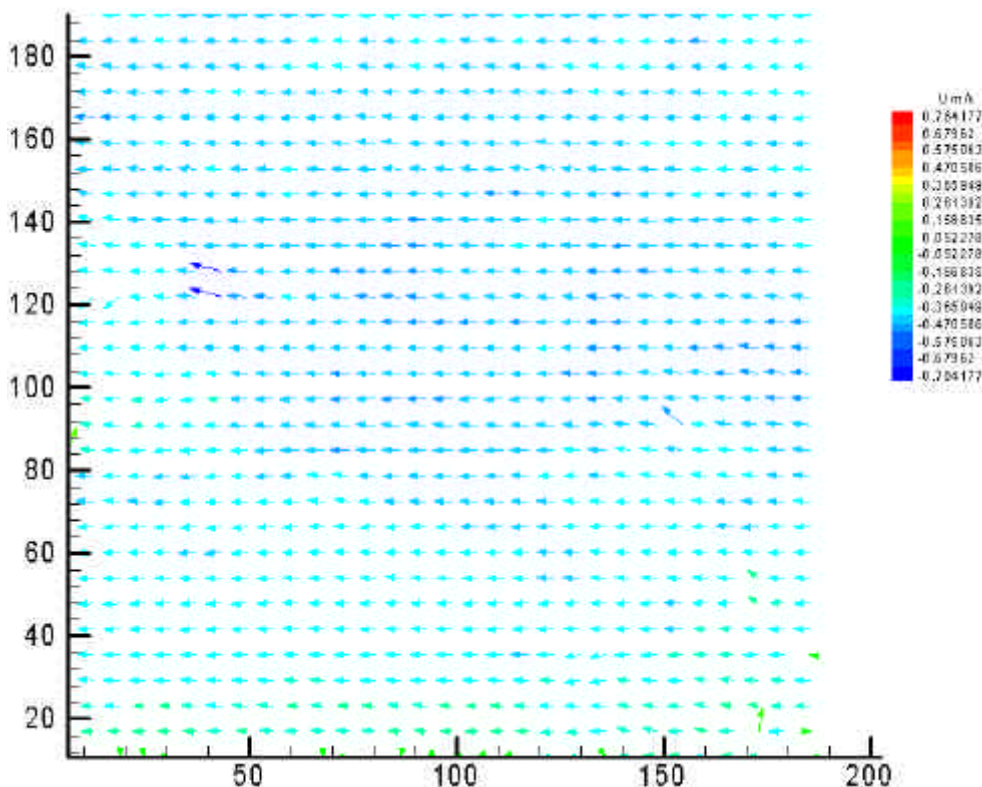| Amp (%)	10	20	30	40	50	60	70	80	90	100
u_{max} (m/s)	0.12	0.24	0.35	0.43	0.55	0.67	0.71	0.77	0.82	0.81
u_{min} (m/s)	0.02	0.01	0.03	0.04	0.06	0.03	0.05	0.08	0.17	0.20
u_{mean} (m/s)	0.08	0.16	0.27	0.34	0.44	0.52	0.58	0.57	0.73	0.74
Re (10^4)	2.3	4.4	7.2	9.1	11.9	14.0	15.6	15.4	19.5	19.7

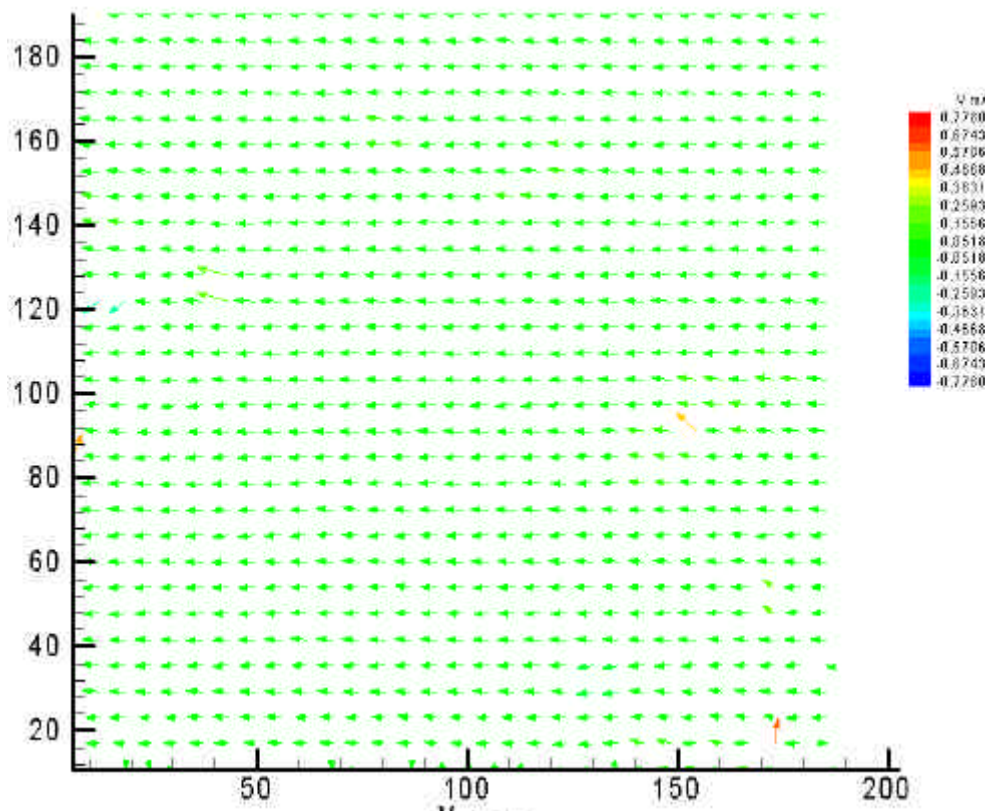Figure 4-31 Example of vector field of mainstream velocity

67

Figure 4-32 Example of vector field of vertical velocity
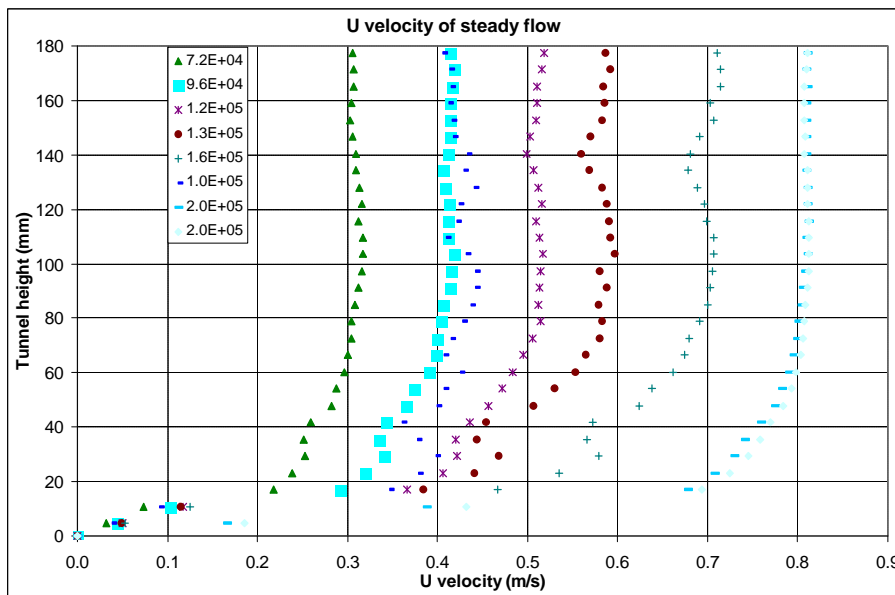

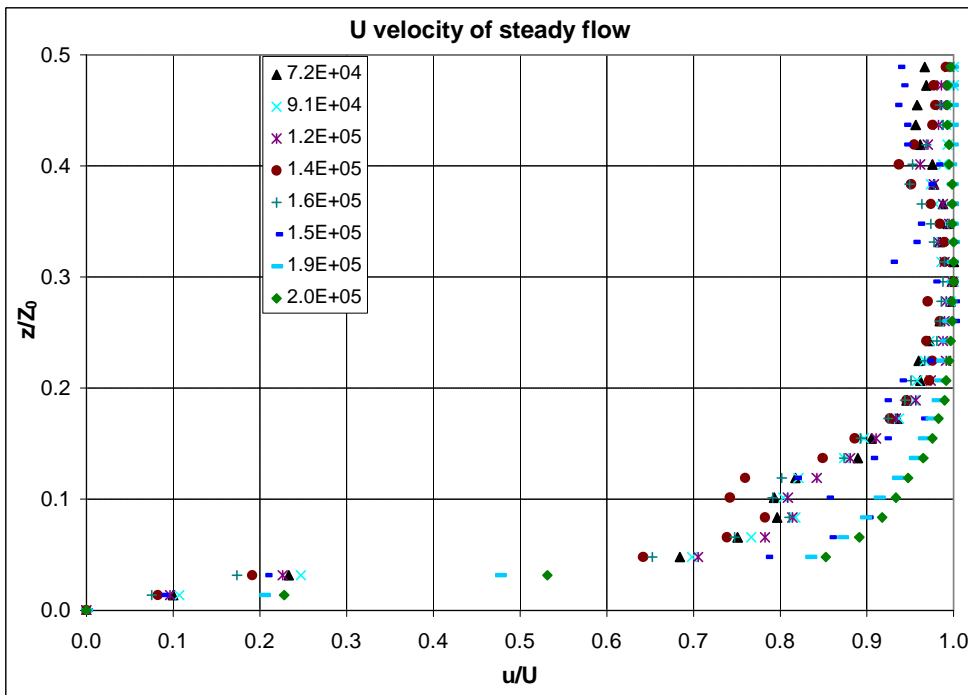Figure 4-33 Mainstream velocity profiles of steady flow

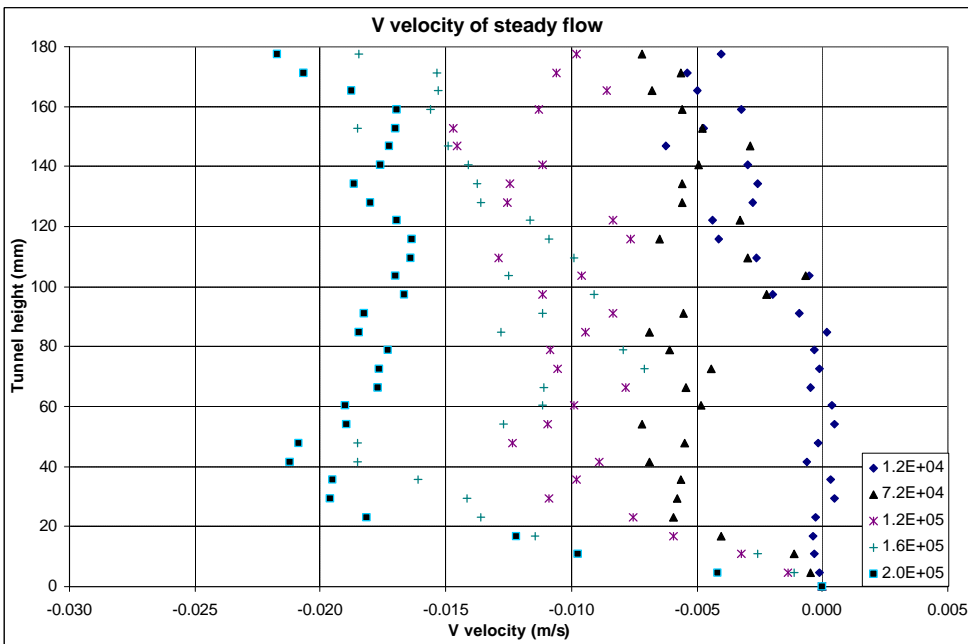Figure 4-34 Dimensionless mainstream velocity of steady flow

Figure 4-35 Vertical velocity profiles of steady flow (Fewer profiles are shown for vertical velocity to make the figure readable)

The velocity profiles of stationary flows measured are shown in Figure 4-33 to Figure 4-35. Each profile in Figure 4-33 to Figure 4-35 is the velocity distributions of a flow regime, i.e., a stationary flow with identical flow rate. This is different from the velocity profile figure for oscillatory flow shown later, in which all profiles in one figure are from the same oscillatory flow regime.

Each profile in Figure 4-33 to Figure 4-35 was obtained by averaging 50 pairs of PIV pictures taken continuously, i.e., by averaging 50 space averaged profiles. The sampling rate of PIV was 1Hz for the cases shown. The sampling time for a flow regime was 50 s. The legends in Figure 4-33 to Figure 4-35 are marked as the Reynolds numbers as listed in Table 4-5.

Figure 4-33 shows the absolute mainstream velocity profiles by PIV.

Figure 4-34 shows the dimensionless mainstream velocity profiles by PIV. z is the height of the point in vertical direction, from the bottom of the test duct; Z_0 is the total height of the duct, $Z_0 = 350$ mm for the test duct with roughness inner layer; u is the instant velocity of the point; U is the maximum velocity of the flow tested (u_{max} in Table 4-5).

Figure 4-35 is the profiles of vertical velocity of the same stationary flows.

Only the lower half of velocity profile is shown in Figure 4-33 to Figure 4-35 for velocity symmetry about the centreline was assumed along the tunnel height.

From Figure 4-34 to Figure 4-35 we can see:
- For all cases shown, the velocity was smaller than 50% of the maximum velocity only in the narrow area near to the boundary wall, which took less than 5% of the tunnel height.
- The mainstream velocity was close to the maximum value of velocity for more than 80% of the tunnel height.
- At least in the time of the sampling period, the velocity profiles were not straight flat and smooth, though the variation was only about 3-5% of the maximum mainstream velocity.
- The vertical velocity was quite small generally. It always fluctuated around zero point. The fluctuating range was smaller for points near to the wall and becoming larger and larger when the points were nearer to the centreline of the test duct. The vertical velocity increased along with the tunnel height too.

4.6 PIV Velocity of Pure Oscillatory Flow

As defined in the Chapter 1.1.2, Pure Oscillatory Flow was the oscillatory flow without base stationary flow (bulk flow). It was oscillating around the zero point, or *x-axis* in a 2D coordinate system

About 60 flow regimes of Pure Oscillatory Flow were measured. It is difficult to present all the velocity profiles and waveforms from PIV measurement in this thesis. Only examples of the test results are shown below.

4.6.1 Velocity of constant frequency and variable amplitude

Examples of measured mainstream velocity *u* with different oscillating amplitude are shown in Figure 4-36 to Figure 4-53. Followings are the summary of the flow specifications:
- Oscillatory frequency: 0.01 Hz
- Oscillatory amplitude: 10% -- 90% of the full pump load, 9 amplitudes were measured. i.e., 9 flow regimes were measured.

– Maximum velocity range: 0.069– 1.029 m/s, detail velocity statistics is listed in Table 4-6:

Table 4-6 Specific velocities of the flows

Amp (%)	10	20	30	40	50	60	70	80	90
u_{max} (m/s)	0.07	0.17	0.24	0.34	0.46	0.57	0.69	0.80	1.03
u_{min} (m/s)	-0.07	-0.18	-0.26	-0.35	-0.49	-0.59	-0.74	-0.86	-0.96
u_{mean} (m/s)	0.00	0.00	0.00	-0.01	0.00	-0.01	0.00	-0.04	0.01

– Maximum flow rate range: 5.3 – 79.2 l/s, detail flow rate statistics is listed in Table 4-7:

Table 4-7 Specific flow rates of the flows

Amp (%)	10	20	30	40	50	60	70	80	90
Q_{max} (l/s)	5.31	12.86	18.29	26.53	35.59	43.68	53.12	61.35	79.23
Q_{min} (l/s)	-5.06	-13.49	-20.27	-27.09	-37.48	-45.31	-57.03	-66.30	-73.96
Q_{mean} (l/s)	0.07	-0.23	0.19	-0.49	0.18	-0.71	-0.15	-3.14	0.55

– Number of PIV pictures taken in one session: 125 pairs

– Number of PIV pictures taken in each oscillatory period: K = 25 pairs

– Total measuring time: W = 5 oscillatory periods (500 seconds)

A pair of figures is shown for each flow regime. One is the velocity profile from the tunnel bottom to the tunnel centre. The other is the velocity waveform at different vertical locations of the test duct. For example, Figure 4-36 is the velocity profiles of flow with oscillating amplitude of 10% of the full pump load, frequency of 0.01Hz; and Figure 4-37 is the velocity by phase angle of the same flow. There are 25 profiles in each profile figure (1/3 are shown in the simplified version). There are 30 points on each profile. There are 30 waveforms in each figure of velocity by phase (1/3 are shown in the simplified version). There are 25 points on each waveform. Phase interval between two profiles in profile figure and two points on waveform is 14.4° (as mentioned above, simplified version of velocity profile and waveform is presented in this chapter, in which the phase interval is times of 14.4°, due to the omission of profiles and waveforms in between. A full version of the figures is available in Appendix D).

Figure 4-36 Velocity profiles at amp=10%, f_r=0.01Hz

Figure 4-37 Velocity waveforms at amp=10%, f_r=0.01Hz

71

Figure 4-38 Velocity profiles at amp=20%, f_r=0.01Hz

Figure 4-39 Velocity waveforms at amp=20%, f_r=0.01Hz

Figure 4-40 Velocity profiles at amp=30%, f_r=0.01Hz

Figure 4-41 Velocity waveforms at amp=30%, f_r=0.01Hz

Figure 4-42 Velocity profiles at amp=40%, f_r=0.01Hz

Figure 4-43 Velocity waveforms at amp=40%, f_r=0.01Hz

Figure 4-44 Velocity profiles at amp=50%, f_r=0.01Hz

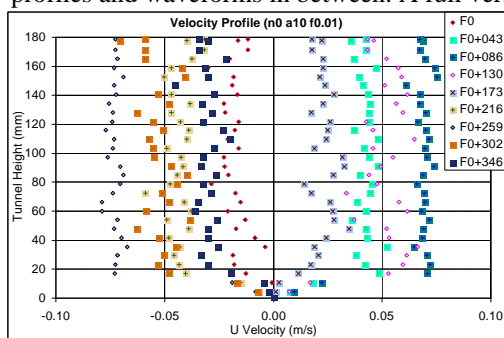Figure 4-45 Velocity waveforms at amp=50%, f_r=0.01Hz
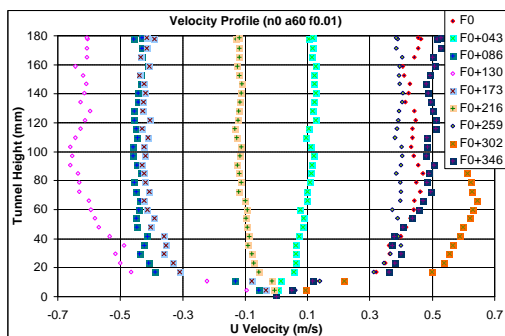
Figure 4-46 Velocity profiles at amp=60%, f_r=0.01Hz
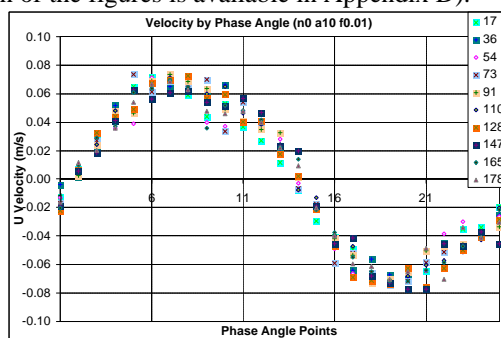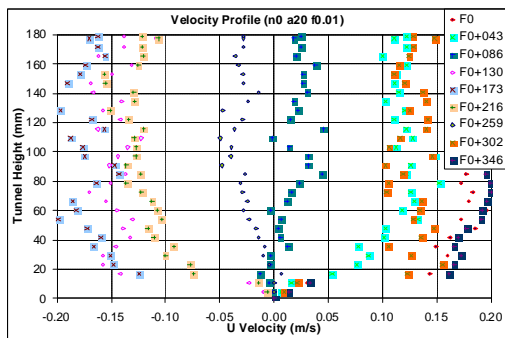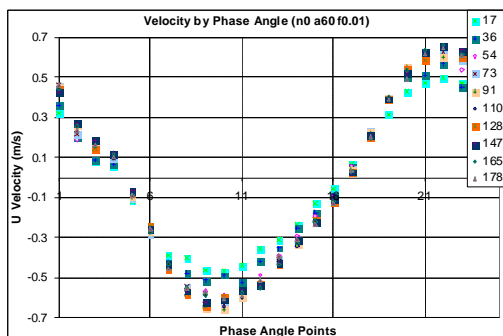

Figure 4-47 Velocity waveforms at amp=60%, f_r=0.01Hz
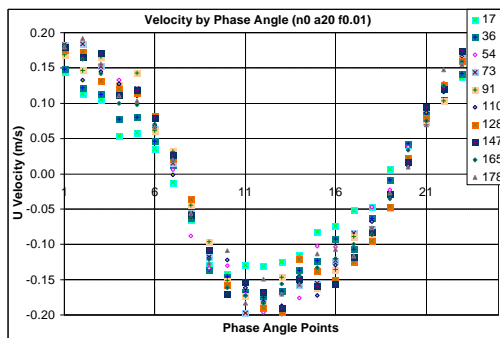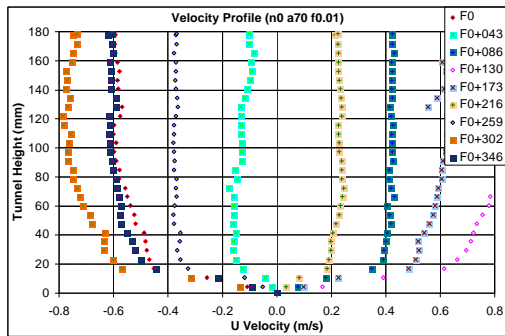

Figure 4-48 Velocity profiles at amp=70%, f_r=0.01Hz
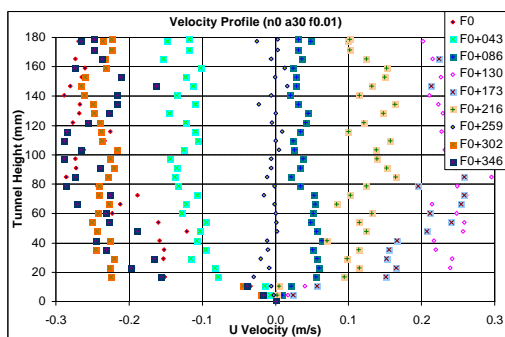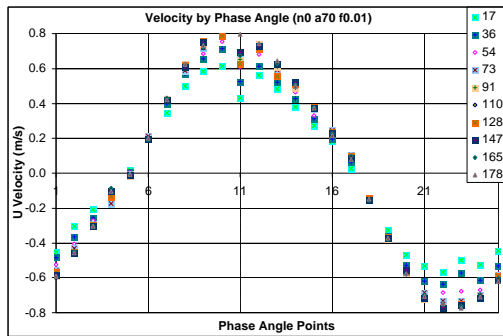

Figure 4-49 Velocity waveforms at amp=70%, f_r=0.01Hz
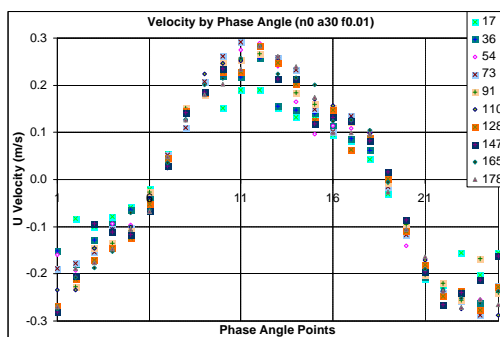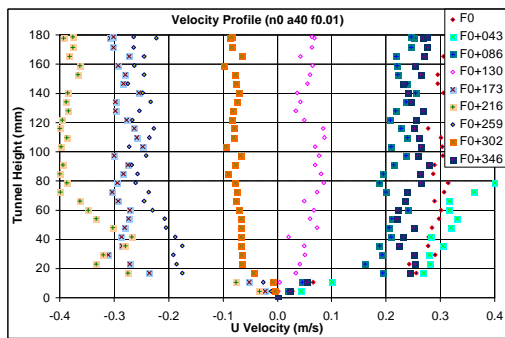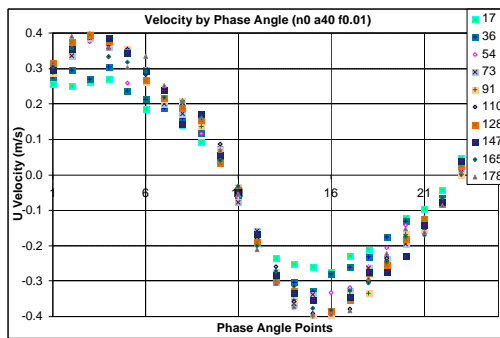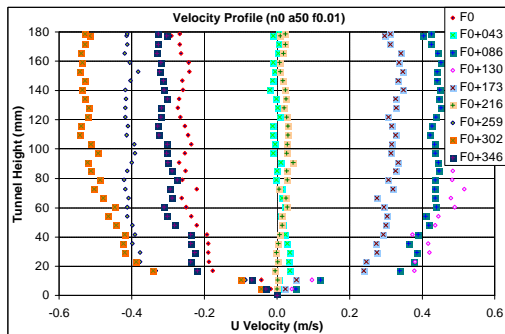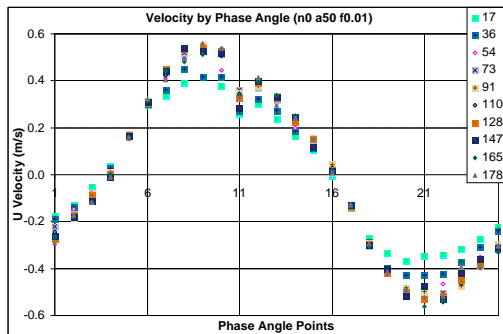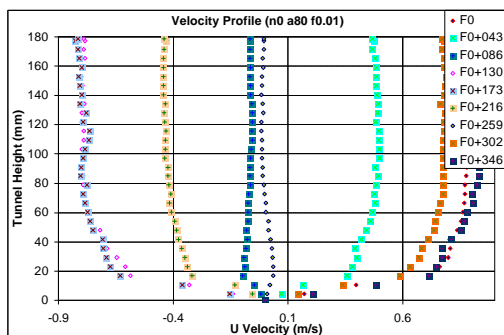
Figure 4-50 Velocity profiles at amp=80%, f_r=0.01Hz
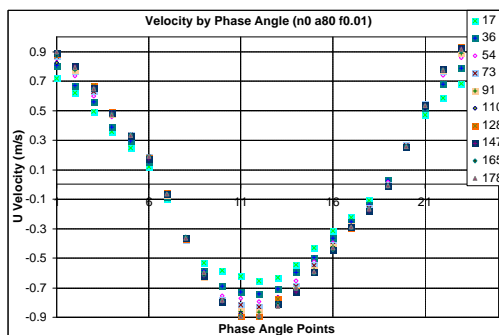
Figure 4-51 Velocity waveforms at amp=80%, f_r=0.01Hz
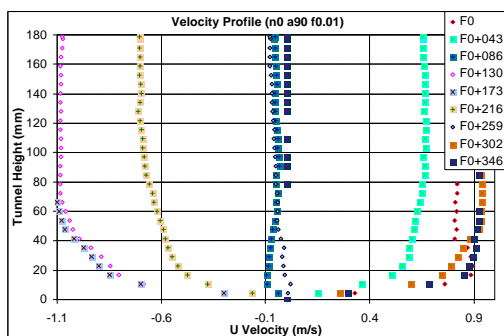
Figure 4-52 Velocity profiles at amp=90%, f_r=0.01Hz
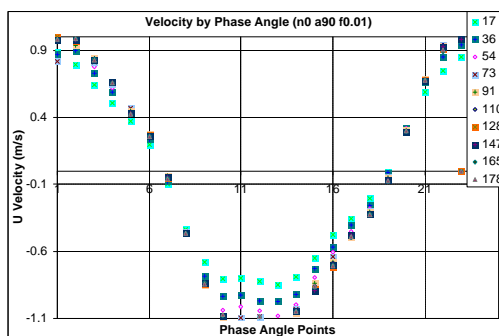
Figure 4-53 Velocity waveforms at amp=90%, f_r=0.01Hz

It is shown from Figure 4-36 to Figure 4-53 that:

- At lower flow rate, the velocity profile was not as smooth as that of the higher flow rate. The flow was more dominant by the mainstream at higher flow rate. The fluctuation played more roles relatively at the lower flow rate.

- At higher flow rate, the velocity profiles were more flat. The velocity profiles wer more parabolic at lower flow rate. When the oscillatory amplitude was higher, the velocity profile was quite flat and smooth even though at the phase angles when the absolute velocity magnitude was quite small.

- At the oscillatory frequency of 0.01 Hz, annular effect (Richardson E.G, 1929 [19] and Schlichting Hermann, 1979 [22]) was not obvious in all cases shown. This was due to that the velocity changed direction very slowly and the flow in one direction vanishes completely before the flow in another direction was developed.

- In all cases shown, only the velocity in the area very close to the boundary wall was small. The velocity increased very fast after that (about 10 mm from the wall).

- In all cases shown, the velocity waveform at any vertical location was single frequency harmonic wave, exactly similar to the control waveform of water supply pumps.

- The phase change of velocity from the point close to the wall to the point near to the centreline at the same time instant was insignificant.

− The velocity shown for pure oscillatory flow was not symmetric across the zero velocity. This was resulted from the unsymmetrical layout of the rig. The distances from two pumps to the sampling point were not equal.

4.6.2 Velocity of variable frequency and constant amplitude

To display the influence of oscillatory frequency on the velocity, velocity profiles and velocities by phase angle for different oscillatory frequencies are shown in Figure 4-54 to Figure 4-59.

− Figure 4-54 and Figure 4-55 are the velocity profiles and velocity waveforms of pure oscillatory flow with frequency of 0.05Hz, amplitude of 50% of the full pump load. K = 20, W = 5, sampling rate is 1Hz, sampling time is 100 s, phase interval is times of 18° for the simplified version.

− Figure 4-56 and Figure 4-57 are the velocity profiles and velocity waveforms of pure oscillatory flow with frequency of 0.10Hz, amplitude of 50% of the full pump load. K = 25, W = 5, sampling rate is 2.5Hz, sampling time is 50 s, phase interval is times of 14.4° for the simplified version.

− Figure 4-58 and Figure 4-59 are the velocity profiles and velocity waveforms of pure oscillatory flow with frequency of 0.50Hz, amplitude of 50% of the full pump load. K = 30, W = 4, sampling rate is 15Hz, sampling time is 8 s, phase interval is times of 12° for the simplified version.

− The velocity profiles and velocity waveforms for similar flow with frequency of 0.01 Hz were already shown in Figure 4-44 and Figure 4-45.

Figure 4-54 Velocity profiles of 0.05Hz, amp=50%
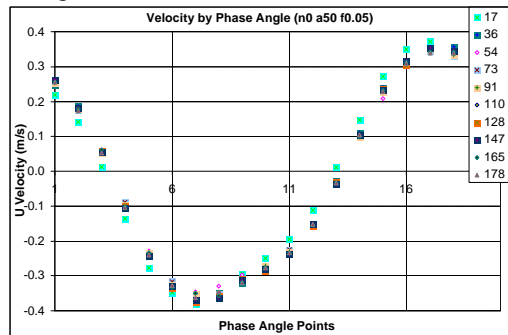
Figure 4-55 Velocity waveforms of f_r=0.05Hz, amp=50%
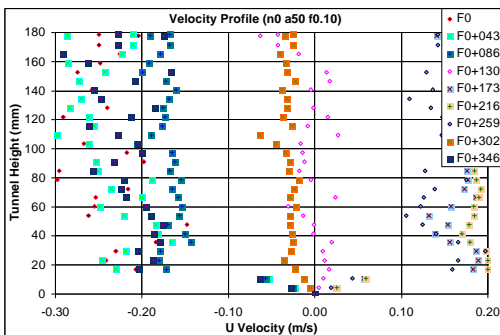
Figure 4-56 Velocity profiles of 0.10Hz, amp=50%

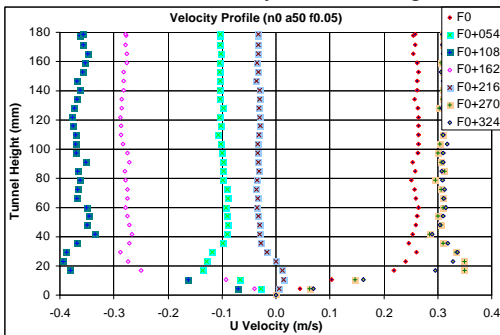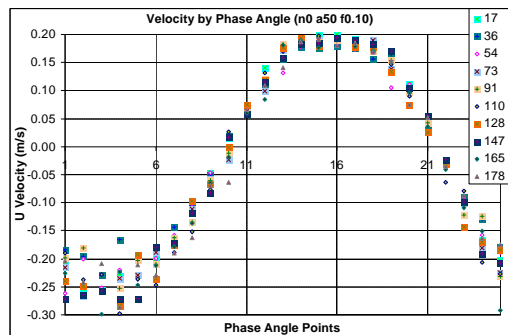
Figure 4-57 Velocity waveforms of f_r=0.10Hz, amp=50%

75
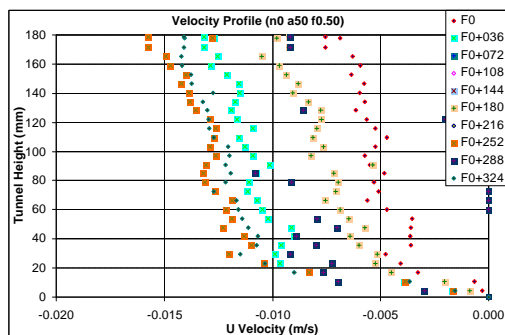
Figure 4-58 Velocity profiles of 0.50Hz, amp=50%
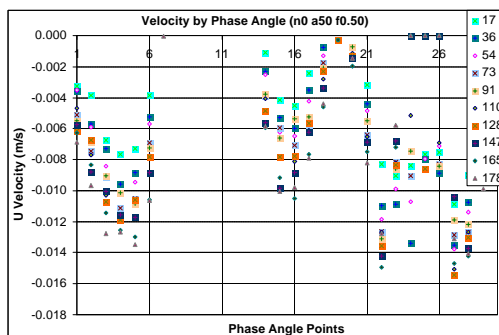
Figure 4-59 Velocity waveforms of f_r=0.50Hz, amp=50%

Comparing the velocity shown in Figure 4-54 to Figure 4-59 to the velocity shown in Figure 4-44 and Figure 4-45, it is noted that:

−   The annular effect was observed in most cases shown in Figure 4-54 to Figure 4-59. Generally, the higher of the maximum velocity, the more obvious the annular effect was. The complex actions of oscillatory frequency and amplitude determined the magnitude of the annular effect.

−   Thought the input oscillatory amplitude to the pumps kept unchanged for the flows shown in Figure 4-44, Figure 4-54, Figure 4-56 and Figure 4-58, the actual maximum velocity decreased along with the increase of frequency. For the highest oscillatory frequency shown, $f_r = 0.50$ Hz, the flow was almost stand still, only with velocity lower than 0.01 m/s, which was about 1/40 of that of for $f_r = 0.01$ Hz. When the oscillating frequency was high enough, the flow could not be fully developed in one direction before it was forced to run in another direction. The maximum velocity reached at higher frequency was smaller, comparing with that of the flow at lower oscillatory frequency. More discussion on this is presented in the next chapter.

−   The velocity waveform at any location was harmonic wave when the oscillatory frequency was lower than 0.10 Hz (included). The velocity waveform was complex when the oscillatory frequency was 0.50Hz. The reason was unclear.

−   For all frequencies shown, the phase change of velocity from the point near to the wall to the point near to the centreline at the same time instant was insignificant.

4.6.3 Vertical velocity

Examples of vertical velocity in the flow for different amplitudes of pump input are shown in Figure 4-60 to Figure 4-63.

−   Figure 4-60 is the velocity profiles of flow with oscillating amplitude of 60% of the full pump load, frequency of 0.01Hz, corresponding to the flow of Figure 4-46. 25 profiles are shown in the figure, with a phase interval of 14.4° in between two adjacent profiles; Figure 4-61 is the velocity by phase angle of the same flow. 25 waveforms of velocity are shown in the figure for different vertical locations in the test duct. This figure is corresponding to Figure 4-47.

−   Figure 4-62 is the velocity profiles of flow with oscillating amplitude of 90% of the full pump load, frequency of 0.01Hz, corresponding to the flow of Figure 4-52. 25 profiles are shown in the figure, with a phase interval of 14.4° in between two adjacent profiles; Figure 4-63 is the velocity by phase angle of the same flow. 25 waveforms of

velocity are shown in the figure for different vertical locations in the test duct. This figure is corresponding to Figure 4-53.

− The parameters mentioned above are for the full version of figures shown in Appendix D. The simplified version shown here has 1/3 of profiles and waveforms respectively.
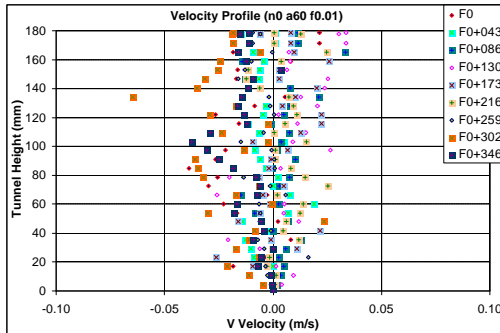
Figure 4-60 Profiles of velocity *V* at amp=60%, f_r=0.01Hz
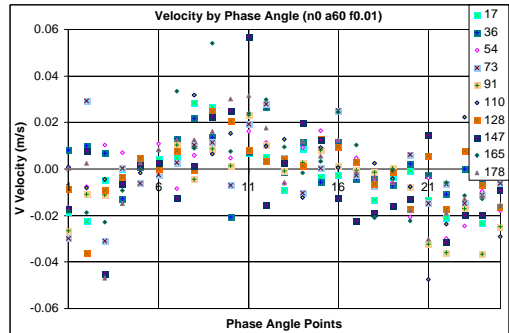
Figure 4-61 Waveforms of velocity *V* at amp=60%, f_r=0.01Hz
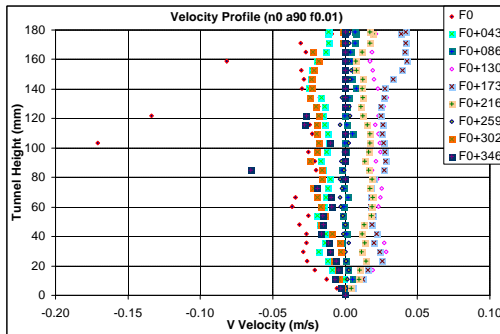
Figure 4-62 Profiles of velocity *V* at amp=90%, f_r=0.01Hz
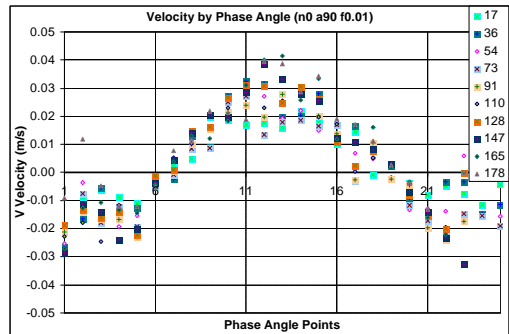
Figure 4-63 Waveforms of velocity *V* at amp=90%, f_r=0.01Hz

It is shown from Figure 4-60 to Figure 4-63 that:

− The magnitude of velocity in the vertical direction was quite small. All velocities distributed around the zero point.

− The general distribution tendency of vertical velocity was similar to that of the mainstream velocity. Annular effects could be observed at some phase angles.

− The vertical velocity was also in harmonic waveform, though the amplitude was quite small.

− The phase of the vertical velocity was different from that of mainstream velocity for 180°.

4.6.4 Summary of PIV velocity for pure oscillatory flow

From the measured results shown above, it is summarized that:

− The velocity of pure oscillatory flow varied across the zero point.

− Both velocity components were harmonic waveform with a single frequency; both velocity components increased from the boundary wall to the centreline of the duct and

fluctuated along a horizontal line. Velocity increased very fast vertically in the close to boundary region. The velocity was close to mainstream maximum velocity in more than 80% of the duct height.

- Velocity profile depended on both the oscillatory frequency and amplitude. For bigger oscillatory amplitude, the velocity profile was more flat, though at the phase angle where the absolute velocity was small.

- Annular effect was resulted from the comprehensive actions of oscillatory frequency and amplitude.

4.7 PIV Velocity of Combined Oscillatory Flow

We defined in the Chapter 1.1.2 that Combined Oscillatory Flow was the oscillatory flow with nonzero base stationary flow (bulk flow). It oscillates around the base stationary flow, or bulk flow. This flow regime was more practical in engineering applications.

Combined Oscillatory Flow took the most part of measurements that carried out; about 250 flow regimes of Combined Oscillatory Flow were measured. It is difficult to present all the velocity profiles and waveforms from PIV measurement in this thesis. Only typical examples of the test results are shown below.

4.7.1 Velocity of variable amplitude, constant base flow and frequency

In this section, measuring results of following flows are presented:
- Oscillatory frequency: 0.10 Hz
- Base stationary flow: 40% of full pump load
- Oscillatory amplitude: 10% -- 60% of the full pump load, 6 amplitudes was measured, i.e., 6 flow regimes were tested.
- Maximum velocity: 0.439– 0.741 m/s, detail velocity statistics is listed in Table 4-8:

Table 4-8 Velocities of the flow

Amp (%)	10	20	30	40	50	60
u_{max} (m/s)	0.44	0.50	0.58	0.67	0.74	0.74
u_{min} (m/s)	0.34	0.30	0.30	0.29	0.28	0.23
u_{mean} (m/s)	0.39	0.39	0.43	0.46	0.49	0.49

- Maximum flow rate range: 33.84 – 57.03 l/s, detail flow rate statistics is listed in Table 4-9:

Table 4-9 Flow rate of the flow

Amp (%)	10	20	30	40	50	60
Q_{max} (l/s)	33.84	38.79	44.82	51.66	56.80	57.03
Q_{min} (l/s)	26.03	23.45	22.82	22.02	21.48	18.09
Q_{mean} (l/s)	29.71	30.40	32.93	35.61	37.83	37.70

- Number of PIV pictures taken in one session: 125 pairs
- Number of PIV pictures in each oscillatory period: $K = 25$ pairs
- Total measuring time: $W = 5$ oscillatory periods (50 seconds)

The velocity profiles and velocity waveforms at different vertical location in the test duct of the flows mentioned above are shown in Figure 4-64 to Figure 4-75. For the full version of velocity profile and waveform figure, which is shown in Appendix D, there are 25 profiles in

78

each profile figure; there are 30 points on each profile; there are 30 waveforms in the figure of velocity by phase; there are 25 points on each waveform; phase interval between two profiles in profile figure and two points on waveform is 14.4°. Only a simplified version of these figures is shown in this chapter, in which 1/3 of profiles or waveforms are shown and the phase interval in between profiles or points on waveforms is times of 14.4°.
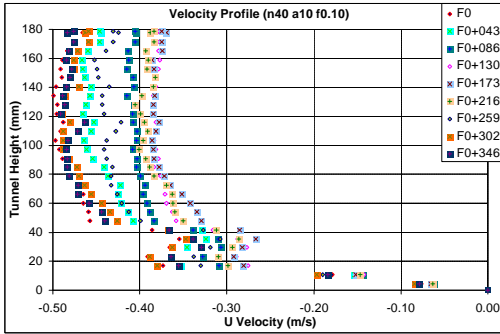
Figure 4-64 Velocity profiles at amp=10%, n_0=40%, f_r=0.10Hz
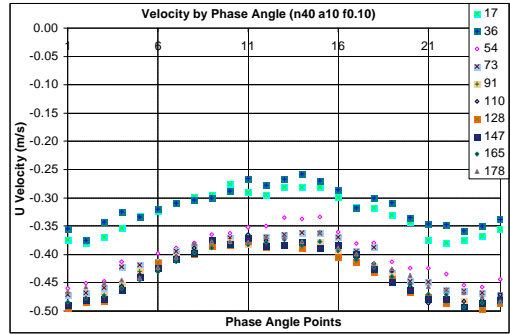
Figure 4-65 Velocity waveforms at amp=10%, n_0=40%, f_r=0.10Hz
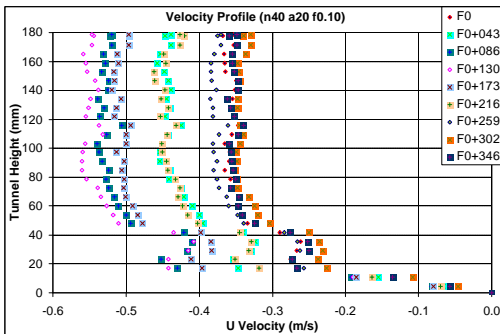
Figure 4-66 Velocity profiles at amp=20%, n_0=40%, f_r=0.10Hz
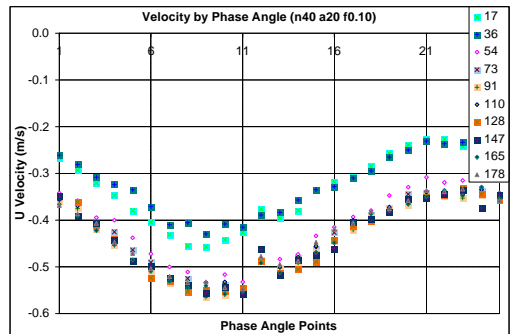
Figure 4-67 Velocity waveforms at amp=20%, n_0=40%, f_r=0.10Hz
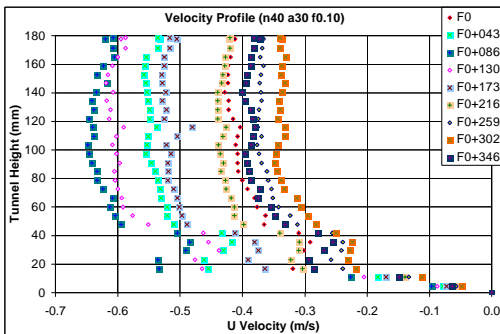
Figure 4-68 Velocity profiles at amp=30%, n_0=40%, f_r=0.10Hz
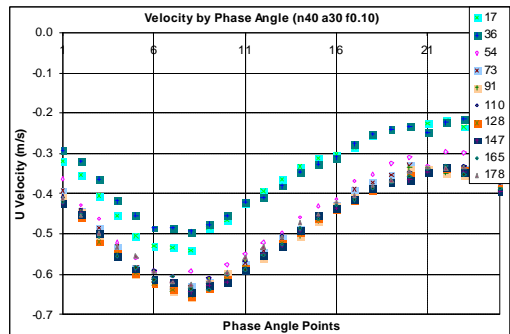
Figure 4-69 Velocity waveforms at amp=30%, n_0=40%, f_r=0.10Hz

79
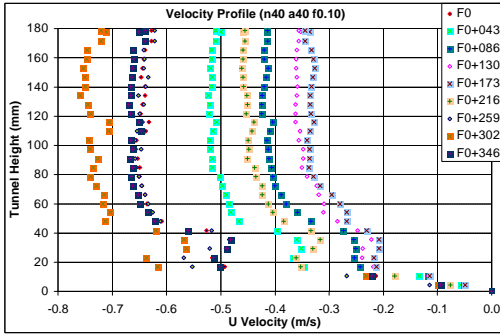
Figure 4-70 Velocity profiles at amp=40%, n_0=40%, f_r=0.10Hz
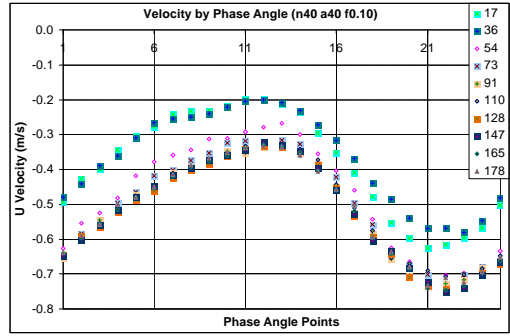
Figure 4-71 Velocity waveforms at amp=40%, n_0=40%, f_r=0.10Hz
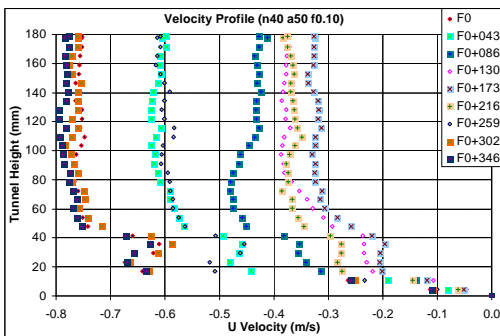
Figure 4-72 Velocity profiles at amp=50%, n_0=40%, f_r=0.10Hz
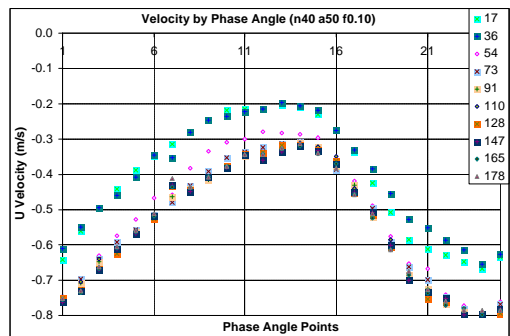
Figure 4-73 Velocity waveforms at amp=50%, n_0=40%, f_r=0.10Hz
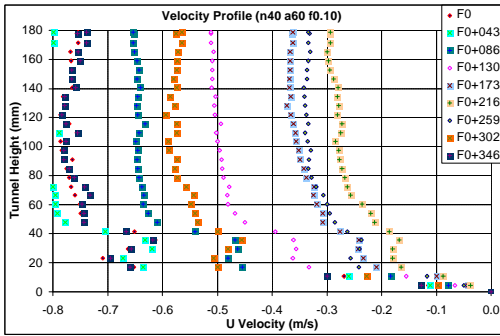
Figure 4-74 Velocity profiles at amp=60%, n_0=40%, f_r=0.10Hz
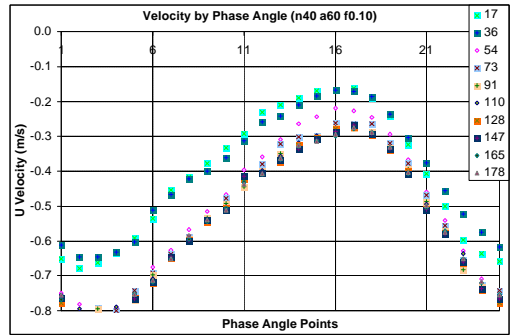
Figure 4-75 Velocity waveforms at amp=60%, n_0=40%, f_r=0.10Hz

It is shown from Figure 4-64 to Figure 4-75 that:

– Generally speaking the velocity profile and waveform of combined oscillatory flow were similar to those of pure oscillatory flow. The difference was that the velocity of pure oscillatory flow oscillated across the zero point and velocity of combined oscillatory flow oscillated around a nonzero value.

– For all cases shown, the velocity waveform at any location in the test duct was always harmonic wave with single frequency.

- Only within the area very close to the boundary wall, the velocity was very low. The velocity increases very fast afterwards to the maximum velocity.
- The flow only ran in one direction, without inverse flow in any case shown, even for the case where oscillatory amplitude was bigger than the stationary base flow, inverse pump input was introduced then.
- General annular effect was not observed in most velocity profiles shown. However, "overshooting" of velocity existed in lot of cases shown, here the "overshooting" was smaller than the maximum velocity in the mainstream, but bigger than the velocity in the nearby area.
- The phase variation of velocity from the point close to the wall to the point near to the centreline at the same time instant was insignificant.

4.7.2 Velocity of variable frequency, constant base flow and amplitude

To show the influence of oscillatory frequency on the velocity of combined oscillatory flow, velocity profiles and velocity waveforms of flows with the same stationary flow level, the same oscillatory amplitude level and different frequencies are shown in Figure 4-76 to Figure 4-83.

The corresponding flows of Figure 4-76 through Figure 4-83 have a stationary base flow level of 40% of the full pump load and oscillatory amplitude level of 30% of the full pump load. The oscillatory frequencies of the flows are ranged from 0.01Hz to 0.50Hz:

- Figure 4-76 and Figure 4-77 are the velocity profiles and velocity waveforms of combined oscillatory flow with frequency of 0.01Hz. $K = 25$, $W = 5$, sampling rate is 0.25Hz, sampling time is 500 s, phase interval is times of 14.4°.
- Figure 4-78 and Figure 4-79 are the velocity profiles and velocity waveforms of combined oscillatory flow with frequency of 0.05Hz. $K = 20$, $W = 5$, sampling rate is 1Hz, sampling time is 100 s, phase interval is times of 18°.
- Figure 4-80 and Figure 4-81 are the velocity profiles and velocity waveforms of combined oscillatory flow with frequency of 0.20Hz. $K = 25$, $W = 5$, sampling rate is 5Hz, sampling time is 25 s, phase interval is times of 14.4°.
- Figure 4-82 and Figure 4-83 are the velocity profiles and velocity waveforms of combined oscillatory flow with frequency of 0.50Hz. $K = 30$, $W = 4$, sampling rate is 15Hz, sampling time is 8 s, phase interval is times of 12°.
- Similar flow for frequency of 0.10Hz was shown in Figure 4-68 and Figure 4-69.
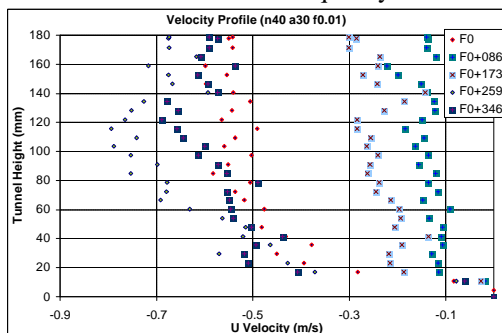
Figure 4-76 Velocity profiles of f_r=0.01Hz , amp=30%, n_0=40% (to make it easier to read, fewer profiles shown)
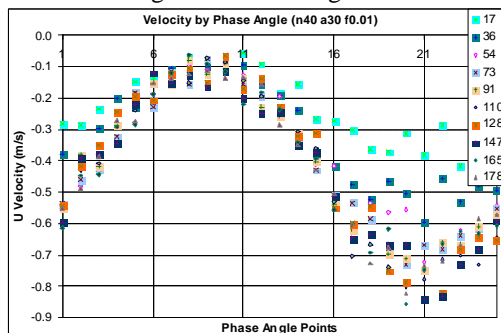
Figure 4-77 Velocity waveforms of f_r=0.01Hz, amp=30%, n_0=40%
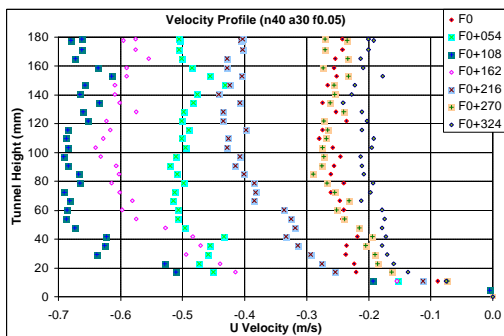
Figure 4-78 Velocity profiles of f_r=0.05Hz, amp=30%, n_0=40%
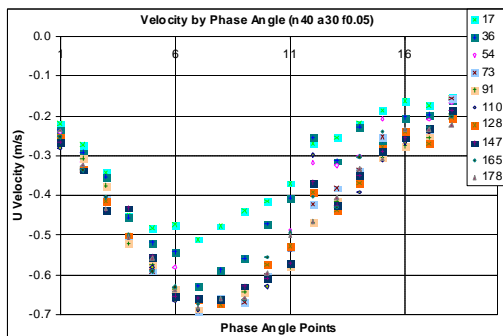
Figure 4-79 Velocity waveforms of f_r=0.05Hz, amp=30%, n_0=40%
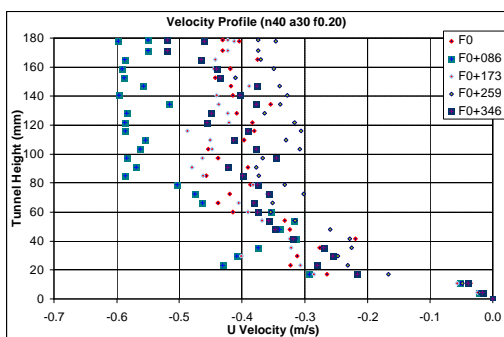
Figure 4-80 Velocity profiles of f_r=0.20Hz, amp=30%, n_0=40% (to make it easier to read, fewer profiles shown)
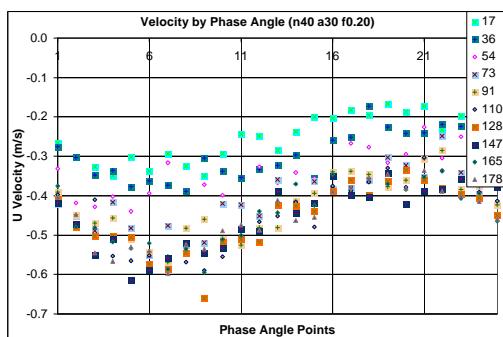
Figure 4-81 Velocity waveforms of f_r=0.20Hz, amp=30%, n_0=40%
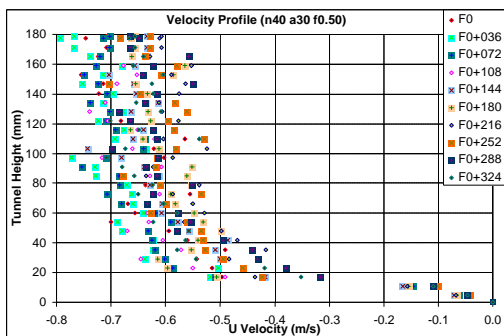
Figure 4-82 Velocity profiles of f_r=0.50Hz, amp=30%, n_0=40%
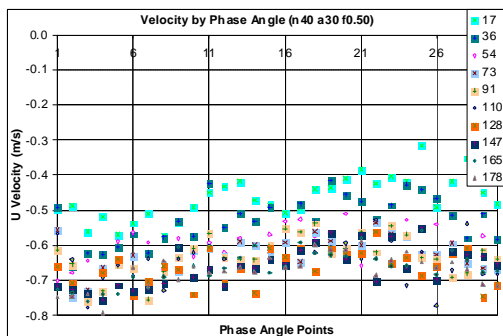
Figure 4-83 Velocity waveforms of f_r=0.50Hz, amp=30%, n_0=40%

It is shown from Figure 4-76 to Figure 4-83, Figure 4-68 and Figure 4-69 that:

− The general shapes and developing tendencies of the velocity profiles and waveforms were similar to those shown in the previous section. Most of the points concluded from the previous section were valid and will not be discussed again here.

- At lower oscillatory frequency, the velocity varied across a relative wide range in an oscillating period, and at higher frequency the velocity only varied within a relative narrow range in an oscillating period.
- The same as the results from pure oscillatory flow, when the oscillating frequency was sufficient high, the flow could not be developed sufficiently in any direction before it was forced to change directions. The absolute velocity of flow became smaller along with the increase of frequency even though the input levels to the pumps were constant.

4.7.3 Velocity of variable base flow, constant frequency and amplitude

To show the influence of base flow level on the velocity of combined oscillatory flow, velocity profiles and velocity waveforms of flows with the same oscillatory frequency, the same oscillatory amplitude level and different base flow levels are shown in Figure 4-84 to Figure 4-93. Both the oscillatory amplitude level and the base flow level here refer to the pump load input level.

The corresponding flows of Figure 4-84 to Figure 4-93 have an oscillatory amplitude level of 40% of the full pump load and oscillatory frequency of 0.10Hz. The stationary base flow levels are ranged from 10% to 60%, except 40%, results of which are shown in Figure 4-70 and Figure 4-71. Other specifications of these flows are the same as the flows of the same frequency presented in the previous sections.
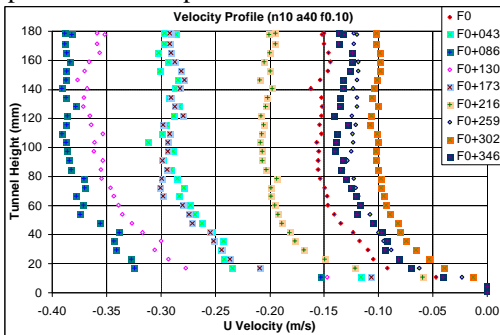
Figure 4-84 Velocity profile of n_0=10%, amp=40%, f_r=0.10Hz
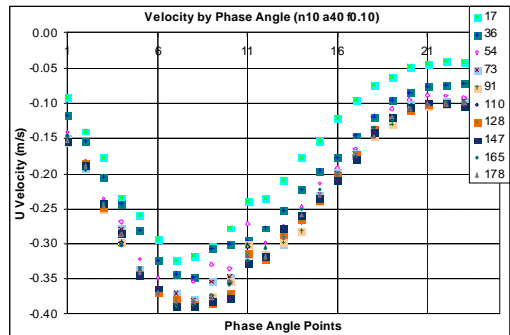
Figure 4-85 Velocity waveforms of n_0=10%, amp=40%, f_r=0.10Hz
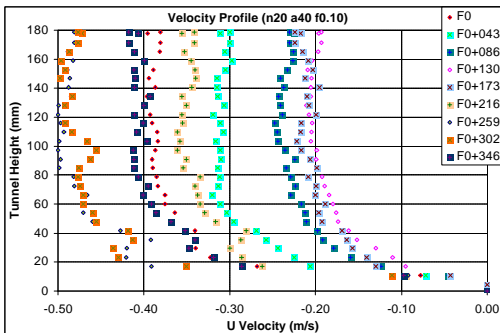
Figure 4-86 Velocity profile of n_0=20%, amp=40%, f_r=0.10Hz
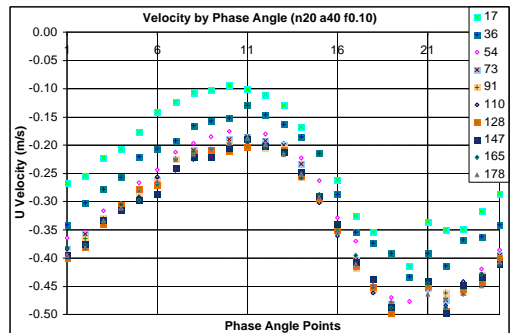
Figure 4-87 Velocity waveforms of n_0=20%, amp=40%, f_r=0.10Hz
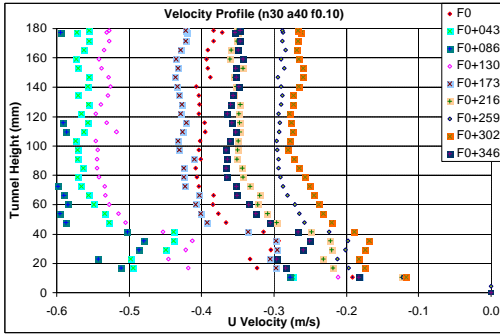
Figure 4-88 Velocity profile of n_0=30%, amp=40%, f_r=0.10Hz
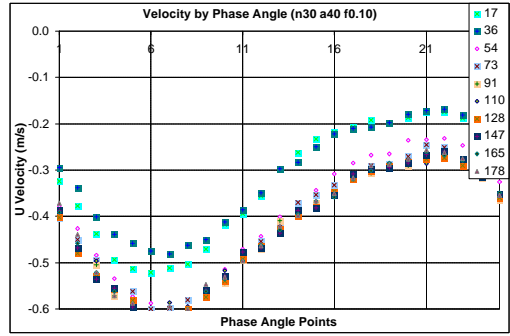
Figure 4-89 Velocity waveforms of n_0=30%, amp=40%, f_r=0.10Hz
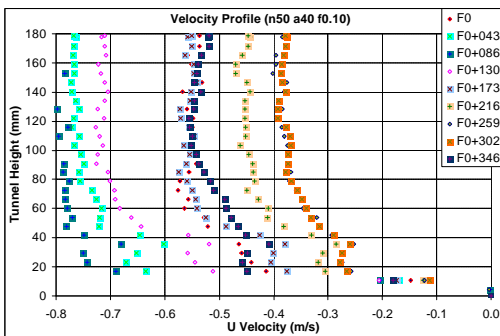
Figure 4-90 Velocity profile of n_0=50%, amp=40%, f_r=0.10Hz
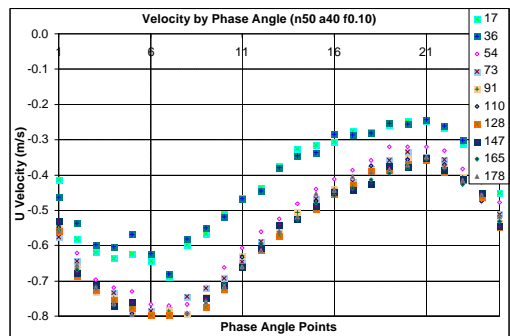
Figure 4-91 Velocity waveforms of n_0=50%, amp=40%, f_r=0.10Hz
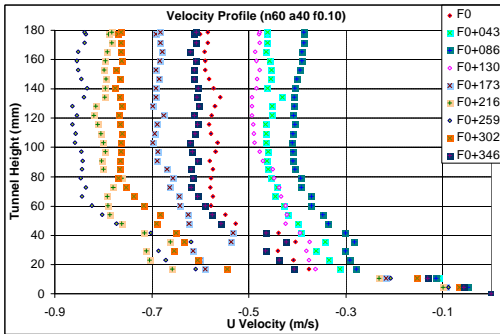
Figure 4-92 Velocity profile of n_0=60%, amp=40%, f_r=0.10Hz
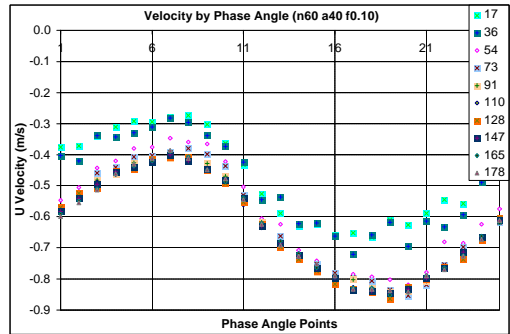
Figure 4-93 Velocity waveforms of n_0=60%, amp=40%, f_r=0.10Hz

It is shown from Figure 4-84 to Figure 4-93, Figure 4-70 and Figure 4-71 that:

– The general shapes and developing tendencies of velocity profile and waveform were similar to those shown in the previous section. Most of the points concluded from the previous section were valid and was not repeated here.

– The velocity profile and waveform did not have obvious difference among oscillating dominant flow (Figure 4-84 to Figure 4-87), balanced flow (Figure 4-88 to Figure 4-91, Figure 4-70 and Figure 4-71) and stationary dominant flow (Figure 4-92 and

Figure 4-93). It seems that the percentage of base flow level did not have significant effects on the general shapes of the velocity profile and waveform.

−   The velocity variation in one period of oscillating dominant flow was bigger than that of balanced flow and stationary dominant flow.

−   The bigger of the base flow, the bigger of the maximum velocity in any location of the duct and in any phase angle of an oscillating period.

4.7.4 Vertical velocity

Three examples of the vertical velocity of the combined oscillatory flow are shown in Figure 4-94 to Figure 4-99. These are typical vertical velocities of stationary dominant flow (Figure 4-94 and Figure 4-95, $n_0 = 40\%$, amp = 10%, $f_r = 0.10$Hz), balanced flow (Figure 4-96 and Figure 4-97, $n_0 = 40\%$, amp = 40%, $f_r = 0.10$Hz) and oscillating dominant flow (Figure 4-98 and Figure 4-99, $n_0 = 40\%$, amp = 60%, $f_r = 0.10$Hz) respectively. Figure 4-94 and Figure 4-95 corresponding to Figure 4-64 and Figure 4-65. Figure 4-96 and Figure 4-97 corresponding to Figure 4-70 and Figure 4-71. Figure 4-98 and Figure 4-99 corresponding to Figure 4-74 and Figure 4-75. Refer to the previous section for the specifications of flows and measurements.
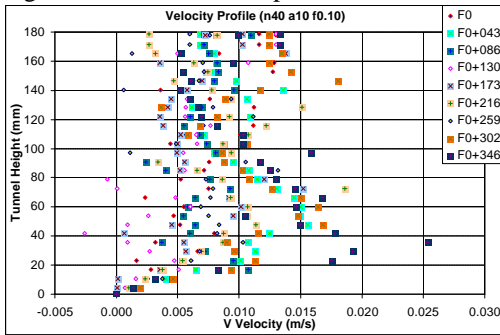
Figure 4-94 Velocity profiles of *V* at amp=10%, n₀=40%, f$_r$=0.10Hz
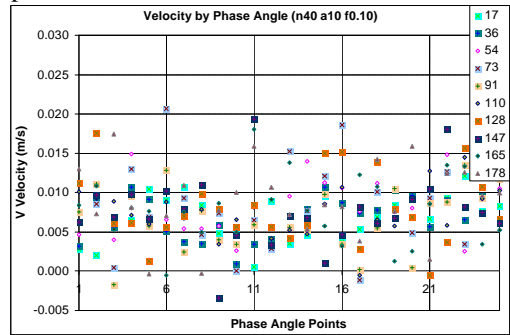
Figure 4-95 Velocity waveforms of *V* at amp=10%, n₀=40%, f$_r$=0.10Hz
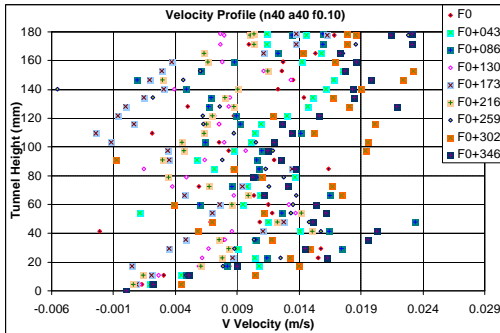
Figure 4-96 Velocity profiles of *V* at amp=40%, n₀=40%, f$_r$=0.10Hz
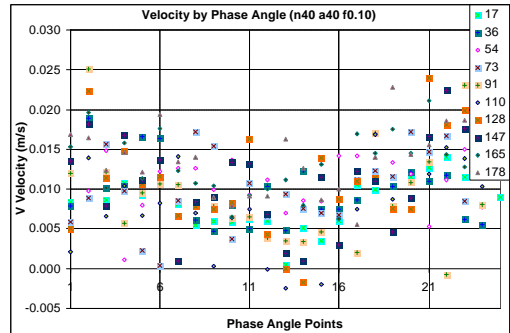
Figure 4-97 Velocity waveforms of *V* at amp=40%, n₀=40%, f$_r$=0.10Hz
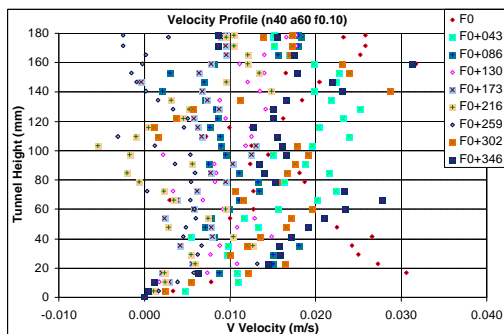
Figure 4-98 Velocity profiles of *V* at
amp=60%, n_0=40%, f_r=0.10Hz
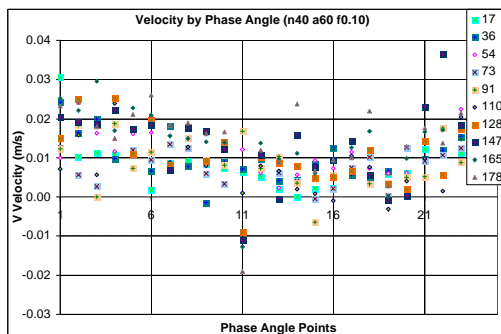
Figure 4-99 Velocity waveforms of *V* at
amp=60%, n_0=40%, f_r=0.10Hz

It is shown from Figure 4-94 to Figure 4-99 that:

− Generally, comparing with the mainstream velocity, the vertical velocity was very small, always oscillating in the narrow area near to zero within an oscillatory period of the flow.

− Relatively to the vertical velocity itself, the magnitude of vertical velocity was quite small at the narrow area near to the boundary wall and bigger in the mainstream area.

− The vertical velocity had a waveform roughly in the shape of harmonic wave.

− The phase of the vertical velocity was different from that of horizontal mainstream velocity for 180°.

4.7.5 Summary of PIV velocity for combined oscillatory flow

From the measured results shown above, it is summarized that:

− The velocity for combined oscillatory flow varied around a constant velocity in an oscillatory period.

− Both velocity components were in harmonic waveform with single frequency; both velocity components increased from the boundary wall to the centreline of the duct and fluctuate a little randomly along a horizontal line. Velocity increased very fast vertically in the region close to boundary. The velocity was close to mainstream maximum velocity in more than 80% of the duct height.

− Velocity profile depended on both the oscillatory frequency and amplitude. The influence of base flow on the velocity distribution was insignificant.

− Annular effect was not obvious in the cases shown for combined oscillatory flow. Regional overshooting was observed instead, which was also resulted from the complex actions of oscillatory frequency and amplitude.

− The general shapes and developing tendencies of velocity profile and velocity waveform were similar among stationary dominant flow, balanced flow and oscillation dominant flow, though the magnitudes of velocity variation in one period were different among different types of flows.

Chapter 5

Frequency Dependent Head Loss

Main topics of this chapter:

- Wave speed calculation

- Basic theory of friction head loss

- Head loss of steady flow

- Head loss of pure oscillatory flow

- Head loss of combined oscillatory flow

- Analysis head loss in frequency domain

5.1 Wave Speed in the Test Duct

As described in Chapter 2 Experimental Setup, the test duct was made of Plexiglas. The sides of the rectangular section of the test conduit would deflect and create an expanded cross section if the pressure increased in the conduit (Figure 5-1). The flexible walls would then cause a pressure wave propagating along the test conduit while the pressure was changing (Figure 5-2). This would affect the water head variation streamwise. The extent of the influence of the pressure wave on the water head variation along the tunnel was dependent on the ratio of the pressure wave speed to the flow velocity.
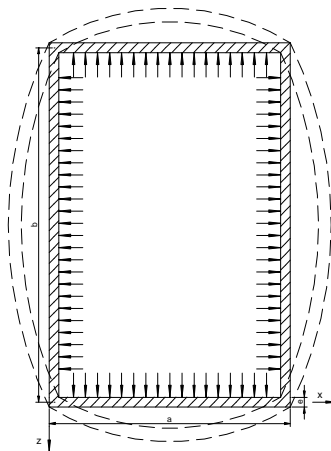
Figure 5-1 Deflection of a rectangular duct

<div style="text-align:center">

p
ρ
c
A

p + Δp
ρ + δρ
c + Δv
A + δA
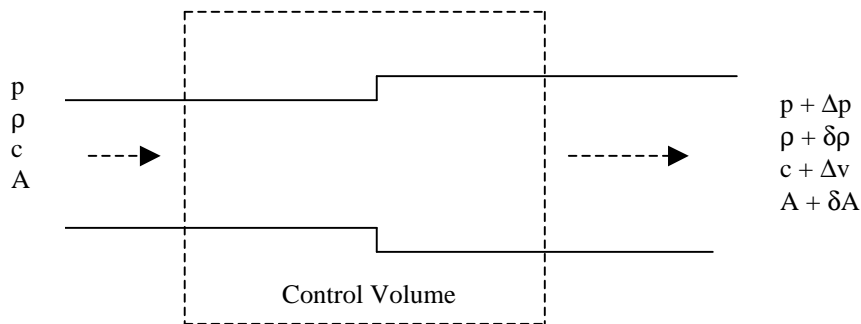
Control Volume

Figure 5-2 Control volume in oscillatory flow

</div>

p	Initial pressure		Δp	Pressure increment
ρ	Initial density		δρ	Density increment
c	Wave speed		Δv	Flow velocity increment
A	Initial cross section area of duct		δA	Area increment

To estimate the possible influence of the pressure wave on the water head variation along the tunnel, the pressure wave speed in the test conduit was calculated. The wave speed was dependent on the flexibility of the walls of the conduit. The sidewall of the conduit was taken as a plate, the deflection of which was calculated first. Area variation of the test duct resulted from the sidewall deflection was evaluated afterwards. The pressure wave speed could be calculated when the area variation was available. The detail calculation can be found in Appendix A.3 Wave Speed Calculation. The main points are listed below:

1.   Wave speed equation

(5-1) $$c = \left[r\left(\frac{1}{K} + \frac{1}{A}\frac{dA}{\Delta p} \right) \right]^{-\frac{1}{2}}$$

This is the general equation to calculate the wave speed of transient pressure propagation of liquid in pipes or tunnels. The term with bulk modulus K represents the elasticity of the fluid, and the term with area variation per unit change in pressure $\dfrac{dA}{\Delta p}$, denotes the elasticity of the conduit.

2.   Area variation with simple boundary conditions

For the test duct, if it is assumed that a unit strip from the wall deflects in the way as that of a simple beam, no deflection at both ends of the beam, no reacting moment at the ends, no axial force to prevent the ends from axial movements, and all unit strips deflect in the same way, then the area variation can be written as:

(5-2) $$\frac{1}{A}\frac{dA}{\Delta p} = \frac{(a^5 + b^5)}{a \cdot b} \cdot \frac{1}{30 \cdot E \cdot e^3}$$

The wave speed calculated with this area variation was:

(5-3) $c = \left[r \left(\dfrac{1}{K} + \dfrac{1}{A} \dfrac{dA}{\Delta p} \right) \right]^{-\frac{1}{2}} = \underline{\underline{63.085}}(m/s)$

3.   Area variation with more strict boundary conditions

If it is assumed that the ends of unit strip can not move to each other, axial reaction forces exist to prevent the movement; the ends of unit strip can not rotate freely, reaction moments exist around the corner of the duct to prevent the rotation, then the area variation can be written as:

(5-4)

$$\frac{1}{A}\frac{dA}{dp} = \frac{1}{a \cdot b} \cdot \frac{1}{dp} \left[\begin{array}{l} \dfrac{C_1}{k}(e^{ka}-1) - \dfrac{C_2}{k}(e^{-ka}-1) + \dfrac{p \cdot a^2}{12k^2 D} + \dfrac{M_0 a}{k^2 D} - \dfrac{pa}{k^4 D} \\[2mm] + \dfrac{C_1}{k}(e^{kb}-1) - \dfrac{C_2}{k}(e^{-kb}-1) + \dfrac{p \cdot b^2}{12k^2 D} + \dfrac{M_0 b}{k^2 D} - \dfrac{pb}{k^4 D} \end{array} \right]$$

$$= \frac{1}{a \cdot b} \left\{ \frac{a+b}{k^4 D} - \frac{1}{2k^3 D} \left[a^2 \frac{1+e^{-k \cdot a}}{1-e^{-k \cdot a}} + b^2 \frac{1+e^{-k \cdot b}}{1-e^{-k \cdot b}} \right] + \frac{a^3 + b^3}{12k^2 D} \right\}$$

The wave speed calculated with this area variation was much higher than the result from Equation (5-3). Iteration is needed to finish the calculation.

4.   Discussions and Conclusions

From the results shown above and in Appendix A.3, the wave speed was ranged from 35.725 m/s to 79.832 m/s in the test duct. The peak velocity measured in the test was around 1 m/s, much smaller than the wave speed. The interference between them ought to be quite small. The highest oscillatory frequency of flow tested was 1.0 Hz; the lowest oscillatory frequency of flow tested was 0.01 Hz. The period of flow ranged from 1.0 s to 100 s. The distance between the two connection points of differential pressure sensor was 9 m. It took about 0.25 s for the pressure wave to travel from one connection point to another if the wave speed was 35 m/s, took about 0.11 s if the wave speed was 80 m/s. For flow with lower oscillatory frequency, the time was negligible. For flow with higher oscillatory frequency, the time might be too big for accurate measurement.

In the rig, enforcement ribs were glued to the sides of the duct. The distance between two adjacent ribs was 0.75 m. This resisted the deflection of the wall and increased the pressure wave speed a lot.

The inner rough layer was not taken into account in above evaluations. The inner rough layers were fixed to the walls of test duct tightly. It also helped to resist the bend and deflection effect of the walls.

Briefly, the actual speed of pressure wave ought to be quite bigger than 35 m/s. The time taken for pressure wave to travel between the two sampling points of differential pressure sensor ought to be small enough to get a relatively accurate result. The influence of the wave speed on the water head variation along the test conduit was negligible.

5.2 Friction Head Loss Analysis

Oscillatory flow accelerates and decelerates all of the time. Thus, the head variation along the mainstream of oscillatory flow has two components:

–   Friction head loss: head loss caused mainly by friction or shear stress in the flow near to the boundary.

–   Accelerative head: head variation caused by the accelerating and decelerating of the flow.

89

The reading of differential pressure sensors used in the measurement was the sum of these two components.

5.2.1 Dynamic equation of unsteady flow

For a liquid element along a streamline in a real fluid, both shear stress and normal pressure act on the surface of the fluid element, as shown in Figure 5-3.
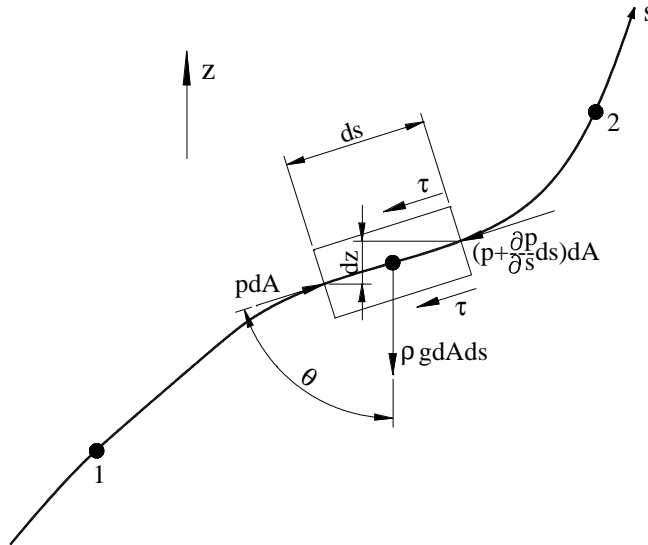
Figure 5-3 Fluid element on a streamline and forces acting on it

Symbols in Figure 5-3

p	Pressure at left side of the element	dA	Cross section area of element
V	Velocity of the element	ds	Length of element
ρ	Density of fluid	dz	Altitude variance of element
τ	Shear stress	$(\partial p/\partial s)ds$	Pressure increment
g	Gravity acceleration	θ	Angle between p and g

If the fluid element in Figure 5-3 is regarded as a cylinder of radius r and length ds, the area over which the shear stress acts along the streamline is $2\pi r\ ds$. Apply Newton's second law of motion for the accelerating fluid element:

$$\boldsymbol{r} \cdot dA \cdot ds \frac{dV}{dt} = -\frac{\partial p}{\partial s} ds \cdot dA - \boldsymbol{r}g \cdot dA \cdot ds \cdot \cos\boldsymbol{q} - 2\boldsymbol{pr} t \cdot ds$$

or

(5-5)
$$\frac{dV}{dt} = -\frac{1}{\boldsymbol{r}} \frac{\partial p}{\partial s} - g\cos\boldsymbol{q} - \frac{2t}{\boldsymbol{r} \cdot r}$$

The fluid velocity V is a function of the independent variables of displacement s and time t, and $ds/dt=V$, then:

(5-6)
$$\frac{dV}{dt} = \frac{\partial V}{\partial t} + V\frac{\partial V}{\partial s}$$

90

The first term on the right hand side of Equation (5-6) is the *local* or *temporal acceleration*, which represents the local change in velocity with time, and the second term is *convective acceleration*, which represents the change in velocity along a streamline.

Insert Equation (5-6) into Equation (5-5) and replace $cos\boldsymbol{q}$ with $\partial z/\partial s$, then:

$$(5\text{-}7) \qquad \frac{\partial V}{\partial t} + V\frac{\partial V}{\partial s} = -\frac{1}{\boldsymbol{r}}\frac{\partial p}{\partial s} - g\frac{\partial z}{\partial s} - \frac{2\boldsymbol{t}}{\boldsymbol{r}\cdot\boldsymbol{r}}$$

Integrate Equation (5-7) along a streamline between point 1 and point 2 separated by a distance l, as shown in Figure 5-3:

$$(5\text{-}8) \qquad \frac{V_1^{\,2}}{2} + \frac{p_1}{\boldsymbol{r}} + gz_1 = \frac{V_2^{\,2}}{2} + \frac{p_2}{\boldsymbol{r}} + gz_2 + \int_1^2 \frac{2\boldsymbol{t}}{\boldsymbol{r}\cdot\boldsymbol{r}}\,ds + \int_1^2 \frac{\partial V}{\partial t}\,ds$$

This is the general form of one-dimensional dynamic equation for unsteady flow of real incompressible fluid. The test rig is composed of horizontal rectangular duct, i.e., $z_1 = z_2$, and the density can be treated as constant, then

$$(5\text{-}9) \qquad \frac{V_1^{\,2}}{2} + \frac{p_1}{\boldsymbol{r}} = \frac{V_2^{\,2}}{2} + \frac{p_2}{\boldsymbol{r}} + \frac{1}{\boldsymbol{r}}\int_1^2 \frac{2\boldsymbol{t}}{\boldsymbol{r}}\,ds + \int_1^2 \frac{\partial V}{\partial t}\,ds$$

Set

$$g\cdot h_f = \frac{1}{\boldsymbol{r}}\int_1^2 \frac{2\boldsymbol{t}}{\boldsymbol{r}}\,ds$$

$$g\cdot h_a = \int_1^2 \frac{\partial V}{\partial t}\,ds$$

where h_f is the friction head loss between point 1 and 2 on the streamline, h_a is the *accelerative head* from point 1 to point 2 on the streamline. Then:

$$(5\text{-}10) \qquad h_f = \frac{1}{\boldsymbol{r}\cdot g}\int_1^2 \frac{2\boldsymbol{t}}{\boldsymbol{r}}\,ds$$

$$(5\text{-}11) \qquad h_a = \frac{1}{g}\int_1^2 \frac{\partial V}{\partial t}\,ds$$

5.2.2 Friction head loss of oscillatory flow

The test rig is a horizontal duct. For mass oscillatory flow, it is supposed that $V_1 = V_2$. From Equation (5-9),

$$\frac{p_1 - p_2}{\boldsymbol{r}} = \frac{1}{\boldsymbol{r}}\int_1^2 \frac{2\boldsymbol{t}}{\boldsymbol{r}}\,ds + \int_1^2 \frac{\partial V}{\partial t}\,ds = g\cdot h_f + g\cdot h_a$$

or

(5-12)
$$\frac{\Delta p}{\boldsymbol{r} \cdot g} = h_f + h_a$$

Equation (5-12) shows that:
- For oscillatory flow, the pressure difference between two points along the streamline caused from not only friction head loss h_f, but also accelerative head h_a.
- For oscillatory flow, the measured value of a differential pressure sensor in the test is composed of both parts.
- If h_a was evaluated from the velocity measured from the velocimetry, h_f could be evaluated from Equation (5-12) based on the reading of differential pressure cell.
- For steady flow, the accelerative head does not exist. The pressure difference between two points along the streamline is only resulted form the friction head loss. The reading of a differential pressure sensor along the streamline is the friction head loss of the flow.

For stationary flow, Darcy-Weibach formula could be used to estimate the friction head loss:

(5-13)
$$h_f = \boldsymbol{f}(R_e, \frac{\boldsymbol{e}}{d}) \frac{V^2 l}{2gd} = f \frac{l}{d} \frac{V^2}{2g}$$

where
- Re: Reynolds number of the flow
- ε/d: relative roughness of the duct
- d: diameter of the duct
- $f = \boldsymbol{j}$ $(Re, \varepsilon/d)$: friction factor of the flow in the duct

C. F. Colebrook (1939) and C. M. White (1932) establish the expressions for friction factor as follows:

(5-14)
$$\frac{1}{\sqrt{f}} = 1.14 - 2\log\left(\frac{\boldsymbol{e}}{d} + \frac{9.35}{R_e \cdot \sqrt{f}}\right)$$

For smooth pipe, $\varepsilon \rightarrow 0$, then the friction factor for smooth pipe, from Equation (5-14), is:

(5-15)
$$\frac{1}{\sqrt{f}} = 2\log\left(R_e \cdot \sqrt{f}\right) - 0.8$$

This is the famous Prandtl's universal law of friction for smooth pipes.

If Re $\rightarrow$ 8 , then Equation (5-14) transforms to the following form:

(5-16)
$$\frac{1}{\sqrt{f}} = 1.14 - 2\log\left(\frac{\boldsymbol{e}}{d}\right)$$

This is the resistance formula proposes by J. Nikuradse for completely rough region based on his famous experiment of sand roughness. It is observed by J. Nikuradse that at sufficiently large values of Reynolds number of flow the friction factor depends only on the parameter ε/d and becomes independent of the Reynolds number of flow.

Equation (5-14) is implicit. Iteration has to be conducted to compute the friction factor. Haaland (1983) proposes an explicit approximation formula as:

$$(5\text{-}17) \qquad \frac{1}{\sqrt{f}} \approx -1.8\log\left(\left(\frac{e/d}{3.7}\right)^{1.11} + \frac{6.9}{R_e}\right)$$

This equation may be solved immediately for friction factor and varies by less than ±2% from the result of Equation (5-14). A better way is to evaluate the friction factor from Equation (5-17) first and iterate again by Equation (5-14) on the basis of the value from Equation (5-17). The iteration takes less time by this two -step method.

The test rig was a rectangular duct. The diameter d in the above equations ought to be replaced by the hydraulic diameter D_h of the duct. If the side lengths of the rectangular were a and b respectively, then:

$$(5\text{-}18) \qquad D_h = \frac{4A}{P} = \frac{4ab}{2(a+b)} = \frac{2ab}{a+b}$$

D_h was also used in the calculation of Reynolds number for the above equations.

$$(5\text{-}19) \qquad Re = V \cdot D_h / \boldsymbol{n}$$

where

- $\boldsymbol{n}$: kinematics viscosity of water $\boldsymbol{n} = 1.007 \times 10^{-6}$ m^2/s

The relative roughness of the inner rough layer was ε/D_h.

When Equation (5-13) was used to estimate the friction head loss for stationary flow, mean velocity was used to evaluate the Reynolds number, friction factor and the friction head loss.

It is reasonable to estimate the friction head loss with Equation (5-13) for unsteady flow, if the instant mean velocity of flow is available. Use the instant mean velocity to compute the Reynolds number, friction factor and the friction head loss at the instant. A time series can be built up if same calculation is applied to a series of consecutive instant velocity.

- If the unsteady flow accelerates or decelerates monotonously, the results by this estimation ought to be accurate enough.
- If the turning from accelerating to decelerating or vice versa is very slow, the results by this estimation ought to be accurate too.
- If the turning from accelerating to decelerating or vice versa is fast, the results by this estimation could result in big error around the turning point.

For oscillatory flow, if the velocity V along a streamline is expressed as:

$$(5\text{-}20) \qquad V = V_0 + V_{amp}\,\sin(\boldsymbol{w}t + \boldsymbol{j}_0)$$

where

- V_0 is the bulk flow velocity (base flow velocity)
- V_{amp} is amplitude of the oscillatory velocity
- $\boldsymbol{w}$ is the oscillatory angle frequency, $\boldsymbol{w} = 2\pi f_r$ (f_r is oscillatory frequency in Hz)
- $\boldsymbol{j}_0$ is the initial phase angle of the oscillatory velocity

For any instance t in the oscillatory period, insert Equation (5-20) into Equation (5-19) to get the Reynolds number; use Equation (5-17) and Equation (5-14) to get the friction factor; and use Equation (5-13) to get the friction loss at instance t.

Generally, to simplify the calculation it is assumed that $\boldsymbol{j}_0 = 0$. V_0 and V_{amp} can be obtained from the measured value of velocity.

- V_0 is the mean velocity of oscillatory flow over periods.
- V_{amp} is half of the difference between the peak velocity and V_0 of oscillatory flow.
- V is the mean velocity across the section at any instant.

There were two ways to get the instant mean velocity V. Only tiny difference existed between the results from these two methods:

- By integrating the PIV velocity to get the flow rate at any instant; then compute velocity with this flow rate.
- Averaging the velocity fields from PIV at any instant directly.

5.2.3 Dynamic head of oscillatory flow

Assume that the cross section of the stream tube is constant, which is accurate in the test rig discussed, $\partial V/\partial t$ keeps constant throughout the length of the tube, and then:

$$(5-21) \qquad\qquad h_a = \frac{l}{g}\frac{dV}{dt}$$

where l is the length of the stream tube between point 1 and 2 as shown in Figure 5-3.

According to the oscillatory velocity in Equation (5-20), then:

$$(5-22) \qquad\qquad \frac{dV}{dt} = V_{amp}\boldsymbol{w}\cos(\boldsymbol{w}t + \boldsymbol{j}_0)$$

Insert this relation into Equation (5-21), then:

$$(5-23) \qquad\qquad h_a = \frac{l}{g}V_{amp}\boldsymbol{w}\cos(\boldsymbol{w}t + \boldsymbol{j}_0)$$

In this equation, if V_{amp} and $\boldsymbol{j}_0$ are known, dynamic head can be evaluated. In the practice of measurement, V_{amp} and $\boldsymbol{j}_0$ were available from the analysis of PIV or LDA measuring results (refer to the previous section).

As shown in Equation (5-23), there is a 90 degrees phase shift between the accelerative head and the oscillatory velocity. When the oscillatory velocity reached the maximum and minimum value, the dynamic head was equal to zero. When the oscillatory velocity equalled to zero, the dynamic head reached its peak value.

Differential pressure sensor was used to get the pressure change between two points along the test duct. Friction head loss of oscillatory flow could be evaluated by Equation (5-12) afterwards if the accelerative head was computed from Equation (5-23):

$$(5-24) \qquad\qquad h_f = -\frac{\Delta p}{\boldsymbol{r}\cdot g} + \frac{l}{g}V_{amp}\boldsymbol{w}\cos(\boldsymbol{w}t + \boldsymbol{j}_0)$$

where

- Δp is the readings of the differential pressure cell.
- l is the distance between the two sampling points of differential pressure cell.

Comparisons could be carried out then:

- Comparison of computed friction head loss from Equation (5-13) with measured friction head loss of steady flow.
- Comparison of friction head loss between steady flow and oscillatory flow.

- Compare the friction head loss got from Equation (5-24) to the results from the method described in the previous section.

It should be noted that in Equation (5-24), when it is applied to oscillatory flow, all three items, i.e., Δp, h_f, h_a, have the same phase angle at every instant, 90 degrees shift from that of the velocity.

5.3 Friction Head Loss of Steady Flow

As an example and reference for further analysis, following is a case study of friction head loss calculation of steady flow. The friction factor was obtained by iteration with Equation (5-14) at first. Friction head loss was computed afterwards with Equation (5-13). At last, the computation results were compared with the measured results from differential pressure sensor.

5.3.1 Description of the calculation

The calculation was based on the measured flow rate Q. The calculation of friction factor was conducted in following steps:

- Compute approximate friction factor by Equation (5-17).
- Iterate friction factor by Equation (5-14) on the result from the previous step.

Multiple ways were used to iterate the friction factor by Equation (5-14):

- A special iterating code was made to do this
- Use the Solver of MS Excel
- Numeric Solver of pocket calculator (TI-89 from Texas Instrument).

Only the results from the first method are shown below (f_2 in Table 5-2).

The iterated friction factor was inserted into Equation (5-13) to get the friction head loss from the empirical formula. Following comparison was made:

- Comparison of the friction factor from Equations (5-14) and (5-17)
- Comparison of the friction head loss computed with the measured differential pressure on the same length of the duct.

The known physical and geometrical parameters of the test rig are listed in Table 5-1.

Table 5-1 Known physical and geometry parameters

Variables	a	b	ε	A	P	D	ε/D	n	l_1	l_2
Units	m	m	m	m^2	m	m	-	m^2/s	m	m
Values	0.35	0.22	0.0005	0.077	1.14	0.2701	0.00185	$1.01\cdot10^{-6}$	9.0	6.0

5.3.2 Results of the calculation

The calculation result is shown in Table 5-2 and Figure 5-4, in which:

- f_1: friction factor from Equation (5-17)
- f_2: friction factor from Equation (5-14) by iteration with a special made code
- **Df** (%): $(f_2 - f_1)/f_1 \times 100\%$
- h_{f1}: friction head loss from Equation (5-13) with conduit length $l = 9$ m.
- $dP1$: reading of differential pressure cell $dP1$ ($l = 9$ m)
- **Dh_{f1}** (%):$(h_{f1} - dP_1)/h_{f1} \times 100\%$
- h_{f2}: friction head loss from Equation (5-13) with conduit length $l = 6$ m.

− dP_2: reading of differential pressure cell $dP2$ ($l = 6$ m)
−   **Dh_{f2}** (%):$(h_{f2} - dP_2) / h_{f2} \times 100\%$

Table 5-2 Data for friction head loss calculation of steady flow

Q (l/s)	19.69	39.63	60.09	79.82	99.30	119.60
V (m/s)	0.2557	0.5146	0.7804	1.0366	1.2896	1.5532
Re	68607.56	138068.94	209382.16	278121.04	345990.28	416718.11
f_1	0.02521	0.02416	0.02378	0.02359	0.02347	0.02339
f_2	0.02539	0.02424	0.02382	0.02360	0.02347	0.02338
Df (%)	0.70%	0.34%	0.17%	0.07%	0.00%	-0.04%
h_{f1} (m)	0.00282	0.01091	0.02465	0.04311	0.06635	0.09588
dP_1(m)	0.00352	0.00980	0.02221	0.04187	0.06914	0.10534
Dh_{f1} (%)	25.00%	-10.17%	-9.90%	-2.87%	4.19%	9.86%
h_{f2} (m)	0.00188	0.00727	0.01643	0.02874	0.04423	0.06392
dP_2	0.00224	0.00670	0.01528	0.02871	0.04573	0.06941
Dh_{f2} (%)	19.23%	-7.85%	-7.01%	-0.10%	3.37%	8.59%
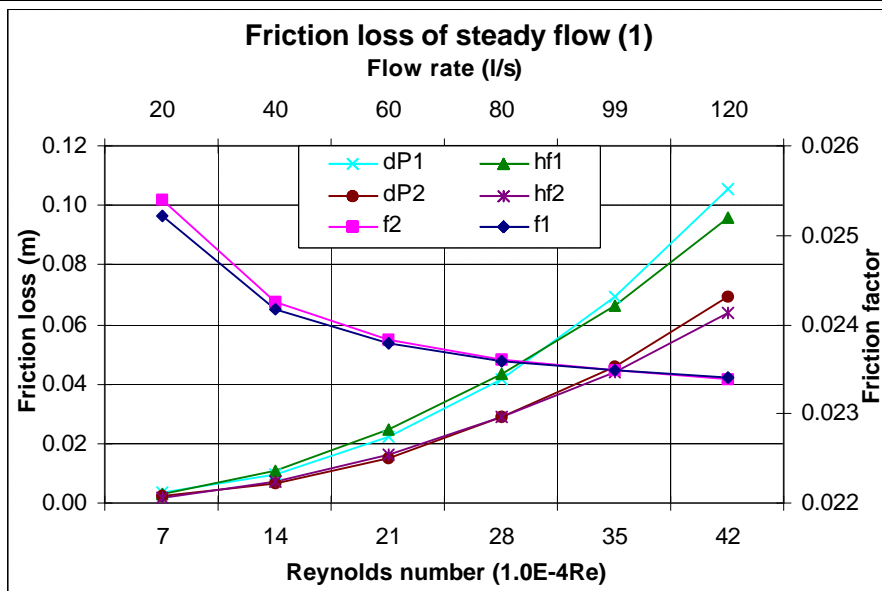
Figure 5-4 Friction head loss of steady flow

From Table 5-2 and Figure 5-4, the calculation is summarized as:

−   Generally, the difference of frictional factors from Equation (5-17) and Equation (5-14) was very small, less than ±1% in all cases shown here. The difference was near to zero at higher Reynolds number, which was about 210 000 in the results shown

−   If the relative roughness was deviated from the correct value, the difference between the frictional factors from Equation (5-17) and Equation (5-14) was bigger than ±2%. For example, in the former calculation, if the relative roughness value decreased 20%, the difference increased up to 5%. And the higher the Reynolds number, the bigger the difference in the range tested.

- At lower Reynolds number, frictional factor from Equation (5-17) was always greater than the frictional factor from Equation (5-14) in the cases shown.

- At high Reynolds number, the friction factor kept almost constant. In the cases shown, the friction factor was independent of the Reynolds number when Reynolds number was higher than 300 000.

- At higher Reynolds number, the friction loss increased faster with Reynolds number. It was proportional to the square of mean velocity. At lower Reynolds number, friction loss was not really proportional to the square of mean velocity due to the chain relation from velocity to Reynolds number to friction factor and to the friction loss.

- The precision of iteration of friction factor was always higher than 10^{-7}, i.e., the difference of left hand side and right hand side of (5-14) was less than 10^{-7}. Actually for most cases the difference was zero when iterate with pocket calculator and Solver of MS Excel.

- The difference in percentage between friction head loss calculated by equation (5-13) and differential pressures measured values reached the minimum point at Reynolds number of 300 000. Greater difference existed at higher and lower end of the Reynolds number. This was true for comparing both dP_1 with h_{f1} and dP_2 with h_{f2}. At lower Reynolds number, the magnitude of differences between dP_1 and h_{f1}, dP_2 and h_{f2} was quite small. At higher Reynolds number, the magnitude of differences between dP_1 and h_{f1}, dP_2 and h_{f2} was increasing with the increase of Reynolds number.

5.4 Friction Head Loss of Pure Oscillatory Flow

As defined in the subchapter 1.1.2, *Pure Oscillatory Flow* was the oscillatory flow without base flow (bulk flow).

5.4.1 Measured differential pressure

Typical waveforms of differential pressure sensor, after phase averaging the readings, are shown in Figure 5-5 to Figure 5-10 for oscillatory flow with frequency ranged from 0.01Hz to 0.50Hz and oscillatory amplitude from 10% to 60% of the full pump rotating speed. It is important to note that the reading of differential pressure sensors including both the friction head loss and dynamic head of oscillatory flow.

Figure 5-5 Oscillatory amplitude amp=10%

Figure 5-6 Oscillatory amplitude amp=20%

Figure 5-7 Oscillatory amplitude amp=30%

Figure 5-8 Oscillatory amplitude amp=40%

Figure 5-9 Oscillatory amplitude amp=50%

Figure 5-10 Oscillatory amplitude amp=60%

It is shown from Figure 5-5 to Figure 5-10 that:

−   The head variation along the streamline of pure oscillatory flow was amplitude dependent. As an example, the maximum readings of differential pressure sensor for oscillatory flow with frequency 0.05 Hz are listed in Table 5-3.

Table 5-3 Maximum values of dP for $f_r = 0.05Hz$

Amp (%)	10	20	30	40	50	60
dPmax (m)	0.004	0.013	0.021	0.029	0.039	0.047

−   The head variation along a streamline of pure oscillatory flow was frequency dependent. As an example, the maximum readings of differential pressure sensor for oscillatory flow with amplitude 40% of full pump rotating speed are listed in Table 5-4.

Table 5-4 Maximum values of dP for POF of Amp = 40%

Freq. (Hz)	0.01	0.05	0.10	0.20	0.50
dPmax (m)	0.02943	0.080595	0.077293	0.049125	0.024523

−   At lower frequency the reading of dP increased with the frequency and at high frequency the readings of dP decreased with frequency. More details on this will be discussed later.

5.4.2 Accelerative head

The velocity of different flow regimes of pure oscillatory flow measured with Particle Image Velocimetry (PIV) are listed below. Table 5-5 is the mean velocities of pure oscillatory flows and Table 5-6 is the velocity amplitudes of oscillatory flows. It is important to note that the velocity is not constant either by mean or by amplitude for different flow regimes.

Table 5-5 Mean values of oscillatory velocity from PIV (V_0)

		Amp (%)					
		10	**20**	**30**	**40**	**50**	**60**
Freq. (Hz)	0.01	0.0009	-0.0030	0.0024	-0.0064	0.0024	-0.0092
	0.05	0.0050	0.0067	0.0126	0.0009	-0.0017	-0.0085
	0.10	-0.0003	0.0140	0.0152	0.0237	0.0276	0.0236
	0.50	0.0015	0.0047	0.0067	0.0053	0.0042	

Table 5-6 Amplitudes of oscillatory velocity from PIV (V_{amp})

		Amp (%)					
		10	**20**	**30**	**40**	**50**	**60**
Freq. (Hz)	0.01	0.0681	0.1700	0.2351	0.3509	0.4599	0.5766
	0.05	0.0148	0.0586	0.1456	0.2412	0.3492	0.4492
	0.10	0.0099	0.0426	0.0780	0.1393	0.2115	0.2980
	0.50	0.0019	0.0071	0.0082	0.0076	0.0095	

With the value from Table 5-5 and Table 5-6, the waveform of the pure oscillatory velocity was built and the accelerative head was calculated with Equation (5-23). The waveforms of dynamic head for oscillatory flow with frequencies ranged from 0.01 Hz to 0.50 Hz and amplitudes ranged from 10% to 60% of the full pump rotating speed are shown in Figure 5-11 to Figure 5-16.
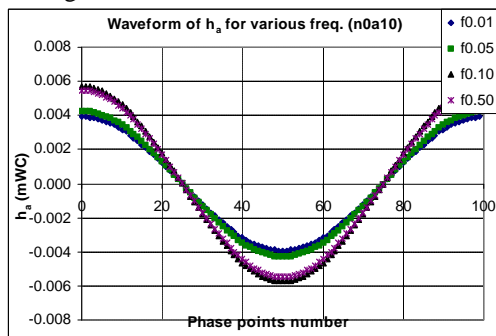
Figure 5-11 Oscillatory amplitude amp=10%
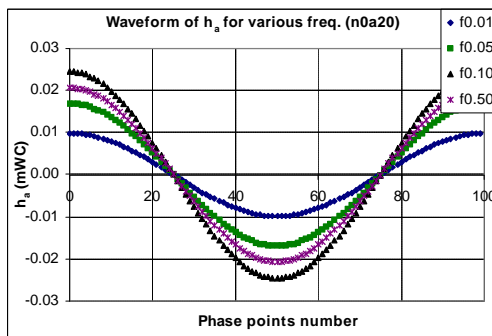
Figure 5-12 Oscillatory amplitude amp=20%
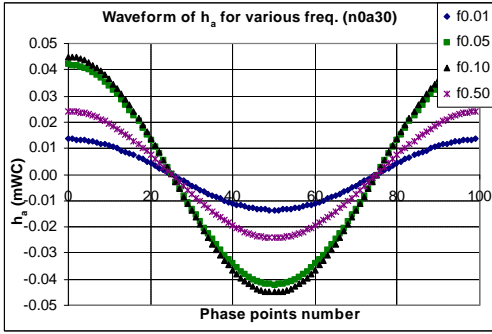
Figure 5-13 Oscillatory amplitude amp=30%
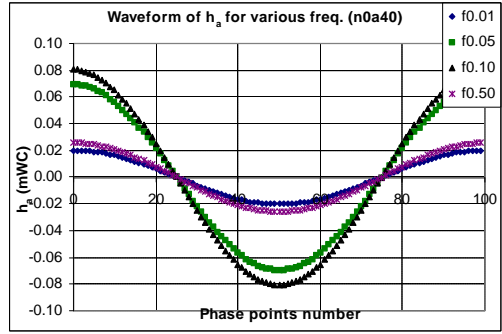
Figure 5-14 Oscillatory amplitude amp=40%
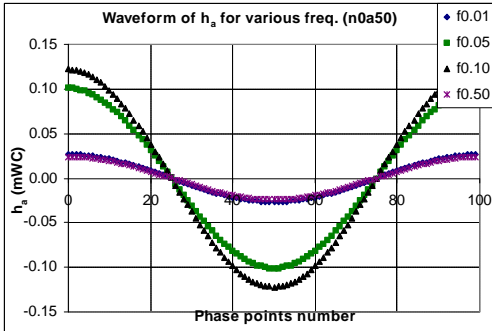
Figure 5-15 Oscillatory amplitude amp=50%
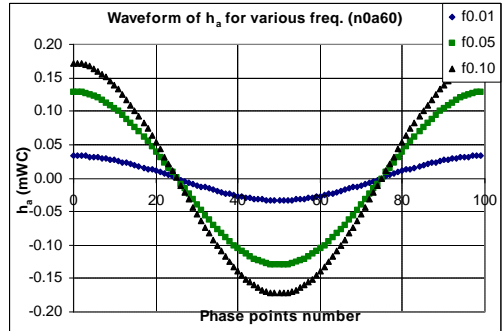
Figure 5-16 Oscillatory amplitude amp=60%

5.4.3 Friction head loss

According to Equation (5-24), the friction head loss could be obtained by subtracting the accelerative head from the readings of differential pressure sensor. The waveforms got in this way are shown in Figure 5-17 to Figure 5-22.
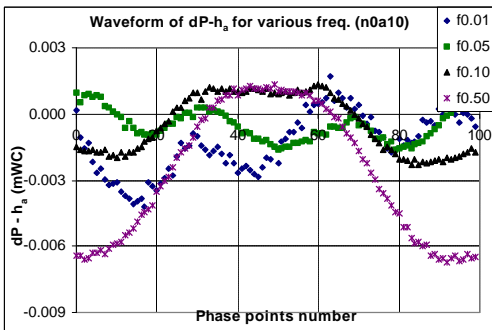
Figure 5-17 Oscillatory amplitude amp=10%
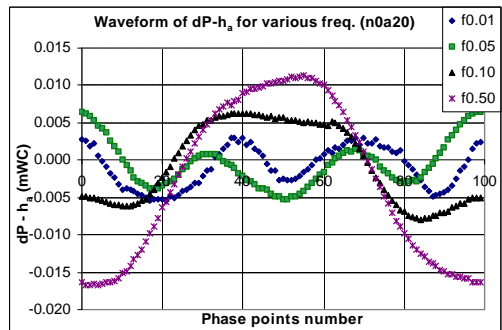
Figure 5-18 Oscillatory amplitude amp=20%
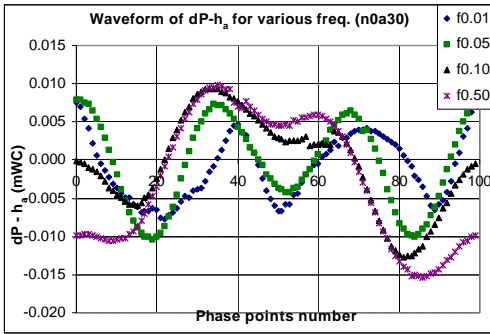
Figure 5-19 Oscillatory amplitude amp=30%
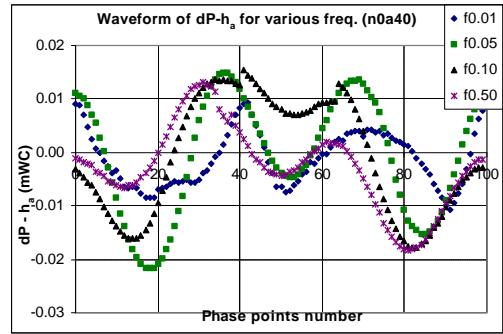
Figure 5-20 Oscillatory amplitude amp=40%
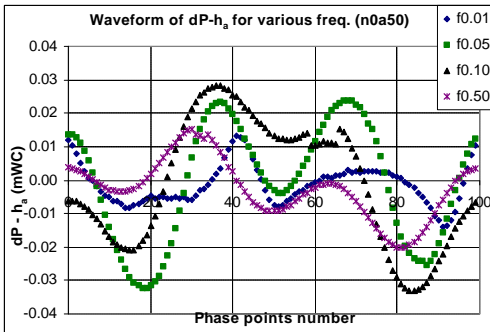
Figure 5-21 Oscillatory amplitude amp=50%
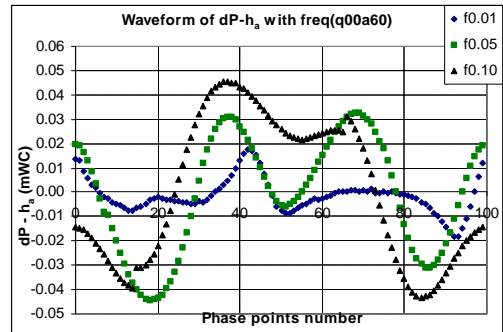
Figure 5-22 Oscillatory amplitude amp=60%

Another way to get the waveform of head loss of oscillatory flow was to calculate head loss by Equation (5-13) with the velocity data listed in Table 5-5 and Table 5-6. The result waveforms are shown in Figure 5-23 to Figure 5-28. In the figures, the two half periods are shown on the same side of x-axis. The friction head loss from equation (5-13) is always positive.
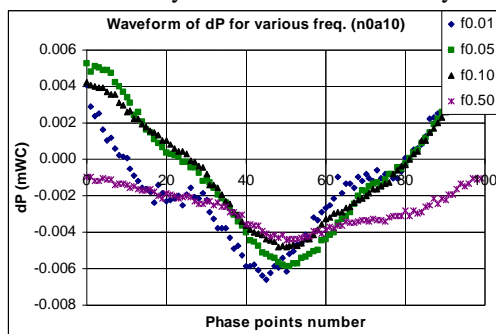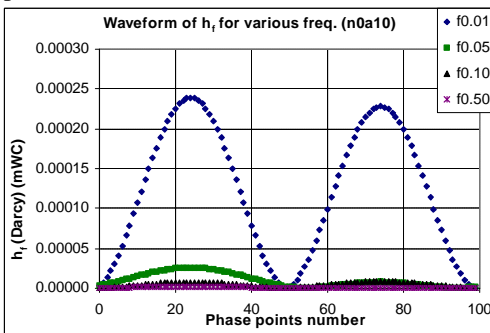

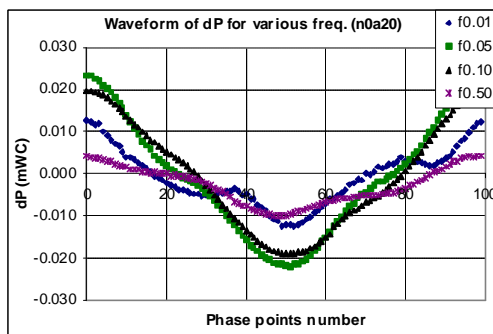Figure 5-23 Oscillatory amplitude amp=10%
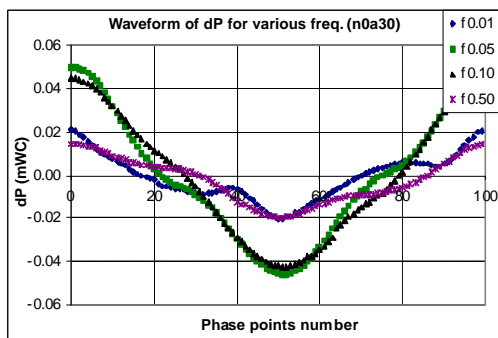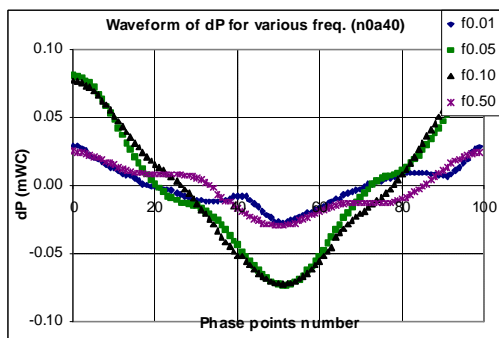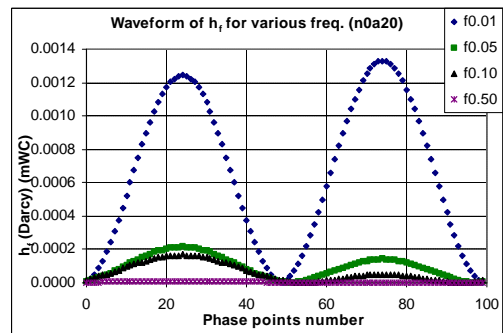

Figure 5-24 Oscillatory amplitude amp=20%
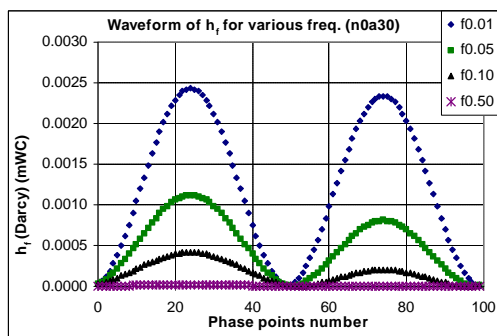
Figure 5-25 Oscillatory amplitude amp=30%
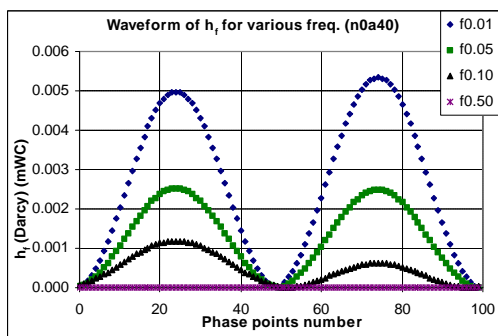
Figure 5-26 Oscillatory amplitude amp=40%
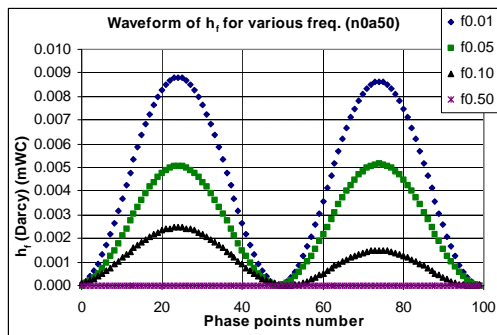
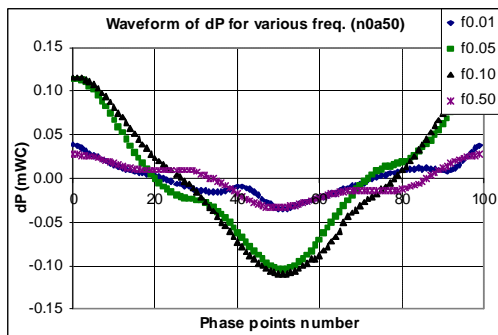Figure 5-27 Oscillatory amplitude amp =50%
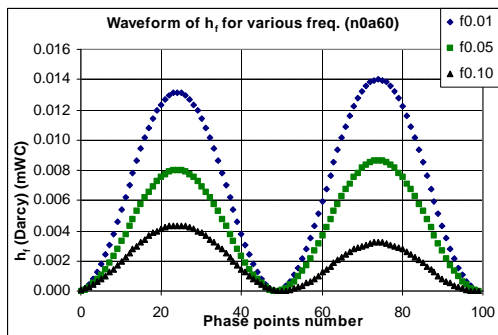
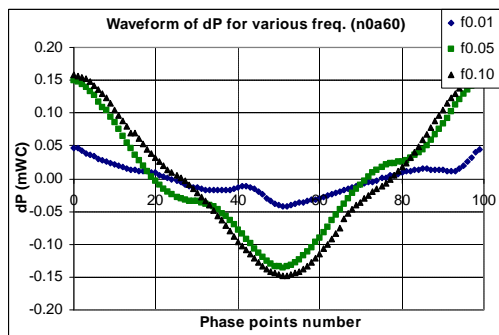Figure 5-28 Oscillatory amplitude amp=60%

5.4.4 Frequency dependency of friction head loss

The peak head loss for different flow regimes of pure oscillatory flow is shown in Figure 5-29. It is displayed that the head loss increased with frequency when frequency was smaller than approximately 0.10Hz; the head loss decreased with frequency when frequency was higher than approximately 0.10 Hz.

To compare the difference of head loss between stationary flow and oscillatory flow, Figure 5-30 gives out the ratio of head loss between two types of flow based on the measuring results. The ratio shown in Figure 5-30 decreased along with the increase of the amplitude of pump rotating speed applied. This was due to the logarithm relation of head loss to flow rate in stationary flow that the head loss increased faster when the flow rate was bigger. Otherwise the relation between head loss and flow rate of pure oscillatory flow was near to linear for bigger flow rate.
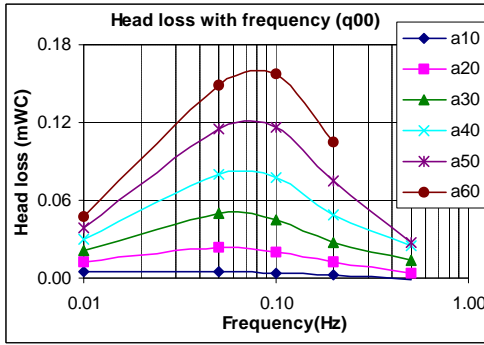
Figure 5-29 Head loss with frequency
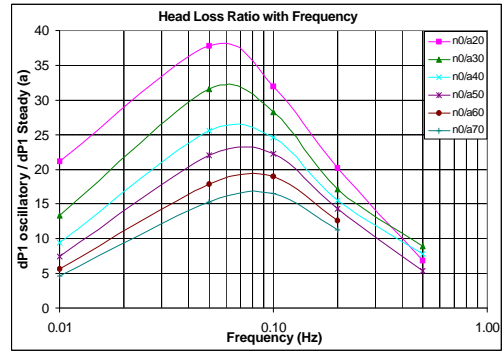
Figure 5-30 Head loss ratio

When the same rotating amplitude signal was applied to the pump at different frequencies, the actual flow rate output from the pump varied with the frequency. The peak flow rate of pump at different frequencies and rotating amplitudes is shown in Figure 5-31. Only in the case of oscillatory frequency 0.01Hz, the peak flow rate of pure oscillatory flow was near to the mean flow rate of stationary flow with the same pump rotating speed input; others have differences of various magnitudes. The flow rate was quite small and increased very slow with pump input amplitude when the oscillatory frequency was 0.50Hz.

The relation of peak head loss of pure oscillatory flow and the flow rate in the system is shown in Figure 5-32. The peak head loss of pure oscillatory flow increased with flow rate in a linear manner for all cases tested.
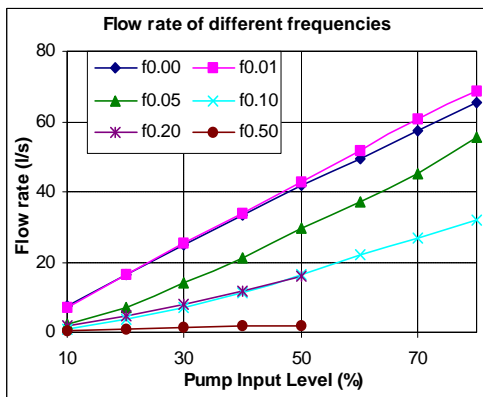
Figure 5-31 Flow rate of different flow
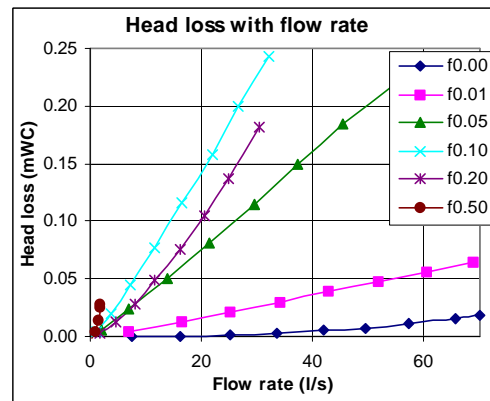
Figure 5-32 Head loss with flow rate

By using the results from Figure 5-31 and Figure 5-32, rebuild Figure 5-29 and Figure 5-30 on the basis of flow rate. The results are shown in Figure 5-33 and Figure 5-34.
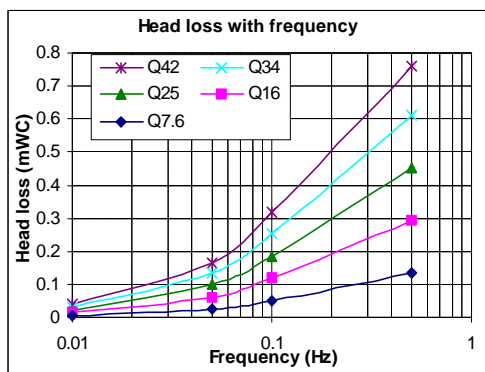
Figure 5-33 Head loss with frequency   Figure 5-34 Head loss ratio
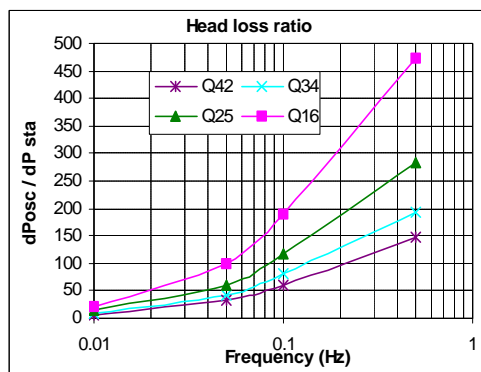
From Figure 5-33 and Figure 5-34, following conclusions of the head loss of pure oscillatory flow may be drawn:

- The peak head loss of pure oscillatory flow increased along with the increase of frequency for all frequencies tested.
- At lower frequency, the slope of curves in Figure 5-33 was smaller and became bigger at higher frequency.
- At lower frequency, the curves in Figure 5-33 were in nonlinear form and the curves were near to linear lines at higher frequency.
- It was also shown that the bigger of the flow rate the faster of the increment of peak head loss along with the frequency.
- All curves in Figure 5-34 demonstrated similar tendency of development as the curves in Figure 5-33. i.e., the head loss ratio had the same developing tendency to frequency as that of peak head loss value itself.
- It was very impressive that the ratio of head loss between pure oscillatory flow and stationary flow could be hundreds times at higher frequency if the flow rate kepts constant.

The head losses shown in Figure 5-29 to Figure 5-34 are the general head losses of pure oscillatory in the test duct of a specific length. The corresponding dynamic heads along with frequency are shown in Figure 5-35 and Figure 5-36. It is shown from the figures that:

- The peak values of the accelerative head were frequency dependent, increasing along with the frequency, except the last frequency point on the curves.
- The mean values of the accelerative head were developing in a similar manner as that of following transfer function, except the last frequency point on the curves

$$\frac{y}{x} = \frac{1}{C1 \cdot s + C2}$$

where $C1$ and $C2$ are constants; y is the output and x is the input of the transfer function.

- The mean values of the accelerative head were quite small, near to zero.
- The accelerative head was calculated from the measured velocity (flow rate), its accuracy was dependent on the accuracy of the measured velocity. The problems of pumps at high frequency and full load affected this calculation too.

104

– The oscillatory amplitude also played a role in the accelerative head development. The curve was steeper when the amplitude was bigger.
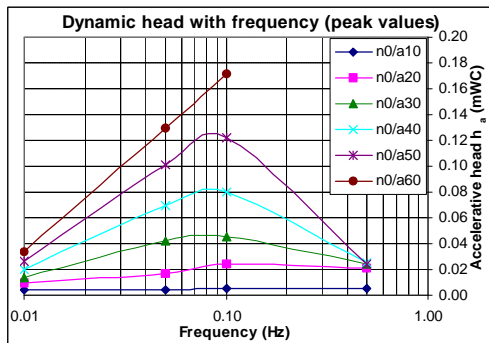
Figure 5-35 Peak values of dynamic head
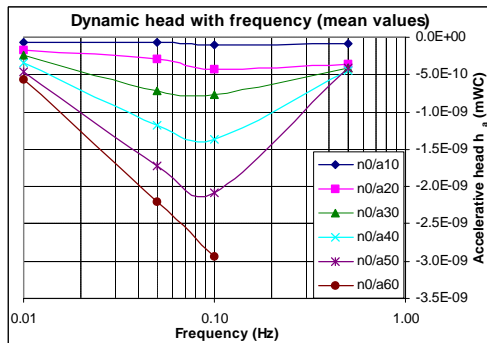
Figure 5-36 Mean values of dynamic head

5.5 Friction Head Loss of Combined Oscillatory Flow

As defined in subchapter 1.1.2 that *Combined Oscillatory Flow* is the oscillatory flow with nonzero base flow (bulk flow). It is oscillating around the base flow, or bulk flow. These flow regimes are more practical in engineering applications.

5.5.1 Measured differential pressure

Complete series of combined oscillatory flow were measured, with oscillatory frequency from 0.01 Hz to 1.00Hz, base flow from 10% to 70% and oscillatory amplitude from 10% to 90% (the sum of base and amplitude was smaller than or equal to100%). Totally more than 200 flow regimes were tested. It is difficult to present all test results here. Only results from some typical example flow regimes are shown below, i.e., base flow is 40% of the pump rotating speed of full load, oscillatory amplitude varies from 10% to 60%. The waveforms of the readings from differential pressure sensor are shown in Figure 5-37 to Figure 5-40.
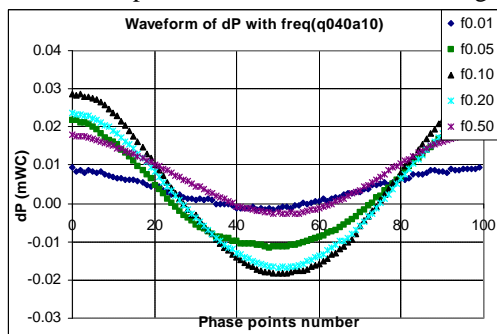
Figure 5-37 Oscillatory amplitude amp=10%
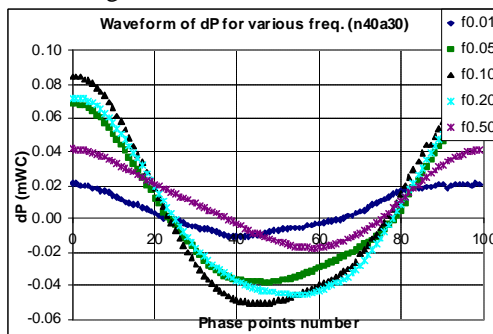
Figure 5-38 Oscillatory amplitude amp=30%

– From Figure 5-37 to Figure 5-40, it is shown that, for combined oscillatory flow (COF), the waveform of head variation was harmonic wave for all cases. The mean value of head variation for COF was deviated from the zero. The waveforms were more like a standard sine wave for stationary dominant flow (SDF, Figure 5-37 in

105

which base flow was 40% and oscillatory amplitude was 10% of full load pump rotating speed). The waveform deformed from standard sine wave for oscillation dominant flow (ODF, Figure 5-40 in which base flow was 40% and oscillatory amplitude was 60% of full load pump rotating speed). For balanced flow, the head variation oscillated in a manner between that of SDF and ODF (BF, Figure 5-38 and Figure 5-39 in which base flow was 40% and oscillatory amplitude was 30% and 40% of full load pump rotating speed respectively), the wave shape deformation was not as obvious as in the case of ODF.

− Comparatively, the waveforms of head variation of pure oscillatory flow (POF), shown in the previous section, were similar to the head loss waveform of ODF, and deformed significantly from the standard sine wave. But the mean value of head variation in POF was approximately equal to zero.
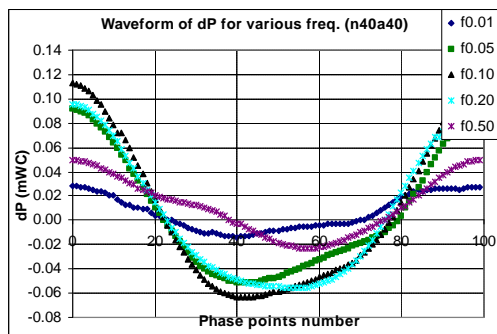
Figure 5-39 Oscillatory amplitude amp=40%   Figure 5-40 Oscillatory amplitude amp=60%
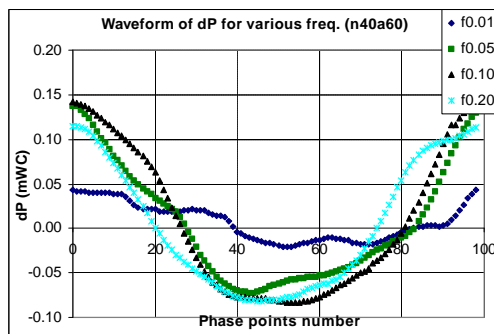
− The head variation along a streamline of COF was amplitude dependent. As an example, the maximum readings of differential pressure sensor for oscillatory flow with frequency 0.05 Hz and base flow 40% are listed in Table 5-7.

Table 5-7 Maximum values of dP for f_r = 0.05Hz

Amp (%)	10	20	30	40	50	60
dPmax (m)	0.02296	0.04475	0.06830	0.09182	0.11478	0.13757

− The head variation along a streamline of COF was frequency dependent. As an example, the maximum readings of differential pressure sensor for flow with base flow 40% and oscillatory amplitude 30% of full pump rotating speed are listed in Table 5-8.

Table 5-8 Maximum values of dP for COF of n0 = 40% and Amp = 30%

Freq. (Hz)	0.01	0.05	0.10	0.20	0.50
dPmax (m)	0.02189	0.06830	0.08458	0.07194	0.04113

− At lower frequency the readings of dP increased with the frequency and at high frequency the readings of dP decreased with frequency. More details on this will be discussed later.

5.5.2 Accelerative head

To evaluate the accelerative head, the measured result from PIV was used. Table 5-9 is the mean velocity of combined oscillatory flow with base flow of 40% of full load pump rotating speed. Table 5-10 is the velocity amplitude of the same oscillatory flows.

106

With the values in Table 5-9 and Table 5-10, the velocity waveform of the combined oscillatory was build and the accelerative head was calculated with Equation (5-23). The waveforms of accelerative head for COF with frequencies ranged from 0.01 Hz to 0.50 Hz, base flow of 40%, oscillatory amplitude ranged from 10% to 60% of the full pump rotating speed are shown in Figure 5-41 to Figure 5-44.

Table 5-9 Mean oscillatory velocity from PIV (V_0)

		Amp (%)					
		10	**20**	**30**	**40**	**50**	**60**
Freq. (Hz)	0.01	0.374	0.364	0.372	0.383	0.389	0.367
	0.05	0.364	0.373	0.381	0.409	0.424	0.426
	0.10	0.386	0.395	0.428	0.462	0.491	0.490
	0.20	0.330	0.353	0.384	0.440	0.456	0.401
	0.50	0.509	0.542	0.585	0.637	0.646	

Table 5-10 Amplitude of oscillatory velocity from PIV (V_{amp})

		Amp (%)					
		10	**20**	**30**	**40**	**50**	**60**
Freq. (Hz)	0.01	0.099	0.191	0.289	0.409	0.434	0.499
	0.05	0.078	0.158	0.238	0.284	0.345	0.366
	0.10	0.054	0.109	0.155	0.209	0.246	0.251
	0.20	0.037	0.076	0.093	0.136	0.172	0.180
	0.50	0.040	0.048	0.082	0.062	0.064	
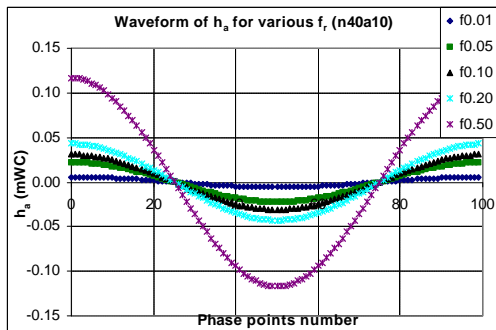
Figure 5-41 Oscillatory amplitude amp=10%
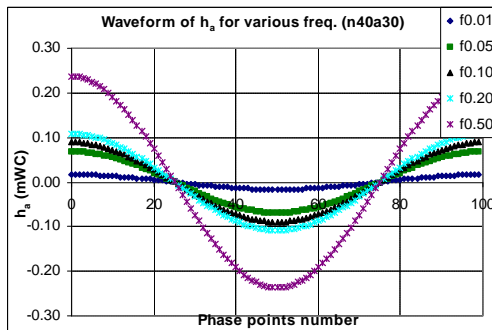
Figure 5-42 Oscillatory amplitude amp=30%
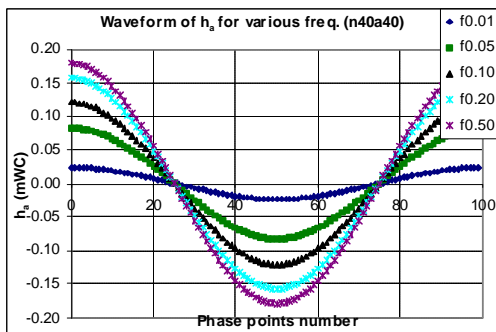
Figure 5-43 Oscillatory amplitude amp=40%
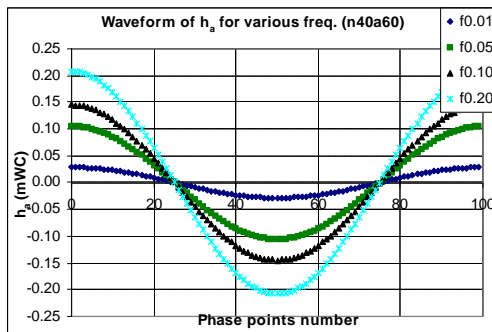
Figure 5-44 Oscillatory amplitude amp=60%

107

5.5.3 Friction head loss

According to Equation (5-24), subtracting the dynamic head from the readings of differential pressure sensor, the friction head loss was obtained. The waveforms obtained in this way for COF with base flow of 40% and oscillatory amplitude from 10% to 60% are shown in Figure 5-45 to Figure 5-48. It is obviously that the friction of head loss is dependent on the frequency for all cases shown.
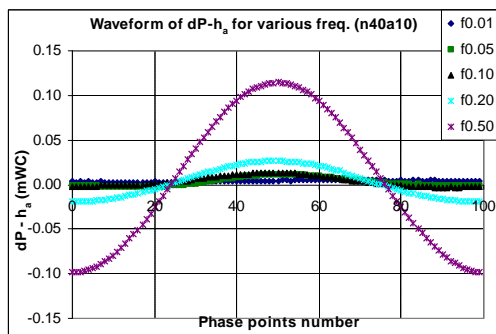
Figure 5-45 Oscillatory amplitude amp=10%
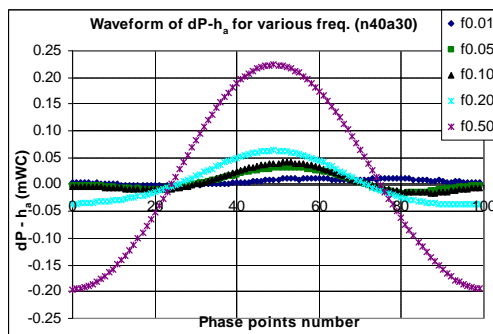
Figure 5-46 Oscillatory amplitude amp=30%
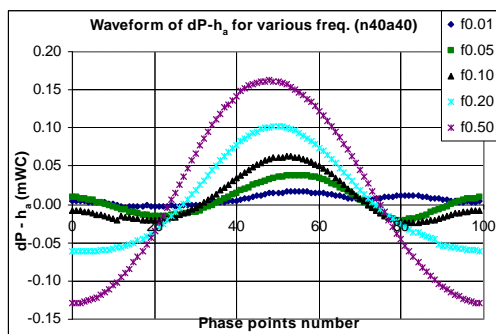
Figure 5-47 Oscillatory amplitude amp=40%
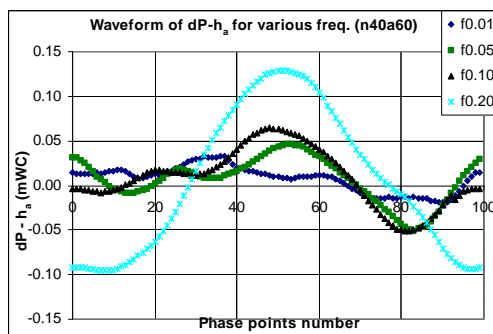
Figure 5-48 Oscillatory amplitude amp=60%

Theoretically, the waveform of friction head loss of oscillatory flow can be built by calculating it with Equation (5-13), using the velocity data listed in Table 5-9 and Table 5-10. The result waveforms are shown in Figure 5-49 to Figure 5-52.

There was a bottom flat in lot curves shown in Figure 5-50 to Figure 5-52. The flat happened at high oscillatory amplitude and low absolute velocity. It was also frequency dependent, the lower of the frequency, the wider of the flat part.

After checking the velocity, Reynolds number and friction factor of the places where the bottom flat occurred, it was found that the friction factor was almost constant at higher oscillatory amplitude shown above. However, there was a special pop up of friction factor when the absolute velocity was cross zero point. There must be a short transition area of flow characteristics around zero velocity point.
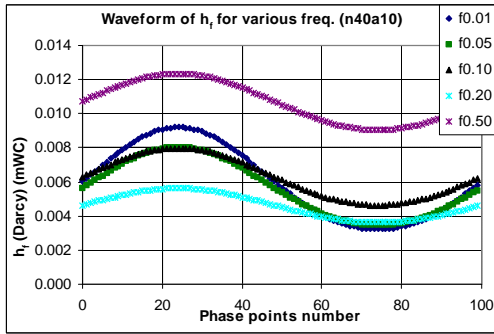
Figure 5-49 Oscillatory amplitude amp=10%
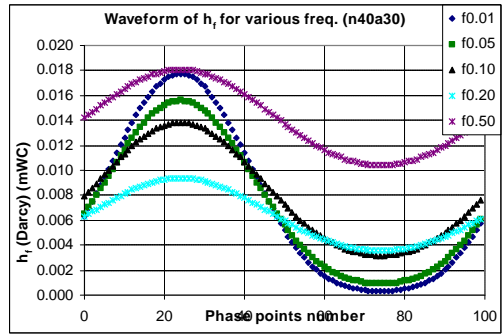
Figure 5-50 Oscillatory amplitude amp=30%
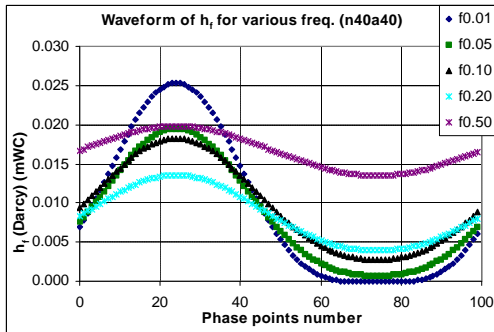
Figure 5-51 Oscillatory amplitude amp=40%
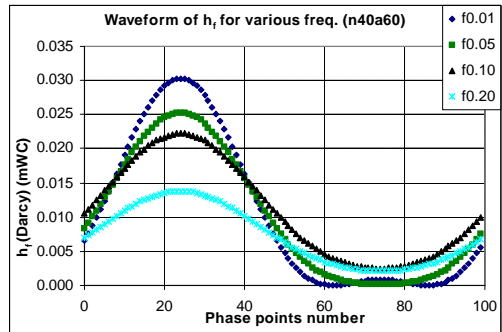
Figure 5-52 Oscillatory amplitude amp=60%
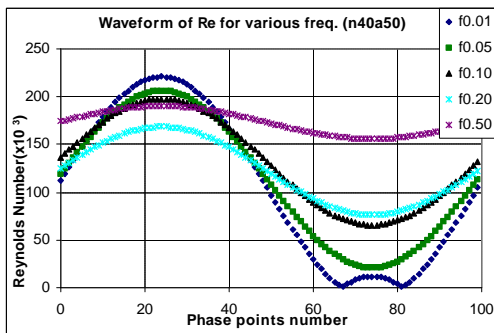
Figure 5-53 Reynolds number amp=50%
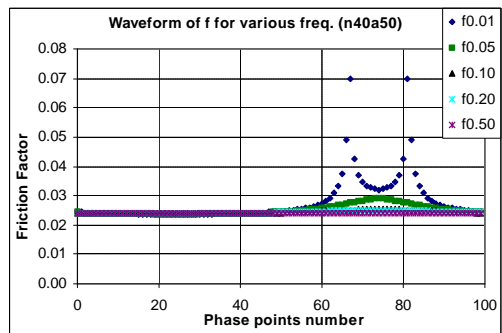
Figure 5-54 Friction factor amp=50%

The Reynolds number and friction factor for COF with base flow of 40% and oscillatory amplitude of 50% are shown in Figure 5-53 and Figure 5-54.

Within the transition area, the relation of velocity and Reynolds number, friction factor, friction head loss was becoming more complicate. Use only Equation (5-13) to get the friction head loss, Equation (5-14) or Equation (5-17) to calculate friction factor, were not accurate for the whole transition area.

5.5.4 Frequency dependency of friction head loss

The mean head variation and peak head variation measured for COF with frequencies from 0.01Hz to 0.50Hz, oscillatory amplitudes from 10% to 60% and base flow 40% of full load pump rotating speed are shown in Figure 5-55 and Figure 5-56.

The mean head variation over oscillatory periods kept almost constant when frequency was smaller than 0.05 Hz, and increased slowly in the frequency range of 0.05 Hz to 0.10 Hz. The mean head variation increased quite fast after the frequency was higher than 0.10 Hz.

For the peak head variation in an oscillatory period, its developing tendency along with frequency was different from that of mean head variation over periods due to the acceleration and deceleration effects of oscillatory flow and other reasons (discussed below). When the frequency was smaller than 0.10Hz, the peak head variation increased along with oscillatory frequency. When the frequency was higher than 0.10Hz, however, the peak head variation decreased along with the increase of oscillatory frequency.
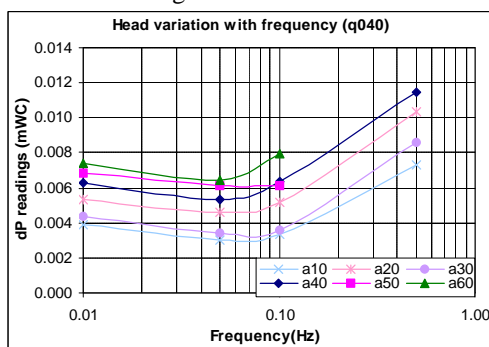
Figure 5-55 Mean head variation
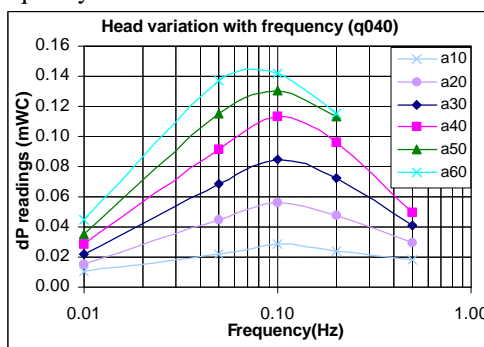
Figure 5-56 Peak head variation

To compare the head variation between COF and POF, COF and SF, the head variations between COF and POF with the same oscillatory amplitude are shown in Figure 5-57; the head variations between COF and SF with the same oscillatory amplitude are shown in Figure 5-58.
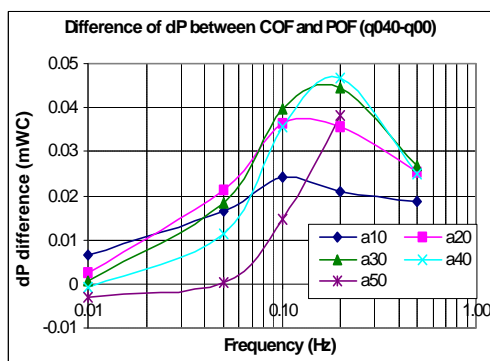
Figure 5-57 dP difference of COF and POF
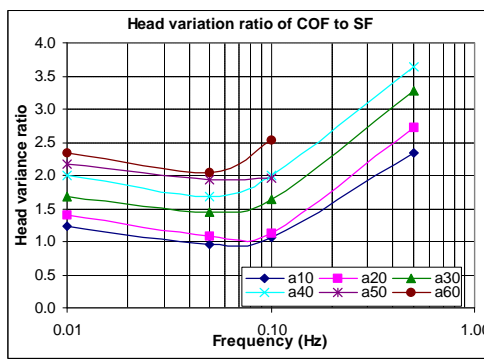
Figure 5-58 dP ratio of COF and SF

Accelerative head was removed from the values in Figure 5-57. For most cases, the peak head loss without accelerating and decelerating parts still had the similar developing tendency as the peak head loss with accelerating and decelerating effects included as shown in Figure

5-56. This indicated that though the mean head loss over periods did not increase along with frequency at lower frequency, the peak head loss in a period increased along with frequency even at lower frequency.

The ratios of mean head variation over periods of oscillatory flow with base flow percentage 40% to that of stationary flow with same base flow percentage were ranged from 1.0 to 4.0 as shown in Figure 5-58, for oscillatory amplitudes from 10% to 60% and oscillatory frequencies from 0.01 Hz to 0.50 Hz. The developing tendency of this ratio was similar to that of the mean head variation over periods shown in Figure 5-55.

As in the case of pure oscillatory flow, when the same rotating amplitude signal was applied to the pumps at different frequencies, the actual flow rate output from the pump varied with the frequency. The peak flow rates of pumps at different frequencies and rotating amplitudes are shown in Figure 5-59.
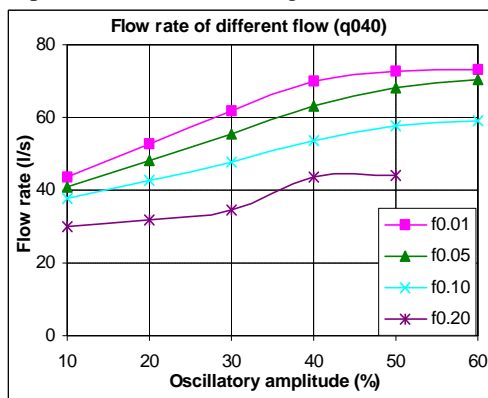
Figure 5-59 Flowrate with amplitude
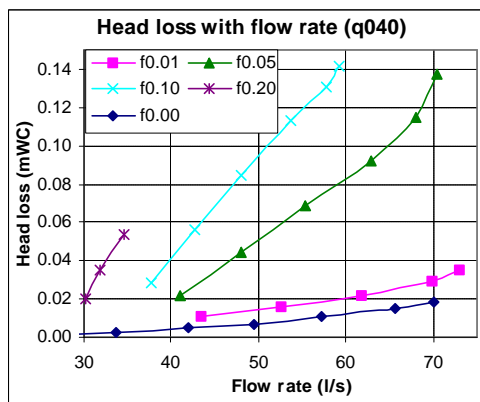
Figure 5-60 Head variation with flow rate

The relation of peak head variation of COF and flow rate in the system is shown in Figure 5-60. The peak head variation of pure oscillatory flow increased with flow rate in a near to linear manner for most cases tested.

By using the results from Figure 5-59 and Figure 5-60, Figure 5-55 and Figure 5-58 on the basis of flow rate was rebuilt. The results are shown in Figure 5-61 and Figure 5-62.
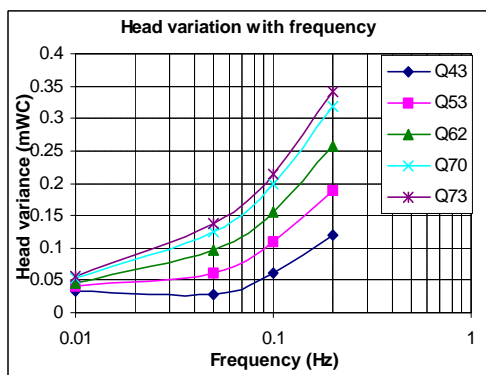
Figure 5-61 Mean head variation
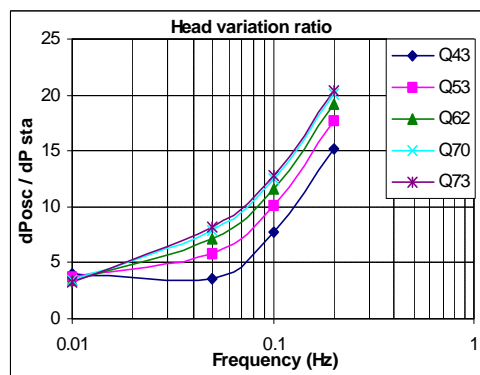
Figure 5-62 Head variation ratio

It is shown in Figure 5-61 and Figure 5-62 that the head variation increased with frequency in all the frequency range tested, slower at lower frequency and faster at higher frequency for all flow rates showed. The ratio of head variation between the oscillatory flow and stationary flow with the same flow rates had the similar developing tendency as the head variation itself of oscillatory flow as shown, increased along with the frequency. The minimum value of the ratio was about 4 located at the lowest frequency tested, 0.01 Hz, and the maximum ratio was almost 20 at maximum frequency shown, 0.20 Hz.

The head losses shown in Figure 5-55 to Figure 5-62 were the general head losses of combined oscillatory flow in the test duct of a specific length. The corresponding accelerative heads along with frequency are shown in Figure 5-63 and Figure 5-64. It is shown from the figures that:

- Thought the magnitudes of the accelerative head was quite small, the developing tendency of the accelerative head along with the frequency was very clear and promising to get a conclusion.

- The peak values of the accelerative head were frequency dependent, increasing along with the frequency.

- The mean values of the accelerative head are developing in a similar manner as that of following transfer function

$$\frac{y}{x} = \frac{1}{C1 \cdot s + C2}$$

   where $C1$ and $C2$ are constants; y is the output and x is the input of the transfer function.

- The mean values of the accelerative head were quite small, near to zero.

- The accelerative head was calculated from the measured velocity (flow rate), its accuracy was dependent on the accuracy of measured velocity. The problems of pumps at high frequency and full load affected this calculation too.

- The oscillatory amplitude also played a role in the accelerative head development. The curve was steeper when the amplitude was bigger.
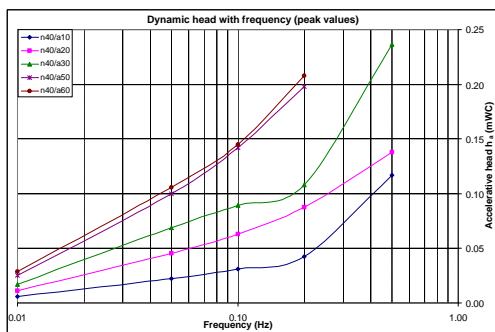
Figure 5-63 Peak values of dynamic head
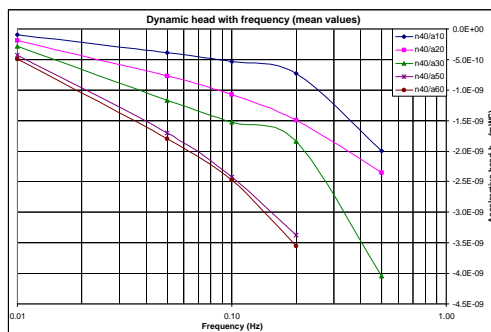
Figure 5-64 Mean values of dynamic head

5.6 Accelerative Head Loss in Frequency Domain

The analysis of head loss presented till now is mainly in time domain. Alternatively, analysis of head loss of oscillatory flow in frequency domain is more commonly used. Following is an example of analysis of head loss in frequency domain for the oscillatory flows measured.

5.6.1 Expression of time constant

A section of the flow is illustrated as Figure 5-65: the water runs from point 1 to point 2 with a flow rate of Q m^3/s. The water head at point 1 is H_1 mWC and the water head at point 2 is H_2 mWC. The cros sectional area of the duct is A m^s.

Obviously, the head loss H and the flow rate Q from point 1 to point 2 can be expressed as:

$$H = H_1 - H_2$$

$$Q = V A$$

where V is the mean velocity of the flow.
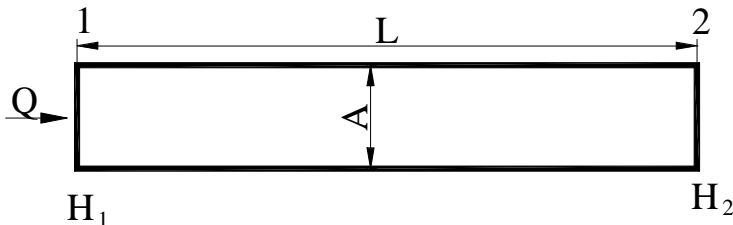
Figure 5-65 A section of the flow

At the same time, the head loss from point 1 to point 2 can be expressed by Bernoulli equation as:

(5-25) $$H = \zeta \frac{V^2}{2g}$$

where $\zeta = \lambda L$ and $\lambda = f(R_h)$ (Moody). Differentializing equation (5-25)

(5-26) $$dH = 2\left(\frac{\zeta}{2g}\right) \cdot V \cdot dV$$

At steady state condition:

$$V = V_0$$

$$H = H_0$$

i.e.,

(5-27) $$\frac{H_0}{V_0} = \left(\frac{\zeta}{2g}\right) \cdot V_0$$

$$dH = 2\left(\frac{\zeta}{2g}\right) \cdot V_0 \cdot dV$$

Dimensionless variables

$$\frac{dH}{H_0} = \frac{2\left(\dfrac{\zeta}{2g}\right) \cdot V_0 \cdot dV}{\left(\dfrac{\zeta}{2g}\right) \cdot V_0^2} = 2\frac{dV}{V_0}$$

or

$$\frac{dV}{V_0} = \frac{1}{2} \cdot \frac{dh}{H_0}$$

Using Laplace transformed dimensionless variables, the above relation can be expressed as:

(5-28) $$\hat{V} = \frac{1}{2}\hat{h} \quad \text{or} \quad 2\hat{V} = \hat{h}$$

Apply Newton's second law to the flow

$$F = ma = m\frac{dV}{dt}$$

$$m = \rho AL$$

$$F = \rho g H \cdot A$$

Then

$$\rho g A \cdot dH = \rho AL \frac{\partial(dV)}{\partial t}$$

$$dH = \frac{L}{g}\frac{\partial(dV)}{\partial t}$$

Dimensionless form is:

(5-29) $$\frac{dH}{H_0} = \frac{V_0}{H_0}\frac{L}{g}\frac{\partial(\dfrac{dV}{V_0})}{\partial t}$$

Apply Laplace transformation $s = \dfrac{\partial}{\partial t}$ to equation (5-29) and introduce:

$$\hat{h} = \frac{dH}{H_0} \quad \text{and} \quad \hat{V} = \frac{dV}{V_0}$$

Then

$$\hat{h} = \left(\frac{V_0}{H_0}\frac{L}{g}\right) \cdot \hat{V} \cdot s$$

or

(5-30) $$\hat{V} = \frac{H_0 g}{V_0 L} \cdot \hat{h} \cdot \frac{1}{s}$$

Now it is possible to establish the connection between equation (5-28) and equation (5-30) as a block diagram as Figure 5-66:
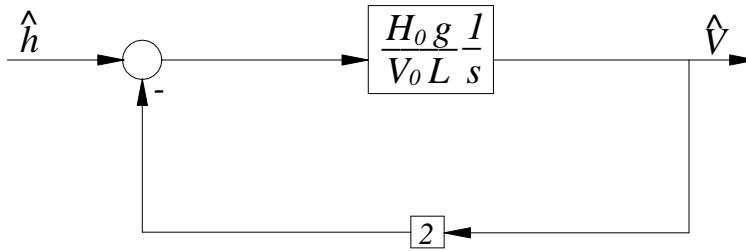
Figure 5-66 Block diagram of the flow

Then

(5-31)
$$\frac{\hat{h}}{\hat{V}} = \frac{\dfrac{1}{2}}{1 + \dfrac{V_0}{2H_0}\dfrac{L}{g}s} = \frac{\dfrac{1}{2}}{1 + T_w s}$$

Here the time constant of the flow in the test duct is

(5-32)
$$T_w = \frac{V_0}{2H_0}\frac{L}{g}$$

Insert equation (5-27) into (5-31)

$$\frac{\hat{h}}{\hat{V}} = \frac{\dfrac{1}{2}}{1 + \left(\dfrac{2g}{\zeta}\right)\dfrac{1}{V_0}\dfrac{L}{2g}s} = \frac{\dfrac{1}{2}}{1 + \dfrac{1}{V_0}\dfrac{L}{\zeta}s} = \frac{\dfrac{1}{2}}{1 + T_w s}$$

or

(5-33)
$$\frac{\hat{h}}{\hat{V}} = \frac{\dfrac{1}{2}}{1 + T_w s}$$

This is the final transfer function of dimensionless head loss and velocity of the oscillatory flow discussed.

5.6.2 Time constant calculation

Comparing equation (5-25) with the Darcy-Weibach formula of friction head loss, equation (5-13), following expression can be developed:

(5-34)
$$\zeta = \lambda L = f\frac{L}{d}$$

From Table 5-2 and Figure 5-4, friction factors for flow rate from 20 l/s to 120 l/s are available for stationary flows. And in the measurement:
  − $L = 9$ m

– $d = D_h = 0.27$ m

The corresponding values of z and T_w can be calculated by equation (5-34) and (5-32) respectively. The results calculated are listed below in Table 5-11.

Table 5-11 Time constants at different flow rates

Q (l/s)	19.69	39.63	60.09	79.82	99.30	119.60
V_0 (m/s)	0.2557	0.5146	0.7804	1.0366	1.2896	1.5532
Re	68607.56	138068.94	209382.16	278121.04	345990.28	416718.11
f_1	0.02521	0.02416	0.02378	0.02359	0.02347	0.02339
f_2	0.02539	0.02424	0.02382	0.02360	0.02347	0.02338
z_1	0.8403	0.8053	0.7927	0.7863	0.7823	0.7797
z_2	0.8463	0.8080	0.7940	0.7867	0.7823	0.7793
T_{w1} (s)	41.8868	21.7178	14.5484	11.0419	8.921	7.4317
T_{w2} (s)	41.5899	21.6452	14.5246	11.0363	8.921	7.4355

5.6.3 The bode diagrams

Based on the time constant in Table 5-11, and the transfer function equation (5-33), the Bode diagrams of the flow at different flow rates are shown below from Figure 5-67 to Figure 5-72.
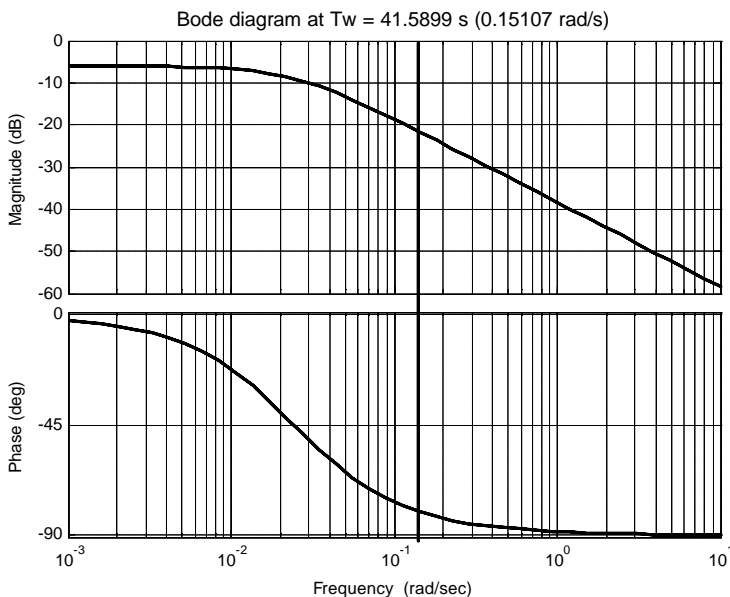
Figure 5-67 Bode diagram at Q = 20 l/s, T_w = 41.5899 s
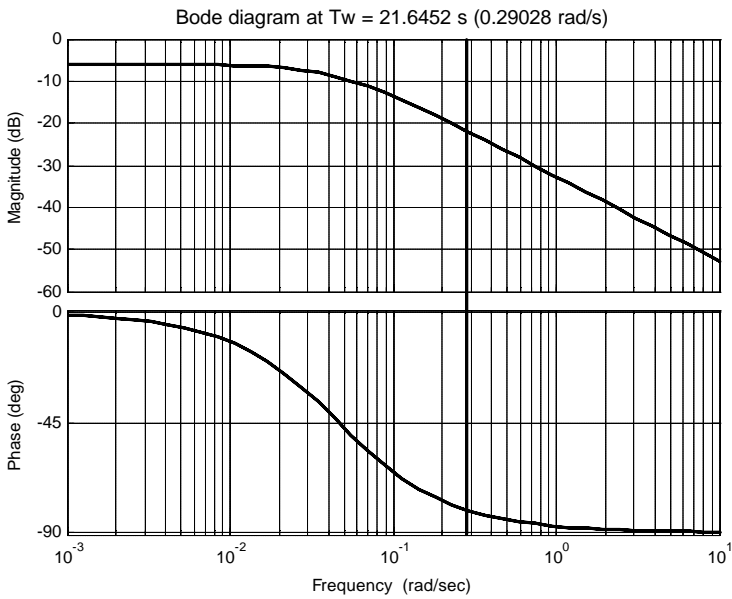
Figure 5-68 Bode diagram of $Q = 40$ l/s, $T_w = 21.6452$ s
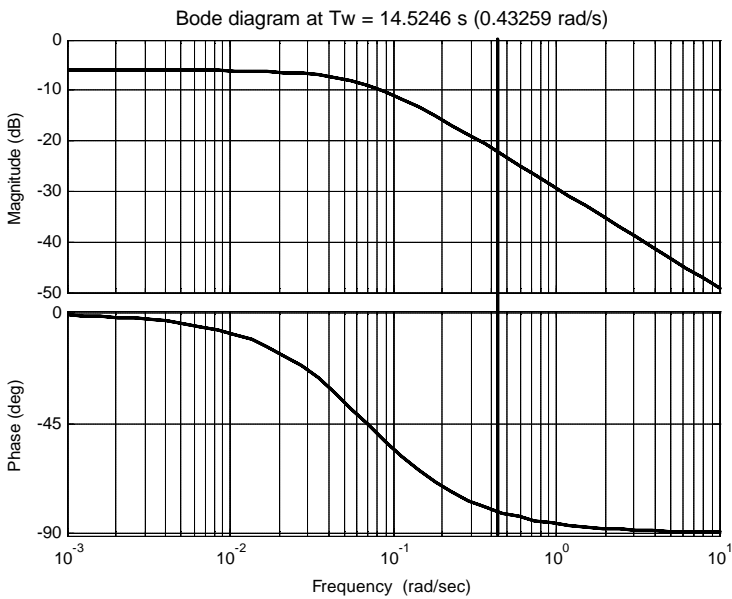
Figure 5-69 Bode diagram of $Q = 60$ l/s, $T_w = 14.5246$ s
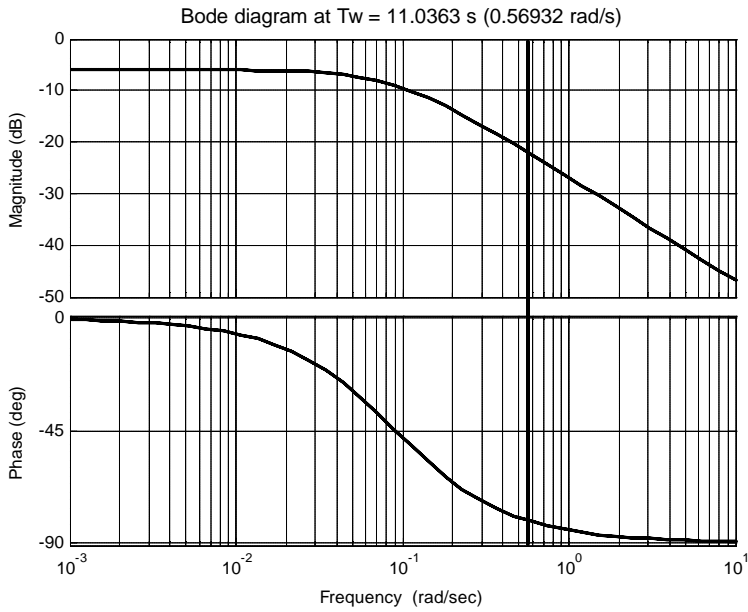
Figure 5-70 Bode diagram of Q = 80 l/s, T_w = 11.0363 s
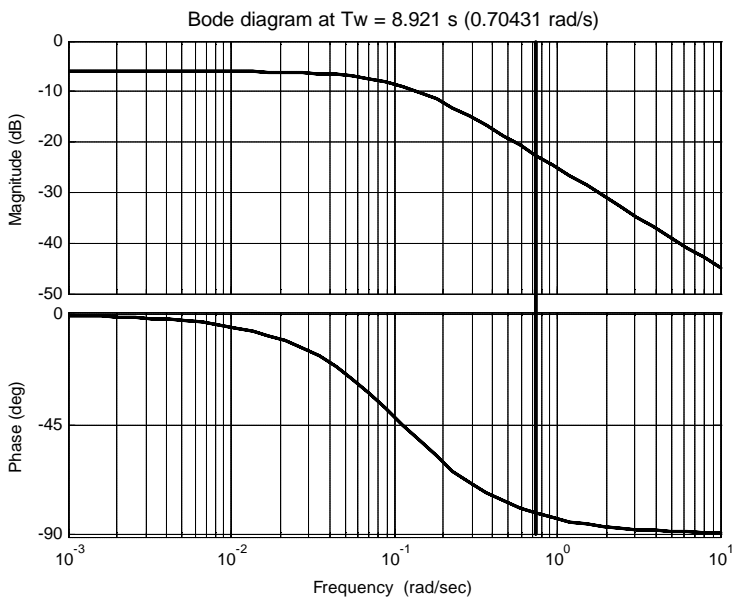
Figure 5-71 Bode diagram of Q = 100 l/s, T_w = 8.921 s
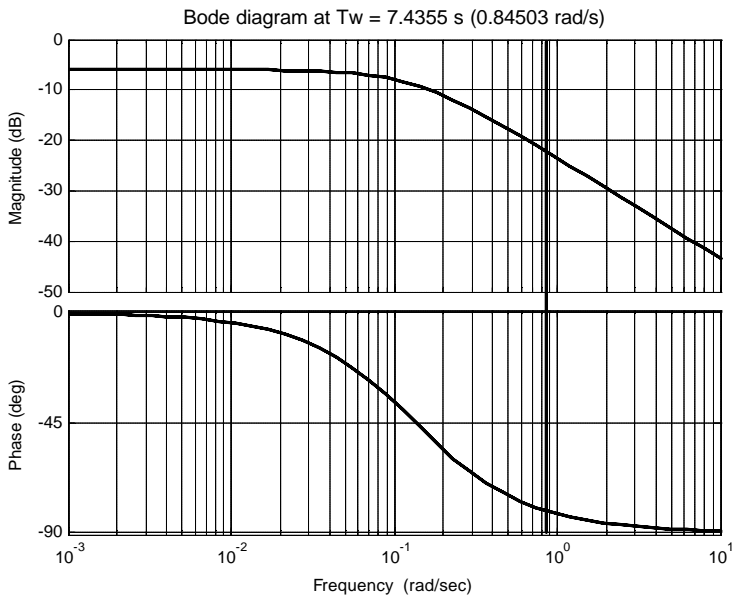
Figure 5-72 Bode diagram of Q = 120 l/s, T_w = 7.4355 s
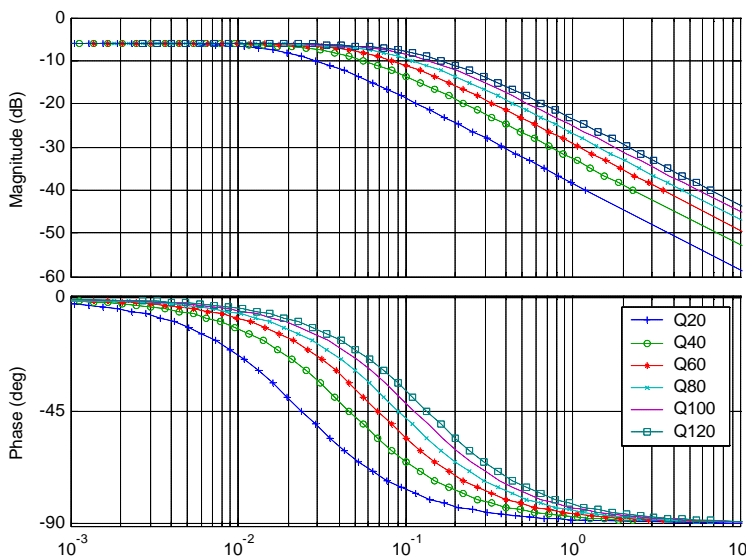
Figure 5-73 Bode diagrams for Q = 10 to 120 l/s

5.6.4 Discussions of time constant and phase shift

From the time constants calculated above, it is clearly shown that the time constant decreased along with the increases of the flow rate.

The Bode diagrams of flow rates from 20 l/s to 120 l/s are shown in Figure 5-73. It is shown in the figure that the magnitudes of the Bode diagram move to right (higher frequency direction) with the increase of the flow rate. This was coincidence with the theoretical analysis.

One of the advantages of analyzing the head loss in frequency domain and representing it in the form of transfer function and Bode diagram is that it is easier to get the phase shift between the head loss and the flow rate, i.e., the mean velocity. It is shown in Figure 5-67 to Figure 5-72 that the phase shift between the head loss and the mean velocity increases along with the increases of the velocity.

The time constant and Bode diagram shown above are based on the measured differential pressure from steady flow. If a method could be used to make dimensionless the measured differential pressure of oscillatory flow shown in previous sections of this chapter, it would be possible to get the dynamic head loss in oscillatory flow and presented it in a similar form as Figure 5-67 to Figure 5-72, i.e., in frequency domain. The author did not find a simple method to do this due to the limitation of time, data available and the complexity of the flow regimes measured.

Chapter 6

Discussion and Conclusion

Main topics of this chapter:

- Conclusions of Oscillatory Velocity

- Conclusions of Head Loss

- Discussions

6.1 Conclusions and Discussion of Oscillatory Velocity

From the results shown in Chapter 4, it is concluded that:

1. Velocity profile:

Velocity profiles of all flows tested had similar shape, for both stationary flow and oscillatory flow. The velocity fluctuated around the centreline mainstream velocity, or the maximum instant velocity in more than 80% of the duct height. The velocity, which was smaller than 50% of the centreline mainstream velocity, was only found in a very narrow area next to the boundary wall, less than 10% of the duct height.

The flow tested was completely turbulence. The velocity could be very low when the phase angle of pure oscillatory flow was crossing zero. The velocity profile was quite flat at the low velocity, similar to that of higher velocity. No transition between laminar and turbulence was observed.

The velocity of the flow tested fluctuated in both directions of a PIV sampling plane. The velocity increased from the boundary wall to the centreline, following the general profile of turbulent flow. On the other hand the velocity fluctuated a little locally along with the general increasing tendency of velocity from the boundary wall to the centreline. The flow oscillated as mass oscillation in a general view, fluctuations were spotted from points with the same horizontal coordinate.

2. Velocity waveform

Velocity waveforms of most oscillatory flows tested were single frequency harmonic wave. The waveform was complex when oscillating frequency was higher than 0.50 Hz, when the absolute value of the velocity was very small due to the limitation of the pumps (could be out of the bandwidth of the pump to response to a input signal).

3. Annular effect

Annular effect was dependent on not only oscillatory amplitude and frequency, but also the ratio of stationary part to oscillatory part. The general actions of all these factors determined the magnitude of annular effect. Generally, annular effect was not obvious at lower frequency and

small oscillation. It was easy to be observed at higher frequency, especially when the oscillatory amplitude was bigger.

"Sub-annular effect" was observed in lot of oscillatory flows while exact annular effect did not exist, the "overshooting" of which was smaller than the centreline mainstream velocity, but obviously was bigger than the adjacent velocity. "Sub-annular effect" was located in the area where annular effect happened if existed.

4.   Phase shift

The phase change of velocity from the point near to the wall to the point near to the centreline at the same time instant was insignificant for both pure oscillatory flows and various combined oscillatory flows tested.

5.   Dependency of amplitude, frequency and stationary part

The shape and developing tendency of both the velocity profile and waveform were not obviously dependent on either the oscillatory frequency, or the oscillatory amplitude, or the percentage of stationary flow.

However, the amplitude of velocity was dependent on the frequency when the pump input signal kept unchanged, the higher of the frequency, and the lower of the maximum velocity. It would be ideal if this dependency did not exist. This was due to the limitations of the pumps when operating at higher frequency.

6.   Mainstream velocity and vertical velocity

Mainstream velocity and velocity in the vertical direction had the similar distribution and waveform. The magnitude of velocity in the vertical direction was quite small comparing with mainstream velocity. The mainstream velocity and velocity in the vertical direction have a phase difference of 180° in all physical locations.

7.   LDV velocity and PIV velocity

The velocities from LDV and PIV were quite similar. More samples were collected from LDV for each flow regime and the statistics results were smoother, comparing with the PIV velocity, which did not collect large amount of samples. This was obvious in the case of steady flow. The difference of results between LDV and PIV was insignificant in the case of oscillatory flow.

8.   Velocity errors

Velocity errors could result from the test condition, environmental conditions and so on. These errors would not influence the conclusions mentioned above. The author believed that the PIV velocity was quite accurate except for some cases when big air bubbles existed in the water. This happened when the oscillatory amplitude was near to the full pump load, the absolute velocity in the test duct was quite high and the head in the flow was quite low.

6.2 Conclusions and Discussion of Head Variation

From the results shown in Chapter 5, we can get following points

1.   Head variation

The head variation from differential pressure sensors along the test duct oscillated in a similar manner as the velocity, with the same oscillating frequency, single peak value in one period, but the waveform deformed from the standard simple harmonic wave.

The head variation increased with frequency all the way in the frequency range tested, increasing slower at lower frequency and increasing faster at higher frequency for all flow rates

measured. The ratio of head variation between the oscillatory flow and stationary flow with the same flow rate showed the same tend as the head variation itself of oscillatory flow, increasing along with the frequency. The minimum value of the ratio was about 4 located at the lowest frequency tested, 0.01 Hz, and the maximum ratio was almost 20 at maximum frequency showed, 0.20 Hz.

2. Accelerative head

Accelerative head discussed in the thesis was a theory value based on the measured velocity. It oscillated as harmonic wave in the same frequency as the velocity. There was a phase shift of 90° between the mean velocity and the accelerative head.

Accelerative head was in the same phase as that of head variation mentioned above.

3. Friction head loss

Friction head loss discussed in the thesis was the difference between head variation and accelerative head. It had similar characteristics to head variation.

4. Frequency dependency

It was clearly shown that the head variation from differential pressure sensor, the accelerative head and the friction head loss in the test duct was frequency dependent if the flow rate kept constant. The ratio of various heads of oscillatory flow to the stationary flow was different for different oscillatory flows. The ratio was bigger for pure oscillatory flow and was smaller for combined oscillatory flow.

5. Amplitude dependency

It was also shown that the peak value of various heads of oscillatory flow was amplitude dependent, the bigger of the amplitude, the higher of the head variation or head loss along the test duct.

Chapter 7

Further Work

Measurement costs a lot of time and money. Process and analysis of the experimental data are very time consuming and needs lot of tricks. Due to the limitation of time and fund, lot of experiment and theory work to discover more details about the mechanism of head loss in the tunnel with oscillatory flow could not be carried out in the working period of this thesis. To get a better understanding of the head loss in the tunnel with oscillatory flow, the author suggests that following researches should be carried out in the future:

1.   Measurement of rougher inner layer

Sand roughness was used in the measurement carried out. Other roughnesses, which are rougher than sand roughness, should be deployed and measurement on various oscillatory flow regimes ought to be carried out with the new roughness. For example, the roughness in the test tunnel can be build by gluing stone particles with different sizes to the tunnel wall. The author supposes that there is difference on the head loss mechanism and its dependency on oscillating frequency and amplitude between various roughnesses. The boundary layer plays a more important role in head loss analysis when roughness is of higher scale.

At least two more roughness could be tested. If the sand roughness is called small-scale roughness, medium roughness (10 times rougher) and large roughness (80—100 times rougher) should be the next objects to measure.

2.   Improvement of the rig

Improvement to the test rig is helpful to get more accurate measuring results. For instance, a symmetry layout of the rig, which is not the case in the measurement presented, is essential to get a balanced flow in both directions; more rigidity test tunnel wall is needed to test the flow with high oscillatory amplitude, when errors in measurement resulted from vibration of the tunnel wall and wave speed ought to be limited; make the boundary darker so that PIV or LDV can get more information of the boundary layer. It would be much better to rebuild the rig based on the problems bumped in the measurement presented here before any new measurement is conducted.

3.   Theory development

Both theory and experimental research on unsteady water flow are not sufficient till now. Especially the research on non-circular duct with unsteady flow is very limited. However there are many engineering applications related to this flow regime. Most available theory and experiment on unsteady flow is about circular pipe. There should be significant difference between circular pipe and non-circular duct on the head loss mechanism and its dependency on oscillating frequency and amplitude. The secondary flow located near to the corner of non-circular duct is unique in non-circular duct. It transports momentum from the center to the corner of the duct and generates high velocity in the area near to the corner. This phenomenon would be more complicate when higher roughness is applied. It will contribute more to the head loss in the duct.

More theory work should be done on this. The theory could base on the experimental result and as a basis for further experiment.

4.   Further analysis of the data obtained

A large amount of the data obtained from the measurement presented. The results presented here are just derived from a small part of the data. Further detail analysis of the data is needed. More results can be got from digging into the data. The author is very sure of this point. For example, detail comparison of the test results based on the mean flow rate is needed for a more concrete conclusion; dimensionless of the velocity measured and compares it with the turbulence models.

Only example data from LDV measurement is presented in Appendix. Other data measured should be studied too. Characteristics like turbulence intensity, velocity gradient, vorticity and so on can be derived from LDV data and / or PIV data. More details of the flow structure can be displayed.

5.   More start up and stop test

The measurement presented here is mainly about the fully developed oscillatory flow. Some start-up tests were carried out and the result is briefly presented in Appendix B. More measurement on start-up can be carried out, not only with stationary flow, but also with oscillatory flow. PIV can be put into action during the start-up measurement to see how the flow is developed. It is difficult for LDV to get enough information in the start-up period. PIV can get enough pictures to show the process of how the flow is build up. Stop test (valve close) is difficult to be carried out with the rig configuration used. Actually stop test is more meaningful to the application in hydropower plant. Lot of theory and experiment are available for stop test, mainly on circular pipe.

Bibliography

[1]   Binder G., Kueny J. L. (1982) Measurements of the periodic velocity oscillations near the wall in unsteady turbulent channel flow. Turbulent Shear Flows Third-International Symposium on Turbulent Shear Flows. Springer Verlag, Berlin, West Germany. pp 6-17.

[2]   Borghei S. M. (1982) Oscillatory boundary layer over fixed rough beds. Univ-Nottingham

[3]   Brekke Hermod (1984) A stability study on hydro power plant governing including the influence from quasi nonlinear damping of oscillatory flow and from the turbine characteristics. The Norwegian University of Science and Technology, Troondheim, Norway.

[4]   Clauser. F. H., 1956, The Turbulent Boundary Layer', Advances in Applied Mechanics, vol.4, pp.1-51, Academic Press, Inc.

[5]   Colebrook, C. F. (1939): Turbulent flow in pipes with particular reference to the transtion region between the smooth and rough pipe laws. J. Institution Civil Engineerings

[6]   Fox J. A. (1989) Transient Flow in Pipes, Opend Channels and Sewers. Ellis Horwood Limited, New York.

[7]   Gere James M., Timoshenko Stephen P. (1990) Mechanics of Materials, Third Edition. PWS-KENT Publishing Company, Boston.

[8]   Jonsson L. (1991) Mean velocity profiles in transient flows. Proc Int Meeting on Hydraulic transients and column separation. , Valencia, Spain. pp 99-113.

[9]   Jonsson I. G. (1980) A new Approch to Oscillatory Rough Turbulent Boundary Layers. Ocean Engineering Vol. 7, 1980 pp 109 -152 , Pergamon Press Ltd., Great Britain.

[10]   Lawrence W. Carr (1981) A Compilation of Unsteady Turbulent Boundary Layer Experimental Data. Technical Editing and Reproduction Ltd, London.

[11]   Li Pingju (2001) Preliminary Measurement of Oscillatory Tunnel Flow with PIV. 10th IAHR WG on the Behaviour of Hydraulic Machinery Under Steady Oscillatory Conditions. , Trondheim Norway.

[12]   Li Pingju, Brekke Hermod (2002) Experimental Study on Head Loss of Combined Oscillatory Flow in Rough Rectangular Duct. In Proceedings of the Hydraulic Machinery and Systems 21st IAHR Symposium. , September 9-12, 2002 Lausanne, Switsland.

[13]   Li Pingju, Svingen B. (2000) Preliminary Measurement of Model Tunnel Flow. In Procedings Eighth international symposium onStochastic hydraulics. , Beijing China.

[14]   Li Pingju, Svingen B., Selanger Karl (1999) Losses in Transient and Oscillating Flow in Pipes and Tunnels. In 9th IAHR WG on the Behaviour of Hydraulic Machinery Under Steady Oscillatory Conditions.

[15]   Lodahl C. R., Sumer B. M., Fredsoe J. (1998) Turbulent combined oscillatory flow and current in a pipe. Journal of Fluid Mechanics 373, 313-348.

[16]   Raffel Markus, Willert Christian E., Kompenhans Jürgen (1998) Particle Image Velocimetry. Springer, Berlin.

[17]   Ramaprian B. R., Tu S. W. (1983) Fully developed periodic turbulent pipe flow. II. The detailed structure of the flow. Journal of Fluid Mechanics 137, 59-81.

[18]   Ramaprian B. R. and Tu S. W. (1979) Experiments on Transitional Oscillatory Pipe Flow, IIHR Report No. 221, Iowa Institute of Hydraulic Research, The University of Iowa , August 1979, Iowa City, Iowa 52242, USA

[19]   Richardson E.G. and Tyler E. (1929) The Transverse Velocity Gradient Near the Mouth of Pipes in which an Alternating or Continuous Flow of Air is Established. Proc. Phys. Soc. London 42, 1-15

[20]   Roy D. N. (1988) Applied fluid mechanics. Chichester : Ellis Horwood.

[21]   Skåre Per Egil (1994), Experimental Investigation of an Equilibrium Boundary Layer in Strong Adverse Pressure Gradient, the Norwegian University of Science and Technology, Trondheim Norway

[22]   Schlichting Hermann (1979) Boundary-layer theory. Mcgraw-Hill, Inc, New York

[23]   Schlichting Hermann, Gersten Klaus (2000) Boundary-layer theory. Springer, Berlin.

[24]   Svingen Bjørnar and Roar Vennatrø, Transient og oscillerende hydraulisk demping I rør, SINTEF Rapport STF84 A96441, SINTEF Energiforskning, Desember, 1996

[25]   Thorley A. R. D. (1991) Fluid Transients in Pipeline Systems. D. & L. George Ltd.

[26]   Tu S. W., Ramaprian B. R. (1983) Fully developed periodic turbulent pipe flow. I. Main experimental results and comparison with predictions. Journal of Fluid Mechanics 137, 31-58.

[27]   Vennatrø Roar (2000), An Experimental and Theoretical Analysis of Non-steady Turbulent Flow in Circular Smooth Pipes. Norwegian University of Science and Technology, Trondheim Norway.

[28]   Ventsel Eduard, Krauthammer Theodor (2001) Thin Plates and Shells, --Theory, alalysis, and applications. Marcel Dekker Inc., New York, NY 10016.

[29]   White C. M (1932): Fluid friction and its relation to heat transfer, Trans. Inst. Chem. Eng. 10, 66

[30]   White Frank M. (1991) Viscous Fluid Flow. McGraw-Hill, Inc., Singapore.

[31]   Wylie E. Benjamin, Streeter Victor L., Suo Lisheng (1993) Fluid Transient in Systems. Prentice Haa, Inc., New Jersey.

Appendix A Auxiliary Processing / Computation

A.1 Waveform Points Rearrange and Curve Fitting

A.1.1 Background

In the measurement, the following variables of the flow were in sine waveform when oscillatory flow applied:

1.   Velocity at one point in the test duct

2.   Flow rate at one point in the test duct

3.   The dynamic pressure at one point in the test duct

4.   The differential pressure between two points along the mainstream.

In the cases of (3) and (4), the waveforms might not be exactly in the form of a sine wave, but in the form of quasi-sine wave.

   Due to the samplings were not started from the identical phase angle for all flow regimes, the waveforms of the same variable got from different flow regimes could have "phase difference", which could cause confusion when one try to compare the results of the same variable from different flow regimes.
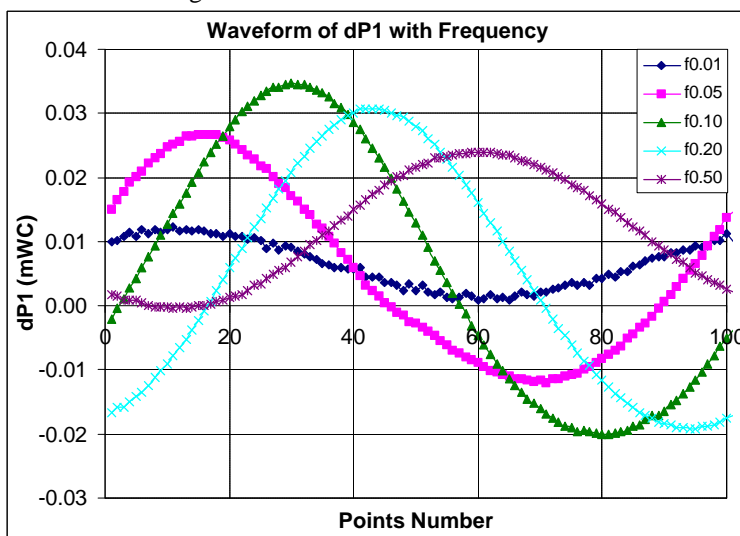
Figure A-1 Waveform before processing

   Figure A-1 is an example of the case. The maximum value of waveform of flow with frequency $f_r = 0.05Hz$ was located at about 17th sample point. The maximum value for $f_r = 0.50$ Hz was located at far downstream, about 60th sample point. In Figure A-1, it is not too difficult to compare the difference between flow regimes. However, it is easy to be confused that there is phase shift between different flow regimes, which is meaningless here.

   There were two basic ways to fix this so that the waveform for different flow regimes could be shown in a synchronized mode, i.e., started from the same phase angle and developed in the same tendency. One of the ways was to take one waveform as the norm and shift others to the

129

norm, i.e., rearrange the sequences of the discrete points for other waveforms. Another way was to find the mathematical expression of the waveform and redraw the waveform of all flow regimes with the expressions by the same initial phase angle.

A.1.2 Rearrange the discrete points

Each waveform in Figure A-1 is composed of the same amount of discrete points. If we took the waveform of $f_r = 0.10Hz$ as the norm. Then we rearranged the discrete points of other waveforms so that their maximum points could be located at the same place of *x-axis*.

1.   Find the location of maximum point on each waveform, listed in Table A-1.

<p align="center">Table A-1 Maximum value locations</p>

ID	f0.01	f0.05	f0.10	f0.20	f0.50
Maximum value location	11	17	30	43	60
Maximum value	0.0122	0.0267	0.0347	0.0308	0.0240
New location	25	25	25	25	25

2.   Rearrange the samples and redraw the waveforms, as shown in Figure A-2
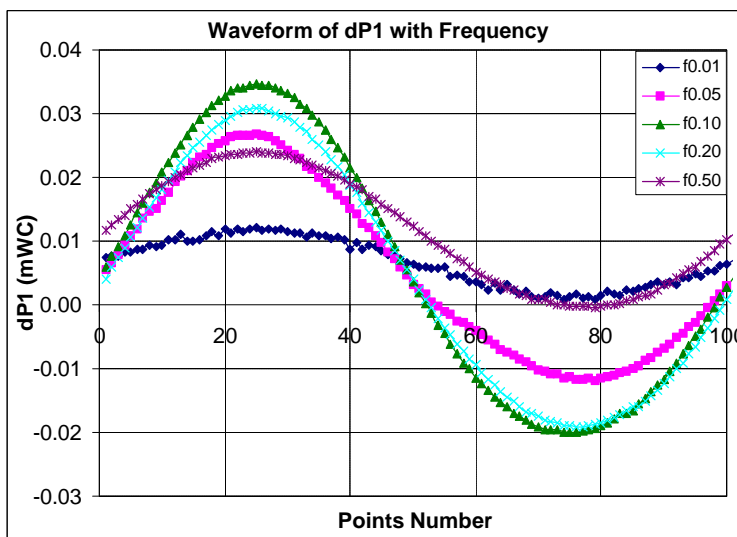
<p align="center">Figure A-2 Waveform after points rearrange</p>

This processing was applied to the data handling for the measurement.

A.1.3 Waveform fitting

If the waveform was expressed as

(A-1) $$y = y_0 + y_{amp} \sin(\varphi_0 + \Delta\varphi)$$

where y_0 could be represented by the mean values of samples, y_{amp} could be the expressed by the difference of maximum value and mean value of samples, and $\Delta\boldsymbol{j}$ was the phase difference between sample points. Information of the frequency and time instant was included in the value of $\Delta\boldsymbol{j}$. Then y_0 and y_{amp} were known, at least the approximate values could be known from the

measured values. The only unknown in Equation (A-1) was j_0. Insert the values of any sample point into Equation (A-1), the unknown j_0 could be evaluated.

In the case of mean value of y_0 and oscillatory amplitude y_{amp} were not available, or for the purpose to verify the values, it was possible to insert three set samples of y and Δj into Equation (A-1), then we get

$$(A\text{-}2) \qquad\qquad y_1 = y_0 + y_{amp}\, \sin(\varphi_0 + \Delta\varphi_1)$$

$$(A\text{-}3) \qquad\qquad y_2 = y_0 + y_{amp}\, \sin(\varphi_0 + \Delta\varphi_2)$$

$$(A\text{-}4) \qquad\qquad y_3 = y_0 + y_{amp}\, \sin(\varphi_0 + \Delta\varphi_3)$$

By Equation (A-2) - (A-3) being divided by Equation (A-3) - (A-4), then

$$(A\text{-}5) \qquad\qquad \frac{y_1 - y_2}{y_2 - y_3} = \frac{\sin(\varphi_0 + \Delta\varphi_1) - \sin(\varphi_0 + \Delta\varphi_2)}{\sin(\varphi_0 + \Delta\varphi_2) - \sin(\varphi_0 + \Delta\varphi_3)}$$

where only j_0 was unknown and could be found with numeric method quite easily. Then y_0 and y_{amp} could be calculated by Equation (A-6) and Equation (A-7) as following

$$(A\text{-}6) \qquad\qquad y_{amp} = \frac{y_2 - y_3}{\sin(\varphi_0 + \Delta\varphi_2) - \sin(\varphi_0 + \Delta\varphi_3)}$$

$$(A\text{-}7) \qquad\qquad y_0 = y_1 - y_{amp}\, \sin(\varphi_0 + \Delta\varphi_1)$$

After the control parameters of the waveform, i.e., mean, amplitude, initial phase angle, were obtained from the process shown above, Equation (A-1) could be used to calculate the time series of y. Compare the calculated values with the original values to verify if the parameters got from waveform fitting were good enough.

To minimize the error caused by the deviation of original sample data, the phase interval $\Delta j_1 - \Delta j_2$ and $\Delta j_1 - \Delta j_2$ ought not be too small. And to minimize the fitting error, multiple parameters y_0, y_{amp} and j_0 could be calculated from different sets of sample data y and Δj. Then average the results to get the mean as y_0, y_{amp} and j_0 in Equation (A-1) to build the time series.

A.1.4 Discussion

If the waveform was not in the form of standard sine wave, it was difficult to express it with Equation (A-1). It was difficult to use the method of "wave fitting" to process the data set. The method of "Rearrange the discrete points to shift the waveform" could be applied in most of the cases if there was only single peak in one period of the wave form. If there were multiple peaks located in one period, the problem was more complicate.

The initial phase angle of all variables ought to be the same if start all data acquisitions at the same instant. This was the case for the variables in the measurement of one flow regime. It was possible to start each measurement from the same phase point for all flow regimes. This was the case used in the last stage of the measurement. However, first this method was not applied at the start stage of the measurement; secondly there was a distance between different sensors, i.e., they were not deployed at the same location of the test tunnel, it was quite difficult to start collecting data from each sensor at the exactly the same phase angle of the flow; thirdly, the phase shifts of flow among the sensors at different locations were different from flow to flow.

A.2 PIV Velocity Integration

When comparing the measurement on the basis of flow rate, and when trying to calculate accelerative head and friction head loss from Darcy-Weibach formula, mean flow rate or mean velocity of oscillatory flow was needed. The mean flow rate and mean velocity of oscillatory flow could be integrated from the velocity field measured by Particle Image Velocimetry.

A.2.1 PIV data brief

The Particle Image Velocimetry (PIV) system took the picture of a target flow. Velocity data could be extracted from the pictures by special algorithm. First, the pictures were meshed into grids as shown in Figure A-3.
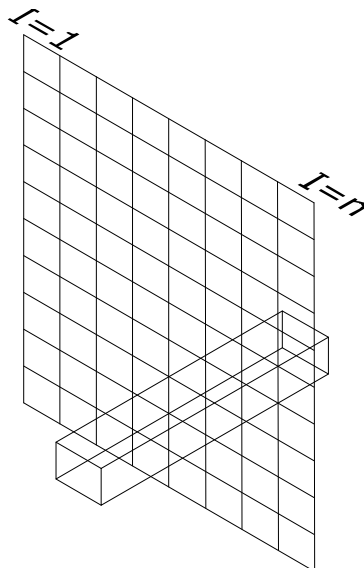
Figure A-3 Element box of PIV flow rate

The velocity of each cell was calculated according to the displacement of particle in the flow of the cell. Supposed

–   all particles in one specific cell moved in the same velocity

–   the flow velocity kept constant in the box shown in Figure A-3.

where the box was normal to the flow direction, with a length equalled to the width of test tunnel, and a cross section equalled to the area of the cell mentioned above.

The velocity field was available after the velocity of each cell was calculated. This was the basic information stored in the vector field files of PIV velocity.

The grid of velocity field was indexed as $I = 1$ to n in the mainstream direction, and as $j = 1$ to m in the vertical direction. The velocity was denoted as u in the mainstream direction and v in the vertical direction.

Mean flow rate of the flow could be calculated from the velocity and geometry of every cell by integrating method.

In most case the flow was dominated by the mainstream flow or the velocity element u contributed most of the flow rate and the velocity element v was insignificant in the flow rate calculation. The flow rate would be integrated from the mainstream velocity component only. The flow rate calculated by this way was just an approximation of the real flow rate. There were

other factors that were not taken into account, such as the boundary layer, annular effect area in both ends of the box in Figure A-3, where the velocity was much different from that of the centreline part.

A.2.2 Flow rate calculation

1. Mirror the data to the whole height

The height of the tunnel was about 360 mm and it is too high for the PIV to capture the flow of full height in one PIV frame and it was not necessary to do so. The cross section of test tunnel was a rectangular. It was assumed that the velocity distribution across the section was symmetrical (left of Figure A-4, in which the flow direction was perpendicular to the paper, flowing out or in the paper).
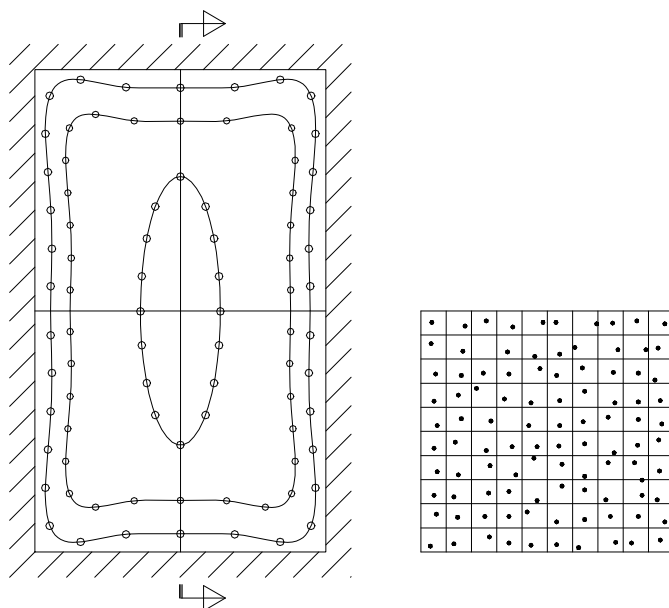
Figure A-4 Velocity in a rectangular tunnel

In practice, only the lower half of the tunnel height was measured, as shown in the right part of Figure A-4. It was a section view of the left part of Figure A-4, as shown in the figure by arrows. The full height velocity distribution could be obtained by mirror the lower half to the upper half. To calculate the flow rate in the tunnel, first integrate the velocity of the lower half along the height and the total mean flow rate was two times of the integrated results.

2. Element flow rate

The element flow rate was the flow passing through the vertical side surface of the box in Figure A-3 in a unit time. If the length of a PIV frame was L *(x axis)*, the width of the tunnel was B *(y axis)* and the height of the tunnel was $2H$ *(z axis)*. The dimension of box was as follows:

  −   length of the box $b = B$
  −   width of the box $l = L / (n – 1)$
  −   height of the box $h = H / (m – 1)$

The area of the vertical side surface of the box was $h \times b$. If the flow velocity of the cell was u, then the cell flow rate passing through the box was $q = u \times h \times b$.

3.   Instant flow rate

Theoretically, instant flow rate Q_i of the tunnel could be obtained by integrating the cell flow rate q along the tunnel height. As a simplification, Q_i was approximately equal to the sum of all element flow rates along the height of the tunnel.

(A-8)
$$Q_i = \sum_{j=1}^{m-1} q_j$$

For each PIV picture, n Q_i were calculated with this equation.

4.   Flow rate average along streamline

The fluid was assumed to be uncompressed. To make the calculation more accurate, average the instant flow rate Q_i along the streamline within one PIV frame.

(A-9)
$$Q = \frac{1}{n-1} \sum_{i=1}^{n-1} Q_i$$

For each PIV picture, a Q was calculated with this equation.

5.   Flow rate average over phase

For oscillatory flow, the flow rate waveform was composed of a sequence of Q_i from equation (A-8) or Q from equation (A-9). By averaging the flow rate Q_i or Q over phase, final waveform of flow rate was built up. If the sampling frequency of PIV was f_{piv} (Hz), the total number of PIV picture for one flow regime measured was N_{piv}, the time taken for the measurement was $t_{piv} = N_{piv} / f_{piv}$. If the period of the flow was T_{flow}, the number of periods measured was $n_{flow} = t_{piv} / T_{flow}$. The picture number for each period was $n_{piv} = N_{piv} / n_{flow}$.

From equation (A-8), a series of instant flow rate was obtained: Q_{i1}…… Q_{iNpiv}

From equation (A-9), a series of instant flow rate eas obtained: Q_1…… Q_{iNpiv}

For each phase angle, the mean flow rate was

(A-10)
$$Q_{mean}(\phi) = \frac{Q_{i1} + Q_{in_{piv}+1} + ... + Q_{i(n_{flow}-1)(n_{piv}+1)}}{n_{flow}}$$

or

(A-11)
$$Q_{mean}(\phi) = \frac{Q_1 + Q_{n_{piv}+1} + ... + Q_{(n_{flow}-1)(n_{piv}+1)}}{n_{flow}}$$

6.   Implementation of the calculation

Totally 312 flow regimes were tested for each roughness. It meant there were 312 waveform of flow rate to be calculated. Each waveform consisted of 15 points or more. The flow rate of each point would come from each PIV picture first and phase averaged later. Table A-2 is the statistics of the calculation. It is shown in Table A-2 that the flow rate of each point on the phase averaged waveform was based on several thousands PIV grid datum. Each flow rate waveform came from more than one hundred PIV data files. The amount of calculation was huge. A special code was made for this purpose.

Table A-2 Statistics of flow rate calculation

Frequency (Hz)	0.01	0.05	0.10	0.20	0.50	1.00
Flow regimes	52	52	52	52	52	32
PIV pictures/style	125	100	125	125	150	150
PIV Data file	6500	5200	6500	6500	7800	4800
I index	30	30	30	30	30	30
J Index	30	30	30	30	30	30
Total points ($\times 10^6$)	5.85	4.68	5.85	5.85	7.02	4.32
Period No.	5	5	5	5	10	10
Points/period	25	20	25	25	30	15

The code carried out the calculation as following:

- Set the flow regime parameters: frequency, base flow, amplitude of oscillatory. Located the PIV data file on disk by the parameters.
- Determine the number of PIV data files for the specific flow regime. Determine the number of points on one period.
- Open the first PIV data file. Read the velocity data for each PIV grid node.
- Average the velocity of points with same vertical coordinates (height) and different horizontal coordinates (along the streamline).
- Determine the general cell height, which is the same for most cells except the one at bottom and the one trimmed at the centre line.
- Determine the height of bottom cell (the lowest cell) and trim the centreline cell in the middle of the tunnel according to the internal height of the tunnel 350.
- Calculate the cell flow rate and integrate from bottom to the centreline.
- Save the flow rate calculated in one cell of Excel worksheet.
- Open next PIV data file. Go through step 3) to 8). For the same flow regime, the results from 5) and 6) should keep constant, can be reused in the processing of all PIV data files of the same flow regime.
- After all PIV data files for one flow regime is processed, average the calculated flow rate over phase and save the averaged value in another Excel worksheet.
- After phase average finish. Find the maximum, minimum flow rate and calculate the mean flow rate.
- Extract the phase-averaged data of flow rate meter reading from the corresponding data file.
- Create the waveform in one chart for both the calculated flow rate from PIV data and the flow rate meter readings.
- Save the Excel workbook file.
- Go to another flow regime.

7.   Comparison of the calculated value to the readings of flow rate meter

It was a little bit difficult to compare the instant value of calculated flow rate and the readings of the flow rate meter for oscillatory flow.

- Both were discrete values.
- The start points of measurement are different for PIV and flow rate meter. If the start point of PIV was corresponding to phase angle j_1 of the oscillatory flow, the reading start point of flow rate meter was corresponding to phase angle j_2 of the flow. The

chance for $j_1 = j_2$ was very low. PIV and flow rate meter were located in two different points in the rig. The distance between them was about 12.5 meters.

- The sampling rates of PIV and flow rate meter were different in most cases. The phase increment y_1 between consecutive points of PIV measurement was seldom equals to the phase increment y_2 between consecutive readings of the flow rate meter.

Only qualitatively comparison can be made by

- The waveform of flow rate from two different ways.
- The characteristic value of flow rate from two different ways, i.e. the mean, maximum and minimum value.

This was enough for the purposes

- Verifying the flow rate of different measurements carried out at different stages, among which some accidents had happened to the rig.
- Take the calculated flow rate as the reference parameter for other analysis, such as the comparison of the measured head loss (differential pressure).

8. Discussion of the calculation

- As mentioned above, the vertical boundary was not taken into account in the flow rate calculation. This would cause some errors.
- Also mentioned above, the comparison was only qualitative.
- In the calculation practice, the PIV grid was not even trimmed at the bottom and the centreline of the flow.
- In fact, the lower half of the flow was not 100% symmetry to the upper half flow in the tunnel due to the gravity of the flow. This would not cause any significant error.
- One PIV frame included about 900 nodes, if the indexes for two dimensions were 30 respectively. Not all velocity data at each node was valid in lot of cases. The invalid node had to be discarded during the calculation.
- In some cases, the velocity in one PIV frame was not correlated completely. It was difficult to get a valid point of flow rate from the frame. The frame was discarded from the calculation.
- If there was a PIV frame or frames discarded from calculation in one flow regime, phase average on the flow regime was carried out in a special way.

A.3 Wave Speed Calculation

A.3.1 Pressure variance

When an oscillatory flow is applied to a straight duct, a pressure wave travels back and forth of the duct. If the wave speed is c and flow velocity is v, the speed relative to the duct is $(c + v)$ when wave speed is in the same direction as the flow and $(c - v)$ when wave speed is in the reverse direction to the flow. Set a control volume in the flow and specify the flow condition as shown in Figure A-5.

Apply Newton's Second Law, the conservation of linear momentum, to the control volume. The net force across the control volume is equal to the net loss in linear momentum from it:

(A-12) $$\Delta p \cdot A = M \cdot \left[(c + \Delta v) - c \right]$$

where M is the mass flow rate. For the test flow in the measurement, the flow velocity change Δv is negligible comparing to the wave propagation speed, c, and the mass flow rate M through the control volume is:

(A-13) $M = \boldsymbol{r}\, A\, c$

Insert Equation (A-13) into Equation (A-12) and we get:

(A-14) $\Delta p = -\boldsymbol{r} \cdot c \cdot \Delta v$

or

(A-15) $\Delta v = -\dfrac{\Delta p}{\boldsymbol{r} \cdot c}$
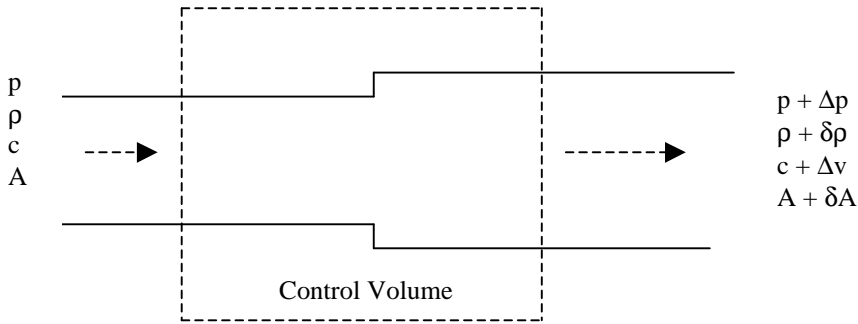
Figure A-5 Control volume in oscillatory flow

The symbols used in Figure A-5 are listed below:

p	Initial pressure	Δp	Pressure increment
ρ	Initial density	δρ	Density increment
c	Wave speed	Δv	Flow velocity increment
A	Initial cross section area of duct	δA	Area increment

A.3.2 Wave speed equation

According to the Law of Conservation of Mass, the flow out of the control volume is equal to the flow into the control volume. Then we can get:

$$(\boldsymbol{r}+\boldsymbol{dr}) \cdot (A+dA) \cdot (c+\Delta v) \cdot = \boldsymbol{r} \cdot A \cdot c$$

Divide the left hand side by the right hand side, and substitute Δv with Equation (A-14):

$$(1+\frac{\boldsymbol{dr}}{\boldsymbol{r}}) \cdot (1+\frac{dA}{A}) \cdot (1-\frac{\Delta p}{\boldsymbol{r} \cdot c^2}) = 1$$

Multiplying out and remove the product of infinitesimals:

(A-16) $\dfrac{\boldsymbol{dr}}{\boldsymbol{r}} + \dfrac{dA}{A} - \dfrac{\Delta p}{\boldsymbol{r} \cdot c^2} = 0$

The density increment $\delta\boldsymbol{r}$ can be expressed by the Bulk Modulus K of water as:

$$\dfrac{\boldsymbol{dr}}{\boldsymbol{r}} = \dfrac{\Delta p}{K}$$

137

Insert this relation into Equation (A-16) we get:

(A-17)
$$c = \left[r \left(\frac{1}{K} + \frac{1}{A} \frac{dA}{\Delta p} \right) \right]^{-\frac{1}{2}}$$

This is the general equation to calculate the wave speed of transient pressure propagation of liquid in pipes or tunnels. The term with bulk modulus K represents the elasticity of the fluid, and the term with area strain per unit change in pressure $\dfrac{dA}{\Delta p}$, denotes the elasticity of the conduit.

A.3.3 Area strain for rectangular duct and wave speed

The test tunnel is a duct with rectangular cross section as shown in Figure A-6

The actual width of top and bottom wall is 325 mm. The part on which the pressure force acts is the part within the range of left and right sidewalls, i.e., the effective width of top and bottom is equal to the inner space of the duct, 230 mm.

The inner rough layer is fixed on four sides of the duct tightly. It may help the wall to defend the deflection. To simplify the calculation, this improvement is neglected in the following calculation of area strain of the duct.

We start the calculation from the deflection of the sidewall. First the sidewall of the conduit is taken as a plate, the deflection of which is calculated. A simple way to calculate the deflection of the plate is to take out a strip from the plate and regard it as a beam as shown in Figure A-7.
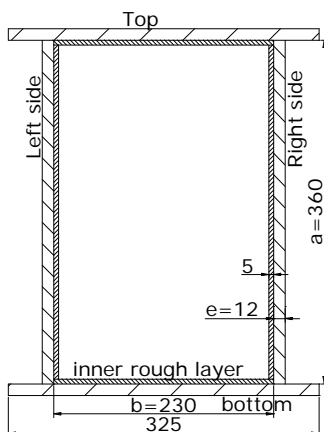
Figure A-6 Test duct cross section

A.3.3.1   Basic definitions and deflection calculation

1.   Definition of Simple Beam

Simple Beam is a planar structure, all loads act in the bending plane, all deflections occur in the bending plane, supported with PIN support in one end and ROLLER support at the other end; as shown in Figure A-7.
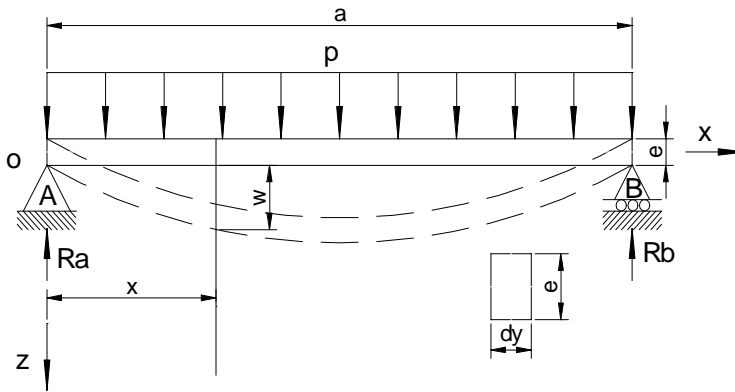
Figure A-7 Deflection of simple beam

2.   Feature of a simple beam

Table A-3 lists the features of a simple beam.

Table A-3 Features of a simple beam

	PIN support (A)		**Roller support (B)**	
	Horizontal	Vertical	Horizontal	Vertical
Translation	No	No	Yes	Yes
Rotation	Yes in bending plane		Yes in bending plane	
Reaction force	Yes	Yes	No	Yes
Reaction moment	No		No	

3.   Hook's Law for a bar and a beam with linear elasticity

(A-18) $\boldsymbol{s} = E \cdot \boldsymbol{e}$

4.   Hook's Law for infinite plate supported along the edges

Hook's Law for plane stress, taking into account the Poisson's ratio, i.e., the ratio of strain in the lateral direction to the strain in the axial direction, the 2D relation of strain and stress can be written as (suppose $\boldsymbol{s}_z = 0$):

(A-19) $\boldsymbol{s}_x = \dfrac{E}{1-\boldsymbol{n}^2}(\boldsymbol{e}_x + \boldsymbol{n} \cdot \boldsymbol{e}_y)$

(A-20) $\boldsymbol{s}_y = \dfrac{E}{1-\boldsymbol{n}^2}(\boldsymbol{e}_y + \boldsymbol{n} \cdot \boldsymbol{e}_x)$

5.   Deflection of a simple beam

Deflection at any point of a beam, with coordinates x along its longitude axis, is

(A-21) $w = \dfrac{p \cdot x}{24 \cdot E \cdot I}(a^3 - 2 \cdot a \cdot x^2 + x^3)$

Maximum deflection happens at the middle point of the beam

(A-22) $w_{max} = \dfrac{5 \cdot p \cdot a^4}{384 \cdot E \cdot I}$

where moments of inertia of areas I is equal to:

(A-23) $I = \dfrac{dy \cdot e^3}{12}$

Equation (A-21) can be written as:

$$w = \frac{p \cdot x}{2 \cdot E \cdot dy \cdot e^3}(a^3 - 2 \cdot a \cdot x^2 + x^3)$$

Let $dy = 1$, as unit width, we get:

(A-24) $w = \dfrac{p \cdot x}{2 \cdot E \cdot e^3}(a^3 - 2 \cdot a \cdot x^2 + x^3)$

6.   Deflection of a plate in cylindrical bending

The governing differential equation for the deflection of thin plate bending analysis based on Kirchhoff's assumptions is:

(A-25) $\dfrac{\partial^4 w}{\partial x^4} + 2\dfrac{\partial^4 w}{\partial x^2 \partial y^2} + \dfrac{\partial^4 w}{\partial y^4} = \dfrac{p}{D}$

where flexural rigidity of the plate D is:

(A-26) $D = \dfrac{E \cdot e^3}{12(1 - n^2)}$

It plays the same role as the flexural rigidity EI does in beam bending. However $D > EI$; hence, a plate is always stiffer than a beam of the same span and thickness.

For an infinite long plate in the y-axis direction, subjected to a transverse load $p = constant$ along x-axis, all the strips of a unit width parallel to the x-axis and isolated from the plate will bend identically. The plate as a whole is found to be bent over the cylindrical surface $w = w(x)$. Setting all the derivatives with respect to y equal to zero in Equation (A-25), we obtain the following equation for the deflection of any elementary strip:

(A-27) $\dfrac{d^4 w}{dx^4} = \dfrac{p}{D}$

This equation coincides with the corresponding equation of bending of a beam if the flexural rigidity of a beam EI is replaced by the flexural rigidity of a plate D.

By integrating and applying the boundary condition to the integration, we get the deflection of an elementary strip under transverse constant load p:

(A-28) $w = \dfrac{p \cdot x}{48 \cdot D}\left(3 \cdot a^2 x - 5 \cdot ax^2 + 2 \cdot x^3\right)$

It should be noted that the boundary conditions used are:

(A-29) $w = 0\big|_{x=0}, \dfrac{dw}{dx} = 0\big|_{x=0}$ and $w = 0\big|_{x=a}, M_x = -D\dfrac{d^2 w}{dx^2} = 0\big|_{x=a}$

Equation (A-28) can be rewritten as:

(A-30) $w = \dfrac{p \cdot x \cdot (1 - \mathbf{n}^2)}{4 \cdot E \cdot e^3} \left(3 \cdot a^2 x - 5 \cdot ax^2 + 2 \cdot x^3 \right)$

Compare Equation (A-24) and (A-30) we can see that the difference of deflection between a beam and a plate strip is not only relied on the Poisson's ratio, i.e.,

(A-31) $w_{plate} \neq \dfrac{w_{beam}}{1 - \mathbf{n}^2}$

A.3.3.2   Area variance of the rectangular duct due to deflection

As shown in Figure A-8, the area variance of a rectangular duct due to deflection under inner pressure force is:

(A-32) $\Delta A = 2 \left(\displaystyle\int_0^b w_z \, dx + \int_0^a w_x \, dz \right)$

Based on equation (A-30) :

(A-33) $w_z = \dfrac{p \cdot z \cdot (1 - \mathbf{n}^2)}{4 \cdot E \cdot e^3} \left(3 \cdot b^2 z - 5 \cdot bz^2 + 2 \cdot z^3 \right)$

(A-34) $w_x = \dfrac{p \cdot x \cdot (1 - \mathbf{n}^2)}{4 \cdot E \cdot e^3} \left(3 \cdot a^2 x - 5 \cdot ax^2 + 2 \cdot x^3 \right)$
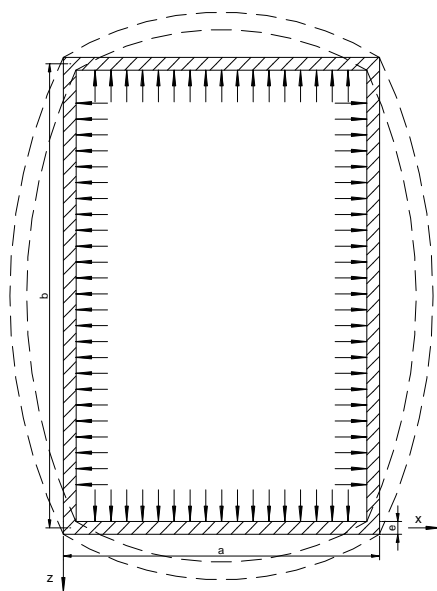
Figure A-8 Deflection of a rectangular duct

Then the following expression is obtained

(A-35)

$\Delta A = 2 \left(\displaystyle\int_0^a \dfrac{p \cdot x \cdot (1 - \mathbf{n}^2)}{4 \cdot E \cdot e^3} \left(3 \cdot a^2 x - 5 \cdot ax^2 + 2 \cdot x^3 \right) dx + \int_0^b \dfrac{p \cdot z \cdot (1 - \mathbf{n}^2)}{4 \cdot E \cdot e^3} \left(3 \cdot b^2 z - 5 \cdot bz^2 + 2 \cdot z^3 \right) dz \right)$

141

By integration the following expression can be developed:

(A-36) $\Delta A = \dfrac{3}{40} \cdot \dfrac{p \cdot (1 - \mathbf{n}^2)}{E \cdot e^3} \cdot \left(a^5 + b^5 \right)$

The area variance due to the pressure transient $\mathbf{dp}$ is

(A-37) $\mathbf{dA} = \dfrac{3}{40} \cdot \dfrac{\mathbf{dp} \cdot (1 - \mathbf{n}^2)}{E \cdot e^3} \cdot \left(a^5 + b^5 \right)$

Then

(A-38) $\dfrac{1}{A} \dfrac{\mathbf{dA}}{\mathbf{dp}} = \dfrac{3}{40} \cdot \dfrac{1}{a \cdot b} \cdot \dfrac{(1 - \mathbf{n}^2)}{E \cdot e^3} \cdot \left(a^5 + b^5 \right)$

This is a similar to the results of Hill (1970)

(A-39) $\dfrac{1}{A} \dfrac{\mathbf{dA}}{\Delta p} = \dfrac{(a^5 + b^5)}{a \cdot b} \cdot \dfrac{1}{30 \cdot E \cdot e^3}$

A.3.4 Wave speed in the test duct

The test duct is made of Plexiglas and its properties are listed in Table A-4. The properties of water are listed in Table A-5.

Table A-4 Properties of test duct

a	Longer side of the duct	0.36	M
b	Shorter side of the duct	0.23	M
e	Wall thickness	0.012	M
E	Elastic modulus	3.3	GN/m^2
n	Poisson's ratio	0.5	

Table A-5 Properties of water

r	Water density	998	kg/m^3
K	Bulk Modulus	2.19	GN/m^2

Insert the values in Table A-4 and Table A-5 into Equation (A-38)

(A-40) $\dfrac{1}{A} \dfrac{\mathbf{dA}}{\mathbf{dp}} = 2.5132 \cdot 10^{-7}$

Then the wave speed of pressure transient in the duct is

(A-41) $c = \left[\mathbf{r} \left(\dfrac{1}{K} + \dfrac{1}{A} \dfrac{\mathbf{dA}}{\Delta p} \right) \right]^{-\frac{1}{2}} = \underline{\underline{63.085}} (m/s)$

As comparison, if we calculate the wave speed in the test duct on the basis of deflection from Equation (A-24), the result is:

(A-42) $\dfrac{1}{A} \dfrac{\mathbf{dA}}{\mathbf{dp}} = 1.4169 \cdot 10^{-6}$

(A-43) $c = \underline{\underline{26.5881}} (m/s)$

A.3.5 More practical boundary conditions in the test duct

In the previous discussion, boundary condition used (Equation (A-29)) is quite unrealistic. For the case of rectangular duct used in the measurement:

1. The ends of the elementary strip (corners of the test duct) can not move to each other; reaction forces exist along x axis to prevent the movement, which are denoted as S in Figure A-9.

2. The ends of the element strip (corners of the test duct) cannot rotate freely; reaction moments exist around the corners to prevent the rotation, which are denoted as M_0 in Figure A-9.

Taking an element strip of unit width from the plate, as shown in Figure A-9. The bending moment at any cross section of the strip is:

(A-44) $M = \dfrac{p \cdot a}{2} x - \dfrac{p \cdot x^2}{2} - S \cdot w + M_0$

The cylindrical bending curve can be expressed as

(A-45) $\dfrac{d^2 w}{dx^2} = -\dfrac{M}{D}$
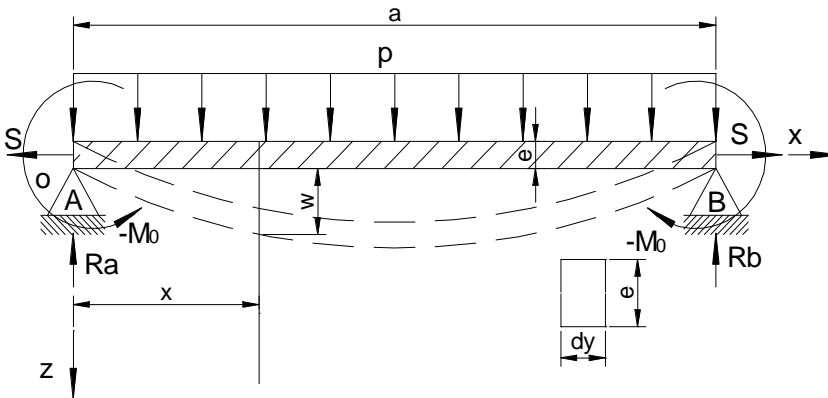
Figure A-9 Element strip and forces acting on it

Insert Equation (A-44) into Equation (A-45), we obtain:

(A-46) $\dfrac{d^2 w}{dx^2} - \dfrac{S}{D} w = \dfrac{p \cdot x^2}{2D} - \dfrac{p \cdot a \cdot x}{2D} - \dfrac{M_0}{D}$

This is a second order non-homogeneous differential equation in the form of

(A-47) $w'' + k_1 w' + k_2 w = P(x)$

where constants $k_1 = 0$ and $k_2 = -S/D$, and

(A-48) $P(x) = \dfrac{p \cdot x^2}{2D} - \dfrac{p \cdot a \cdot x}{2D} - \dfrac{M_0}{D}$

The general solution of Equation (A-47) is:

(A-49) $w = w_h + w_p$

where w_h is the general solution to the homogenous differential equation

(A-50) $w'' + k_1 w' + k_2 w = 0$

and w_p is the particular solution to the second order non-homogeneous differential equation. The characteristic equation of Equation (A-47) is

(A-51) $\lambda^2 + k_1\lambda + k_2 = 0$

For the case of $k_1 = 0$ and $k_2 = -S/D$, the roots of Equation (A-51) are:

(A-52) $\lambda_1 = \sqrt{S/D}$ and $\lambda_2 = -\sqrt{S/D}$

λ_1 and λ_2 are real and $\lambda_1 \neq \lambda_2$, the general solution to equation (A-50) is

(A-53) $w_h = C_1 e^{\lambda_1 x} + C_2 e^{\lambda_2 x}$

and the particular solution to Equation (A-47) is

(A-54) $w_p = \dfrac{1}{\lambda_1 - \lambda_2}\left[e^{\lambda_1 x}\int e^{-\lambda_1 x}P(x)dx - e^{\lambda_2 x}\int e^{-\lambda_2 x}P(x)dx\right]$

Introducing the notation

(A-55) $\dfrac{S}{D}\cdot\dfrac{a^2}{4} = u^2$

The general solution of Equation (A-46) can be written in the following form:

(A-56) $w = C_1\sinh\dfrac{2ux}{a} + C_2\cosh\dfrac{2ux}{a} + \dfrac{pa^3 x}{8u^2 D} - \dfrac{pa^2 x^2}{8u^2 D} - \dfrac{pa^4}{16u^4 D} + \dfrac{M_0 a^2}{4u^2 D}$

The deflection curve of the element strip is symmetrical with respect to the middle of the strip, the integration constants C_1 and C_2, the reaction moment M_0 can be determined from the following conditions:

(A-57) $\left.\dfrac{dw}{dx} = 0\right|_{x=0}, \left.\dfrac{dw}{dx} = 0\right|_{x=\frac{a}{2}}, \left.w = 0\right|_{x=0}$

Then we get:

(A-58) $C_1 = -\dfrac{pa^4}{16u^3 D}, C_2 = \dfrac{pa^4}{16u^3 D}\coth u$

(A-59) $M_0 = -\dfrac{pa^2}{4u^2} - \dfrac{pa^2}{4u}\coth u = -\dfrac{pa^2}{12}\cdot\dfrac{3(u-\tanh u)}{u^2\tanh u}$

Then the deflection w is therefore given by expression:;

(A-60) $w = -\dfrac{pa^4}{16u^3 D}\sinh\dfrac{2ux}{a} + \dfrac{pa^4}{16u^3 D}\coth u\cosh\dfrac{2ux}{a} + \dfrac{pa^3 x}{8u^2 D} - \dfrac{pa^2 x^2}{8u^2 D} - \dfrac{pa^4}{16u^4 D}\coth u$

By further simplification, we obtain:

(A-61) $w = \dfrac{pa^4}{16u^3 D\tanh u}\left\{\dfrac{\cosh\left[u\left(1-\dfrac{2x}{a}\right)\right]}{\cosh u} - 1\right\} + \dfrac{pa^2(a-x)x}{8u^2 D}$

Obviously it is not easy to integrate Equation (A-61) to calculate the area variance in a rectangular duct.

We noticed that the right hand side of the second order non-homogeneous differential equation (A-46) is a polynomial of degree 2. Then the particular solution to equation (A-46) could be:

$$(A-62) \quad w_p = \frac{1}{k_2}\left[P(x) - \frac{k_1}{k_2}P'(x) + \frac{k_1^2 - k_2}{k_2^2}P''(x)\right] = \frac{1}{k_2}P(x) - \frac{1}{k_2^2}P''(x)$$

From Equation (A-48) we know that

$$(A-63) \quad P''(x) = \frac{p}{D}$$

Insert it into Equation (A-62), we obtain

$$(A-64) \quad w_p = -\frac{p \cdot x^2}{2S} + \frac{p \cdot a \cdot x}{2S} + \frac{M_0}{S} - \frac{pD}{S^2}$$

Then the general solution to equation (A-46) is

$$(A-65) \quad w = C_1 e^{\sqrt{\frac{S}{D}}x} + C_2 e^{-\sqrt{\frac{S}{D}}x} - \frac{p \cdot x^2}{2S} + \frac{p \cdot a \cdot x}{2S} + \frac{M_0}{S} - \frac{pD}{S^2}$$

Apply boundary conditions as shown in Equations (A-57), we can get

$$(A-66) \quad C_1 = \frac{pa}{2S}\sqrt{\frac{D}{S}} \cdot \frac{e^{-\sqrt{\frac{S}{D}} \cdot a}}{1 - e^{-\sqrt{\frac{S}{D}} \cdot a}}$$

$$(A-67) \quad C_2 = \frac{pa}{2S}\sqrt{\frac{D}{S}} \cdot \frac{1}{1 - e^{-\sqrt{\frac{S}{D}} \cdot a}}$$

$$(A-68) \quad M_0 = \frac{pD}{S} - \frac{pa}{2}\sqrt{\frac{D}{S}} \cdot \frac{1 + e^{-\sqrt{\frac{S}{D}} \cdot a}}{1 - e^{-\sqrt{\frac{S}{D}} \cdot a}}$$

Introducing the notation $\mathbf{k} = \sqrt{S/D}$, then

$$(A-69) \quad w = C_1 e^{\mathbf{k}x} + C_2 e^{-\mathbf{k}x} - \frac{p \cdot x^2}{2\mathbf{k}^2 D} + \frac{p \cdot a \cdot x}{2\mathbf{k}^2 D} + \frac{M_0}{\mathbf{k}^2 D} - \frac{p}{\mathbf{k}^4 D}$$

$$(A-70) \quad C_1 = \frac{pa}{2D}\frac{1}{\mathbf{k}^3} \cdot \frac{e^{-\mathbf{k} \cdot a}}{1 - e^{-\mathbf{k} \cdot a}}$$

145

(A-71) $C_2 = \dfrac{pa}{2D} \dfrac{1}{\boldsymbol{k}^3} \cdot \dfrac{1}{1 - e^{-\boldsymbol{k} \cdot a}}$

(A-72) $M_0 = \dfrac{p}{\boldsymbol{k}^2} - \dfrac{pa}{2} \dfrac{1}{\boldsymbol{k}} \cdot \dfrac{1 + e^{-\boldsymbol{k} \cdot a}}{1 - e^{-\boldsymbol{k} \cdot a}}$

Thus the deflections of the element strip depend on the quantity $\boldsymbol{k}$, which is a function of the axial force S. S can be determined from the condition that the ends of the strip do not move along the x-axis. Hence the extension of the strip produced by the force S is equal to the difference between the length of the arc along the deflection curve and the chord length a. This difference for small deflection can be presented by the formula:

(A-73) $\Delta l = \dfrac{1}{2} \displaystyle\int_0^a (\dfrac{dw}{dx})^2 \, dx$

Assume that lateral strain of the strip in the y-direction is zero and use Hook's Law for plate, i.e., Equation (A-19) and (A-20), we get

(A-74) $\Delta l = \dfrac{1 - \boldsymbol{n}^2}{E} \cdot \dfrac{S \cdot a}{e} = \dfrac{1}{2} \displaystyle\int_0^a (\dfrac{dw}{dx})^2 \, dx$

From Equation (A-69), we can get

(A-75) $\dfrac{dw}{dx} = C_1 \boldsymbol{k} e^{kx} - C_2 \boldsymbol{k} e^{-kx} - \dfrac{p \cdot x}{\boldsymbol{k}^2 D} + \dfrac{p \cdot a}{2\boldsymbol{k}^2 D}$

$\left(\dfrac{dw}{dx} \right)^2 = \left(C_1 \boldsymbol{k} e^{kx} - C_2 \boldsymbol{k} e^{-kx} - \dfrac{p \cdot x}{\boldsymbol{k}^2 D} + \dfrac{p \cdot a}{2\boldsymbol{k}^2 D} \right)^2$

(A-76) $= \left(C_1 \boldsymbol{k} e^{kx} \right)^2 + \left(C_2 \boldsymbol{k} e^{-kx} \right)^2 + \left(\dfrac{p \cdot x}{\boldsymbol{k}^2 D} \right)^2 + \left(\dfrac{p \cdot a}{2\boldsymbol{k}^2 D} \right)^2$

$- 2C_1 C_2 \boldsymbol{k}^2 - 2C_1 e^{kx} \dfrac{p \cdot x}{\boldsymbol{k} D} + 2C_2 e^{-kx} \dfrac{p \cdot x}{\boldsymbol{k} D} + C_1 e^{kx} \dfrac{p \cdot a}{\boldsymbol{k} D} - C_2 e^{-kx} \dfrac{p \cdot a}{\boldsymbol{k} D} - \dfrac{p^2 ax}{\boldsymbol{k}^4 D^2}$

Insert it into Equation (A-74) and carry out the integration on the right hand side, we obtain

(A-77) $\dfrac{1 - \boldsymbol{n}^2}{E} \cdot \dfrac{S \cdot a}{e} = \dfrac{1}{2} \left\{ \begin{array}{l} \left[\dfrac{1}{2} C_1^2 \boldsymbol{k} (e^{2ka} - 1) \right] - \left[\dfrac{1}{2} C_2^2 \boldsymbol{k} (e^{-2ka} - 1) \right] + \dfrac{1}{12} \dfrac{p^2 a^3}{\boldsymbol{k}^4 D^2} - 2C_1 C_2 \boldsymbol{k}^2 a \\[2ex] - 2C_1 \dfrac{p}{\boldsymbol{k}^3 D} \left[e^{ka} (\boldsymbol{k}a - 1) + 1 \right] - 2C_2 \dfrac{p}{\boldsymbol{k}^3 D} \left[e^{-ka} (\boldsymbol{k}a + 1) - 1 \right] \\[2ex] + C_1 \dfrac{p}{\boldsymbol{k}^2 D} (e^{ka} - 1) + C_2 \dfrac{p}{\boldsymbol{k}^2 D} (e^{-ka} - 1) \end{array} \right\}$

This is an implicit expression of S for $\boldsymbol{k}$ is a function of S. Maybe the easiest way to get the value of S is iteration.

Then we can integrate Equation (A-65) to get the area variance of the test duct along side a.

$$\begin{aligned}
dA_1 &= \int_0^a \left(C_1 e^{kx} + C_2 e^{-kx} - \frac{p \cdot x^2}{2k^2 D} + \frac{p \cdot a \cdot x}{2k^2 D} + \frac{M_0}{k^2 D} - \frac{p}{k^4 D} \right) dx \\
\text{(A-78)} \quad &= \frac{C_1}{k}(e^{ka} - 1) - \frac{C_2}{k}(e^{-ka} - 1) + \frac{p \cdot a^2}{12 k^2 D} + \frac{M_0 a}{k^2 D} - \frac{pa}{k^4 D}
\end{aligned}$$

Similarly we can get the expression of S and area variance for side b of the test duct:

$$\text{(A-79)} \quad w = C_1 e^{kx} + C_2 e^{-kx} - \frac{p \cdot x^2}{2k^2 D} + \frac{p \cdot b \cdot x}{2k^2 D} + \frac{M_0}{k^2 D} - \frac{p}{k^4 D}$$

$$\text{(A-80)} \quad C_1 = \frac{pb}{2D} \frac{1}{k^3} \cdot \frac{e^{-k \cdot b}}{1 - e^{-k \cdot b}}$$

$$\text{(A-81)} \quad C_2 = \frac{pb}{2D} \frac{1}{k^3} \cdot \frac{1}{1 - e^{-k \cdot b}}$$

$$\text{(A-82)} \quad M_0 = \frac{p}{k^2} - \frac{pb}{2} \frac{1}{k} \cdot \frac{1 + e^{-k \cdot b}}{1 - e^{-k \cdot b}}$$

$$\text{(A-83)} \quad \frac{1 - n^2}{E} \cdot \frac{S \cdot b}{e} = \frac{1}{2} \left\{ \begin{aligned}
&\left[\frac{1}{2} C_1^2 k(e^{2kb} - 1) \right] - \left[\frac{1}{2} C_2^2 k(e^{-2kb} - 1) \right] + \frac{1}{12} \frac{p^2 b^3}{k^4 D^2} - 2 C_1 C_2 k^2 b \\
&- 2 C_1 \frac{p}{k^3 D} \left[e^{kb}(kb - 1) + 1 \right] - 2 C_2 \frac{p}{k^3 D} \left[e^{-kb}(kb + 1) - 1 \right] \\
&+ C_1 \frac{p}{k^2 D}(e^{kb} - 1) + C_2 \frac{p}{k^2 D}(e^{-kb} - 1)
\end{aligned} \right\}$$

$$\begin{aligned}
dA_2 &= \int_0^b \left(C_1 e^{kx} + C_2 e^{-kx} - \frac{p \cdot x^2}{2k^2 D} + \frac{p \cdot b \cdot x}{2k^2 D} + \frac{M_0}{k^2 D} - \frac{p}{k^4 D} \right) dx \\
\text{(A-84)} \quad &= \frac{C_1}{k}(e^{kb} - 1) - \frac{C_2}{k}(e^{-kb} - 1) + \frac{p \cdot b^2}{12 k^2 D} + \frac{M_0 b}{k^2 D} - \frac{pb}{k^4 D}
\end{aligned}$$

And finally, we get

$$dA = dA_1 + dA_2$$

$$\begin{aligned}
\text{(A-85)} \quad &= \frac{C_1}{k}(e^{ka} - 1) - \frac{C_2}{k}(e^{-ka} - 1) + \frac{p \cdot a^2}{12 k^2 D} + \frac{M_0 a}{k^2 D} - \frac{pa}{k^4 D} \\
&+ \frac{C_1}{k}(e^{kb} - 1) - \frac{C_2}{k}(e^{-kb} - 1) + \frac{p \cdot b^2}{12 k^2 D} + \frac{M_0 b}{k^2 D} - \frac{pb}{k^4 D}
\end{aligned}$$

147

$$(A\text{-}86) \quad \frac{1}{A}\frac{dA}{dp} = \frac{1}{a \cdot b} \cdot \frac{1}{dp} \left[\begin{array}{l} \dfrac{C_1}{k}(e^{ka}-1) - \dfrac{C_2}{k}(e^{-ka}-1) + \dfrac{p \cdot a^2}{12k^2 D} + \dfrac{M_0 a}{k^2 D} - \dfrac{pa}{k^4 D} \\[2mm] + \dfrac{C_1}{k}(e^{kb}-1) - \dfrac{C_2}{k}(e^{-kb}-1) + \dfrac{p \cdot b^2}{12k^2 D} + \dfrac{M_0 b}{k^2 D} - \dfrac{pb}{k^4 D} \end{array} \right]$$

$$= \frac{1}{a \cdot b}\left\{ \frac{a+b}{k^4 D} - \frac{1}{2k^3 D}\left[a^2 \frac{1+e^{-k \cdot a}}{1-e^{-k \cdot a}} + b^2 \frac{1+e^{-k \cdot b}}{1-e^{-k \cdot b}} \right] + \frac{a^3+b^3}{12k^2 D} \right\}$$

Insert this area variance into the equation of wave speed we can calculate the wave speed in the test duct. For different water head applied into the duct, different S can be evaluated from the equations mentioned above by iteration and the wave speed can be computed. The result is quite higher than the value shown in Equation (A-41).

A.3.6 Calculations from others

Several researchers have made some efforts to calculate the area strain of rectangular duct. Hill (1970) was among the first to study wave speed in a rectangular duct. He used steady state bending theories to sidewall deflection of the duct and showed that for a thin-wall rectangular duct (e.g. $a/e > 20$, for the test duct discussed, $a/e = 30 > 20$), the term of area strain in Equation (A-17) is:

$$(A\text{-}87) \quad \frac{1}{A}\frac{dA}{\Delta p} = \frac{(a^5+b^5)}{a \cdot b} \cdot \frac{1}{30 \cdot E \cdot e^3}$$

The Bulk Modulus K and the Modulus of rigidity of the test rectangular duct are listed in Table A-6. Other properties of the test duct and water are listed in Table A-4 and Table A-5.

Table A-6 Properties of test duct

K	Bulk Modulus	2.19	GN/m^2
G	Modulus of rigidity	1.1	GN/m^2

Insert the value of variables for the test duct into Equation (A-87), we get the area strain of the duct:

$$\frac{1}{A}\frac{\delta A}{\Delta p} = 4.723 \cdot 10^{-7}$$

The wave speed can be evaluated from Equation (A-17) as:
$$c = \underline{\underline{46.037}}(m/s)$$

In his analysis, Hill (1970) assumed that each sidewall of the duct be treated as a simple beam having "built in ends" and which deforms under the action of a uniformly distributed load. Assumption also made on that the corners do not rotate and that they remain at fixed points in space. The inertia of the duct wall and the longitudinal restraints are also neglected.

Jenkner (1971) examined the case of thin-wall rectangular duct in more details and with less assumption. The corner may rotate and does not restrict them to be fixed in space, so that the stretch of the wall is taken into account as well as the bending deflections. Steady state bending theory is used and the resulting expression of area strain for rectangular duct is:

$$(A\text{-}88) \quad \frac{1}{A}\frac{dA}{\Delta p} = \frac{a}{b} \cdot \frac{a^3}{15 \cdot E \cdot e^3} \cdot R$$

where

(A-89)
$$R = \frac{1}{2}(6-5a) + \frac{1}{2}\left(\frac{b}{a}\right)^5\left[6-5a\left(\frac{a}{b}\right)^2\right]$$

and

(A-90)
$$a = \frac{1+\left(b/a\right)^3}{1+\left(b/a\right)}$$

Insert the value for the test duct into Equation (A-90), Equation (A-89) and Equation (A-88),

$$\alpha = 0.7693 \, , \ R = 0.8945 \ \text{and} \ \frac{1}{A}\frac{\delta A}{\Delta p} = 7.637\cdot 10^{-7}$$

The wave speed from Equation (A-17) is

$$c = \underline{36.211}(m/s)$$

Thorley et al (1976) added an item in the area strain to represents the influence of shear force on the bending deflection, for the shear force effects may be significant in thick-wall ducts, i.e., where *a / e < 20*. The changes in internal cross sectional area of the duct due to bending and stretching of the sidewalls are determined separately for each side and the two effects added together. The area strain is:

(A-91)
$$\frac{1}{A}\frac{dA}{\Delta p} = \frac{f(a,b)}{a\cdot b\cdot E\cdot e^3}$$

where

(A-92) $f(a,b) = \dfrac{a^3+b^3}{2(a+b)}\left(\dfrac{a^3}{6}+\dfrac{a^2 b}{2}-\dfrac{b^3}{3}\right)-\dfrac{a^5}{20}-\dfrac{a^2 b^3}{4}+\dfrac{b^5}{5}+\dfrac{Ee^2}{4G}(a^3+b^3)+\dfrac{abe^2}{2}(a+b)$

Insert the value for the test duct into Equation (A-92) and Equation (A-91), we get

$$f(a,b) = 3.705\cdot 10^{-4} \ \text{and} \ \frac{1}{A}\frac{\delta A}{\Delta p} = 7.846\cdot 10^{-7}$$

The wave speed from Equation (A-17) is

$$c = \underline{35.725}(m/s)$$

According to Thorley et al (1979), the area strain term in Equation (A-17) for non-circular duct may be expressed in a more general and simplified was as:

(A-93)
$$\frac{1}{A}\frac{dA}{\Delta p} = \frac{1}{E}\left[\frac{D}{e}+\frac{\tan^4 a}{15}\left(\frac{D}{e}\right)^3\right]+\frac{\tan^2 a}{2G}\left(\frac{D}{e}\right)$$

where

D	Perpendicular distance across the flats of the regular polygon	0.36	m
α	180°/Number of flat sides	45	°

Insert the value for the test duct to Equation (A-93):

$$\frac{1}{A}\frac{\delta A}{\Delta p} = 5.682\cdot 10^{-7}$$

The wave speed from Equation (A-17) is

$$c = \underline{\underline{41.978}}(m/s)$$

If the value of D is b = 0.23 m, the length of the other side of the rectangular, then

$$\frac{1}{A}\frac{\delta A}{\Delta p} = 1.568 \cdot 10^{-7}$$

$$c = \underline{\underline{79.832}}(m/s)$$

A.3.7 Summary of the wave speed calculated

The calculation results from the last sections are listed in Table A-7:

Table A-7 Summary of wave speed calculated

Author	Hill	Jenkner	Thorley	Thorley (a)	Thorley (b)
Wave Speed (m/s)	46.037	36.211	35.725	41.978	79.832

It is shown in the table, the wave speed is ranged from 35.725 m/s to 79.832 m/s. The peak velocity measured in the test is around 1 m/s, much smaller than the wave speed. The interference between them ought to be quite small. The highest oscillatory frequency of flow tested is 1.0 Hz; the lowest oscillatory frequency of flow tested is 0.01 Hz. The period of flow tested is ranged from 1.0 s to 100 s. The distance between the two connection points of differential pressure sensor is 9 m. It takes about 0.25 s for the pressure wave to travel from one connection point to another one if the wave speed is 35 m/s, takes about 0.11 s if the wave speed is 80 m/s. For flow with lower oscillatory frequency, the time is negligible. For flow with higher oscillatory frequency, the time may be too big for accurate measurement.

In the rig, there are enforcement ribs glued to the side of the duct. The distance between two adjacent ribs is 0.75 m. This limited the deflection of the wall of test duct and increase the pressure wave speed a lot.

The inner rough layer was not taken into account in above evaluations. The inner rough layer is fixed to the walls of test duct tightly. It also helps to resist the bend and deflection effect of the walls.

Briefly, the actual speed of pressure wave ought to be quite bigger than 35 m/s. The time taken for pressure wave to travel between the two sampling points of differential pressure sensor ought to be small enough to get a relatively accurate result. The influence of the wave speed on the water head variation along the test conduit is neglecible.

A.4 Reynolds number of flow tested

By definition, Reynolds number is expressed as:

(A-94) $$Re = V \cdot L / \boldsymbol{n}$$

where

- V: Velocity of flow
- L: characteristic length of channel
- $\boldsymbol{n}$: Kinematics viscosity of fluid

For the test rig with a rectangular cross section, characteristic length L is substituted by hydraulic diameter D_h:

(A-95) $$Re = V \cdot D_h / \boldsymbol{n}$$

150

For rectangular duct, D_h is evaluated as:

(A-96)
$$D_h = \frac{4\,A}{P}$$

where

- P: Wet perimeter of the channel, $P = 2\,(a + b)$
- A: Cross section area of the channel, $A = a \cdot b$

then

$D_h = 4\,A\,/\,P = 4\,a \cdot b\,/\,2\,(a + b) = 2\,a \cdot b\,/\,(a + b)$

The parameters and Reynolds numbers calculated are listed in Table A-8.

Table A-8 Parameters and Reynolds numbers

	a	b	P	A	D	D/n	Re
	m	m	m	m2	m		
Smooth	0.36	0.23	1.18	0.0828	0.2807	278726.878	D/n·V
Roughness I	0.35	0.22	1.14	0.077	0.2702	268297.357	D/n·V

We can see from the table, even the mean velocity $V = 0.01\ m/s$, when $Q = 0.736\ (0.682)$ *l/s*, the flow is still turbulence. The minimum flow rate measured was always bigger than *1 l/s*. All flow measured should be turbulence.

For the oscillatory flow, when the flow rate varies between positive value and negative value, there is a short time near to the zero flow rate point when the velocity is so low that the Reynolds number could be small at the time instant. However, for the flow tested, the time is too short to get any flow other than turbulence. Transition always needs time.

Appendix B Other Measurements

B.1 ADV Measurement

Acoustic Doppler Velocimeter (ADV) was used at the first stage of the measurement to get the velocity of the flow.

B.1.1 Brief introduction of ADV

ADV uses the Doppler effects of an acoustic signal to get the velocity of a target flow. It can obtain the 3D velocity of a control volume simultaneously with one sensor unit. The acoustic sensor unit has one transmitting transducer and three receiving transducers. The sampling volume is located away from the sensor unit to provide undisturbed measurements. Doppler
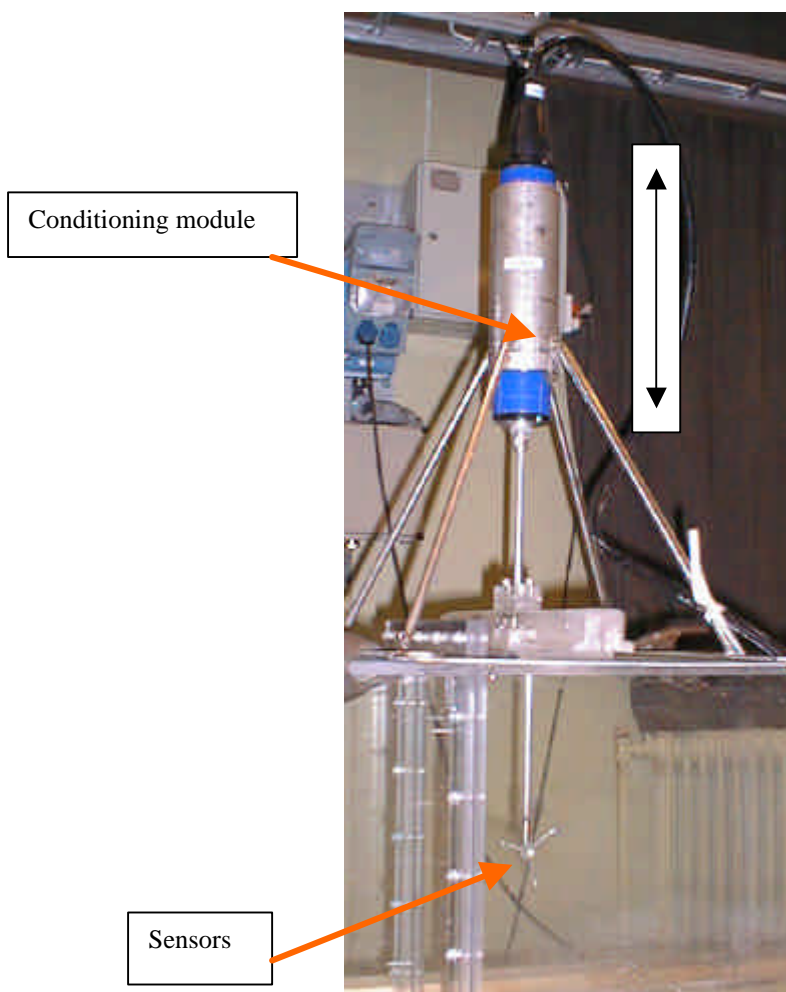
velocity is derived from the acoustic signals scattered by small particles in the flow.

Figure B-1 ADV instrument used in the measurement

The ADV instrument used in the measurement was from Nortek AS (as shown in Figure B-1). It is called as Laboratory Velocimeter by the producer. It consists of three modules:

- the measuring probe, i.e., the transmitter and the receivers: The receiving transducers are mounted on short arms around the transmitting transducer at 120° azimuth intervals. The acoustic beams are oriented so that the receiving beams intercept the transmitting beam at a point located at 50 mm away from the sensor unit. The interception of these four beams, together with the width of the transmitting pulse, defines the sampling volume. This volume is 3 -- 9 mm long and approximately 6 mm in diameter. All three receivers must be submerged to ensure correct 3-D velocity measurements
- the conditioning module with cable
- the processing module: The processing module performs the digital signal processing required for measuring Doppler shifts. In the case of Laboratory Velocimeter, which is the ADV instrument used in the measurement, this computationally intensive task is implemented on a PC-board.

Key specifications of the ADV Velocimeter used are:

- Acoustic frequency: 10 MHz
- Velocity range: ±2.5 m/s
- Velocity accuracy: ±1%, no measurable zero-offset in the horizontal direction
- Random Noise: Approximately 1% of the velocity range at a sampling rate of 25 Hz
- Sampling Rate: Programmable from 0.1 to 100 Hz for PC-based system
- Sampling Volume: Less than 0.25 cm^3
- Minimum water depth: 60 mm for 5-cm probes (probe used in the measurement)
- Minimum Distance from Sampling Volume to Boundary: 5 mm
- Analogy outputs PC-based system (u, v, and w): Optional (±5 V, ±10 V)

The software supplied with the Velocimeter displays the real-time data in graphical and tabular form. The data are recorded to disk in compressed binary files, which can be converted to ASCII format with the data conversion programs supplied with the system

B.1.2 Measuring with ADV

ADV sensor was inserted into the tunnel through a window on the top wall of the test tunnel. The window was designed that it is possible to move the sensor in vertical and/or horizontal directions to get the flow velocity at different locations in the tunnel.

The ADV sensor can only be as near as 8 mm to the top and bottom boundary wall of the tunnel. This is the sum of minimum distance from sampling volume to boundary, 5 mm, required for correct measurement, and the radius of the minimum sampling volume, 3 mm, as specified. The ADV sensor cannot measure the flow more nearer to the boundary wall.

Another limitation of ADV to measure the flow of near wall area is the vibration of the sensor while it is located very near to the wall. The turbulence in the boundary layer and the vibration of wall itself influenced the ADV sensor very obviously, could be easily observed by naked eyes.

The setup and usage of ADV is quite simple and straightforward comparing with that of LDV or PIV.

Figure B-2 is a screenshot of the ADV data acquisition and data processing display. Both the 3D velocity value and the time series of velocity are displayed and updated in real time.

Figure B-2 Screenshot of ADV DAQ and data processing

B.1.3 Example results from ADV

Figure B-3 to Figure B-4 shows the velocity V_x and V_y measured with ADV for flow rates ranged from $Q = 5.0$ l/s to 87.6 l/s. The target flow is stationary flow. The *RMS* of velocity V_x and V_y are shown in Figure B-5 to Figure B-6. Velocity V_z and its *RMS* are not shown in the figures. V_z is very small comparing to V_x and comparable with V_y.
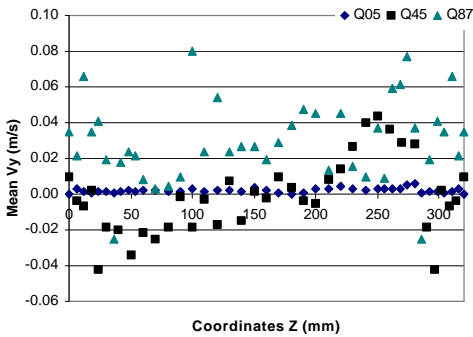

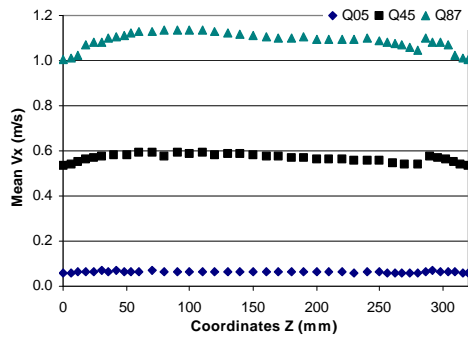Figure B-3 Profile of V_y by ADV
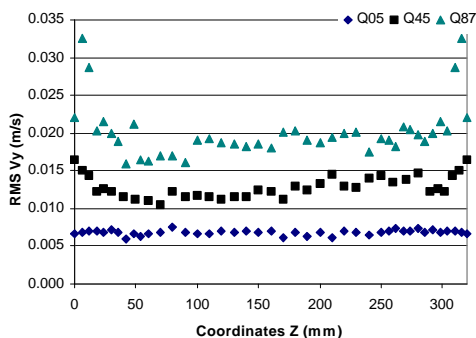

Figure B-4 Profile of V_x by ADV
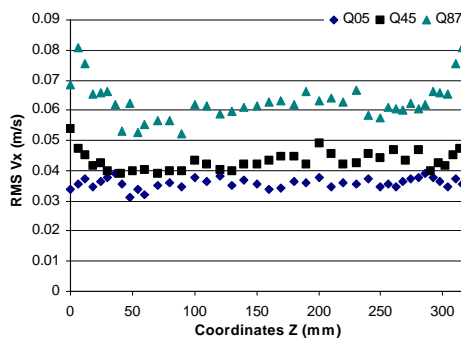
Figure B-5 RMS of V_y by ADV

Figure B-6 Profile of V_x by ADV

We can see from the ADV velocity shown above that the general profiles of velocity in the test tunnel agree with the common known knowledge on the flow. The flow is totally turbulent flow. The profile is quite flat in most of the area. But the information of velocity in the area near to the boundary is too less. When the velocity is too low ($Q = 5$ l/s, $V = 0.06$ m/s in the figures), the ADV velocity profile is almost flat along the whole cross section of the tunnel. Significant error exists in the results of the boundary area.

The sampling volume of ADV is about 50 mm away from the sensor. The sensor does not disturb the flow of sampling volume directly. But it does disturb the flow nearby the sampling volume. This must cause some error in the results.

The move of ADV sensor crossing the flow was done manually along a normal scale during the measurement. The resolution of moving steps was quite low, especially while measuring in the area near to the wall and the absolute moving step was smaller.

Due to these limitations, ADV is only used for a few cases of measurement, mainly for stationary flow, to get a rough approximation of the velocity scale, which can be used for the setup of later measurement with laser.

B.2 Pump Start-up Test

To investigate the pressure surge at the instant of pump start-up, some measurements were carried out when water was totally still and started the pump at full load. The measurement was always conducted in the morning before the first start of the pump.

- First start the data acquisition operation;
- Second set the pump rotating speed;
- Turn on the pump to run in the speed;
- Record the development procedure of the flow

Each pump rotating speed corresponding to a pump output flow rate, or velocity of flow. Table B-1 lists the final mean flow rate and velocity for the 7 cases tested.

Table B-1 List of pump start-up test

No.	1	2	3	4	5	6	7
Final Q(l/s)	10	20	40	60	80	100	120
Final V(m/s)	0.14	0.27	0.54	0.82	1.08	1.36	1.63

The development procedures of differential pressure, dynamic pressure, flow rate and cross section averaged pressure were recorded. As an example, Figure B-7 to Figure B-10 show the time series of differential pressure (*dP1* & *dP2*), dynamic pressure (*dynP1* to *dynP4*), flow rate (*Q*) and cross section averaged pressure (*P1* & *P2*) in the first 25 seconds after pump start up for test No 6 in Table B-1, the final flow rate of which is about 60 l/s.

In the figures shown above, the readings started several seconds before the pump start-up. The readings in the first several seconds are zero. They ought to be removed from the analysis of the start-up characteristics.

The sampling rate for differential pressure, dynamic pressure and flow rate is 50Hz, 1 Hz for the cross section averaged pressure.
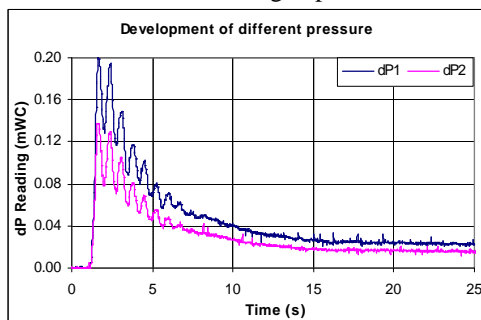
Figure B-7 Development of dP
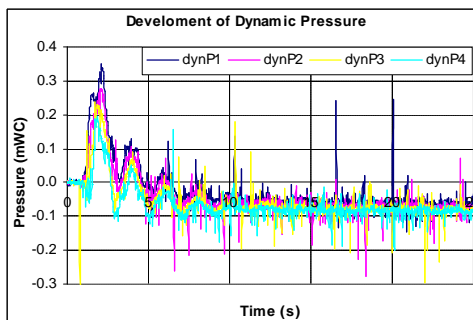
Figure B-8 Develop of dynP
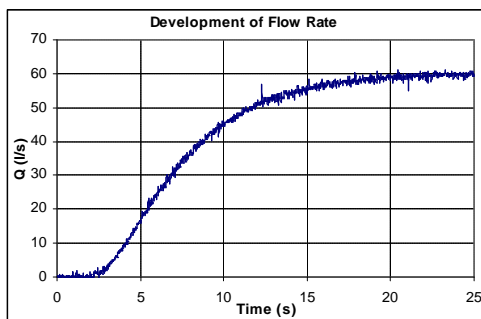
Figure B-9 Development of flow rate
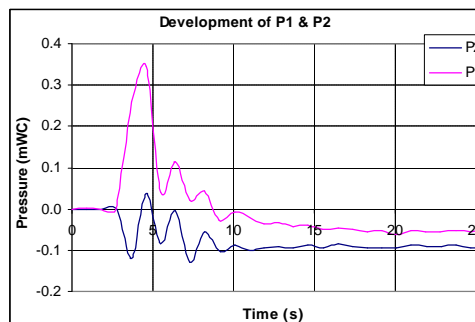
Figure B-10 Develop of averaged pressure

It is displayed in the figures that the time for various variables to reach stable status is different:

–   For flow rate increasing from zero to about 60 l/s, it takes about 20 seconds (Figure B-9).

–   The differential pressures along the main stream reach constant in about 20 seconds (Figure B-7).

–   The dynamic pressure reaches constant in about 10 seconds (Figure B-8).

–   The cross section averaged pressures reach constant in about 15 seconds (Figure B-10).

It is also displayed in the figures that the surge for various variables is different:

–   No surge recorded in the flow rate (Figure B-9). It increases with time steadily; increase faster at the beginning and slower when it is near to the stationary status.

157

- The differential pressures oscillate a lot at the start stage (Figure B-7). The peak differential pressure is almost 10 times of the stable differential pressure for *dP1* and 7 times for *dP2*.
- The dynamic pressure also oscillates some periods (Figure B-8). The peak pressure is several times of the final steady pressure (Note: the zero point here is not zero pressure, it is about 1 meter).
- The cross section averaged pressures oscillate in a similar mode as that of dynamic pressure (Figure B-10).

For other cases tested, the development procedures at pump start-up are similar to the one discussed above. There are differences at the stable time and peak – steady ratio for different final flow status.

B.3 Comparison Between Smooth Tunnel and Rough Tunnel

At the first stage of measurement, tunnel with smooth wall was used. The sand roughness layer was introduced later. Comparative measurements were carried out to get the change of the flow characteristics between smooth tunnel and rough tunnel. Three examples are shown below.

Example 1: mean flow rate was 13.45 l/s for smooth tunnel and 13.34 l/s for rough tunnel; stationary flow.

Table B-2 Compare smooth with rough tunnel at Q = 13 l/s

	Q (l/s)	dynP1 (mWC)	dynP2 (mWC)	dynP3 (mWC)	dynP4 (mWC)	dP1 (mWC)	dP2 (mWC)
Smooth	13.45	-0.007574	-0.008389	-0.008490	-0.009370	0.000733	0.000454
Rough	13.34	-0.003052	-0.003592	-0.005018	-0.003859	0.001085	0.000851
Differ.	-0.76%	0.004522	0.004798	0.003471	0.005511	47.99%	87.24%

Example 2: mean flow rate was 22.83 l/s for smooth tunnel and 22.54 l/s for rough tunnel; stationary flow.

Table B-3 Compare smooth with rough tunnel at Q = 23 l/s

	Q (l/s)	dynP1 (mWC)	dynP2 (mWC)	dynP3 (mWC)	DynP4 (mWC)	dP1 (mWC)	dP2 (mWC)
Smooth	22.83	-0.019592	-0.020735	-0.021310	-0.022327	0.002168	0.001438
Rough	22.54	-0.009680	-0.011368	-0.013613	-0.013134	0.003155	0.002244
Differ.	-1.26%	0.009912	0.009368	0.007697	0.009193	45.53%	56.05%

Example 3: mean flow rate was 31.35 l/s for smooth tunnel and 31.23 l/s for rough tunnel; stationary flow.

Table B-4 Compare smooth with rough tunnel at Q = 31 l/s

	Q (l/s)	dynP1 (mWC)	dynP2 (mWC)	dynP3 (mWC)	DynP4 (mWC)	dP1 (mWC)	dP2 (mWC)
Smooth	31.35	-0.025132	-0.026602	-0.028397	-0.028988	0.003975	0.002723
Rough	31.23	-0.016493	-0.019704	-0.022755	-0.022746	0.006078	0.004178
Differ.	-0.36%	0.008639	0.006898	0.005642	0.006242	52.90%	53.45%

158

In the examples shown above, the difference of flow characteristics between the similar flow in smooth and rough tunnel features:

− The difference between the dynamic pressure was quite small comparing with the static pressure in the flow (about 1 mWC, the values shown in the tables were relative values to a datum)

− The increase of differential pressure (head loss) was obvious, though the absolute increase was not big. The relative increase was about 50% from smooth tunnel to the rough tunnel.

Friction factor of smooth tunnel and rough tunnel could be evaluated on the basis of values listed above using Darcy-Weisbach equation.

The cross section of smooth tunnel was 0.23 * 0.36 m^2 and 0.22 * 0.35 m^2 for rough tunnel.

The measuring distance of *dP1* was 9 meters and 6 meters for *dP2*. The friction factors evaluated from the reading of *dP1* and *dP2* were averaged to get a mean value for each example. The results are listed in Table B-5.

Table B-5 Friction factor of smooth and rough tunnel

	Example 1	Example 2	Example 3	Average
Smooth	0.016401	0.017384	0.017187	0.016991
Rough	0.023137	0.02238	0.022074	0.02253

The friction factor increased about 33% from smooth tunnel to the tunnel with sand roughness. This percentage was lower than that of the head loss increase shown above. This was resulted from the difference of cross sectional area and hydraulic diameter between the smooth and rough tunnel. The difference of mean velocity in the tunnel was much bigger than that of flow rate shown above, between smooth and rough tunnel.

The friction factor for rough tunnel in Table B-5 was similar to the friction factor calculated in Chapter 5 for both stationary flow and oscillatory flow with rough tunnel, using the relative roughness and the empirical formula for friction factor. The difference was about 5%.

Appendix C Summary List Examples of Experimental Data

After all data from PIV and other data acquisition means were processed, including phase average, space average and time average, the specific values (max. min. mean, stdev) of each measured variables (*V, dP1, dP2, dP3, dP4, P1, P2, dynP1, dynP2, dynP3, dynP4* and *Q*) were put together to get the summary lists of experimental data, in order to compare the data from different flow regimes. Two examples are given below. One is the summary list of readings from dP1. The other is the summary list of flow rates integrated from PIV instantaneous velocity fields. From the examples one can have a general view of the dependency of head variation and flow rate on different flow control parameters, i.e., stationary base flow, oscillatory amplitude and frequency.

C.1 Summary List of Averaged Readings of Differential Pressure Sensor dP1

Column names of following tables:
- *No*: ID of the flow regime
- *Max*: Maximum readings of the differential pressure sensor dP1 (mWC)
- *Min*: Minimum readings of the differential pressure sensor dP1 (mWC)
- *Max*: Mean values over periods of dP1 (mWC)
- *Freq*: frequency of the flow in Hz
- *Base*: percentage of the stationary flow (%)
- *Amp*: percentage of the oscillatory amplitude (%)

C.1.1 Stationary flow

No	Max	Min	Mean	Freq	Base	Amp
001	0.000250	−0.000198	0.000005	0.00	0	10
002	0.000837	0.000271	0.000616	0.00	0	20
003	0.001817	0.001360	0.001588	0.00	0	30
004	0.003472	0.002911	0.003151	0.00	0	40
005	0.005437	0.004919	0.005209	0.00	0	50
006	0.009584	0.007011	0.008340	0.00	0	60
007	0.013346	0.010727	0.012096	0.00	0	70
008	0.017861	0.015254	0.016565	0.00	0	80
009	0.020343	0.018057	0.019152	0.00	0	90
008	0.019056	0.016483	0.017626	0.00	0	80

C.1.2 Pure oscillatory flow

No	Max	Min	Mean	Freq	Base	Amp
001	0.004552	−0.006672	−0.001384	0.01	0	10
002	0.013008	−0.013278	−0.000937	0.01	0	20
003	0.021245	−0.020383	−0.001050	0.01	0	30

161

004	0.029706	-0.027822	-0.001143	0.01	0	40
005	0.038655	-0.034772	-0.001241	0.01	0	50
006	0.047174	-0.042320	-0.001331	0.01	0	60
007	0.055560	-0.049557	-0.001579	0.01	0	70
008	0.064682	-0.056249	-0.002134	0.01	0	80
009	0.058195	-0.050398	-0.002256	0.01	0	90
011	0.005422	-0.005871	-0.000530	0.05	0	10
012	0.023316	-0.022123	-0.000525	0.05	0	20
013	0.050046	-0.045811	-0.000532	0.05	0	30
014	0.080595	-0.074060	-0.000610	0.05	0	40
015	0.114550	-0.104421	-0.000411	0.05	0	50
016	0.149343	-0.135470	-0.000258	0.05	0	60
017	0.184719	-0.165862	-0.001801	0.05	0	70
018	0.220409	-0.199961	-0.000807	0.05	0	80
021	0.004205	-0.004806	-0.000489	0.10	0	10
022	0.019647	-0.019108	-0.000646	0.10	0	20
023	0.044898	-0.042206	-0.000869	0.10	0	30
024	0.077293	-0.072769	-0.001076	0.10	0	40
025	0.115872	-0.109295	-0.001618	0.10	0	50
026	0.157751	-0.147349	-0.000189	0.10	0	60
027	0.199860	-0.188312	-0.002019	0.10	0	70
028	0.242640	-0.231115	-0.002877	0.10	0	80
031	0.002534	-0.002731	-0.000111	0.20	0	10
032	0.012411	-0.011521	-0.000295	0.20	0	20
033	0.027294	-0.025993	0.000233	0.20	0	30
034	0.049125	-0.045889	0.000664	0.20	0	40
035	0.074851	-0.069273	-0.000894	0.20	0	50
036	0.105321	-0.096721	-0.001035	0.20	0	60
037	0.136550	-0.124485	0.001746	0.20	0	70
039	0.182000	-0.164439	-0.000310	0.20	0	90
041	-0.000965	-0.004428	-0.002682	0.50	0	10
042	0.004231	-0.010035	-0.002882	0.50	0	20
043	0.014231	-0.019637	-0.002697	0.50	0	30
044	0.024523	-0.030082	-0.002696	0.50	0	40
045	0.027957	-0.033591	-0.002493	0.50	0	50

C.1.3 Combined oscillatory flow

1. Stationary base flow was 10%

No	Max	Min	Mean	Freq	Base	Amp
101	0.005684	-0.004552	-0.000243	0.01	10	10
102	0.014403	-0.007711	-0.000016	0.01	10	20
103	0.024605	-0.015391	0.000261	0.01	10	30
104	0.033043	-0.023870	0.000583	0.01	10	40
105	0.040344	-0.030464	0.000816	0.01	10	50

106	0.049236	−0.038219	0.001114	0.01	10	60
107	0.057771	−0.045669	0.001380	0.01	10	70
108	0.066784	−0.052958	0.000948	0.01	10	80
109	0.074498	−0.060115	0.000247	0.01	10	90
111	0.009639	−0.005242	0.000233	0.05	10	10
112	0.026596	−0.015943	0.000908	0.05	10	20
113	0.052497	−0.035400	0.001588	0.05	10	30
114	0.085473	−0.058260	0.002445	0.05	10	40
115	0.124626	−0.080843	0.003505	0.05	10	50
116	0.170102	−0.108283	0.004809	0.05	10	60
117	0.216784	−0.139219	0.006378	0.05	10	70
118	0.259712	−0.173041	0.008067	0.05	10	80
119	0.290366	−0.206331	0.008763	0.05	10	90
121	0.008750	−0.005505	0.000058	0.10	10	10
122	0.024660	−0.015096	0.000210	0.10	10	20
123	0.048461	−0.032833	0.001061	0.10	10	30
124	0.077794	−0.052464	0.001184	0.10	10	40
125	0.113396	−0.075934	0.000871	0.10	10	50
126	0.153759	−0.101951	0.000646	0.10	10	60
127	0.198204	−0.134825	0.000644	0.10	10	70
128	0.228389	−0.170041	0.000966	0.10	10	80
129	0.232006	−0.204030	−0.000333	0.10	10	90
131	0.006440	−0.004106	0.000482	0.20	10	10
132	0.017776	−0.011389	0.000784	0.20	10	20
133	0.035758	−0.026305	0.000842	0.20	10	30
134	0.059793	−0.047240	0.000719	0.20	10	40
135	0.090993	−0.074271	0.000733	0.20	10	50
136	0.126069	−0.105147	0.000260	0.20	10	60
137	0.164880	−0.139312	0.000371	0.20	10	70
138	0.193194	−0.168625	−0.000404	0.20	10	80
139	0.184255	−0.178438	−0.000897	0.20	10	90
141	0.001018	−0.004488	−0.001689	0.50	10	10
142	0.006969	−0.009145	−0.001489	0.50	10	20
143	0.017285	−0.018086	−0.000856	0.50	10	30
144	0.026673	−0.026212	−0.000010	0.50	10	40
145	0.029181	−0.029185	−0.000235	0.50	10	50

2. Stationary base flow was 20%

No	Max	Min	Mean	Freq	Base	Amp
201	0.006316	−0.004989	0.000527	0.01	20	10
202	0.012445	−0.008297	0.000823	0.01	20	20
203	0.020791	−0.011508	0.001359	0.01	20	30
204	0.032015	−0.017000	0.002114	0.01	20	40
205	0.040907	−0.025593	0.002996	0.01	20	50
206	0.049040	−0.033612	0.003728	0.01	20	60

207	0.057065	−0.041154	0.003571	0.01	20	70
208	0.066077	−0.049029	0.003257	0.01	20	80
211	0.015776	−0.011964	−0.000179	0.05	20	10
212	0.033470	−0.019744	0.000780	0.05	20	20
213	0.054794	−0.029211	0.001482	0.05	20	30
214	0.082453	−0.042600	0.002221	0.05	20	40
215	0.115804	−0.063179	0.003461	0.05	20	50
216	0.154674	−0.082760	0.004351	0.05	20	60
217	0.185469	−0.102270	0.003838	0.05	20	70
218	0.214329	−0.125924	0.003786	0.05	20	80
221	0.016905	−0.011648	0.000611	0.10	20	10
222	0.035766	−0.020484	0.001353	0.10	20	20
223	0.058529	−0.031774	0.001535	0.10	20	30
224	0.087272	−0.049030	0.002177	0.10	20	40
225	0.120622	−0.069553	0.002521	0.10	20	50
226	0.156654	−0.091636	0.003070	0.10	20	60
227	0.186323	−0.117166	0.003325	0.10	20	70
228	0.218473	−0.180146	0.001763	0.10	20	80
231	0.011303	−0.009220	0.000066	0.20	20	10
232	0.024742	−0.016337	0.000494	0.20	20	20
233	0.042653	−0.025865	0.001234	0.20	20	30
234	0.066010	−0.043523	0.001887	0.20	20	40
235	0.095578	−0.067093	0.002371	0.20	20	50
236	0.130625	−0.097086	0.002509	0.20	20	60
237	0.160617	−0.126930	0.002352	0.20	20	70
238	0.168854	−0.147475	0.001682	0.20	20	80
241	0.006826	−0.004235	0.001218	0.50	20	10
242	0.013732	−0.008075	0.002180	0.50	20	20
243	0.023193	−0.013875	0.003376	0.50	20	30
244	0.031294	−0.021952	0.003328	0.50	20	40
245	0.034090	−0.024060	0.003561	0.50	20	50

3. Stationary base flow was 30%

No	Max	Min	Mean	Freq	Base	Amp
301	0.007706	−0.003708	0.001831	0.01	30	10
302	0.012715	−0.008326	0.002241	0.01	30	20
303	0.019045	−0.011422	0.003094	0.01	30	30
304	0.026386	−0.015139	0.003992	0.01	30	40
305	0.039189	−0.017833	0.005058	0.01	30	50
306	0.048041	−0.026839	0.005621	0.01	30	60
307	0.056514	−0.035708	0.005769	0.01	30	70
311	0.018541	−0.012381	0.001044	0.05	30	10
312	0.039347	−0.024164	0.001828	0.05	30	20
313	0.063111	−0.036615	0.002767	0.05	30	30
314	0.085171	−0.046497	0.003945	0.05	30	40

315	0.112389	−0.056825	0.004964	0.05	30	50
316	0.143945	−0.067316	0.005563	0.05	30	60
317	0.175433	−0.078054	0.005351	0.05	30	70
321	0.022855	−0.015985	0.001517	0.10	30	10
322	0.046986	−0.029248	0.001826	0.10	30	20
323	0.071357	−0.040011	0.002454	0.10	30	30
324	0.098547	−0.051375	0.003305	0.10	30	40
325	0.131312	−0.069912	0.004007	0.10	30	50
326	0.156438	−0.093976	0.004392	0.10	30	60
327	0.175458	−0.121295	0.004465	0.10	30	70
331	0.018503	−0.014284	0.000719	0.20	30	10
332	0.037691	−0.026551	0.000830	0.20	30	20
333	0.058172	−0.035871	0.001210	0.20	30	30
334	0.082363	−0.048753	0.001745	0.20	30	40
335	0.110809	−0.067210	0.002638	0.20	30	50
336	0.132714	−0.087914	0.002658	0.20	30	60
337	0.140239	−0.107354	0.004848	0.20	30	70
341	0.012406	−0.003836	0.004037	0.50	30	10
342	0.021627	−0.009428	0.005358	0.50	30	20
343	0.031243	−0.015384	0.006675	0.50	30	30
344	0.039456	−0.020570	0.007631	0.50	30	40
345	0.042076	−0.023192	0.007304	0.50	30	50

4. Stationary base flow was 40%

No	Max	Min	Mean	Freq	Base	Amp
401	0.010940	−0.002214	0.003895	0.01	40	10
402	0.015604	−0.006603	0.004396	0.01	40	20
403	0.021888	−0.010750	0.005312	0.01	40	30
404	0.028976	−0.014352	0.006295	0.01	40	40
405	0.035565	−0.017919	0.006842	0.01	40	50
406	0.044359	−0.021216	0.007391	0.01	40	60
411	0.021955	−0.011485	0.003046	0.05	40	10
412	0.044753	−0.025529	0.003444	0.05	40	20
413	0.068299	−0.037818	0.004591	0.05	40	30
414	0.091819	−0.051639	0.005298	0.05	40	40
415	0.114778	−0.062575	0.006106	0.05	40	50
416	0.137569	−0.072124	0.006410	0.05	40	60
421	0.028557	−0.018390	0.003356	0.10	40	10
422	0.056045	−0.036036	0.003565	0.10	40	20
423	0.084575	−0.050492	0.005143	0.10	40	30
424	0.112948	−0.063342	0.006331	0.10	40	40
425	0.130643	−0.073142	0.006163	0.10	40	50
426	0.141526	−0.083333	0.007983	0.10	40	60
431	0.023491	−0.016714	0.002101	0.20	40	10
432	0.047888	−0.032876	0.002904	0.20	40	20

No	Max	Min	Mean	Freq	Base	Amp
433	0.071942	−0.045280	0.003278	0.20	40	30
434	0.095792	−0.055351	0.005711	0.20	40	40
435	0.112948	−0.065672	0.006853	0.20	40	50
436	0.115449	−0.081303	0.003637	0.20	40	60
441	0.017901	−0.002698	0.007356	0.50	40	10
442	0.029548	−0.010276	0.008584	0.50	40	20
443	0.041127	−0.017552	0.010306	0.50	40	30
444	0.049493	−0.023120	0.011449	0.50	40	40
445	0.051017	−0.025234	0.010939	0.50	40	50

5. Stationary base flow was 50%

No	Max	Min	Mean	Freq	Base	Amp
501	0.012473	0.000382	0.006503	0.01	50	10
502	0.019257	−0.004351	0.007181	0.01	50	20
503	0.025805	−0.008866	0.007793	0.01	50	30
504	0.031814	−0.013921	0.007763	0.01	50	40
505	0.038833	−0.017735	0.008583	0.01	50	50
511	0.026949	−0.011948	0.005638	0.05	50	10
512	0.050277	−0.028125	0.006149	0.05	50	20
513	0.074457	−0.043141	0.006619	0.05	50	30
514	0.098323	−0.055854	0.007178	0.05	50	40
515	0.116667	−0.065837	0.007059	0.05	50	50
521	0.034685	−0.020072	0.005448	0.10	50	10
522	0.065578	−0.040742	0.006763	0.10	50	20
523	0.096658	−0.058093	0.006553	0.10	50	30
524	0.117231	−0.071902	0.007236	0.10	50	40
525	0.125085	−0.079234	0.007452	0.10	50	50
531	0.030779	−0.019243	0.004271	0.20	50	10
532	0.057774	−0.038181	0.004939	0.20	50	20
533	0.086352	−0.055044	0.006630	0.20	50	30
534	0.103007	−0.064187	0.008706	0.20	50	40
535	0.103019	−0.070872	0.008236	0.20	50	50
541	0.023985	−0.000342	0.011608	0.50	50	10
542	0.038291	−0.010343	0.013044	0.50	50	20
543	0.052818	−0.019314	0.014855	0.50	50	30
544	0.059171	−0.024064	0.015819	0.50	50	40
545	0.059833	−0.024972	0.015510	0.50	50	50

6. Stationary base flow was 60%

No	Max	Min	Mean	Freq	Base	Amp
601	0.016287	0.003639	0.009810	0.01	60	10
602	0.020561	−0.001835	0.009725	0.01	60	20
603	0.028660	−0.007350	0.009936	0.01	60	30
604	0.034646	−0.012324	0.009878	0.01	60	40
611	0.026764	−0.007856	0.008324	0.05	60	10

612	0.051162	−0.026036	0.008795	0.05	60	20
613	0.077364	−0.042382	0.009107	0.05	60	30
614	0.097548	−0.055098	0.008804	0.05	60	40
621	0.039934	−0.019848	0.008165	0.10	60	10
622	0.073562	−0.044311	0.008701	0.10	60	20
623	0.097023	−0.062938	0.008955	0.10	60	30
624	0.110298	−0.074909	0.009227	0.10	60	40
631	0.036784	−0.020956	0.006933	0.20	60	10
632	0.068054	−0.044135	0.007599	0.20	60	20
633	0.085418	−0.063212	0.007523	0.20	60	30
634	0.088226	−0.072615	0.007294	0.20	60	40
641	0.031532	0.003159	0.017102	0.50	60	10
642	0.047352	−0.008246	0.018612	0.50	60	20
643	0.056486	−0.015541	0.019664	0.50	60	30
644	0.058949	−0.018900	0.019557	0.50	60	40
651	0.026431	0.007899	0.017026	1.00	60	10
652	0.035820	0.002121	0.018689	1.00	60	20
653	0.039665	0.000288	0.019106	1.00	60	30
654	0.039995	−0.000051	0.019257	1.00	60	40

7. Stationary base flow was 70%

No	Max	Min	Mean	Freq	Base	Amp
701	0.018901	0.006339	0.012579	0.01	70	10
702	0.024329	0.001330	0.012240	0.01	70	20
703	0.029315	−0.003961	0.012145	0.01	70	30
711	0.029815	−0.005068	0.011833	0.05	70	10
712	0.052774	−0.023276	0.011502	0.05	70	20
713	0.074269	−0.038772	0.011141	0.05	70	30
721	0.045185	−0.017885	0.012242	0.10	70	10
722	0.071646	−0.042137	0.011313	0.10	70	20
723	0.087681	−0.059238	0.010851	0.10	70	30
731	0.043611	−0.021014	0.009583	0.20	70	10
732	0.064310	−0.045985	0.009256	0.20	70	20
733	0.071877	−0.061697	0.008490	0.20	70	30
741	0.040093	0.007891	0.023768	0.50	70	10
742	0.050657	−0.001620	0.024324	0.50	70	20
743	0.057234	−0.007831	0.023904	0.50	70	30
751	0.034064	0.013656	0.023727	1.00	70	10
752	0.042093	0.007259	0.024468	1.00	70	20
753	0.044343	0.004649	0.024387	1.00	70	30

C.2 Summary List of Flow Rates Integrated from PIV Velocity

Column names of following tables:

- – *No*: ID of the flow regime
- – *Max*: Maximum flow rates integrated from PIV data (l/s)
- – *Min*: Minimum flow rates integrated from PIV data (l/s)
- – *Max*: Mean flow rates over periods integrated from PIV data (l/s)

Others are the same as those in section C.1.

C.2.1 Stationary flow

No	Max	Min	Mean	Freq	Base	Amp
001	7.994709	6.425780	6.981260	0.00	0	10
002	14.826519	13.011056	13.960516	0.00	0	20
003	22.575116	20.319476	21.454406	0.00	0	30
004	30.182904	26.696279	28.490479	0.00	0	40
005	37.281496	33.514413	35.456964	0.00	0	50
006	43.478758	38.151157	40.811291	0.00	0	60
007	51.576966	45.139022	48.106176	0.00	0	70
008	54.119346	38.788937	49.607340	0.00	0	80
009	59.500732	56.174194	57.923515	0.00	0	90
008	59.880372	56.069087	58.383897	0.00	0	80

C.2.2 Pure oscillatory flow

No	Max	Min	Mean	Freq	Base	Amp
001	5.308851	−5.060899	0.068671	0.01	0	10
002	12.859894	−13.493867	−0.228281	0.01	0	20
003	18.289042	−20.273067	0.186969	0.01	0	30
004	26.526658	−27.094726	−0.489164	0.01	0	40
005	35.592829	−37.479163	0.182544	0.01	0	50
006	43.683805	−45.306726	−0.710833	0.01	0	60
007	53.117791	−57.032259	−0.153391	0.01	0	70
008	61.354889	−66.295551	−3.143700	0.01	0	80
009	79.234151	−73.962138	0.545649	0.01	0	90
011	1.521973	−0.331595	0.385484	0.05	0	10
012	5.023898	−4.079216	0.513287	0.05	0	20
013	12.181590	−10.013317	0.970441	0.05	0	30
014	18.642006	−17.314458	0.071303	0.05	0	40
015	26.754833	−25.633300	−0.134122	0.05	0	50
016	33.928542	−34.031058	−0.655059	0.05	0	60
021	0.742394	−8.329759	−0.020603	0.10	0	10
022	4.357949	−1.370735	1.079765	0.10	0	20
023	7.171026	−5.068914	1.166378	0.10	0	30
024	12.545215	−8.511049	1.821440	0.10	0	40
025	18.407595	−13.884093	2.122782	0.10	0	50
026	24.760563	−20.370388	1.819806	0.10	0	60
027	31.007518	−27.176461	2.064758	0.10	0	70
028	37.005673	−34.015465	1.308010	0.10	0	80

031	1.801633	1.094198	1.470519	0.20	0	10
032	0.004171	0.004171	0.004171	0.20	0	20
033	0.004171	0.004171	0.004171	0.20	0	30
034	0.004171	0.004171	0.004171	0.20	0	40
035	0.004171	0.004171	0.004171	0.20	0	50
037	2.813199	1.741857	2.186764	0.20	0	70
038	38.253185	1.883717	20.038654	0.20	0	80
039	0.862836	0.862836	0.862836	0.20	0	90
041	0.259488	−0.025515	0.113573	0.50	0	10
042	0.910834	−0.200593	0.360737	0.50	0	20
043	1.076854	−0.446064	0.434161	0.50	0	30
044	1.044785	−0.691026	0.360186	0.50	0	40
045	0.904296	−0.627626	0.256217	0.50	0	50

C.2.3 Combined oscillatory flow

1. Stationary base flow was 10%

No	Max	Min	Mean	Freq	Base	Amp
101	10.573283	1.662483	5.562430	0.01	10	10
102	10.523210	−2.978075	2.703179	0.01	10	20
103	10.034431	−4.318467	1.315163	0.01	10	30
104	10.253146	0.000000	0.000000	0.01	10	40
105	7.693897	−3.198574	0.572251	0.01	10	50
106	10.677337	0.000000	0.000000	0.01	10	60
107	5.680738	−2.666872	0.914218	0.01	10	70
108	9.687567	0.000000	0.000000	0.01	10	80
109	7.910556	0.000000	0.000000	0.01	10	90
111	15.664925	11.460217	13.454925	0.05	10	10
112	21.574238	12.043841	16.700449	0.05	10	20
113	28.985337	8.455241	18.661826	0.05	10	30
114	37.996182	2.141467	20.021826	0.05	10	40
115	44.619223	−2.526413	20.713314	0.05	10	50
116	50.214526	−11.039788	21.375919	0.05	10	60
117	49.930765	−18.317409	16.092364	0.05	10	70
118	48.765441	−26.467638	7.596052	0.05	10	80
119	48.317700	−36.513543	5.684601	0.05	10	90
121	10.735766	7.900352	9.169134	0.10	10	10
122	16.227641	9.570135	12.969514	0.10	10	20
123	21.347592	8.114049	14.608827	0.10	10	30
124	27.305607	6.712900	16.193475	0.10	10	40
125	33.170935	4.279230	18.154877	0.10	10	50
126	38.453003	−1.082741	17.895339	0.10	10	60
127	46.278261	−6.604004	17.791764	0.10	10	70
128	48.512425	−13.502253	18.891501	0.10	10	80
129	50.974660	−21.483824	14.857757	0.10	10	90

131	8.274063	6.395533	7.547122	0.20	10	10
132	10.897142	8.125789	9.420072	0.20	10	20
133	14.080411	8.778708	11.433880	0.20	10	30
134	17.664485	7.177120	12.864648	0.20	10	40
135	22.877466	6.934027	14.739377	0.20	10	50
136	27.116176	4.485128	15.396094	0.20	10	60
137	31.188726	1.170652	16.490920	0.20	10	70
138	33.798700	−2.446372	15.467577	0.20	10	80
139	29.363376	−9.414797	9.099266	0.20	10	90
141	12.396213	9.403230	10.820585	0.50	10	10
142	16.091148	11.071751	13.990579	0.50	10	20
143	19.278518	13.532083	17.005486	0.50	10	30
144	21.178145	13.992482	17.907708	0.50	10	40
145	21.504611	13.370664	18.034550	0.50	10	50

2. Stationary base flow was 20%

No	Max	Min	Mean	Freq	Base	Amp
201	15.189310	5.756428	10.416770	0.01	20	10
202	18.639431	2.794243	10.453646	0.01	20	20
203	25.912714	−1.548876	11.368618	0.01	20	30
204	34.983952	−9.828301	11.827406	0.01	20	40
205	41.064884	−18.022481	11.699724	0.01	20	50
206	46.055141	−25.420204	10.548440	0.01	20	60
207	49.599035	−34.044779	9.557741	0.01	20	70
208	55.296533	−43.480307	8.099728	0.01	20	80
211	18.677023	10.478039	15.247500	0.05	20	10
212	28.238344	12.171773	20.539235	0.05	20	20
213	34.932956	12.314970	23.035189	0.05	20	30
214	42.060879	6.911090	23.731640	0.05	20	40
215	50.281490	1.308048	25.154922	0.05	20	50
216	56.150419	−6.648173	23.486095	0.05	20	60
217	58.956672	−15.912109	20.935159	0.05	20	70
218	58.475723	−23.772484	17.164410	0.05	20	80
221	18.472974	13.304276	15.756870	0.10	20	10
222	24.359160	14.120783	18.625581	0.10	20	20
223	29.038714	14.570888	21.535297	0.10	20	30
224	35.549588	13.058498	23.342416	0.10	20	40
225	41.921942	11.033572	25.285331	0.10	20	50
226	48.006293	8.069491	26.638342	0.10	20	60
227	53.018809	3.426003	27.201522	0.10	20	70
228	50.255873	−11.790861	18.996555	0.10	20	80
231	11.480854	8.937443	10.414562	0.20	20	10
232	14.368218	10.569959	12.453796	0.20	20	20
233	18.113212	11.551174	15.125486	0.20	20	30
234	23.361063	14.822015	18.901952	0.20	20	40

170

235	31.563177	14.779381	23.297508	0.20	20	50
236	36.887675	14.021836	25.617132	0.20	20	60
237	42.178144	12.256414	26.671174	0.20	20	70
238	41.796028	7.433179	23.641390	0.20	20	80
241	20.812060	16.514991	18.548660	0.50	20	10
242	23.735642	18.142323	21.299248	0.50	20	20
243	29.666657	24.674611	26.631663	0.50	20	30
244	30.795480	23.230836	27.375540	0.50	20	40
245	30.775035	20.683391	27.391299	0.50	20	50

3. Stationary base flow was 30%

No	Max	Min	Mean	Freq	Base	Amp
301	22.017857	10.960646	17.172568	0.01	30	10
302	32.642363	7.040089	18.996700	0.01	30	20
303	37.714604	3.745470	18.751654	0.01	30	30
304	41.200408	−1.074912	18.782486	0.01	30	40
305	48.474167	−10.691420	19.667031	0.01	30	50
306	54.568698	−19.178313	18.652740	0.01	30	60
307	55.161325	−26.093303	17.108172	0.01	30	70
311	27.292991	14.814201	21.763593	0.05	30	10
312	33.770595	13.244774	23.347925	0.05	30	20
313	41.047791	12.416492	25.881767	0.05	30	30
314	46.696124	9.382326	27.100374	0.05	30	40
315	52.926918	4.842235	26.748291	0.05	30	50
316	59.340296	−0.049500	27.322254	0.05	30	60
317	56.182879	−3.725215	24.770199	0.05	30	70
321	26.384942	19.834136	22.778514	0.10	30	10
322	32.388914	17.917400	24.641131	0.10	30	20
323	37.796745	18.455075	26.917853	0.10	30	30
324	43.032410	18.046861	29.532719	0.10	30	40
325	49.899097	16.818697	31.304823	0.10	30	50
326	54.262899	11.797004	31.974051	0.10	30	60
327	55.155068	6.479866	30.725041	0.10	30	70
331	10.301904	6.810874	8.364231	0.20	30	10
332	11.383926	6.686480	9.170141	0.20	30	20
334	23.312642	10.562821	17.448574	0.20	30	40
335	28.123769	13.614465	19.952753	0.20	30	50
336	39.846928	15.276691	26.123692	0.20	30	60
337	47.805104	20.579359	33.058199	0.20	30	70
341	24.430276	20.319803	22.497973	0.50	30	10
342	34.183463	29.170926	31.423427	0.50	30	20
343	39.733180	34.052969	36.667497	0.50	30	30
344	42.962673	33.633604	38.137464	0.50	30	40
345	44.383475	27.174137	39.596999	0.50	30	50

4. Stationary base flow was 40%

No	Max	Min	Mean	Freq	Base	Amp
401	36.399152	17.829640	28.790246	0.01	40	10
402	42.719754	10.666982	28.023524	0.01	40	20
403	50.877626	7.126687	28.612647	0.01	40	30
404	60.940110	3.741170	29.478537	0.01	40	40
405	63.411001	-0.511808	29.986435	0.01	40	50
406	66.693912	-11.528655	28.263932	0.01	40	60
411	33.956999	16.663593	27.990187	0.05	40	10
412	40.860761	17.506016	28.734679	0.05	40	20
413	47.673464	14.183785	29.351622	0.05	40	30
414	53.363864	12.539200	31.496729	0.05	40	40
415	59.194788	10.460944	32.609479	0.05	40	50
416	60.920877	6.525853	32.765601	0.05	40	60
421	33.837946	26.026857	29.707353	0.10	40	10
422	38.787741	23.448674	30.403994	0.10	40	20
423	44.820703	22.821608	32.927786	0.10	40	30
424	51.662516	22.023897	35.606539	0.10	40	40
425	56.801213	21.475581	37.825032	0.10	40	50
426	57.028051	18.087234	37.697477	0.10	40	60
431	28.261901	23.281657	25.400735	0.20	40	10
432	32.997467	21.809945	27.156340	0.20	40	20
433	36.727422	22.805263	29.536393	0.20	40	30
434	44.360664	24.912768	33.895193	0.20	40	40
435	48.353841	25.433197	35.146617	0.20	40	50
436	44.734365	18.341918	30.858737	0.20	40	60
441	42.292328	28.795162	39.177748	0.50	40	10
442	45.390874	30.653383	41.713158	0.50	40	20
443	51.356716	40.466790	45.037434	0.50	40	30
444	53.806474	44.942921	49.036726	0.50	40	40
445	54.639021	45.801225	49.707414	0.50	40	50

5. Stationary base flow was 50%

No	Max	Min	Mean	Freq	Base	Amp
501	42.639343	29.008278	36.011538	0.01	50	10
502	52.064774	23.351351	36.756055	0.01	50	20
503	58.732904	14.721517	36.275234	0.01	50	30
504	60.621584	9.848066	35.407964	0.01	50	40
505	63.832034	4.047535	36.651133	0.01	50	50
511	40.122131	28.495881	34.033524	0.05	50	10
512	46.499401	23.926928	34.624117	0.05	50	20
513	52.843338	17.812125	34.828253	0.05	50	30
514	59.220326	15.164631	36.893478	0.05	50	40
515	60.228461	13.967513	36.009430	0.05	50	50
521	40.301040	27.536934	35.207073	0.10	50	10

522	45.332730	26.027092	36.010458	0.10	50	20
523	52.090161	25.681628	38.005973	0.10	50	30
524	57.067131	24.271811	39.768481	0.10	50	40
525	59.449387	23.801800	40.901139	0.10	50	50
531	35.856762	27.803750	32.326616	0.20	50	10
532	40.127505	22.295802	34.192848	0.20	50	20
533	46.911883	27.495864	36.804389	0.20	50	30
534	53.413207	30.657904	40.555248	0.20	50	40
535	52.192348	21.661251	39.145479	0.20	50	50
541	51.389101	35.686819	46.457371	0.50	50	10
542	51.607374	39.943880	49.192598	0.50	50	20
543	59.911026	51.885563	55.391857	0.50	50	30
544	61.240170	45.651422	54.238043	0.50	50	40
545	61.032849	46.746893	55.152757	0.50	50	50

6. Stationary base flow was 60%

No	Max	Min	Mean	Freq	Base	Amp
601	49.226305	35.882574	42.307181	0.01	60	10
602	58.010021	29.263732	43.033509	0.01	60	20
603	61.823708	21.621125	43.028590	0.01	60	30
604	64.444108	14.005100	41.378804	0.01	60	40
611	48.709469	35.611023	41.590055	0.05	60	10
612	55.823595	28.291987	41.872071	0.05	60	20
613	60.459412	24.471928	41.992187	0.05	60	30
614	59.881184	19.305463	40.975744	0.05	60	40
621	47.638186	34.477279	41.801554	0.10	60	10
622	53.676033	33.369269	43.069185	0.10	60	20
623	56.940015	29.758712	43.220747	0.10	60	30
624	58.953495	27.243752	43.652151	0.10	60	40
631	42.303103	34.209458	38.076163	0.20	60	10
632	46.717101	31.576545	39.307340	0.20	60	20
633	50.314703	30.820593	40.613826	0.20	60	30
634	52.000576	28.200711	40.233670	0.20	60	40
641	60.407881	53.362618	58.457295	0.50	60	10
642	64.180386	54.019562	60.900081	0.50	60	20
643	67.522617	55.687788	62.800862	0.50	60	30
644	68.249672	56.130785	63.630425	0.50	60	40

7. Stationary base flow was 70%

No	Max	Min	Mean	Freq	Base	Amp
701	55.521511	39.253871	47.946472	0.01	70	10
702	62.218263	34.952035	49.243678	0.01	70	20
703	64.475189	29.498359	48.112835	0.01	70	30
711	55.523869	41.655291	48.243845	0.05	70	10
712	59.783959	35.286094	47.394722	0.05	70	20

173

713	62.056406	29.657573	47.469396	0.05	70	30
721	52.447816	42.506240	47.137195	0.10	70	10
722	56.974277	37.752237	47.631751	0.10	70	20
723	59.679059	31.739812	47.643497	0.10	70	30
731	51.815632	39.170432	46.638848	0.20	70	10
732	54.700750	35.995203	46.436645	0.20	70	20
733	54.571531	30.445004	45.536812	0.20	70	30
741	70.865982	58.740861	68.567209	0.50	70	10
742	71.946729	64.304004	69.001418	0.50	70	20
743	73.652033	63.342096	68.942475	0.50	70	30

Appendix D Full Version of Velocity Profiles

A simplified version of the example velocity profiles and waveforms measured by PIV has been shown in Chapter 4 of this thesis to display the basic information got from PIV measurement. A full version of the velocity profiles and waveforms from the same measurement is shown in this appendix, in the same order and under the same headings as shown in Chapter 4. Refer to Chapter 4 for the analysis and summary of the example velocity profiles and waveforms.

D.1 PIV Velocity of Pure Oscillatory Flow

This is the full version of example velocity profiles and waveforms of pure oscillatory flow measured by PIV. A simplified version of this example is shown in Chapter 4.6

D.1.1 Velocity of constant frequency and variable amplitude

This is the full version of example velocity profiles and waveforms measured by PIV for pure oscillatory flows at the same frequency ($f_r = 0.01$Hz) and different oscillatory amplitudes. The simplified version of this example is shown in Chapter 4.6.1. Please refer to Chapter 4.6.1 for the description of the flow parameters. Figure D-1 to Figure D-18 are the full version of Figure 4-36 through Figure 4-53 respectively.
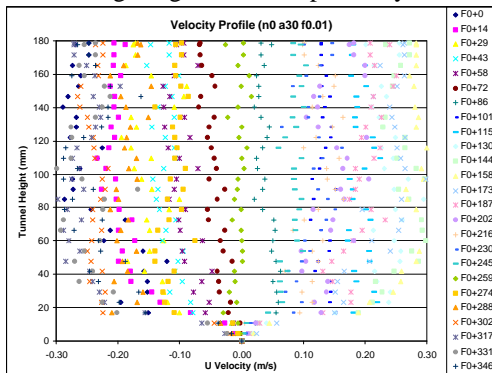
Figure D-1 Velocity profiles (amp=10%)
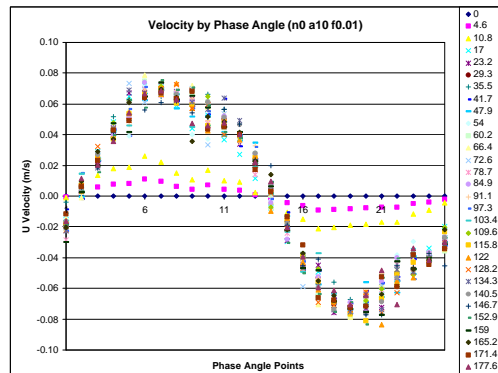
Figure D-2 Velocity waveforms (amp=10%)
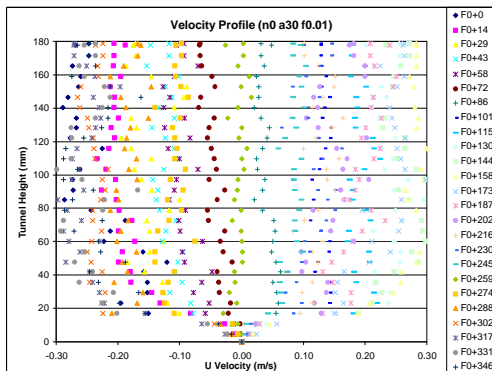
Figure D-3 Velocity profiles (amp=20%)
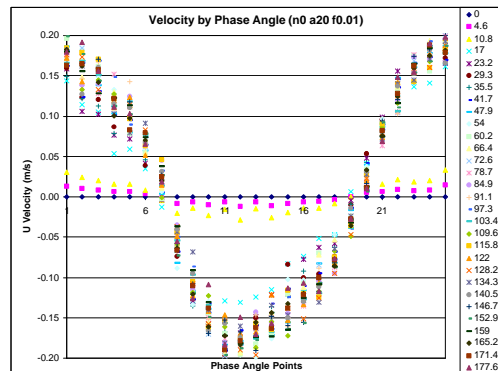
Figure D-4 Velocity waveforms (amp=20%)
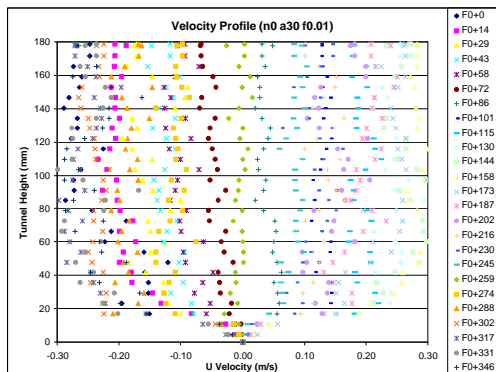
Figure D-5 Velocity profiles (amp=30%)
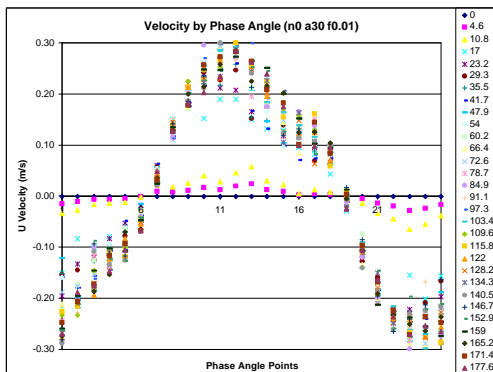
Figure D-6 Velocity waveforms (amp=30%)
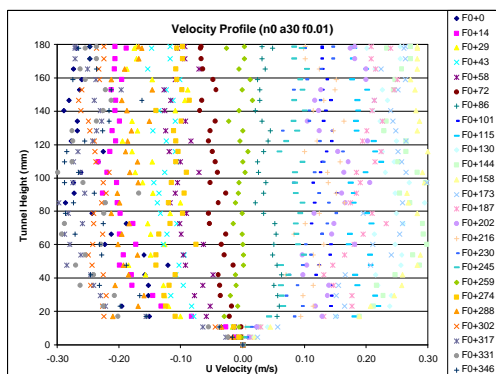
Figure D-7 Velocity profiles (amp=40%)
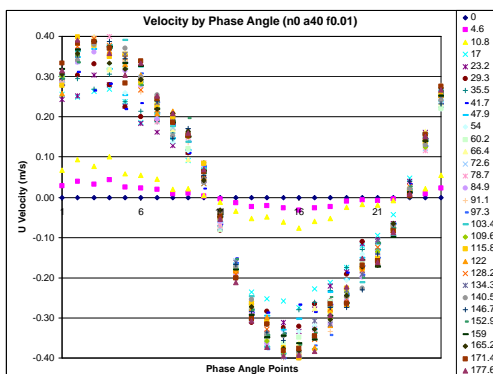
Figure D-8 Velocity waveforms (amp=40%)
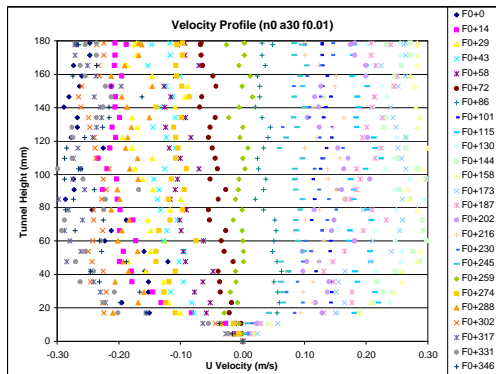
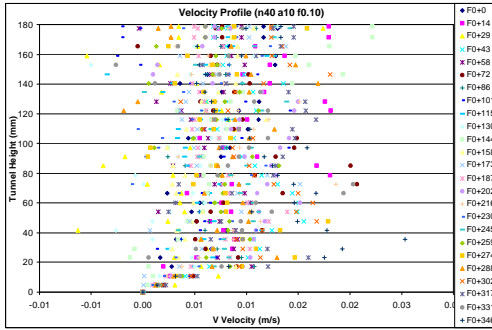Figure D-9 Velocity profiles (amp=50%)
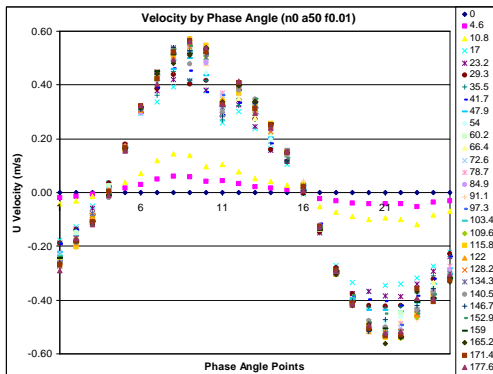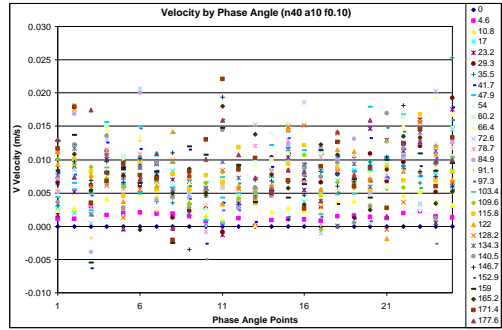

Figure D-10 Velocity waveforms (amp=50%)
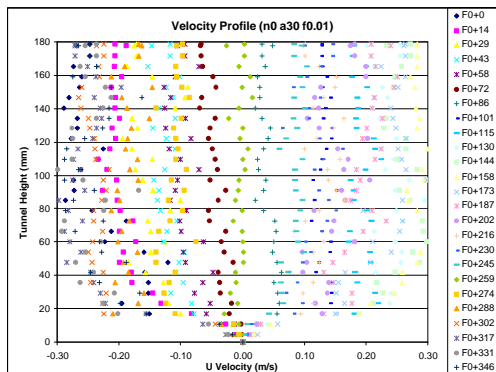
Figure D-11 Velocity profiles (amp=60%)
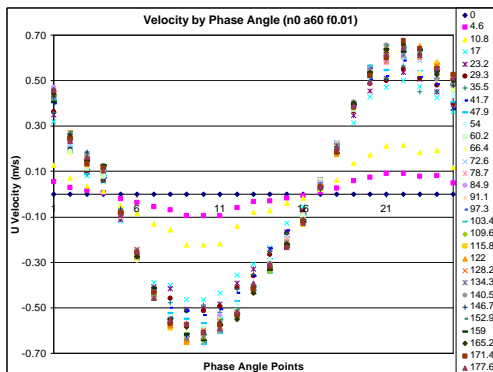
Figure D-12 Velocity waveforms (amp=60%)
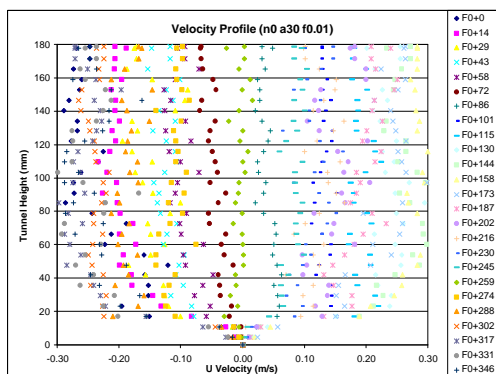
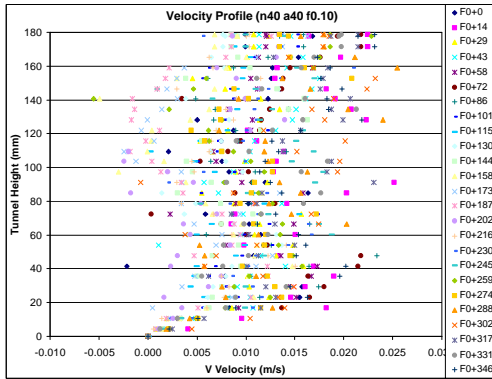Figure D-13 Velocity profiles (amp=70%)
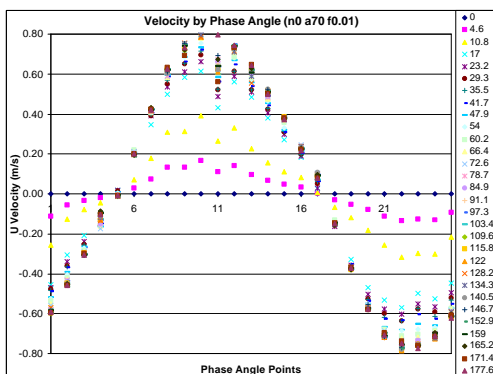
Figure D-14 Velocity waveforms (amp=70%)
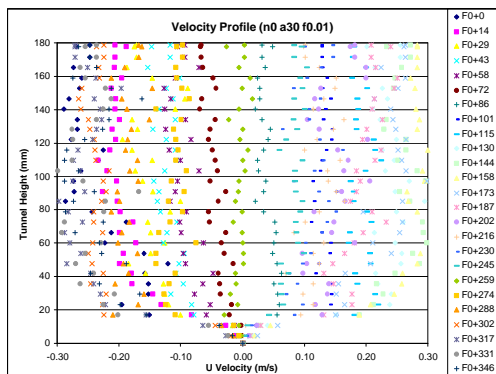
Figure D-15 Velocity profiles (amp=80%)
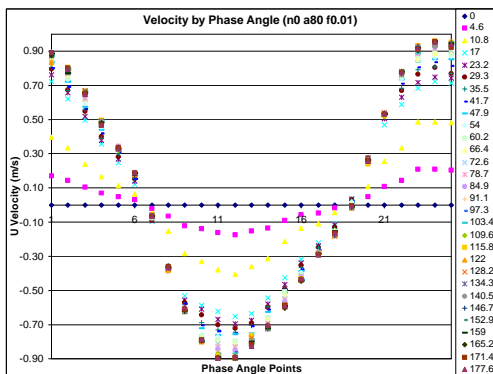
Figure D-16 Velocity waveforms (amp=80%)
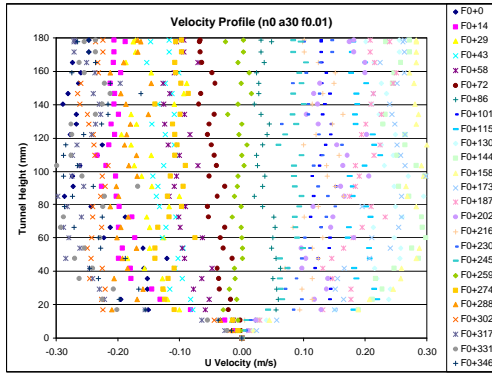
Figure D-17 Velocity profiles (amp=90%)
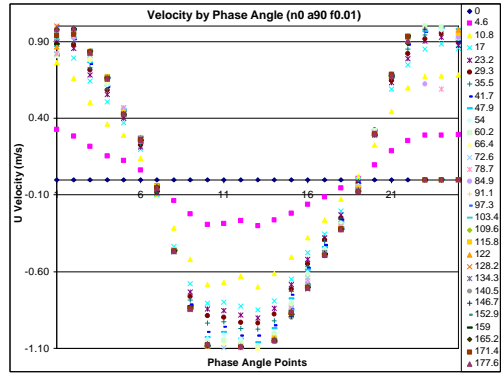
Figure D-18 Velocity waveforms (amp=90%)

D.1.2 Velocity of variable frequency and constant amplitude

This is the full version of example velocity profiles and waveforms measured by PIV for the pure oscillatory flows at different frequencies. The simplified version of this example is shown in Chapter 4.6.2. Please refer to Chapter 4.6.1 for the description of the flow parameters. Figure D-19 to Figure D-24 are the full version of Figure 4-54 through Figure 4-59 respectively.
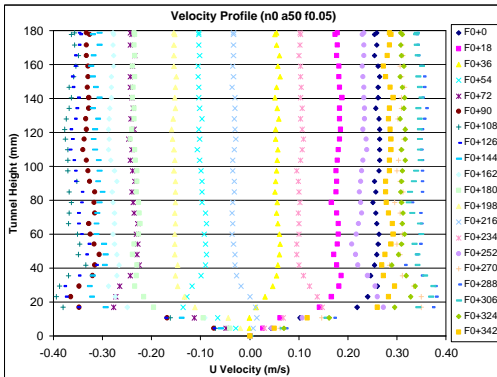
Figure D-19 Velocity profiles of 0.05Hz
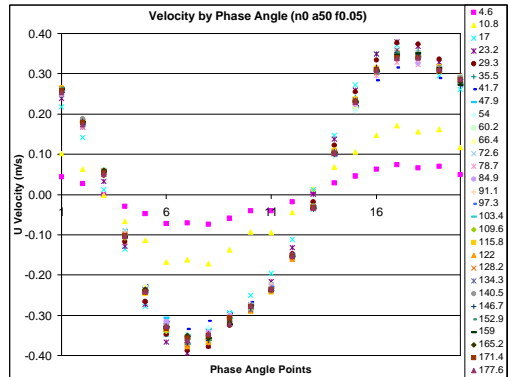
Figure D-20 Velocity waveforms (f_r=0.05Hz)
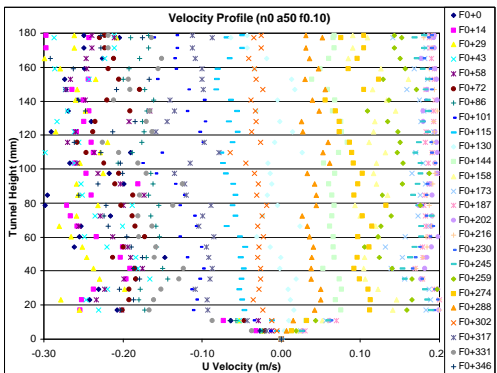
Figure D-21 Velocity profiles of 0.10Hz
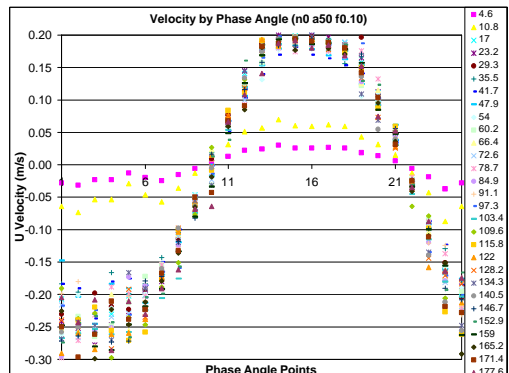
Figure D-22 Velocity waveforms (f_r=0.10Hz)
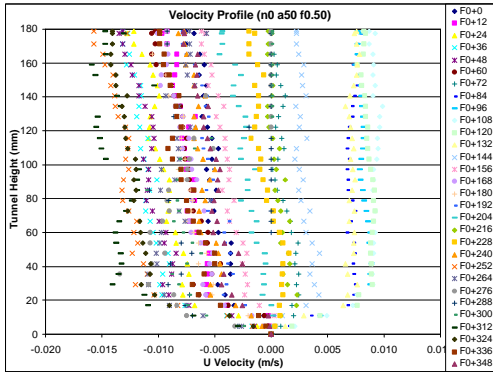
Figure D-23 Velocity profiles of 0.50Hz
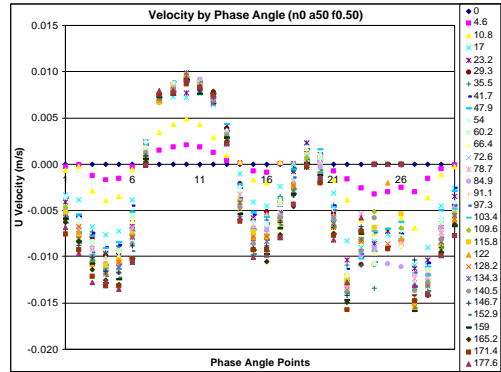
Figure D-24 Velocity waveforms (f_r=0.50Hz)

D.1.3 Vertical velocity

Following is the example vertical velocity profiles and waveforms of pure oscillatory flow at various oscillatory amplitudes. The simplified version of the example is shown in Chapter 4.6.3. Figure D-25 to Figure D-28 are the full version of Figure 4-60 to Figure 4-63 respectively.
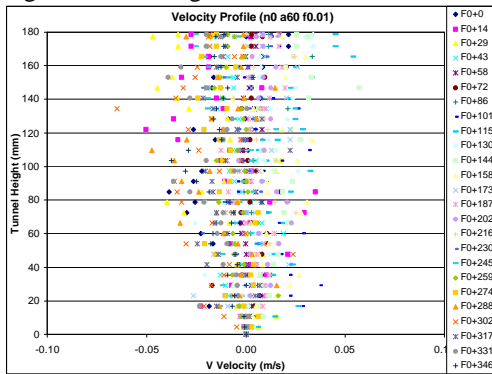
Figure D-25 Velocity profiles of *V* (amp=60%)
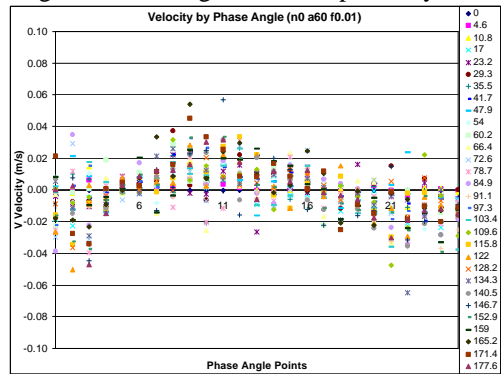
Figure D-26 Velocity waveforms of *V* (amp=60%)
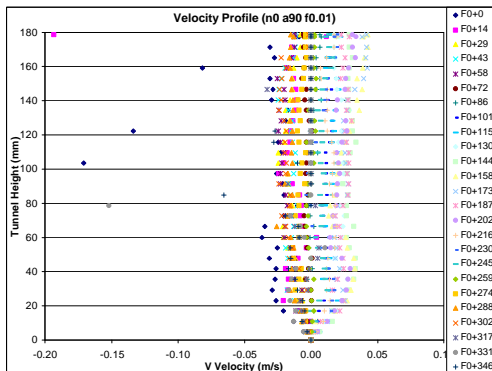
Figure D-27 Velocity profiles of *V* (amp=90%)
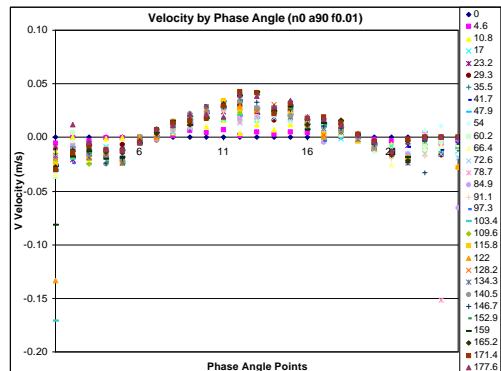
Figure D-28 Velocity waveforms of *V* (amp=90%)

D.2 PIV Velocity of Combined Oscillatory Flow

The full version of example velocity profiles and waveforms of Combined Oscillatory Flow measured by PIV is shown below, the simplified version of which is shown in Chapter 4.7.

D.2.1 Velocity of variable amplitude, constant base flow and frequency

The example of velocity profiles and waveforms measured by PIV velocity for the Combined Oscillatory Flows at different amplitudes is shown in Figure D-29 to Figure D-40 corresponding to Figure 4-64 to Figure 4-75 respectively, as shown in Chapter 4.7.1.
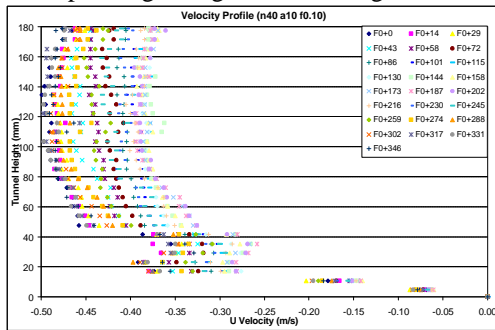
Figure D-29 Velocity profiles at amp=10%
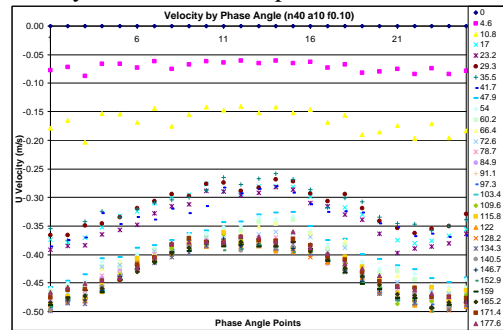
Figure D-30 Velocity waveforms (amp=10%)
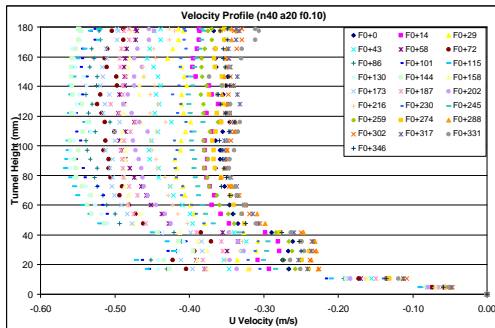
Figure D-31 Velocity profiles at amp=20%
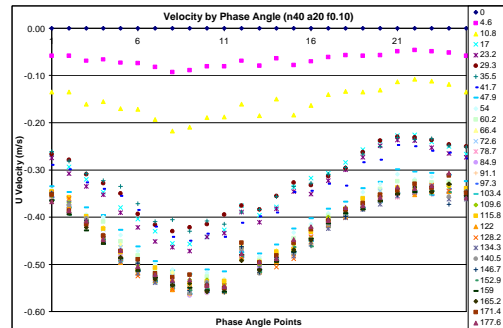
Figure D-32 Velocity waveforms (amp=20%)
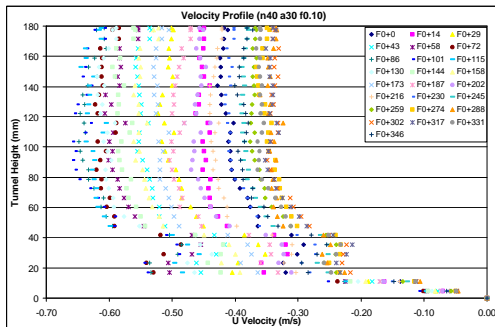
Figure D-33 Velocity profiles at amp=30%
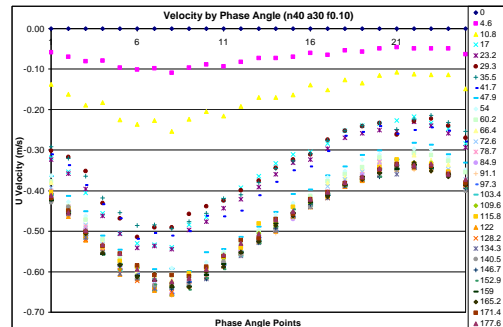
Figure D-34 Velocity waveforms (amp=30%)
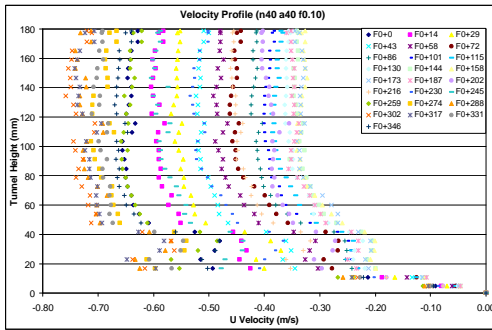
Figure D-35 Velocity profiles at amp=40%
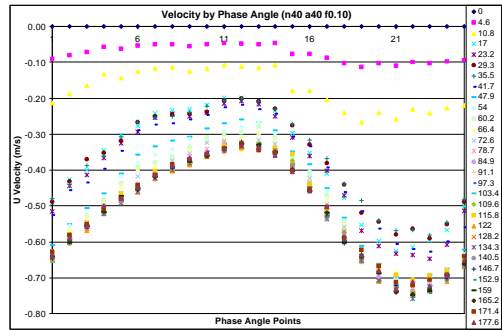
Figure D-36 Velocity waveforms (amp=40%)
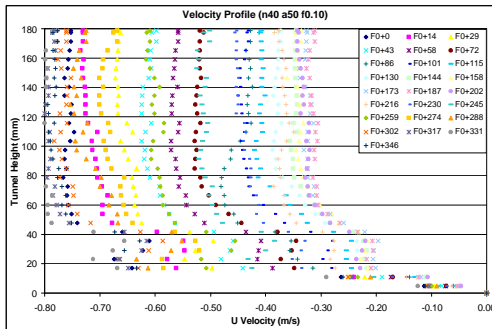
Figure D-37 Velocity profiles at amp=50%
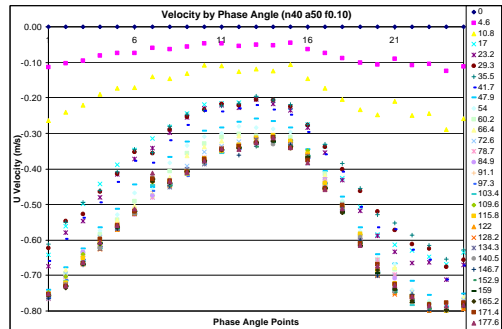
Figure D-38 Velocity waveforms (amp=50%)
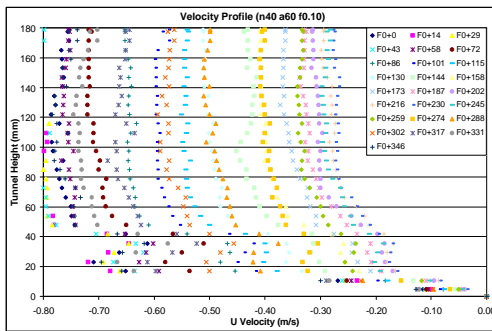
Figure D-39 Velocity profiles at amp=60%
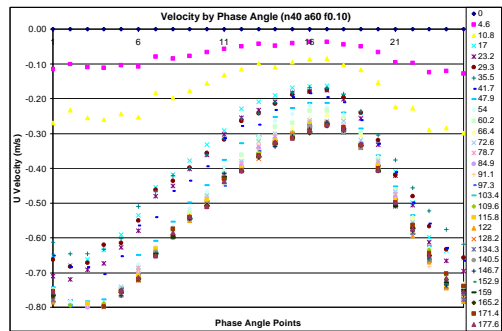
Figure D-40 Velocity waveforms (amp=60%)

D.2.2 Velocity of variable frequency, constant base flow and amplitude

This is the full version of velocity profiles and waveforms measured by PIV for the Combined Oscillatory Flows at different frequencies, the simplified version of which is shown in Chapter 4.7.2. Please refer to 4.7.1 for the description of the flow parameters. Figure D-41 to Figure 4-78 are the full version of Figure 4-76 through Figure 4-83 respectively.
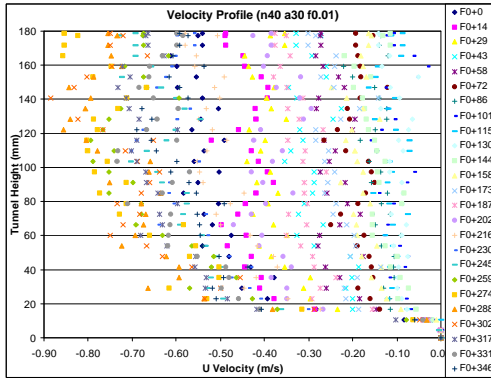
Figure D-41 Velocity profiles of f_r=0.01Hz
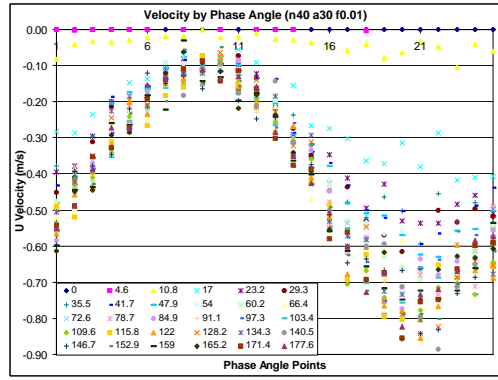
Figure D-42 Velocity waveforms (f_r=0.01Hz)
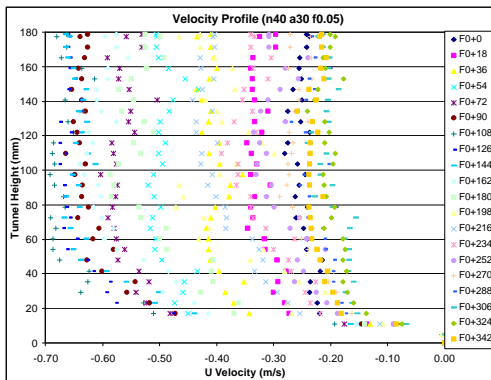
Figure D-43 Velocity profiles of f_r=0.05Hz
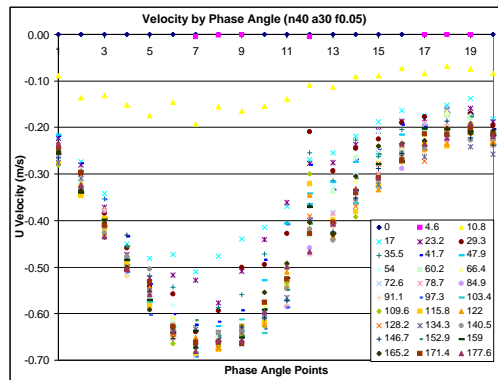
Figure D-44 Velocity waveforms (f_r=0.05Hz)
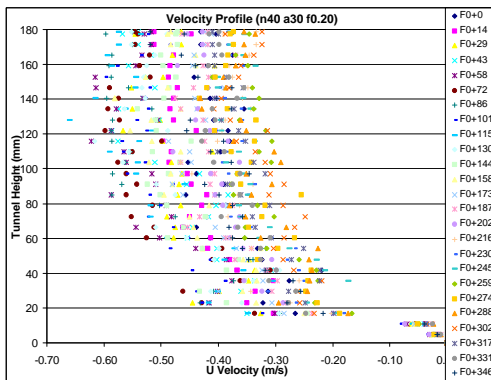
Figure D-45 Velocity profiles of f_r=0.20Hz
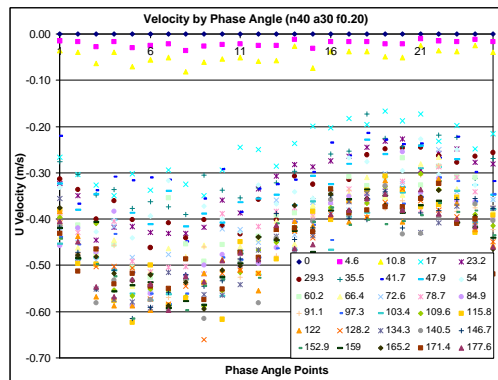
Figure D-46 Velocity waveforms (f_r=0.20Hz)
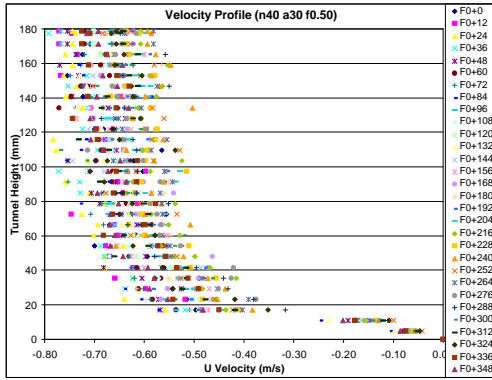
Figure D-47 Velocity profiles of f_r=0.50Hz
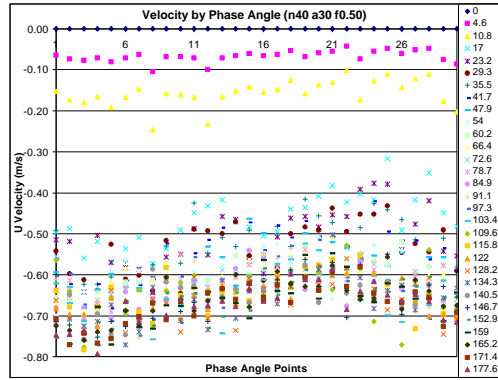
Figure D-48 Velocity waveforms (f_r=0.50Hz)

D.2.3 Velocity of variable base flow, const. freq. and amplitude

This is the full version of velocity profiles and waveforms measured by PIV for the Combined Oscillatory Flows at different base flows, the simplified version of which is shown in Ch. 4.7.3. Figure D-49 to Figure D-58 are the full version of Figure 4-84 through Figure 4-93 respectively
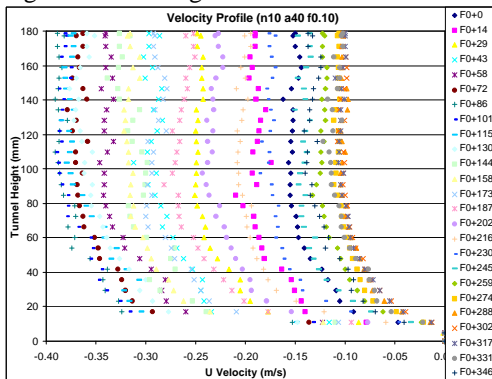
Figure D-49 Velocity profiles of n_0=10%
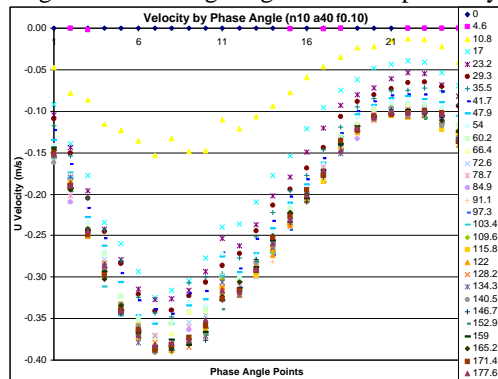
Figure D-50 Velocity waveforms (n_0=10%)
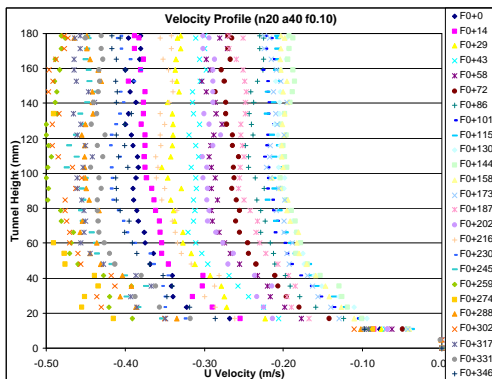
Figure D-51 Velocity profiles of n_0=20%
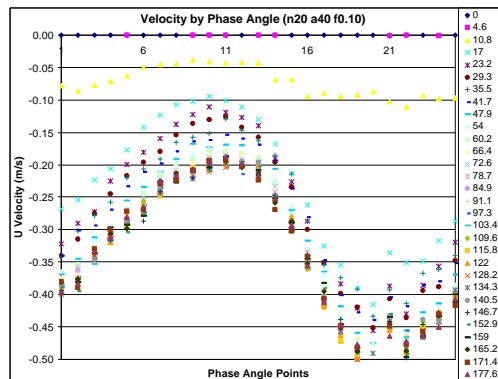
Figure D-52 Velocity waveforms (n_0=20%)
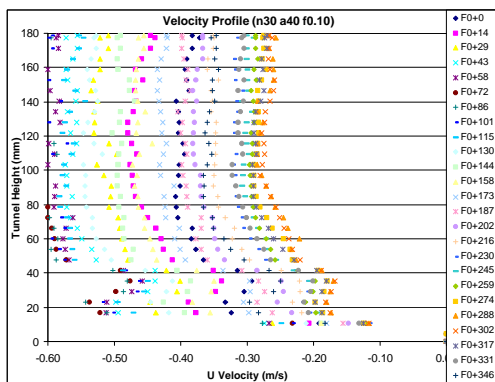
Figure D-53 Velocity profiles of $n_0=30\%$
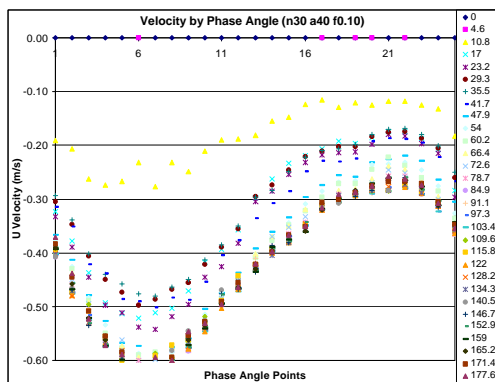
Figure D-54 Velocity waveforms ($n_0=30\%$)
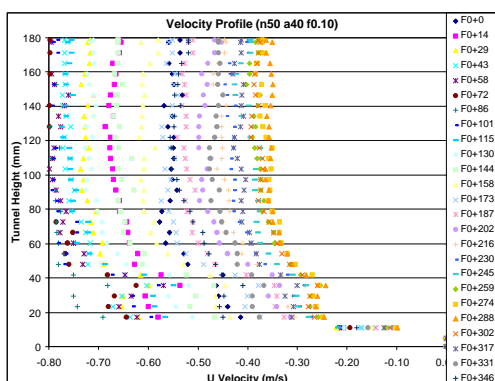
Figure D-55 Velocity profiles of $n_0=50\%$
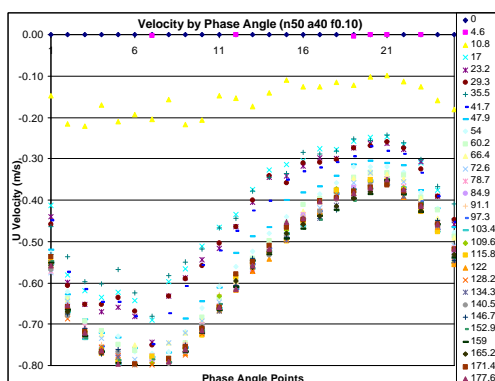
Figure D-56 Velocity waveforms ($n_0=50\%$)
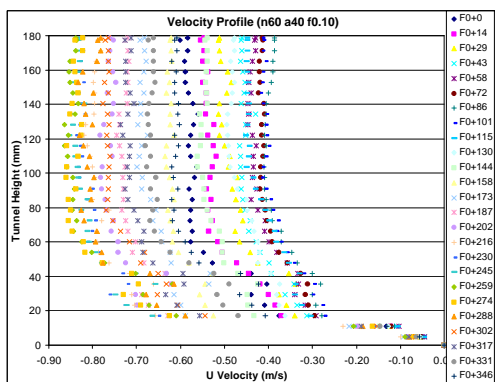
Figure D-57 Velocity profiles of $n_0=60\%$
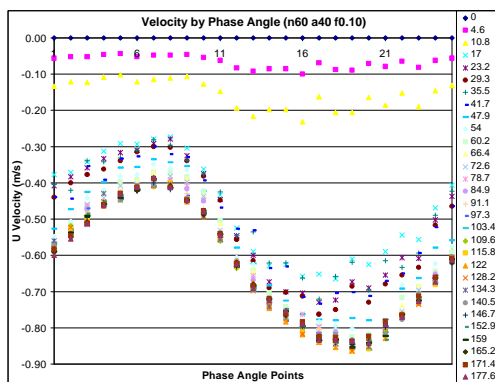
Figure D-58 Velocity waveforms ($n_0=60\%$)

D.2.4 Vertical velocity

The full version of example vertical velocity profiles and waveforms measured by PIV for the combined oscillatory flows at different oscillatory amplitudes is shown in Figure D-59 to Figure

D-64, corresponding to the simplified version of Figure 4-94 through Figure 4-99 respectively, as shown in Chapter 4.7.4. Please refer to 4.7.4 for the description of the flow parameters.

Figure D-59 Velocity profiles of *V* at amp=10%

Figure D-60 Velocity waveforms of *V* (amp=10%)

Figure D-61 Velocity profiles of *V* at amp=40%
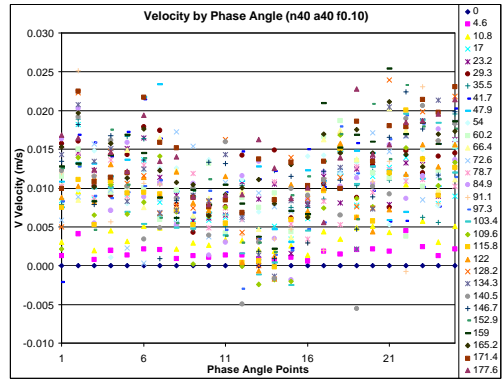
Figure D-62 Velocity waveforms of *V* (amp=40%)
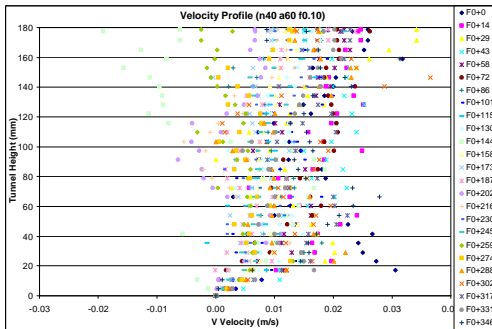
Figure D-63 Velocity profiles of *V* at amp=60%
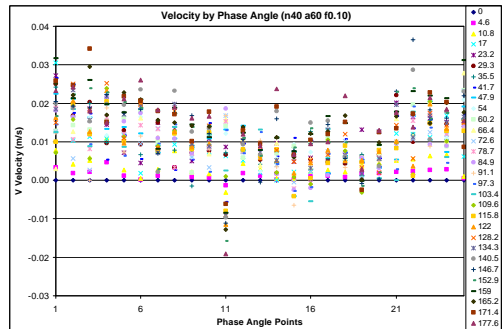
Figure D-64 Velocity waveforms of *V* (amp=60%)

Appendix E Dimensionless Velocity Profiles

A simplified version of the example velocity profiles and waveforms from PIV measurement has been shown in Chapter 4 of this thesis to display the basic information got from PIV. A complete version of the figures is shown in Appendix D. Absolute velocity values were used in the both versions mentioned. To compare the velocity profiles between different flow regimes, dimensionless velocity profiles of the same flow regimes are given in this appendix, in the same order and under the same headings as that of in Chapter 4. Refer to Chapter 4 for the analysis and summary of the example velocity profiles and waveforms.

The dimensionless operation is carried out as follows:

− Velocity: $u^+ = u / U$, $v^+ = v / V$, where U and V are the maximum streamwise and vertical velocities.

− Vertical coordinates: $z^+ = z / Z_0$, where $Z_0 \sim b/2$ is the half height of the test duct.

E.1 PIV Velocity of Pure Oscillatory Flow

The dimensionless velocity profiles of Pure Oscillatory Flow are given below, corresponding to those shown in Chapter 4.6

E.1.1 Velocity of constant frequency and variable amplitude

Followings are the dimensionless velocity profiles of Pure Oscillatory Flows at the frequency of $f_r = 0.01$Hz, the simplified version of which was shown in Chapter 4.6.1. Refer to 4.6.1 for the descriptions of the flow. Figure E-1 to Figure E-9 are the dimensionless version of Figure 4-36 through Figure 4-52 respectively.
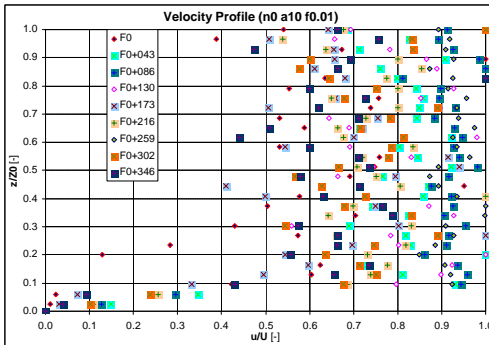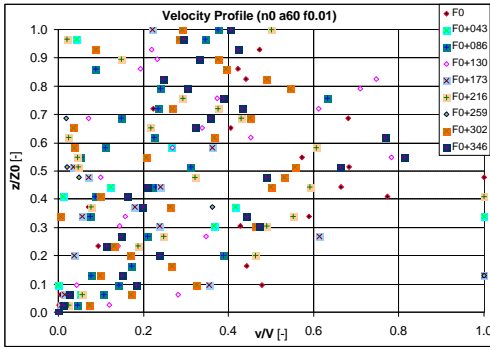

Figure E-1 Velocity profiles at amp=10%
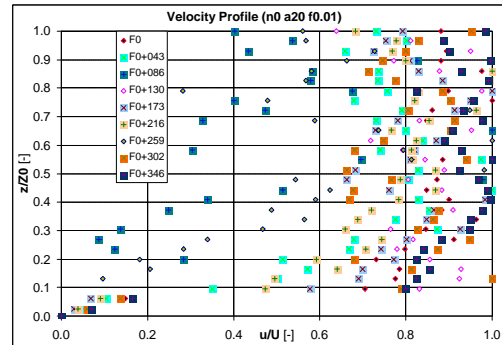
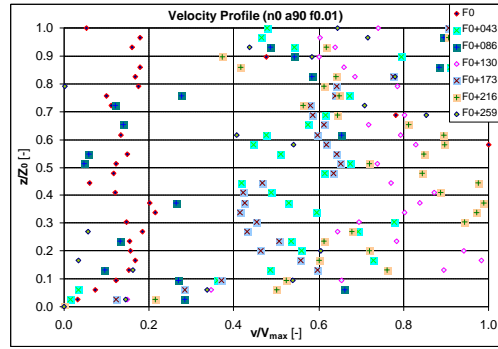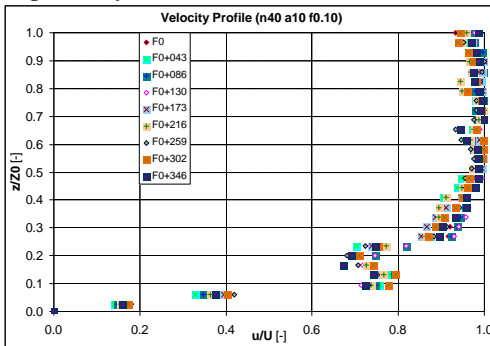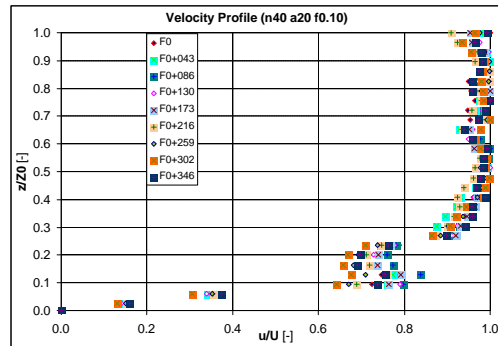Figure E-2 Velocity profiles at amp=20%
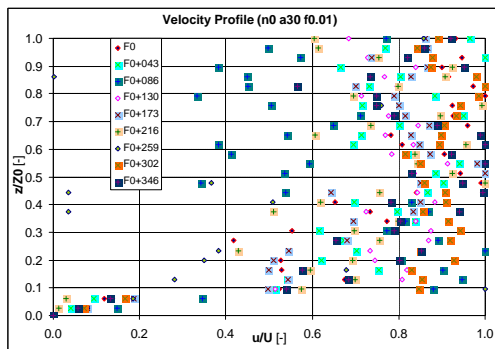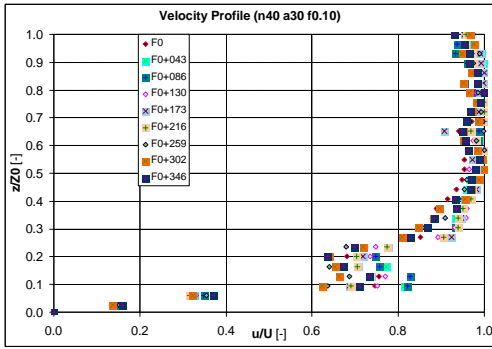
Figure E-3 Velocity profiles at amp=30%
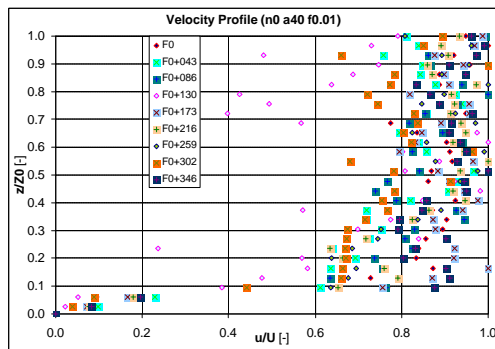
Figure E-4 Velocity profiles at amp=40%
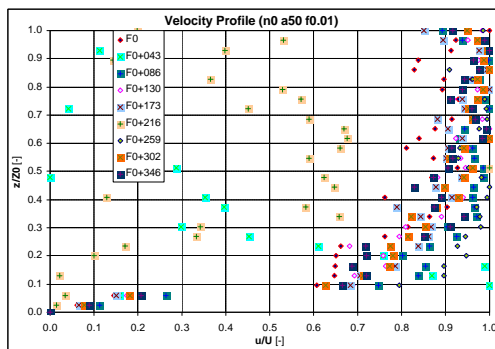
Figure E-5 Velocity profiles at amp=50%
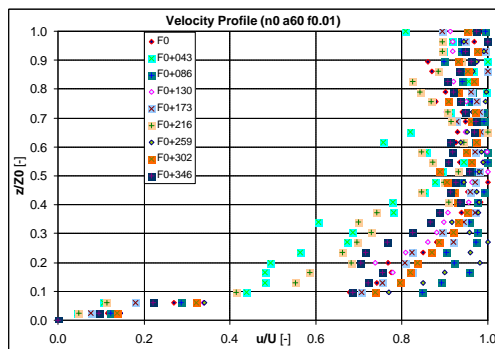
Figure E-6 Velocity profiles at amp=60%
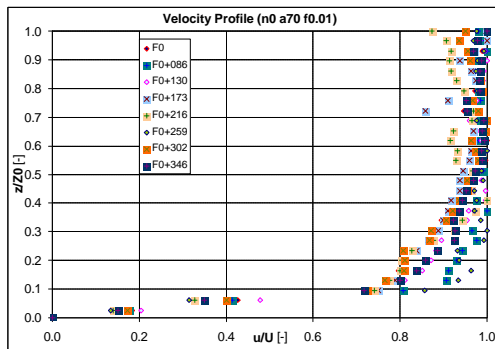
Figure E-7 Velocity profiles at amp=70%
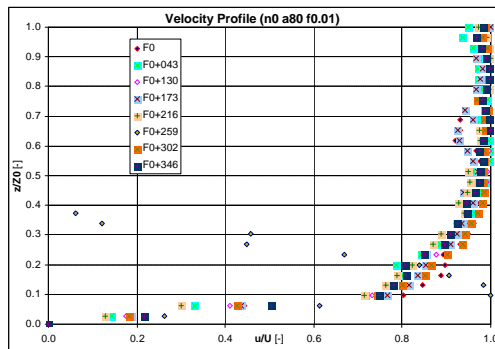
Figure E-8 Velocity profiles at amp=80%
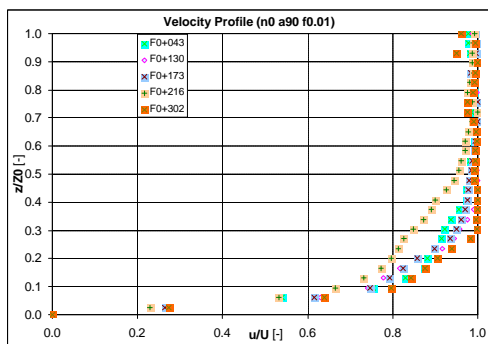
Figure E-9 Velocity profiles at amp=90%
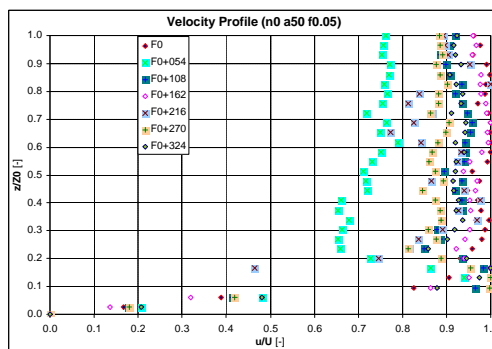
Figure E-10 Velocity profiles of f_r=0.05Hz
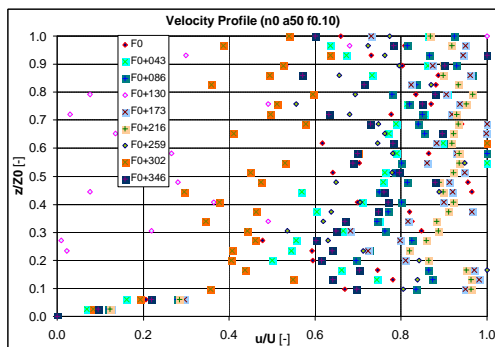
Figure E-11 Velocity profiles of f_r=0.10Hz
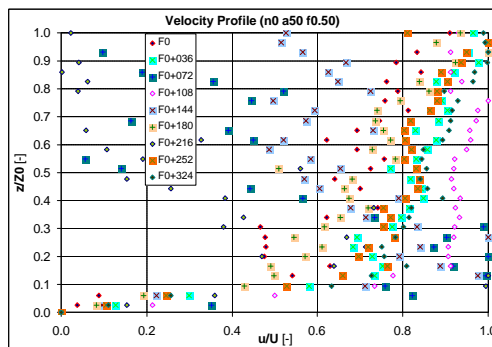
Figure E-12 Velocity profiles of f_r=0.50Hz

E.1.2 Velocity of variable frequency and constant amplitude

The dimensionless velocity profiles of Pure Oscillatory Flows at different frequencies are shown in this section, corresponding to those shown in Chapter 4.6.2. Refer to 4.6.1 for the descriptions of the flow. Figure E-10 to Figure E-12 (shown above) are the dimensionless version of Figure 4-54, Figure 4-56 and Figure 4-58 respectively.

E.1.3 Vertical velocity

Followings are the dimensionless vertical velocity profiles of Pure Oscillatory Flows at different oscillatory amplitudes, corresponding to those shown in Chapter 4.6.3. Refer to 4.6.1 for the descriptions of the flow. Figure E-13 to Figure E-14 are the dimensionless version of Figure 4-60 and Figure 4-62 respectively.
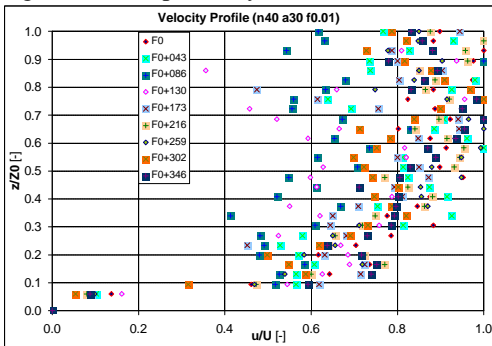
Figure E-13 Velocity profiles of *V* at amp=60%

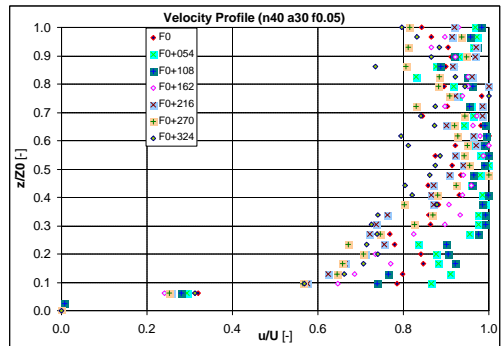Figure E-14 Velocity profiles of *V* at amp=90%

E.2 PIV Velocity of Combined Oscillatory Flow

The dimensionless version of the example velocity profiles of Combined Oscillatory Flow is given below, corresponding to those shown in Chapter 4.7.

E.2.1 Velocity of variable amplitude, constant base flow and frequency

Followings are the velocity profiles of Combined Oscillatory Flows at different amplitudes, corresponding to those shown in Chapter 4.7.1. Refer to 4.7.1 for the descriptions of the flow. Figure E-15 to Figure E-20 are the dimensionless version of Figure 4-64 through Figure 4-74 respectively.

Figure E-15 Velocity profiles of amp=10%

Figure E-16 Velocity profiles of amp=20%

Figure E-17 Velocity profiles of amp=30%
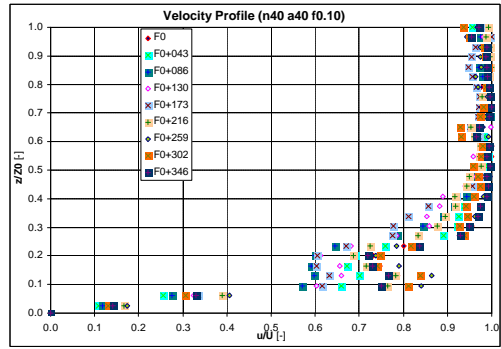
Figure E-18 Velocity profiles of amp=40%
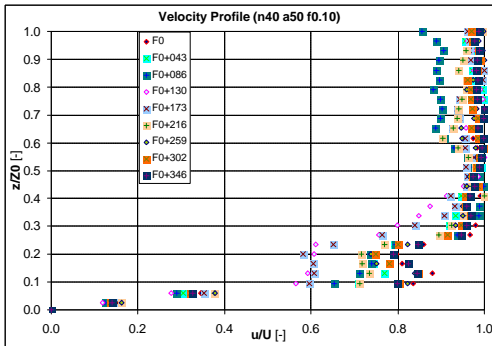
Figure E-19 Velocity profiles of amp=50%
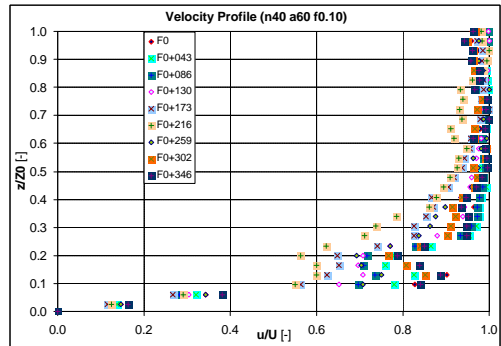
Figure E-20 Velocity profile of amp=60%

E.2.2 Velocity of variable frequency, constant base flow and amplitude

Followings are the dimensionless velocity profiles of Combined Oscillatory Flows at different frequencies, corresponding to those shown in Chapter 4.7.2. Refer to 4.7.1 for the descriptions of the flow. Figure E-21 to Figure E-24 are the dimensionless version of Figure 4-76 through Figure 4-82 respectively.

Figure E-21 Velocity profiles of f_r=0.01Hz

Figure E-22 Velocity profiles of f_r=0.05Hz
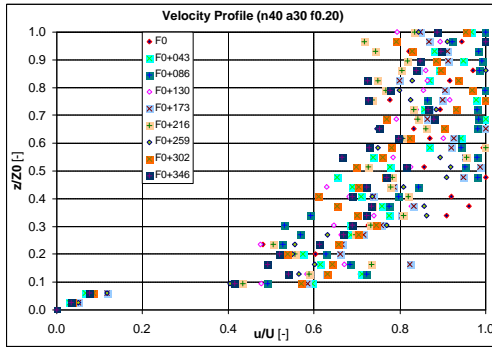
Figure E-23 Velocity profiles of f_r=0.20Hz
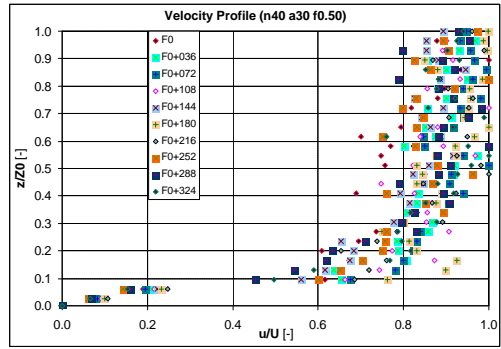
Figure E-24 Velocity profiles of f_r=0.50Hz

E.2.3 Velocity of variable base flow, constant frequency and amplitude

Here are the dimensionless velocity profiles of Combined Oscillatory Flows at different base flows, corresponding to those shown in 4.7.3. Figure E-25 to Figure E-29 are the dimensionless version of Figure 4-84 through Figure 4-92 respectively
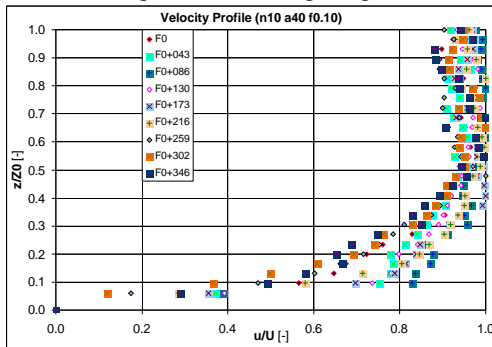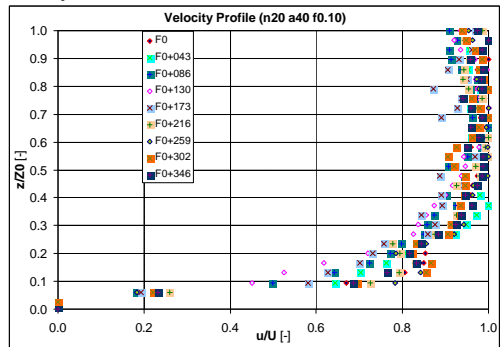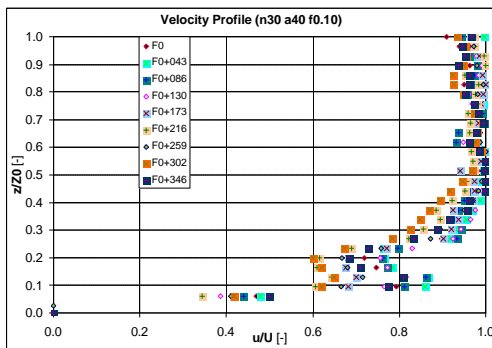

Figure E-25 Velocity profiles of n_0=10%

Figure E-26 Velocity profiles of n_0=20%

Figure E-27 Velocity profiles of n_0=30%
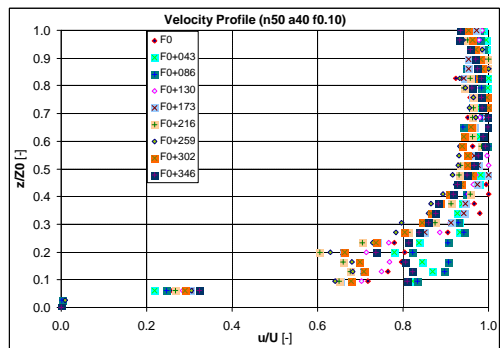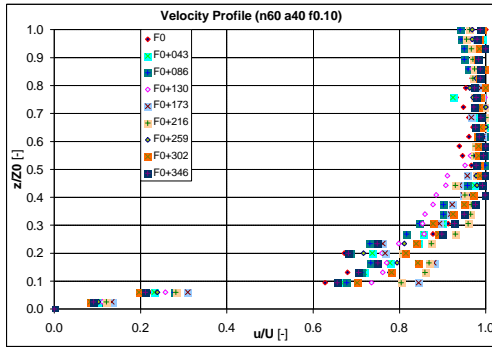

Figure E-28 Velocity profiles of n_0=50%

Figure E-29 Velocity profiles of n_0=60%
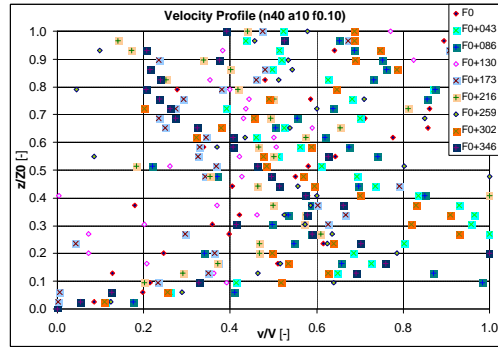

Figure E-30 Velocity profiles of V at amp=10%

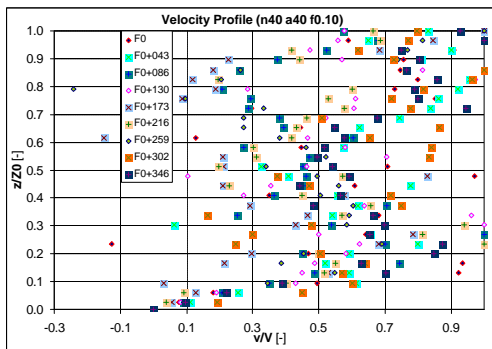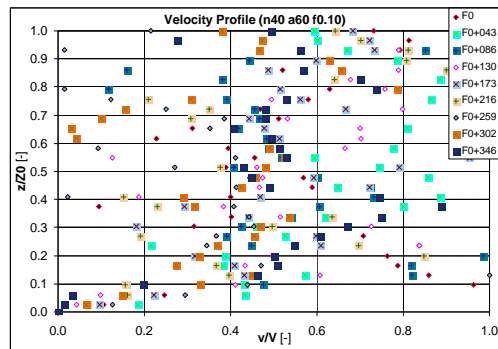Figure E-31 Velocity profiles of V at amp=40%

Figure E-32 Velocity profiles of V at amp=60%

E.2.4 Vertical velocity

The dimensionless vertical velocity profiles of Combined Oscillatory Flows at different oscillatory amplitudes are corresponding to those shown in Chapter 4.7.4. Refer to 4.7.1 for the descriptions of the flow. Figure E-30 to Figure E-32 (shown above) are the dimensionless version of Figure 4-94 through Figure 4-98 respectively

E.3 Discussions of Dimensionless Velocity

1.   Comparison between dimensionless and absolute velocities

From the figures shown above we can see:

– One of the advantages of dimensionless velocity profile is that the velocity profiles are almost identical for flows with different flow parameters, i.e., the velocity profiles are similar for flows with hydraulic similarity.

– One of the disadvantages of dimensionless velocity profile, comparing to the absolute value velocity profiles, is that it is difficult to get information about how the velocity is oscillating with the phase of flow.

2.   Notes from dimensionless velocity profiles

From the figures shown above we can see:

- In most cases the mainstream velocity profiles are similar for different flow regimes, for different flow phases of the same flow regimes.
- The vertical velocity is quite random scattered. It is difficult to get a concrete conclusion for the vertical velocity distribution. Basically the vertical velocity distribution has the similar tendency to that of mainstream velocity.
- For some cases shown, the mainstream velocity is quite scattered. Generally speaking, this happens when the absolute velocity magnitude is too small. This is similar to that of the vertical velocity.

194